NASA CR-54172
PWA-2351, Volume I
Copy 68

DESIGN STUDY OF A HIGH POWER IN-PILE NUCLEAR THERMIONIC SPACE POWERPLANT

by
A. U. Buatti and J. W. Schmitt

prepared for
National Aeronautics and Space Administration

Contract NASw-763

Pratt & Whitney Aircraft DIVISION OF UNITED AIRCRAFT CORPORATION
EAST HARTFORD • CONNECTICUT

NASA CR-54172
PWA-2351, Volume I

copy 68

FINAL REPORT

DESIGN STUDY OF A HIGH POWER IN-PILE NUCLEAR THERMIONIC SPACE POWERPLANT

prepared for
National Aeronautics and Space Administration

Contract NASw-763

July 30, 1964

Technical Management
NASA Lewis Research Center
Space Power System Division
Cleveland, Ohio
Jack F. Mondt

Written by A. U. Buatti, Sen. Anal. Engr.
J. W. Schmitt, Asst. Proj. Engr.

Approved by R. Cohen, Program Manager
W. J. Lueckel, Chief, Space Power Systems

Pratt & Whitney Aircraft DIVISION OF UNITED AIRCRAFT CORPORATION

EAST HARTFORD • CONNECTICUT

FOREWORD

This report presents the results of a design study of a 3.25 megawatt in-pile nuclear thermionic space powerplant conducted by the Pratt & Whitney Aircraft Division of United Aircraft Corporation, East Hartford, Connecticut, under National Aeronautics and Space Administration Contract NASw-763, with the technical direction of J. F. Mondt of Lewis Research Center.

TABLE OF CONTENTS

VOLUME 1

TABLE OF CONTENTS (CONT'D)

LIST OF FIGURES

LIST OF FIGURES(Cont'd)

I. SUMMARY

11041

This report presents the results of preliminary design studies of a 3.25 megawatt in-pile nuclear thermionic space powerplant. The design of the powerplant is based on a systems analysis[1] which varied component and system parameters to determine system performance. In this report, the powerplant is described in detail and an evaluation of its performance is given. Major technical problems and uncertainties are discussed and a number of appendices are included which present supporting detailed design and analytical studies and materials data. The purpose of this study was to determine thermionic system performance, prepare a preliminary design of a system, generate engineering design criteria and identify significant technical problems.

The powerplant selected for design contains a thermionic reactor, a nuclear shield, a primary coolant loop, a multiple-loop heat rejection system and a power-conditioning system. The reactor is fueled with UC-ZrC clad with a tungsten-rhenium alloy. Borated graphite and lithium-7 hydride are the materials used in the shield to protect the radiation sensitive components in the power-conditioning equipment. The main heat rejection system consists of sixteen individual loops, each containing a radiator segment, a heat exchanger and an electromagnetic pump. Lithium is used as the coolant and Cb-1Zr as the containment material for all components of the primary system and the main heat rejection system. The radiators also employ Cb-1Zr as the meteoroid barrier material instead of beryllium. As shown in Report PWA-2319, the use of Cb-1Zr results in a lower powerplant weight, due to its higher allowable operating temperature. The power-conditioning system contains electrical equipment cooled by an auxiliary heat rejection system employing monoisopropylbiphenyl as the coolant and aluminum as the containment material. The powerplant is integrated into a flight configuration with a lightweight titanium support structure designed to support loads in space. The powerplant is supported during launch by a trussed support structure which is jettisoned in space during powerplant startup, along with the aerodynamic fairing and auxiliary startup equipment.

[1] Pratt & Whitney Aircraft, Parametric Study of High Power In-Pile Nuclear Thermionic Space Powerplants, Report PWA-2319

Selection of a high cathode operating temperature is desired to minimize powerplant weight. For high reliability, the cathode temperature in operating converters should be limited to maintain structural integrity and long-life thermionic performance. In addition, because converters in the reactor may have failed due to an open-circuit condition, the temperature level at this condition should not cause structural failures that will lead to progressive reactor failure. For the present study an operating temperature level of 3200°F was selected on the basis of material limits for long-time reactor operation. The 3200°F operating cathode temperature selected also maintains consistency with the previous one-megawatt study[1].

The powerplant requires the use of power-conditioning equipment to convert the low voltage DC thermionic output to a high voltage DC input for the ion engines. The two types of power-conditioning equipment considered were low-temperature (150°F) solid-state devices and high-temperature (1100°F) gas-tube devices. The significant features of powerplants using these devices are shown below:

	Low-Temp. Equipment	High-Temp. Equipment
inflight powerplant specific weight, lbs/KW(e)	23.4	30.7
overall system efficiency, %	10.5	8.8
area (projected one-side) of auxiliary radiator, ft^2	3180	365
weight of auxiliary radiator, lbs	3250	1800
efficiency of power-conditioning equipment, %	93	78
weight of power-conditioning equipment, lbs/KW(e)	4	10

These results are based on the latest available power-conditioning equipment information published by Westinghouse[2]. It should be noted that the system design study described in this report was based on earlier

[1] Pratt & Whitney Aircraft, Design Report, Advanced Nuclear Electric Power Generator Systems Study, Thermionic Nuclear Space Powerplant, Report PWA-2224, Vol. I CRD, Vol. II SRD

[2] Westinghouse Electric Corporation, Aerospace Electrical Division, Space Electric Power Systems Study, Volume 5, NAS5-12134

Westinghouse data presented in PWA-2240[1] because the powerplant study was completed prior to the publication of the new data.

Based on this study the following conclusions can be made:

A. The largest payload weight is obtained by reducing powerplant inflight weight, even if this results in increasing system launch weight. It has been shown that for a given payload weight, up to 3 pounds of powerplant launch weight can be added to save 1 pound of inflight weight (see Appendix 2).

B. A planar radiator configuration results in lower powerplant weight than a cylindrical configuration due predominantly to lower shield weight (see Appendix 2).

C. The selection of NaK as a coolant instead of lithium results in an increase of about 4 lbs/KW(e) in the inflight weight of the powerplant. This increase in specific weight almost eliminates the entire payload capability of the vehicle (see Report PWA-2319 and Appendix 2).

D. Increasing the converter power density to a value greater than that used in this design (approximately 10 watts/cm^2) will not significantly reduce the powerplant specific weight (see p. 110).

E. Development of the anode trilayer is as important to the development of the thermionic fuel element as the development of the nuclear fuel (see p. 114).

F. A 50 per cent change in meteoroid barrier thickness results in only a 5 per cent change in the specific weight of the powerplant. This indicates that the meteoroid barrier criterion, within the thickness range studied, will not significantly affect the powerplant specific weight (see p. 122).

[1] Pratt & Whitney Aircraft, Parametric Study Report, Advanced Nuclear Electric Power Generator System Study, Thermionic Nuclear Space Powerplant, Report PWA-2240

G. Variable converter length with uniform fuel loading results in about the same system performance as constant converter length with variable fuel loading (see Appendix 6).

H. A fuel element designed to contain 100 per cent fission gas release would increase system specific weight by about 30 per cent (see Appendix 7).

I. The largest thermionic reactor that can be reflector-controlled with a 2 per cent shutdown margin is about 53 inches in diameter. For a 3200°F cathode temperature, a reactor of this diameter can produce about 9 megawatts of electrical power (see p. 118).

J. Further systems studies are required to investigate the potential of other reactor fuels and reactor concepts.

K. Further experimental work is required to establish sufficient data for fuel materials, containment materials, electrical insulators, thermionic performance, meteoroid effects and power-conditioning equipment.

L. The following areas require documentation to establish the feasibility of this concept, 1) fuel endurance, 2) cathode endurance, 3) trilayer anode fabrication and endurance, 4) fission product gas disposition, 5) cesium vapor distribution, and 6) radiation effects in electrical insulators.

II. INTRODUCTION

In-pile nuclear thermionic systems are attractive for use as nuclear-electric space powerplants. These powerplants have two potential uses in space vehicles, 1) as propulsive power, and 2) for on-board power. In order to evaluate these systems and to compare them with competitive powerplants, system studies have been conducted for powerplants over a wide range of power output. The design study presented in this report was performed by Pratt & Whitney Aircraft in partial fulfillment of Contract NASw-763 with the Lewis Research Center of the National Aeronautics and Space Administration. The purpose of the study was to investigate performance, to define optimum systems, to identify the significant technical problems that must be resolved before undertaking development of these systems, to establish engineering design criteria for components, and to indicate the objectives for component demonstration programs. A parametric study was performed to identify optimum systems in the power range from 1 to 10 megawatts (electric) and is presented in Report PWA-2319. The design of the 3.25 MWe powerplant presented here was performed to aid in the definition of a high power system.

Similar studies of a one-megawatt powerplant were performed and described earlier by Pratt & Whitney Aircraft under Contract NASw-360[1,2].

As a part of this study certain areas of interest were examined which had been indicated as requiring additional study by the one-megawatt study. These areas are:

1) Selection of radiator configuration
2) Comparison of variable and constant-length converters and variable and uniform fuel loading
3) Establishment of the relative importance of powerplant launch weight and powerplant inflight weight, from a mission standpoint
4) Establishment of the maximum power level of a reflector-controlled thermionic reactor

[1] Pratt & Whitney Aircraft, Parametric Study Report, Advanced Nuclear Electric Power Generator System Study, Thermionic Nuclear Space Powerplant, Report PWA-2240

[2] Pratt & Whitney Aircraft, Design Report, Advanced Nuclear Electric Power Generator Systems Study, Thermionic Nuclear Space Powerplant, Report PWA-2224, Vol. I CRD, Vol. II SRD

5) Determination of overall system weight penalties and reactor size increase for fission gas containment
6) Determination of the effects of design criteria selection on the system
7) Comparison between a system sized to provide full power at beginning of life and a system designed to provide full power at end of life

Although most of the potential missions cannot be precisely defined, selection of a representative mission was desirable to provide general direction for the powerplant investigation. Therefore, for the purposes of this study an unmanned Jupiter-capture mission using electric propulsion was assumed as a model. For this mission the assumption was made that the space vehicle would be launched into an earth orbit by a Saturn 5 vehicle.

During launch and for about 10 hours afterwards, the powerplant would be dormant to allow orbit verification and startup of the system. The propulsion system would then be activated and the vehicle embarked upon a trajectory which included escape and transfer to a heliocentric orbit, followed by a coast until approaching the vicinity of Jupiter, where a capture maneuver would be executed. The vehicle would orbit the planet, make observations, and transmit information back to earth. For this mission, the optimum power level for the powerplant was determined from a mission analysis to be 3.25 megawatts (electric).

The meteoroid hazard is an environmental uncertainty which affects the reliability and design weight of the powerplant for a given mission. Since all missions for this powerplant are not specifically defined, and since the meteoroid hazard itself is not well documented, an assumption of the reliability of the radiator and other components was required. On the basis of a segmented radiator, the system was assumed to provide full power at the start of the mission with all segments and components operational. Meteoroid protection was provided for a 90 per cent probability that three-fourths or more of the radiator segments would be operating at the end of the assumed Jupiter mission of 24,000 hours.

III. RESULTS

A. System Description

The nuclear thermionic space power system whose inflight configuration is shown in Figure 1 is comprised basically of a heat source, an energy conversion device and a heat rejection system. In this system a nuclear reactor is employed as the heat source and thermionic converters as conversion devices. The converters are an integral part of the fuel elements contained within the reactor and are heated directly by the fuel. Electrical power generated in the converters is conducted out of the reactor to power-conditioning equipment which processes the reactor output power characteristics to match those required by the load. A liquid metal coolant circulated by an electromagnetic (EM) pump cools the reactor and transfers waste heat in parallel-connected heat exchangers to the coolants in the heat rejection system. A segmented radiator rejects the waste heat to space. Auxiliary coolant systems are used to control the temperatures of the cesium reservoirs and of the power-conditioning equipment.

A simplified flow diagram for the powerplant is shown in Figure 2. The system components are grouped into three major subsystems, 1) a primary or energy source subsystem, 2) a secondary or heat rejection subsystem, and 3) an auxiliary or power-conditioning subsystem. The components contained in each subsystem are:

Primary Subsystem	Secondary Subsystem	Auxiliary Subsystem
thermionic reactor	heat exchangers (16)	power-conditioning equipment (4 units)
nuclear shield	radiators (16)	auxiliary radiators (4)
primary EM pump	secondary EM pump (16-cell)	centrifugal pumps (4)
primary piping	secondary piping	
cesium reservoir heat rejection system		

B. Powerplant Design

The thermionic powerplant selected for design study is one that delivers 3.25 megawatts electric to a space vehicle assigned to complete a Jupiter-capture mission. This powerplant would be used to supply electric power for both on-board requirements and for electric propulsion. The assumed Jupiter mission requires 20,000 effective full power hours of powerplant operation during a total mission time of 24,000 hours. A typical powerplant power-time profile is given in Section IV. G.

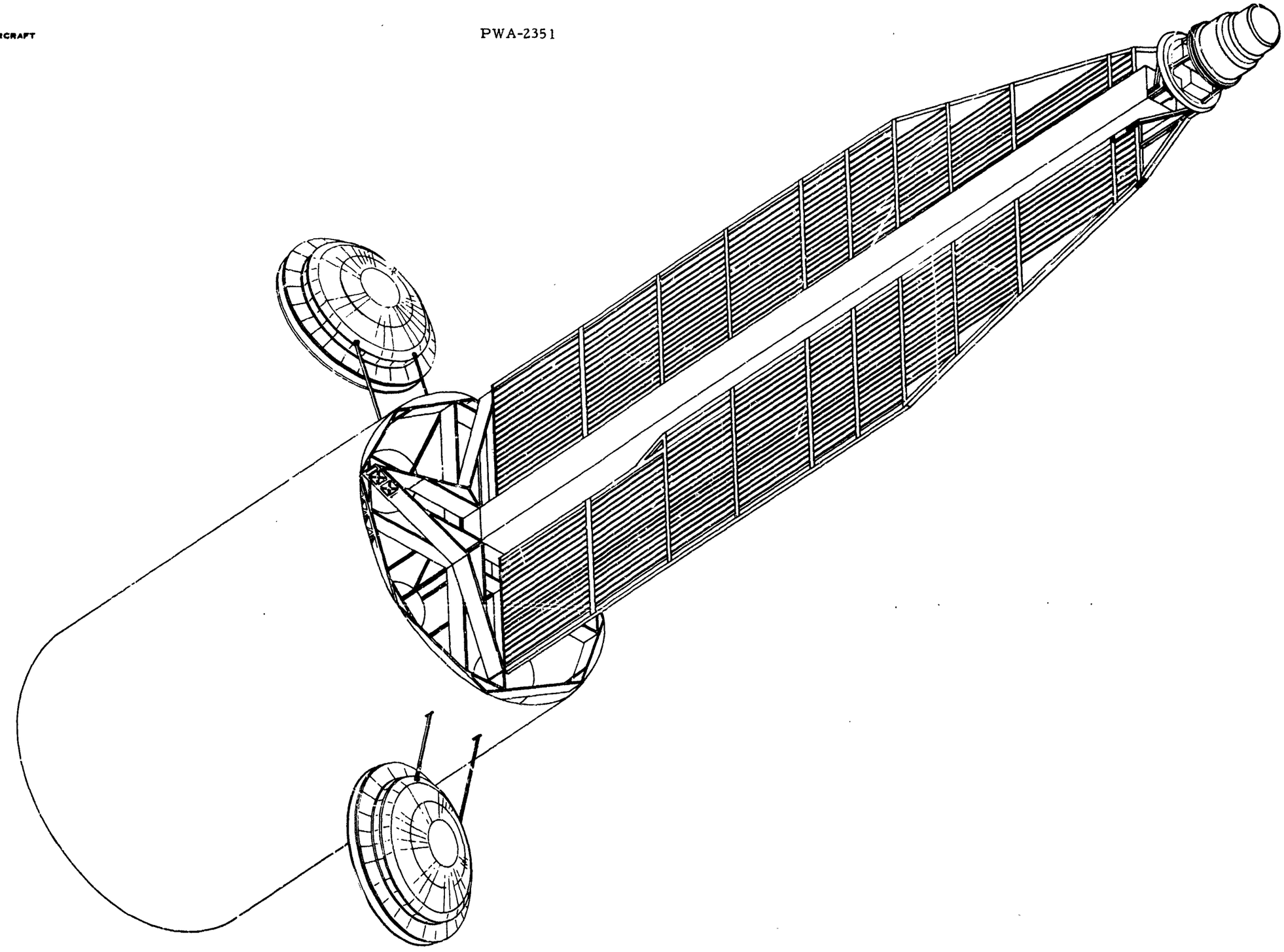

Figure 1 Inflight Powerplant Configuration

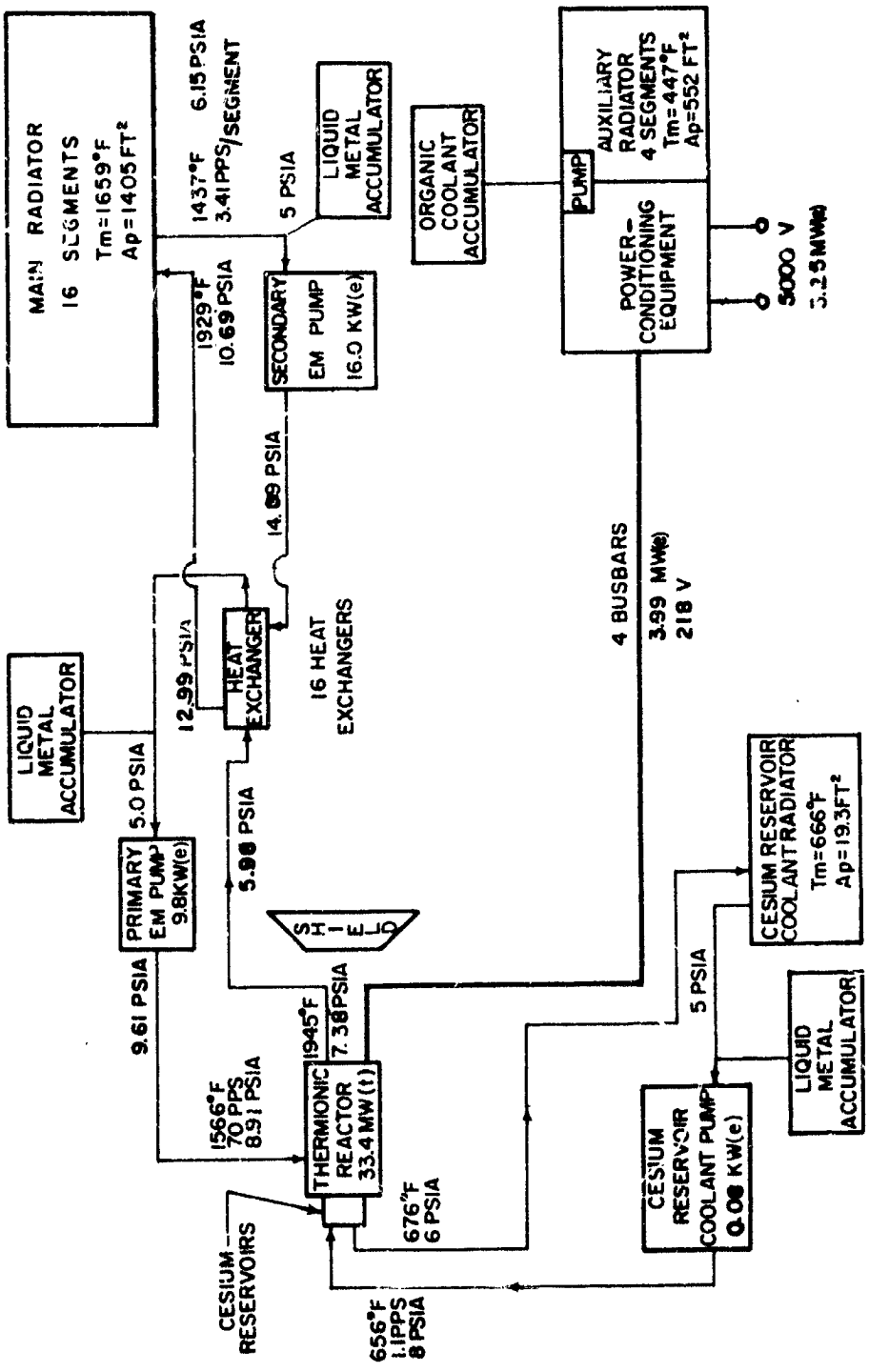

Figure 2 System Cycle Diagram

The design of the powerplant incorporates all necessary system components integrated with a support structure to form a space vehicle. Primary requirements are that the powerplant 1) be contained within the payload envelope of the Saturn 5 launch vehicle, 2) be capable of sustaining acceleration and vibration loads of the launch vehicle (data for the Saturn 1 was used since data for the Saturn 5 was unavailable), 3) be compatible with the nuclear and space environment for the duration of the mission, and 4) fulfill the electric power requirements of the mission.

1. Inflight Configuration

The inflight configuration of the thermionic powerplant integrated with a propulsion system to form a space vehicle is shown in Figure 3. This configuration differs from the launch configuration shown in Figure 4 in that the launch structure, the fairing, and the protective inert gas enclosures have been jettisoned. In this condition the powerplant weighs 76,100 pounds as compared to 123,200 pounds at launch.

The overall arrangement of the vehicle is based primarily upon the shape of the payload envelope for the Saturn 5. Location of the reactor and the radiation-sensitive power-conditioning equipment at opposite ends of the powerplant was done to keep shielding weight to a minimum. The placement of the shield directly behind the reactor also provides minimum weight in the shield. A planar radiator was selected over a cylindrical configuration on the basis that a planar design results in a lighter weight vehicle in space (see Appendix 2), with consequently greater payload. System components were grouped according to their temperatures and located in the plane of the main radiator to reduce heat absorption by low temperature components. The high temperature components are located at the forward end of the vehicle and the low temperature components at the rear. All heavyweight components are so oriented about the principal axis of the powerplant that the center of gravity of the whole vehicle falls on that axis. All heavyweight components supported by the inflight support structure have interconnecting piping designed to sustain thermal expansion.

The primary subsystem is arranged at the forward end of the vehicle with the reactor located at the apex and the shield immediately behind it. Eight reactor control drum drives, the primary coolant pump and the cesium reservoir coolant pump are arranged directly

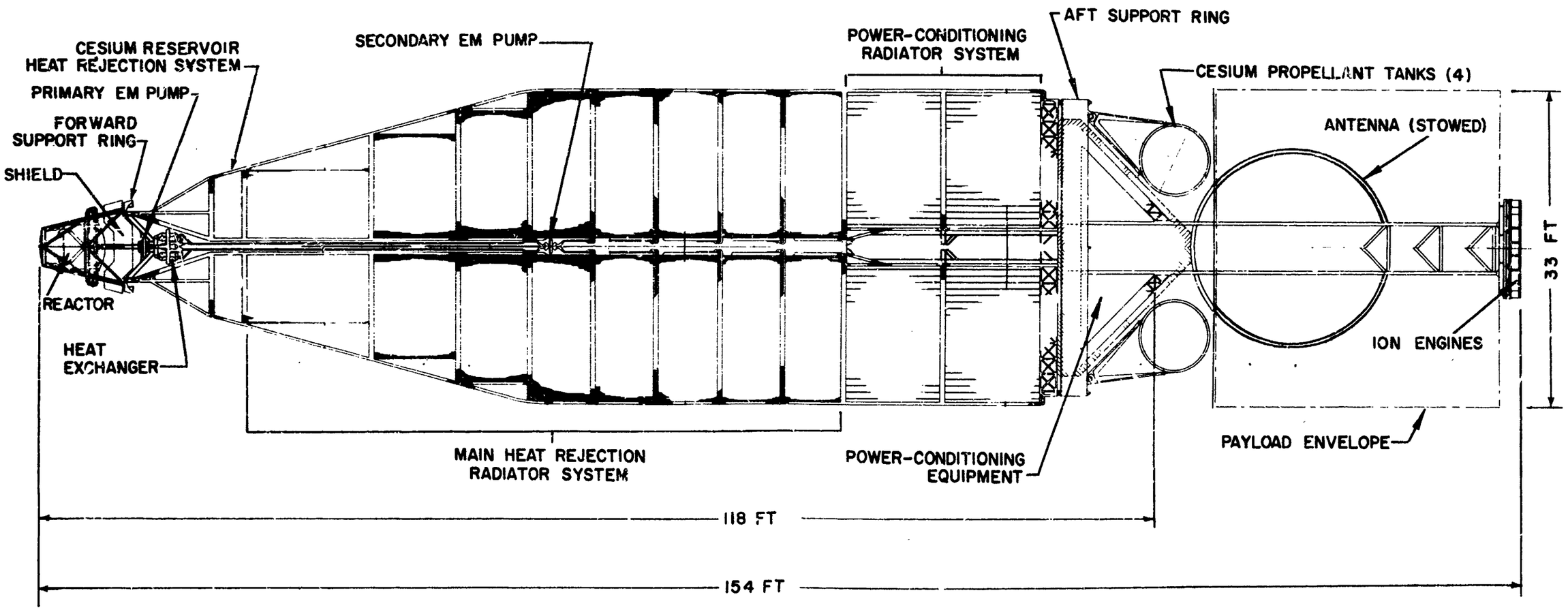

Figure 3 Powerplant Inflight Arrangement

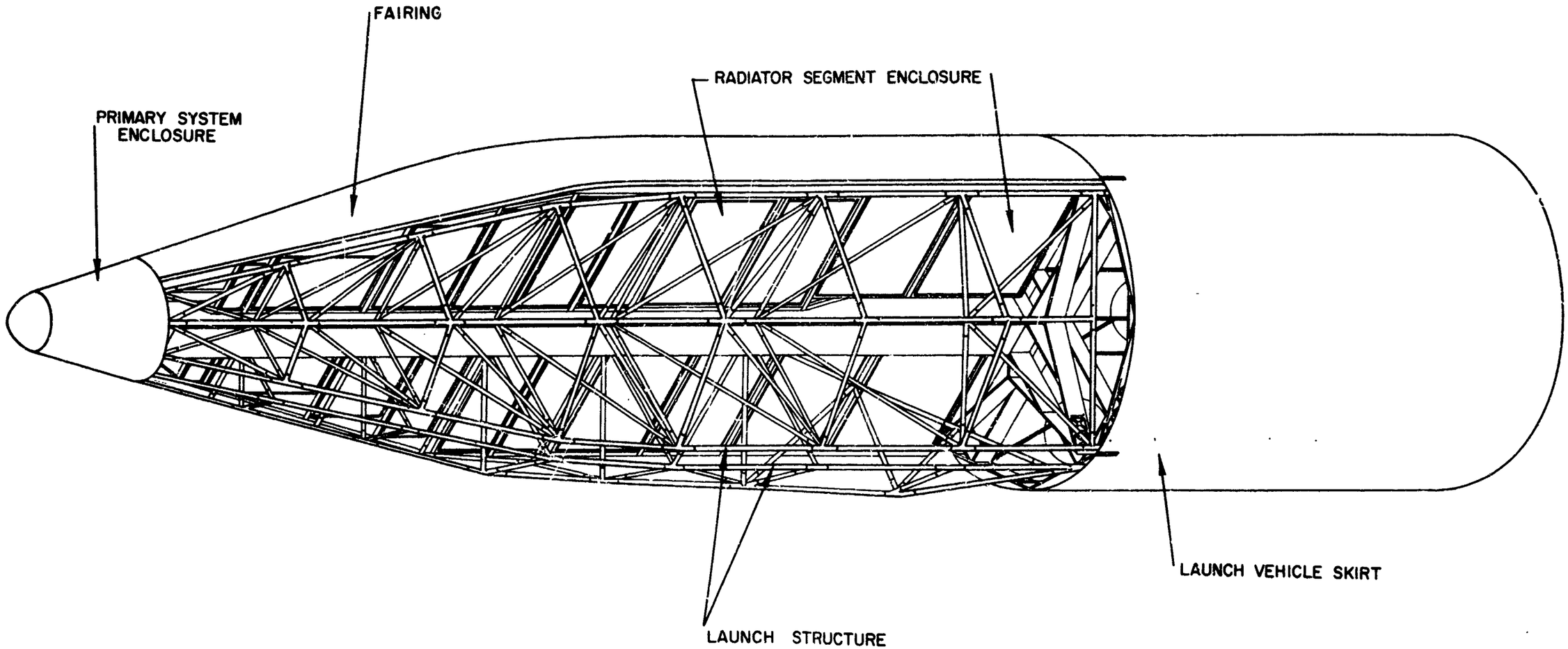

Figure 4 Powerplant Launch Configuration

behind the shield to protect these components from nuclear radiation. The reactor and shield are supported by a truss-type structure which supports these components for both axial and side loads. This structure is attached to the powerplant structure by the forward support ring, and to the reactor by a cylindrical skirt which extends from the top of the reactor, and which is designed to sustain the difference in thermal expansion between the reactor and the structure. Two large-diameter primary pipes extend downward from the reactor and terminate behind the shield in two toroidal manifolds. These manifolds encompass the heat exchanger assembly and are supported by a cruciform structure to remove their weight from the reactor pressure vessel. The cruciform structure which is a part of the forward support ring assembly also supports the primary and cesium reservoir coolant pumps.

The secondary subsystem which comprises the major portion of the powerplant volume is also located behind the shield. Sixteen heat exchangers grouped in a cylindrical cluster are supported by the toroidal inlet manifold and are allowed to expand thermally by the looped piping which connects them to the toroidal outlet manifold. Placing the heat exchangers directly behind the shield is an optimum location since it results in a minimum total weight for both primary and secondary piping. The main radiator, which consists of sixteen separate rectangular segments, is arranged in a plane which determines the overall geometry of the powerplant. Different rectangular shapes for the segments were employed to make as efficient use as possible of the area available in the payload envelope. The various shapes do not affect system weight. Support of the radiators is accomplished by an open-lattice framework which surrounds each of the segments and transmits their loads to the forward support ring. The framework is attached to a central support structure which runs the length of the powerplant along its axis and connects the fore and aft support rings. The cesium reservoir coolant radiator consists of two panels which are located just forward of the main radiator.

The auxiliary subsystem consists of four power-conditioning packages, each with its own coolant system comprised of a pump and a radiator. The radiators are located in the same framework and to the rear of the main radiator. Support of the power-conditioning modules located behind the radiators is afforded by cross-bracing to the aft support ring.

A propulsion system consisting of 55 cesium-ion engines and four propellant tanks is included to show a possible arrangement for the space vehicle. The cesium-ion engines are grouped in a cylindrical array at the rear of the vehicle and are supported by the central support structure. The four propellant tanks are supported at the lower support ring and are located 90 degrees apart about the central axis of the vehicle. Two antennas mounted on telescoping supports are included with the vehicle to provide for communications.

The inflight support structure for the vehicle, shown in Figure 3, consists of a central support column, fore-and-aft support rings, and two framework structures for the radiators. All structural members are constructed of open-lattice titanium beams for light weight. The forward support ring located directly behind the nuclear shield forms the base for the framework which supports both the reactor and the shield. Contained within the diameter of the ring is a beam which supports the heat exchanger assembly, the primary piping and the primary pump. Also contained within the ring are two beams located as chords on either side of and parallel to the diametric beam. These beams aid in supporting the heat exchanger assembly and serve as the connecting members between the forward support ring and the radiator framework supports. The two support structures for the radiators are located symmetrically about the central support column and are divided into ten frames in which are contained the main radiator and auxiliary radiator segments: eight main and two auxiliary segments on each side of the central column. The radiator structures are attached along their entire length to the central column which connects the fore-and-aft support rings and adds rigidity to the entire vehicle structure in a direction perpendicular to the plane of the radiators. The central support column is connected to the lower ring through a cruciform structure which is attached through four expansion joints to an octagonal structure contained within the aft ring (see Figure 1). The purpose of the expansion joints is to allow for thermal expansion of liquid metal components and inflight structure relative to the launch structure. The octagonal structure is cross-braced in its interior to support the power-conditioning equipment. The cross-bracing also serves as the connection between the aft end of the radiator structures and the aft support ring. Four cesium propellant tanks located 90 degrees apart and two communications antennas are also supported from the aft support ring. The central support column protrudes through the aft ring and runs to the rear of the vehicle where it attaches to the support structure for the cesium ion engines. Support of payload packages located be-

tween the aft ring and the ion engines can be obtained by attaching them to the central column.

2. Launch Configuration

The launch configuration of the powerplant shown in Figures 4 and 5 consists of the inflight configuration with the addition of the launch structure, the aerodynamic fairing and the inert gas enclosures. These components are required to protect the vehicle from the rigors of a launch from earth. The launch structure is designed to support the entire weight of the powerplant under launch acceleration and vibration loads. Data for the Saturn 1 used in the calculations gave steady loads of 12G axial and 5G side. The data used for noise and vibration loads are given in Figures 3 and 5 in PWA-2224, Appendix A.

The launch structure shown in Figure 5 is divided into four quadrants, each quadrant forming a trussed column between the fore-and-aft support rings. The quadrants are constructed of four vertical titanium columns trussed at given intervals to prevent buckling. Shear webs are used to connect the quadrants into a single structural unit of high rigidity. Components loads from the primary and secondary subsystems and the auxiliary radiators are transmitted to the forward support ring, then down through the trussed columns into the aft support ring, thence to a cylindrical skirt which extends from the launch vehicle. Loads due to the power-conditioning equipment and the propellant tanks are taken at the aft ring by bracing, while loads due to ion engines and payload packages are transmitted to the aft ring through the extension of the central support column.

Inert gas enclosures are used in the powerplant to protect all columbium - 1 zirconium alloy components from oxidation during the preheat period prior to launch. The primary system is contained within the nose-cone section of the fairing which joins with a cylindrical enclosure around the heat exchanger cluster. The latter enclosure joins with a container which encompasses the central support column, within which are contained the secondary system piping and EM pump. Individual enclosures are employed for each of the main radiator segments. All enclosures are interconnected to allow for a continuous flow of gas during the air evacuation and gas purge cycles prior to filling the system with liquid metal. Disposal of the enclosures occurs in space during the powerplant startup procedures.

The aerodynamic fairing which encompasses the vehicle is a titanium sandwich consisting of a thin sheet on either side of a corregated

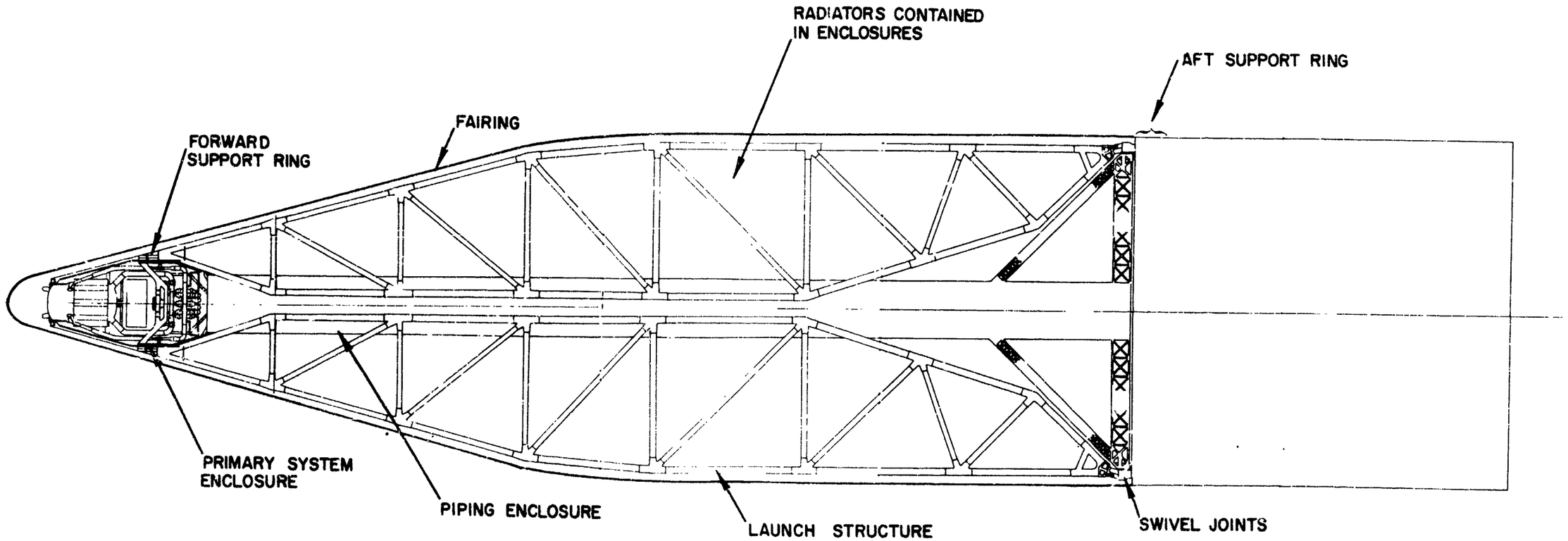

Figure 5 Powerplant Launch Arrangement

sheet. This construction produces a highly rigid fairing. The fairing is separated into two separate sections. The nose-cone section serves not only to protect the vehicle from aerodynamic loads but also as a disposable inert gas enclosure for the primary system. This section is separated from the vehicle at a joint which connects it to the heat exchanger cluster container. The second section of the fairing covering the remaining portion of the vehicle is supported locally by the launch structure and is separated from the vehicle in four parts (see Figure 28). This section mates with the cylindrical skirt extending from the launch vehicle.

C. Component Design

The components of the powerplant system include the thermionic-reactor fuel elements, reactor, reactor shield, high-temperature main radiator, low-temperature auxiliary radiators, heat exchangers, electromagnetic pumps, busbars, and the power-conditioning equipment. The optimization of many of the system parameters is shown graphically in Report PWA-2319, the previous report under this contract. The design parameters for each of the components are given in Table 1.

TABLE 1

Parameters for 3.25 MW Nuclear Thermionic Space Powerplant

Reactor	Units	
thermal power	MW	33.4
gross electric power	MW(e)	3.99
reactor output voltage	volts	218
number of fuel elements	-	2185
average fuel burnup	MWD/ton	10,050
maximum fuel burnup	MWD/ton	11,750
initial critical UC loading	kg	1210
UC loading for temperature effect	kg	9.2
UC loading for burnup	kg	31.4
temperature coefficient of reactivity	$\Delta K/K/°F$	-2.68×10^{-6}
mean fission energy	Mev	.337
nvt core center	neutrons/cm^2	3.26×10^{22}
fuel element power output	watts	1824
fuel element voltage output	volts	11.5
fuel elements per fuel assembly (series connection)	-	19

number of converters in reactor	-	34,960
number of fuel assemblies (parallel connection)	-	115
fuel assembly power output	KW(e)	34.6
fuel assembly voltage output	volts	218
reactor fuel (average composition)	mole fraction	$UC_{.25}ZrC_{.75}$
maximum centerline fuel temperature	°F	3400
core diameter (effective)	inches	38.8
core L/D	-	0.93
coolant volume fraction	-	0.093
reflector material	-	BeO
reflector thickness	inches	2.0
reactor coolant	-	lithium 7
coolant flow rate	lbs/sec	70.0
core pressure drop	psi	1.53
coolant inlet temperature	°F	1566
coolant exit temperature	°F	1945
cesium reservoir coolant	-	lithium 7
cesium coolant flow rate	lbs/sec	1.1
cesium coolant inlet temperature	°F	656
cesium coolant exit temperature	°F	676
pressure vessel and piping material	-	Cb-1Zr
total primary piping pressure drop	psi	2.79
primary piping inside diameter	inches	7.0
primary piping wall thickness	inches	0.199

Fuel Element

converters per fuel element	-	16
average converter power output	watts	114
average converter voltage	volts	0.718
average converter power density	watts/cm^2	4.42
average converter efficiency	%	12.1
fuel outside diameter	inches	0.588
cathode material	-	W-25Re
cathode thickness	inches	0.025
maximum operating cathode temperature	°F	3200
interelectrode gap	inches	0.020
anode material	-	Cb-1Zr
anode thickness	inches	0.031
average anode temperature	°F	1780
insulator material	-	BeO
insulator thickness	inches	0.010

cladding material	-	Cb-1Zr
cladding thickness	inches	0.020
converter length	inches	2.0
cathode lead L/A	in/in^2	15.0
axial converter spacing	inches	0.5
fuel element outside diameter	inches	0.80
fuel element pitch/diameter ratio	-	1.0

Shield

materials	-	C, Li^7H
graphite (C) thickness	inches	8
Li^7H thickness	inches	19.6
dose at power-conditioning equipment		
fast neutrons	nvt, rem	10^{13}, $4x10^5$
gammas	rads	10^7

Main Radiator

radiator material	-	Cb-1Zr
radiator fluid	-	lithium 7
number of segments	-	16
heat rejection per segment	Btu/hr	$5.85x10^6$
radiator area per segment (projected-one side)	ft^2	87.7
emissivity	-	0.9
mean effective radiator temperature	°F	1659
radiator inlet temperature	°F	1929
radiator exit temperature	°F	1437
lithium flow rate per segment	lbs/sec	3.41
tube pressure drop	psi	3.78
manifold pressure drop (1 manifold)	psi	0.76
average piping pressure drop (1 pipe)	psi	2.30
number of tubes per segment	-	120
average radiator tube length	inches	83.3
tube inside diameter	inches	0.148
tube wall thickness (including meteoroid barrier)	inches	0.120
fin width	inches	0.44
fin thickness	inches	0.029
fin efficiency	%	70.1
average manifold length	inches	152
manifold inside diameter	inches	1.5
manifold wall thickness (including meteoroid barrier)	inches	0.140

average pipe length	feet	40
piping inside diameter	inches	1.45
piping wall thickness (including meteoroid barrier)	inches	0.140

Heat Exchanger

type	-	tube-shell
heat exchanger material	-	Cb-1Zr
heat exchanger fluids	-	Li-Li
number of heat exchangers	-	16
primary fluid inlet temperature	°F	1945
primary fluid outlet temperature	°F	1566
secondary fluid inlet temperature	°F	1437
secondary fluid outlet temperature	°F	1929
log mean temperature difference	°F	54.3
primary fluid flow rate (tubeside)	lbs/sec	4.38
primary fluid pressure drop	psi	0.28
secondary fluid flow rate (shell side)	lbs/sec	3.41
secondary fluid pressure drop	psi	0.75
number of tubes per exchanger	-	897
tube inside diameter	inches	0.10
tube wall thickness	inches	0.020
tube length	inches	15.0
tube pitch-to-diameter ratio	-	1.1
shell inside diameter	inches	4.85
shell wall thickness (including meteoroid barrier)	inches	0.140
shell length	inches	20

Auxiliary Radiator

radiator material	-	aluminum
radiator fluid	-	monoisopropylbiphenyl
number of segments	-	4
radiator inlet temperature	°F	500
radiator coolant temperature drop	°F	83.5
radiator mean effective temperature	°F	447
radiator area (projected-one side)	ft^2	552
fin efficiency	%	63.5
average radiator tube length	inches	118
tube inside diameter	inches	0.133
tube wall thickness (including meteoroid barrier)	inches	0.302

average manifold length	inches	169
manifold inlet diameter	inches	0.704
manifold wall thickness (including meteoroid barrier)	inches	0.322
fin width	inches	3.30
fin thickness	inches	0.030
number of tubes per segment	-	23
tube pressure drop	psi	14.0
manifold pressure drop	psi	2.80
radiator coolant flow rate per segment	lbs/sec	1.17

Cesium Reservoir Coolant Radiator

radiator material	-	Cb-1Zr
radiator fluid	-	lithium 7
number of panels	-	2
inlet temperature	°F	676
coolant temperature drop	°F	20
area (projected-one side)	ft^2	19.3
fin efficiency	%	70.1
average radiator tube length	inches	83.3
tube inside diameter	inches	0.148
tube wall thickness (including meteoroid barrier)	inches	0.179
piping inside diameter	inches	1.0
pipe wall thickness	inches	0.199
fin width	inches	0.44
fin thickness	inches	0.020
number of tubes per panel	-	12
coolant flow	lbs/sec	1.1

Main Busbar

material	-	copper
length	ft	100
number of busbars	-	4
cross-sectional area/busbar	in^2	2.15
surface temperature	°F	1000

Pump Busbar

material	ft	copper
length	ft	100
cross-sectional area	in^2	3.01
surface temperature	°F	1000

1. Primary Subsystem

a. Fuel Element

The design features of the thermionic-reactor fuel element are illustrated in Figure 6. The design reflects compromises made between two conflicting goals, 1) attainment of a minimum system specific weight, and 2) achievement of a practical and reliable piece of hardware. System parametric studies (Report PWA-2319) were conducted to determine system performance when component parameters were varied. During these analytical studies, many of the parameters of the reactor fuel element were optimized in order to define the value of each parameter that would result in minimum system weight. However, as design studies progressed, off-optimum values of the parameters had to be selected in most instances to achieve a fuel-element design believed to represent a reasonable engineering approach.

During the initial phase of the design studies, available test data on fuel properties such as fission product gas release rate, burnup limits, swelling, thermal conductivity, thermal expansion coefficient and compatibility were examined. Refractory metal and electrical insulator properties were also reviewed as well as current fabrication techniques. Preliminary design assumptions were based on the available data. The effects of fission product gas contamination of the cesium plasma are unknown. The preliminary design assumptions were made in the direction of conservative engineering practice to develop a design that would indicate the areas of major technical uncertainty needing engineering test data. These assumptions pertained to the use of UC-ZrC fuel, the separation of fission-product gases from the cesium plasma, the use of a refractory metal cathode (fuel cladding) to reduce fuel evaporation and alleviate problems involving fuel cracking, swelling and fission-product contamination of the cesium plasma, and venting of the fission products to space in order to reduce the pressure stress in the fuel cladding. Such reactor concepts as allowing the fission-product gases to mix with the cesium plasma and removing them by the use of a cesium-vapor flush (a continuous process), containment of the fission-product gases in the fuel cladding, electron emission directly from the surface of the fuel, and the use of other fuel materials and other fuel-element configurations are possible

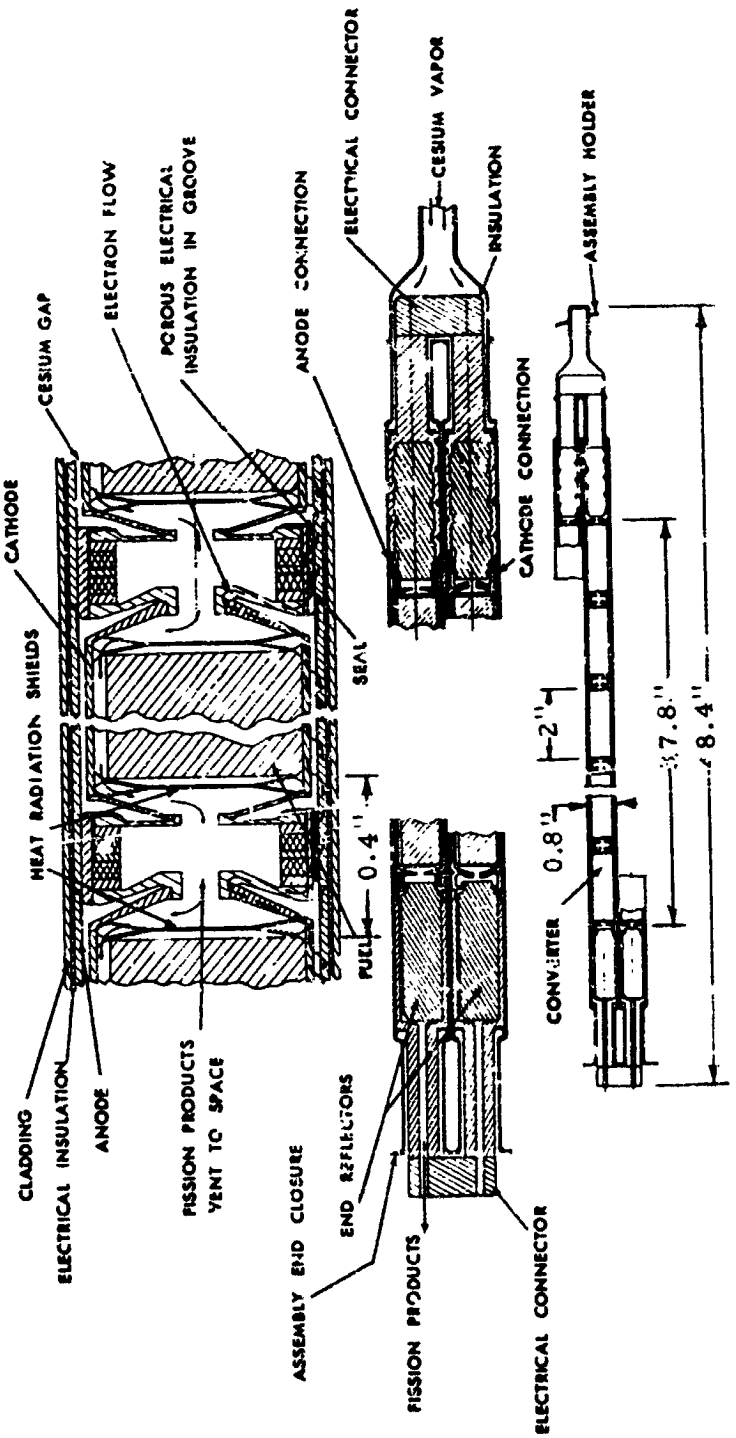

Figure 6 Thermionic Fuel Element

alternates to the preliminary design approach used in this study. These alternate concepts have been the subject of a preliminary examination to determine the unique features of their design and performance. Appendix K of Report PWA-2224 presents the results of a study of a flat-plate element, an internally-cooled element and a cesium-flushed element. Appendix 7 of this report presents the additional study conducted for a fission-gas-contained element.

The thermionic-reactor fuel element shown in Figure 6 was designed to operate in a fast neutron spectrum and in a liquid-lithium environment at temperatures up to 2000°F for 20,000 effective-full-power hours during a total lifetime of 24,000 hours. The element is 0.8 inch in diameter and 48.4 inches in overall length. Each fuel element contains sixteen axially-stacked 2-inch long, cylindrical, cesiated, thermionic converters, with a BeO reflector pellet at each end of the element. The converters are electrically insulated from the liquid lithium coolant of the reactor by a high-density BeO coating on the outside surfaces of the anodes. The coating is protected from the reactor coolant by an outer cladding of columbium alloy.

In the reactor the fuel elements are grouped into nineteen element assemblies and are supported by their upper end enclosures which are joined to a single assembly support plenum. Extending from this plenum is an assembly support stem which houses the cesium reservoir for a complete assembly in its tip. The stem protrudes through the core support plate above which flows a second lithium coolant which controls the pressure of the cesium vapor emanating from the reservoir. The cesium vapor flows down through the assembly support stem and plenum and through the elements in parallel. The vapor permeates the interelectrode spaces in the converters and is isolated from the fission gases by the cathode, the cathode support assemblies and the graded ceramic seal. All of the elements of each assembly are connected structurally at their lower ends by a single enclosure. The elements are connected electrically by Cb-1Zr busbars which are contained within the upper and lower enclosures. Fission gases flow within the cathodes from the uppermost converter in each element down through the following converters and are collected in the lower enclosure. The gases then flow out of the reactor through channels contained in the electrical busbars.

The discussion which immediately follows considers the main design features of the converters, the neutron reflectors and fuel-element end leads, and the element cladding and end enclosures.

1) Converter

Each of the sixteen converters in a fuel element consists of a fuel pellet clad with a thin-walled cylinder (cathode), a thin-walled, cylindrical anode positioned around the cathode, seals, heat-radiation shields, and electrical insulation. An inter-electrode gap is maintained between the cathode and anode by the cathode-to-anode support and the cathode-to-anode electrical lead. The support is located on one end of the cathode and the lead on the opposite end. A graded ceramic seal is positioned between the lead in one converter and the cathode-to-anode support in an adjacent converter, thus insulating adjacent cathodes electrically and sealing fission gases from the cesium vapor. The maximum operating temperature for the cathode is 3200°F, the maximum centerline fuel temperature is 3400°F, the average anode temperature is 1780°F, and the average cesium pressure is 5.3 mm Hg. At these conditions, each converter will produce 114 watts at 0.72 volt and each fuel element will produce 1824 watts at 11.5 volts. A cylindrical converter configuration was chosen on the basis of overall thermionic efficiency, dimensional stability, mechanical integrity, and applicability to reactor configurations. The size of the converters was based on results obtained in the parametric study of this powerplant (Report PWA-2319). The number of converters per fuel element was determined by the required power output of the reactor and the geometry and size of the core. The connection of converters and fuel elements in series was dictated by the voltage output of the individual converters and the required reactor output voltage. It was assumed that the cesium vapor should be separated from fission-gas products in order to prevent contamination in the interelectrode space and consequent decrease in thermionic performance. All passageways for fission gases within the fuel elements were designed to be as large as possible, in an attempt to lessen any susceptibility to clogging by condensable products. However, clogging remains as a potential problem which should be verified experimen-

tally. The supply of cesium vapor to an assembly of fuel elements was chosen on the basis of 1) mechanical simplicity in the method of delivering high-purity cesium to the fuel elements, 2) reliability, and 3) the use of the cesium-reservoir housing as a support for the fuel elements. The cathode-support geometry was so selected as to provide a support that would be mechanically rigid in the radial direction, thus maintaining the interelectrode cesium gap during thermal cycling, and yet having sufficient flexibility in the axial direction to permit thermal expansion at acceptable stress levels. A detailed discussion of the various components of an individual converter assembly, as evolved in the design studies, follows:

2) Cathode

The cathode assembly consists of a cylindrical UC-ZrC fuel pellet, 0.588 inch in diameter, 2 inches in length, and clad with a 0.025-inch thick W-25 Re tube. The diameter of the fuel pellet, the converter length, and the cathode-tube wall thicknesses were determined from system parametric studies and practical engineering considerations.

Thermal and structural analyses described in Report PWA-2224 were conducted for the fuel element designed for the one-megawatt powerplant. Since the element used in this study is very similar, the results of those studies apply here. Based on those studies, thermal stresses in the cathode at operating temperatures should be acceptable.

The carbide fuel [1], although a good thermionic emitter, was designed to be clad with a refractory metal to retain fission gases within the cathode and to provide a metallic electrical conductor. The choice of a W-25 Re cladding was based on fabrication considerations, low evaporation rate, high recrystallization temperature, and fuel compatibility (see Appendix B of Report PWA-2224 and Appendix 8 of this

[1] General Atomics Division, Investigations of Carbides as Cathodes for Thermionic Space Reactors, Final Report, GA-4769, NAS 3-2532

report). It was assumed that this alloy would have the same thermionic performance as tungsten. Circular heat shields were located at both ends of the fuel pellet to reduce radiant heat loss from the end surfaces of the fuel. The maximum centerline fuel temperature is 3400°F for a selected maximum operating cathode temperature of 3200°F.

To minimize the temperature difference across the fuel, the cladding requires good thermal contact with the outside surface of the fuel. An axial slot located on the outside surface of the fuel pellet and around the periphery of the thermal radiation shields allows fission gases to flow within the cathodes from one converter to the next. The axial slot is located on the outside surface of the fuel pellet rather than at the center because of the lower rate of fuel evaporation at the lower temperature outside surface.

A uranium-monocarbide, refractory-metal-carbide, solid-solution alloy was chosen on the basis of the available data on thermionic-reactor fuels (Appendix B of Report PWA-2224 and Appendix 8 of this report). For the preliminary design, ZrC was chosen as the refractory carbide due to its low evaporation rate and density. By alloying UC with ZrC the fuel density is sharply decreased and the fuel melting point is raised significantly. In addition, the ZrC forms a stable carbide by preventing carbide reduction of refractory cathodes[1]. Other refractory metal carbides, such as TaC. form solid solutions with uranium monocarbides. However, their high densitites and a lack of materials data led to a design choice of ZrC. For the fuel compositions listed in Table 3, p. 69, fuel evaporation rate at a cathode temperature of 3200°F should be less than 5 mils per year.

[1] **General Atomics Division, Investigations of Carbides as Cathodes for Thermionic Space Reactors, Final Report, GA-4769, NAS 3-2532**

The higher thermal expansion coefficient of the fuel, compared to that of the cathode tube, will result in good thermal bond, and will tend to reduce the evaporation of the fuel. A radial gap of approximately 2 mils between fuel and cathode under cold conditions should close when operating temperatures are reached. Thermal conductivity data are available at the maximum fuel temperature of 3400°F[1], and a value of 9.5 Btu/hr ft °F has been used. The carbide fuels have good thermal stress integrity at the required power densities and thermal gradients. It is assumed that there will be no fission product retention in the fuel at operating conditions. Fission product condensables will plate out on the cathode support structure, and noncondensables will be vented to space.

The possible difficulties of fuel evaporation, cracking, swelling, and fission-product contamination of the cesium plasma caused a design decision against a carbide cathode and in favor of canning the fuel with a metallic cathode tube. A tungsten-rhenium alloy was chosen for the cathode tube because it had the following desirable properties:

1) low evaporation rate,
2) good thermionic emission qualities,
3) acceptable electrical resistivity,
4) low thermal emittance,
5) high work function,
6) acceptable thermal conductivity,
7) low thermal expansion for good fuel-cathode thermal bonding,

[1] LAMS 2433, Quarterly Status Report of the LASL Plasma Thermocouple Development Program for Period Ending March 20, 1960

8) acceptable cathode fabrication and welding to thermionic-converter leads,
9) acceptable strength, and
10) high recrystallization temperature.

Refractory materials other than tungsten and rhenium were considered for the cathode-tube application. However, all except tantalum were eliminated because of their unsatisfactory evaporation rates, fuel compatibilities, and/or strength characteristics. Although tantalum is workable and ductile at room temperatures, it was rejected for two reasons, 1) its inferior emission characteristics would result in a greater system weight than if tungsten were used, and 2) the rate of diffusivity of zirconium and uranium atoms through tantalum would be higher. It was estimated that Zr and U atoms would diffuse through Ta at the rate of 300μ/50 hours and would contaminate the cathode emission surface.

The tungsten-rhenium alloy (W-25 Re) was considered to be superior to tungsten for the cathode-tube application because of the high brittle-ductile transition temperature (400-600°F) of tungsten, which makes it difficult to fabricate. W-25 Re alloy has room temperature ductility and has been fabricated successfully[1]. However, compatibility with the fuel needs documentation.

3) Anode

The anode is a Cb-1Zr tube. 0.740 inch in outside diameter, 0.031 inch in thickness, 2.3 inches in length, and is positioned around the cathode with a 0.020-inch cathode-to-anode gap maintained by the cathode support and cathode-to-anode lead. The average anode temperature corresponding to minimum system specific weight was calculated to be 1730°F. A cathode-to-anode gap of 0.020 inch is thought to be feasible for a practical thermionic converter at the present

[1]Sims, C.T. and R.I. Jaffee, Properties of Refractory Alloys Containing Rhenium, Trans. of AIME. Soc. for Metals, Vol. 52, 1960, p. 929

time. Cb-1Zr was chosen as the anode material because its compatibility with cesium (see Appendix 8) and because it has a coefficient of thermal expansion approximately equal to that of BeO. Nickel was considered for the anode application because it has a lower electrical resistivity than columbium. Calculations (Appendix B of Report PWA-2224) showed that the system specific weight of a reactor using nickel anodes is less than that of a reactor utilizing columbium anodes. However, these favorable aspects of nickel were offset by the fact that the coefficient of expansion for nickel is much greater than that of either columbium or BeO, so that, for the present converter design, a nickel anode would cause a higher stress in the weld between the cathode support and the anode. Failure of this weld is extremely serious since it constitutes an open circuit in the series-connected converters and would, therefore, result in a disruption in the power output of all the converters in series with the failed converter. Other materials were considered for the anode application as discussed in Appendix B of Report PWA-2224.

4) Cathode-To-Anode Lead and Cathode Support

The purpose of the cathode-to-anode lead is to provide an electrical connection between the cathode of one converter and the anode of an adjacent converter. The lead, which is composed of two discs, provides support for the cathode in the axial and radial directions, and maintains the cathode-to-anode gap and the concentricity of the cathode within the [illegible]. A study of the effects of operation with an eccentric cathode is included in Appendix C of Report PWA-2224.

The dimensions of the lead were based upon an optimum value of 15 in/in^2 for the ratio of lead length to area (L/A ratio), as determined by the system studies. This optimum value was based on minimum system specific weight and was arrived at by minimizing the total power loss in the lead, such loss being the sum of the thermal-conduction and electrical-power losses. The type of lead selected for the application under discussion not only satisfies the optimum L/A ratio value, but also provides adequate support for the cathode. Structural studies (Appendix A of Report PWA-2224)

indicate that although the stresses in the lead are in excess of the yield strengths of the materials of which it is comprised, the lead should be capable of yielding plastically for about 100 thermal cycles.

The cathode support, which is located at the end of the cathode opposite to the lead end, mates with and is insulated from the cathode-to-anode lead of an adjacent converter. The support has a much smaller L/A ratio value than does the lead. It is constructed of a flat disc and a conical disc. This construction makes it more flexible in the axial direction than the lead and allows the support to accommodate thermal expansion of the cathode. The small cross-sectional area of the support not only contributes to the axial flexibility of the cathode, but also reduces heat loss by thermal conduction from the cathode to the anode. As was mentioned previously, the optimum value of the L/A ratio for the cathode lead was calculated on the basis of minimum system specific weight. The optimum value of L/A ratio for the support was based on stress considerations.

One of the two discs comprising the cathode-to-anode lead and one of the two comprising the cathode support are constructed of W-25 Re; the other two discs are of tantalum. Each of the W-25 Re discs is welded at its larger diameter to the W-25 Re cathode and is welded to the tantalum disc at the hole in the center of the disc. The tantalum disc of the cathode lead is welded at its larger diameter to the Cb-1Zr anode of the adjacent converter, thereby providing a series connection between two adjacent converters. The flat tantalum disc of the adjacent converter support is welded to the other Cb-1Zr face of the same seal and is insulated with a 5-mil layer of Al_2O_3 from the cylinder surrounding the seal. The Al_2O_3 in the seal and this layer insulates adjacent cathodes electrically. The lead and the cathode support are bimetallic to match radial expansions of the cathode and anode and thus reduce thermal stresses. Tantalum was chosen as the intermediate metal because of its high ductility and desired thermal expansion properties. The outside diameter of the Cb-1Zr cylinder surrounding the seal contains porous ceramic-filled slots, to reduce electrical leakage between converters through the cesium vapor. An analysis of this leakage problem is given in Appendix D of Report PWA-2224.

5) Electrical Insulators

A high-density coating of BeO covers the outside of all the converters in a fuel element. This coating electrically insulates the anode of adjacent converters and separates the anodes of the converters from the liquid-metal coolant and fuel-element cladding.

The general properties required of the electrical insulation include:

1) high electrical resistivity ($>10^6$ ohm-cm) and adequate thermal conductivity,
2) adequate dielectric strength (imposed voltage is 550 volts maximum)
3) low vaporization rate and outgassing,
4) structural and chemical compatibility with anode, cladding, cesium, fission gases, elements and leads, and cathode supports,
5) high resistance to change in electrical properties with time in a cesium environment,
6) controllability of purity and porosity,
7) close-tolerance controllability of coating thicknesses over large areas, and
8) stability in a high-temperature irradiation environment.

Compared to the oxides, the nitrides have a higher volatility and are more difficult to sinter[1]. The stable carbides have poor electrical insulating properties. The higher melting point nitrides have relatively poor thermal conductivities. Relatively little is known about the electrical insulating properties of the nitrides. Oxide insulators were chosen because they are more stable. However, future data on the high temperature (1800-2000°F) electrical insulating properties of the nitrides may change the choice. Vaporization stability at high-temperature limits the oxide insulator materials to ThO_2, BeO, ZrO_2, and Al_2O_3. ZrO_2 has poor electrical insulating properties at high temperatures (2000°F). ThO_2 is the most stable oxide and has the lowest vaporization rate. However, it has the disadvantage of low thermal

[1]Campbell, I. E., High-Temperature Technology, John Wiley & Sons, Inc., 1956, Chapters 3 and 8

conductivity and of conversion of thorium to U-233, with subsequent fissioning. Ideally, BeO is the best insulator, due to its high thermal conductivity, electrical resistivity, and dielectric strength. At room temperatures, BeO is superior to Al_2O_3 with respect to these properties. Also, BeO has a greater chemical and vaporization stability than Al_2O_3. However, its toxicity requires special consideration during the process of applying BeO insulator coatings.

The greatest lack of electrical data is for breakdown voltages of the oxides in a cesium atmosphere at high temperatures. Data in the literature gives 380 volts per mil breakdown voltage for 99 per cent dense Al_2O_3 at room temperature. At a temperature of 1400°F, the breakdown voltage for Al_2O_3 is approximately 10 per cent of the value at room temperature. BeO has twice the dielectric strength of Al_2O_3 at room temperature, no data being available for high temperatures. The thermal conductivity of BeO is 4 or 5 times greater than that of Al_2O_3. Based on the available data and insulator requirements, BeO was chosen as the high-voltage insulator. Knowledge of the irradiation-stability characteristics of BeO is limited. Reference 1 indicates that BeO specimens remain intact when irradiated with 10^{21} fast neutrons per cm^2 at 1400°F, and helium produced by irradiation was retained in the BeO up to 1900°F. Low density BeO specimens were irradiated up to a fast neutron (1 Mev) dose of 2.9×10^{21} n/cm^2, whereas the dose of high-density BeO was a maximum of 5×10^{20} n/cm^2. Low density specimens, irradiated at 1350-1750°F at a dose of 2.1 to 2.6×10^{21} fast n/cm^2 fractured. A crack was observed in only one capsule of the high-density material which was irradiated to 4.5×10^{20} nvt. According to available data it is not possible to determine whether high-density BeO resists radiation better than low-density BeO, since the two kinds of specimens were subjected to different ranges of radiation dose. Reference 2 also gives some irradiation data for BeO. The effects of neutron irra-

[1]Shields, R., Lee, J., Effects of Fast-Neutron Irradiation and High Temperature on Beryllium Oxide, ORNL-3164

[2]General Electric, Second Annual Report, High Temperature Materials and Reactor Component Development Programs, Vol I. GEMP-177A

diation on the dimensions and thermal conductivity of BeO are shown in Figures 13 and 14 of Appendix 8 of this report. For the preliminary design, the maximum BeO temperature is 2000°F, and the integrated fast neutron (1 Mev) dosage (nvt) is approximately 3.26×10^{22} n/cm^2. Therefore, electrical shorts due to BeO insulator fractures may be a problem. At high irradiation levels, the thermal conductivity of BeO decreases 50-100 per cent and its greatest life capabilities are in the 1400-1900°F range.

The graded ceramic seal that insulates the cathodes of adjacent converters is a cylindrical body having pure Cb-1Zr at both axial ends of the cylinder, pure Al_2O_3 at the center, and graded Cb-Al_2O_3 mixtures in between. Cb-1Zr was chosen for the areas indicated in order to match the thermal expansion properties of the seal and anode materials. A structural analysis of the seal is included in Appendix A of Report PWA-2224.

6) Neutron Reflector and Fuel-Element End Leads

The cylindrical BeO reflector pellets positioned at each end of the fuel elements serve as neutron reflectors for the assembled core. A reflector should have the following properties, 1) high efficiency in reflecting high-energy neutrons from the core, 2) low density, 3) stability at high values of temperature and irradiation, 4) good thermal conductivity, and 5) compatibility with the element end leads and fission products. Consideration of data for Items 1, 2, and 4 led to the choice of a beryllium compound, such as BeO, Be_2C, or an intermetallic beryllide. Data available for Items 3 and 5 leads to BeO as the initial design choice (See Appendix 8). The pellet at the upper end of the fuel element is 0.680 inch in diameter, 2 inches in length, and is clad with Cb-1Zr 0.090 inch thick which serves as an electrical lead. The cladding is welded at one end to the anode or to the cathode support of the end converters, depending on the type of electrical connection required. At the other end of the reflector-pellet cladding, a smaller diameter Cb-1Zr tube protrudes. Fuel elements are connected to each other electrically by a tubular Cb-1Zr bus-bar which is welded to the reflector-cladding protrusions.

Fission gases from the fuel flow through the lower BeO reflector pellet and into the lower assembly enclosure via a flat on the outside surface of the reflector pellet.

The reflector at the top of the fuel element has a spiral groove cut into the outside surface of the Cb-1Zr cladding around the BeO pellet. The groove is coated with high-density BeO to insulate the cladding from the cesium, and is filled with a porous ceramic to provide a path of high electrical resistance for cesium to flow between the cesium reservoir and the converters. A highly resistive path is required because of the high voltage buildup in the series-connected converters, which can cause an electrical breakdown through the cesium between the converters and the cesium reservoir. This problem is analogous to the problem of current loss between converters, but is much more severe due to the high voltage.

A voltage buildup of 550 volts at open-circuit results from the series connection of fuel elements. This voltage existing in busbars raises the problem of breakdown to the enclosure. Therefore, the element-connecting busbars are coated with high-density BeO to prevent electrical breakdown between the busbars and the enclosure assemblies.

The busbars connecting the fuel elements are 0.56 inch in diameter and were sized to yield a minimum weight. A heat transfer analysis indicates that busbar temperature should not exceed 2200°F. The total power loss in the reactor for all end leads is less than 1 per cent of the total reactor power output.

7) Element Cladding and End Enclosures

A 20-mil thick Cb-1Zr cladding is located over the BeO insulation to protect the converters from the reactor coolant. A 20-mil cladding is required to give the element structural integrity. Firm contact must be maintained between the anodes of the converter, the BeO insulation, and the Cb-1Zr cladding throughout operation, since heat conduction through this trilayer will greatly affect the temperature performance of the converters. A method of fabrication must be developed to fabricate a structurally integrated trilayer.

The end enclosures for each pair of fuel elements are constructed of Cb-1Zr. The busbars connecting adjacent fuel elements are contained within these enclosures. Protruding from the upper enclosure plenum is a long Cb-1Zr tube which houses the cesium reservoir in its tip. The stem is hung from the core support plate by a carbide-coated Cb-1Zr nut. This nut screws onto the threaded section of the stem and rests on a tube welded to the core support plate. The upper end enclosures must be capable of supporting pairs of fuel elements while the stem must be capable of supporting a complete assembly of elements under launch loads at a temperature of approximately 700°F. Thermal expansion of the enclosure must not subject the welds to severe stresses because of the possibility of fracturing the welds and because of the increased corrosion in stress locations. The lower end enclosures will not be required to withstand any launch load, but must accommodate very small relative axial movements of the fuel elements.

b. Reactor

Figure 7 shows the design selected for the 3.25 megawatt thermionic reactor. It is a 33.4 MW (thermal), high-temperature, fast reactor, fueled with UC-ZrC and controlled by externally-mounted rotating control drums fabricated from BeO. It is cylindrical in shape and its core has an L/D ratio value of 0.93. The core contains 125.1 kilograms of 93 per cent-enriched UC and 1505 kilograms of ZrC. The reactor core is cooled by a primary high-temperature coolant and the cesium reservoirs for the element assemblies are cooled by a low-temperature coolant. In both instances the coolant is lithium. The total reactor electrical power is 3.99 MW at 218 volts. The principal features of the reactor pressure vessel, the reactor core, the coolant and insulation system, and the reactor control system are discussed in subsequent paragraphs.

1) Reactor Pressure Vessel

The reactor pressure vessel consists of a cylinder with ellipsoidal heads welded to each end. The wall thickness is approximately 0.4 inch with local areas around nozzles shaped to reduce stresses. Cb-1Zr was selected as the construction material for the pressure vessel, as it was for

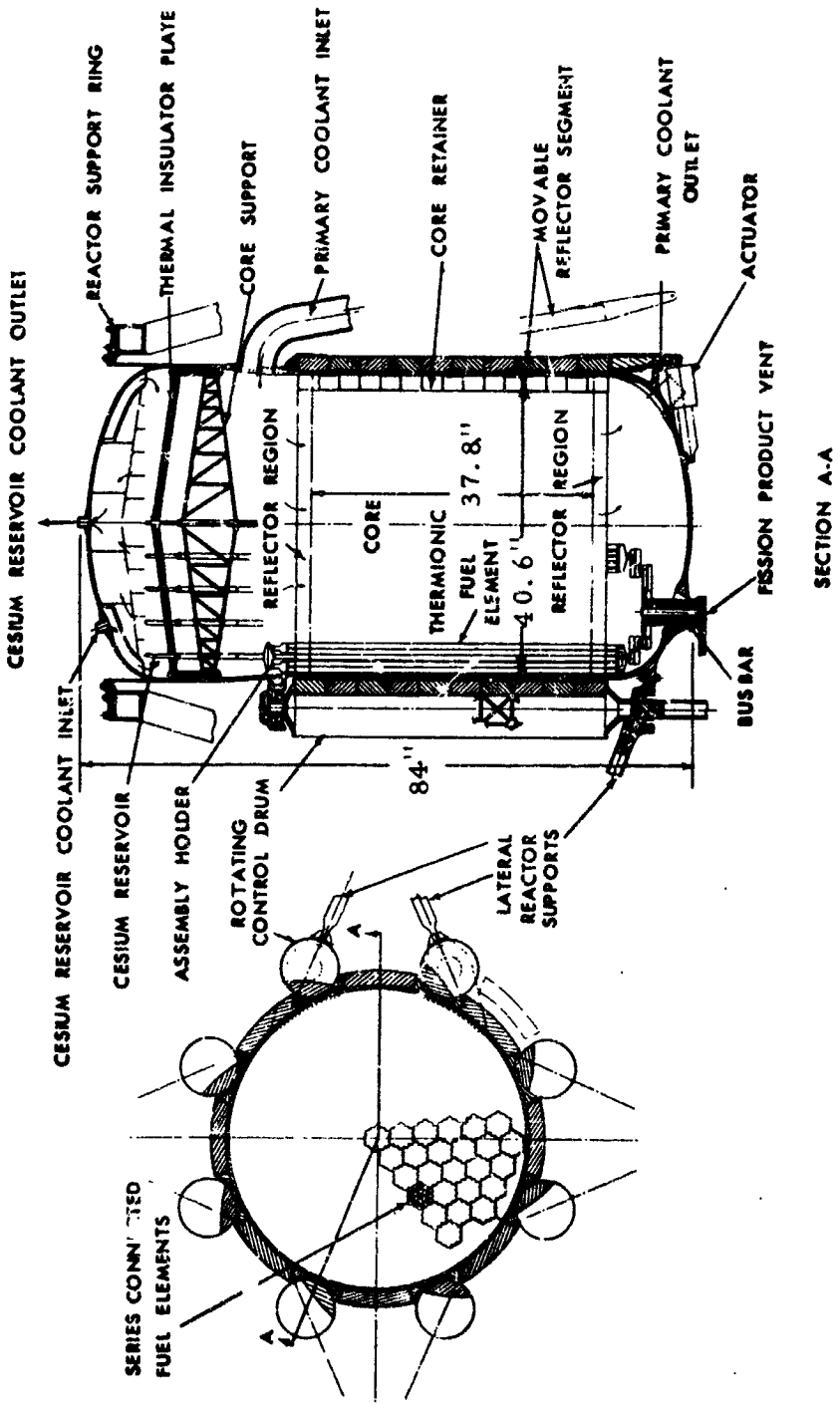

Figure 7 Thermionic Reactor

all other components in contact with lithium (see Appendix B of Report PWA-2224). Pratt & Whitney Aircraft has performed considerable research and development work with Cb-1Zr and has run flow systems with lithium at high temperature (2000°F) for periods up to 10,000 hours[1,2]. A stress analysis of the critical areas of the pressure vessel is presented in Appendix 1 of this report.

2) Reactor Core

The core is designed as an irregular polygon and is composed of 115 hexagonal fuel assemblies held together laterally by baffled guides located at the periphery of the core. This lateral support system maintains the fuel elements in a close-packed, triangular-pitched array. The coolant flows in the cusp-shaped passages between the elements. A detailed temperature analysis of the trilayer anode is presented in Appendix E of Report PWA-2224. The area around the outer edge of the core contains the flow baffles which reduce the coolant flow through this region.

The hexagonal fuel assemblies deliver 34.6 KW at 218 volts each. They are electrically connected in parallel and contain 19 series-connected thermionic fuel elements each. The number of elements connected in series in each assembly determines the voltage buildup in the assembly. Obviously it is desirable to deliver power from the reactor at as high a voltage as possible so as to reduce busbar losses. However, since the anodes of the converters are insulated from the liquid metal system by a layer of BeO, some power will leak through this insulation to ground. In order to select a reactor voltage for the reference design a calculation was performed to determine the system weight increase due to this power loss as a function of reactor output voltage. The results are plotted in Figure 8 which shows that signifi-

[1] Pratt & Whitney Aircraft Design Report, Advanced Nuclear-Electric Power Generator Systems Study, Thermionic Nuclear Space Powerplant, Report PWA-2224, Vol. II SRD, Appendix L

[2] R.I. Strough and A.I. Chalfant, Pratt & Whitney Aircraft, High Temperature Technology for the SNAP 50/SPUR Nuclear-Electric Space Powerplant, SAE and ASME Air Transport and Space Meeting, April 1964

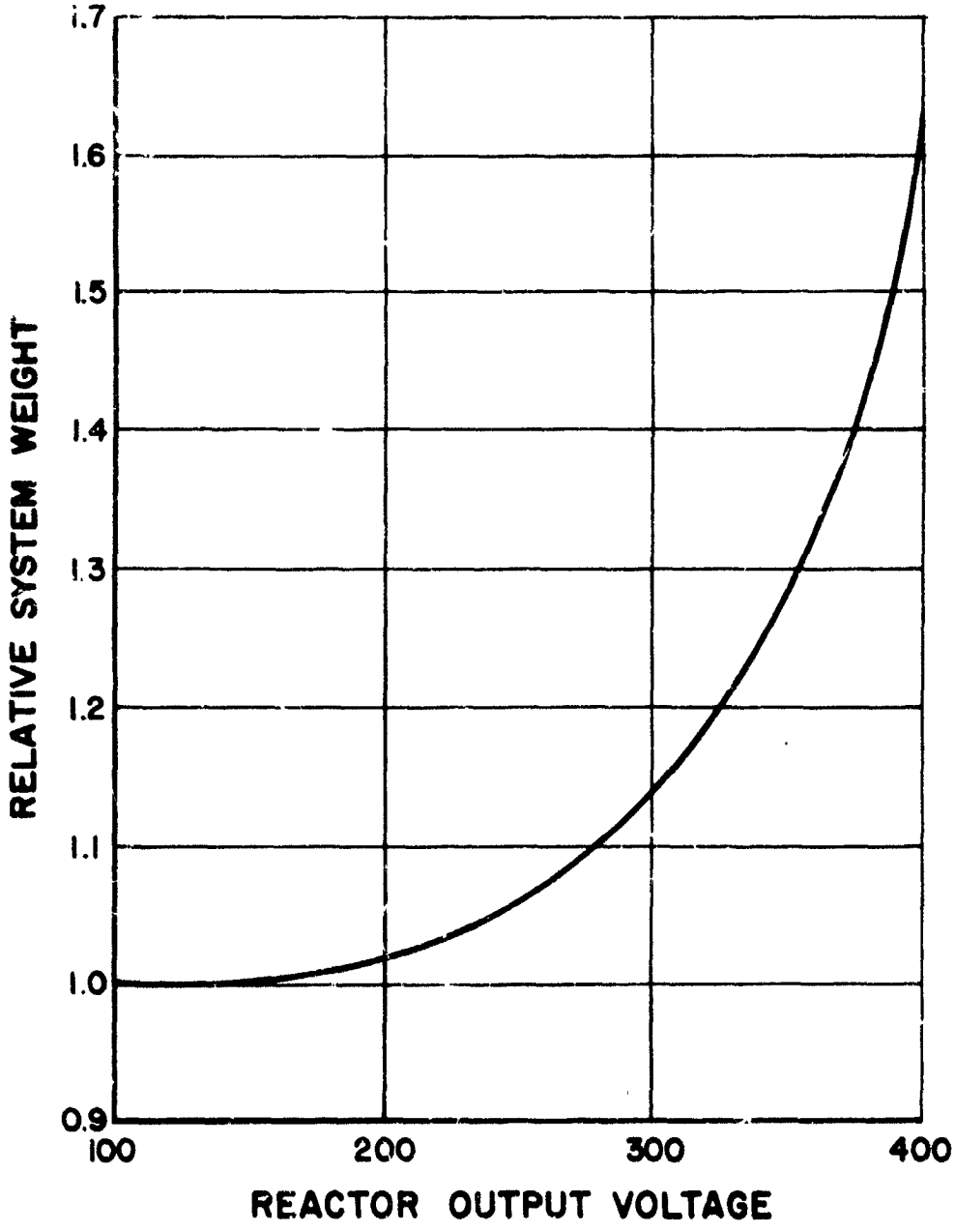

Figure 8 Reactor Output Voltage vs Relative System Weight

cant losses and system weight increases begin to occur at a reactor voltage of about 200 volts. Therefore, an assembly of 19 elements was selected which yields a symmetrical array and produces 218 volts. This voltage produces a system weight increase of only about 3 per cent above optimum. Fewer elements connected in series, which would yield less than 100 volts, result in a system weight increase due to busbar losses, and compound the complexity of the electrical connections required to be made in the reactor. More than nineteen elements yield significant weight increase due to electrical leakage across the trilayer, and increase the probability of arcing within the fuel elements.

The fuel assemblies are arranged in concentric hexagonal arrays, each array containing the same fuel loading. The variation in fuel loadings between arrays is shown in Table 3. The fuel loading within each fuel assembly is varied in three axial regions. A total of fifteen separate fuel regions exist in the core. This design aids in flattening the axial and radial power distributions.

The series-connected fuel elements comprising the hexagonal fuel assemblies are supported in the reactor by hanging them from a core-support plate. The parallel electrical connection of the hexagonal fuel assemblies is accomplished by a collector-ring busbar located in the lower head of the pressure vessel. Cylindrical busbars insulated with BeO protrude from the last fuel element in each assembly and are welded to flexible straps attached to the collector ring. The flexible straps allow axial motion of the elements during launch and thermal cycles. The collector ring is enclosed in a Cb-1Zr enclosure, one face of the busbar being insulated with BeO and in contact with the enclosure. Nuclear heat and I^2R heat generated in the busbar are dissipated to the reactor coolant though this face.

Fission gases, which flow through channels in the fuel-element busbars, pass through the void volume in the collector-ring enclosure and out of the reactor through the cylindrically-shaped busbars. These busbars conduct the current from the collector ring to other busbars located outside the reactor. All of the busbars located within the reactor are constructed of Cb-1Zr alloy. They are sized for minimum weight and shaped to allow for adequate cooling.

The core is supported by a plate constructed of alternating cones and cylinders sandwiched between two shallow conical plates. This type of construction was selected because of its light weight and rigidity. Drilled holes are located in certain regions of the support plate so that liquid metal may circulate and the nuclear heat generated within the plate may be dissipated. The cesium-reservoir stems which support the fuel-element pairs pierce the support plate through tubes mounted in the plate. Columbium carbide-coated nuts mate with the threaded sections of the stems and rest on the upper edge of the tubes. Thus the elements are kept in tension during launch. The weight of the core is transmitted from a support lip to a cylindrical skirt extension on the upper head of the vessel and then to the reactor support structure. Thus the entire weight of the reactor is hung in tension from the skirt. Lateral members extending from the reactor support structure to the lower head of the vessel provide lateral support for the reactor.

3) Coolant and Insulation System

Lithium was selected to be the reactor coolant. This choice was determined in the system parametric studies conducted for this and the former study contract, NASw-360. Lithium possesses a very low vapor pressure at high temperatures and the lithium-7 isotope has a very low neutron absorption cross-section. Pratt & Whitney Aircraft work in lithium technology is summarized in Reference 4 of Appendix 8.

Two lithium-coolant flow paths pass through the pressure vessel. One path channels the primary high-temperature coolant which cools the reactor core. The other channels the low-temperature coolant which cools the cesium reservoirs. The primary coolant enters the reactor from four inlet pipes. The pipe sizes were so selected as to minimize coolant pressure drop. The primary-coolant inlet nozzles are 3.5 inches in diameter and are located in the side of the pressure vessel. The coolant enters the reactor at 1566°F and flows radially across the top and down through the core to the lower pressure-vessel head. The coolant leaves the reactor through two 7-inch diameter nozzles located 180 degrees apart in the lower head. Exit temperature and flow rate for the primary coolant are 1945°F and 70 lbs/sec.

The lithium coolant for the cesium reservoirs enters the pressure vessel through a 1-inch diameter nozzle located at the edge of the upper head of the vessel. It flows through a plenum and across the tops of the fuel-assembly stems,

in which are housed the cesium reservoirs. A flow distributor is located above the stem tips to ensure an even flow distribution across the stems. The coolant leaves the vessel through a 1-inch diameter nozzle located in the center of the upper head. The cesium-reservoir coolant enters the pressure vessel at 656°F and exits at 676°F, with a flow rate of 1.1 lb/sec. The pipes and plenums for the primary-coolant flow system and the cesium-reservoir-coolant flow system were designed to minimize pressure drop and stresses.

An insulator plate is located in the upper plenum of the reactor to reduce heat transfer between the primary high-temperature reactor coolant and the low-temperature cesium-reservoir coolant. This plate, which is filled with ZrO_2 and clad with Cb-1Zr, serves to separate the two coolant flows through the reactor. The pressure of the coolant on either side of the plate must be controlled in order to reduce the seepage of liquid metal through the plate and around the fuel-element stems which protrude through the plate. A ZrO_2 insulator ring is located within the reactor vessel and in contact with the vessel wall. The ring serves to reduce the thermal gradient and the thermal stress existing in the wall because of the temperature difference between the liquid-metal coolants. An analysis of the stresses existing in this section of the vessel wall is given in Appendix 1.

4) Control System

The thermal power of the reactor is controlled by a reflector consisting of eight rotating control drums and eight movable slabs. The slabs are interspersed between the drums and provide additional shutdown margin. Each control drum is pie-shaped, has an open-lattice construction, and contains BeO in its circular sections. Nuclear heat generated in the BeO is dissipated by thermal radiation through the open-lattice framework to space. The control drums are mounted on the pressure vessel by means of ball bearings. Because these bearings will be operating in a high temperature, nuclear, vacuum environment, and will not be continually in motion, they give rise to severe design problems. Means must be provided for preventing welding

between the movable and stationary components of the bearing. The control drums are driven through shafting by motors which are located behind the reactor shield to protect them from the nuclear environment.

The interspersed slabs referred to consist of BeO contained in an open-lattice frame-work. They are movable to allow for reactor shutdown. The slabs are pivoted at their top edges and moved by pneumatically-operated linear actuators mounted on the lower head of the pressure vessel. They will be maintained in the out position during launch and moved to the in position during the initial phase of reactor startup. The pneumatic actuators contain springs for moving the slabs to the out position quickly, in the event that emergency shutdown is required. The slabs are held against the pressure vessel during reactor operation and nuclear heat generated in the BeO is radiated to space.

c. Shield

A nuclear shield is employed in the powerplant to protect the power-conditioning equipment from nuclear radiation. The shield, shown in Figure 3, is located behind the reactor and casts a reduced radiation shadow over the entire powerplant. The selection of the maximum radiation dose for the power-conditioning equipment is based on the allowable dose for solid-state equipment, since data for the gas-tube equipment was unavailable. The total integrated dose over a 24,000-hour period was set at 10^{13} nvt (fast) for neutrons and 10^{7} rads for gammas.

Three materials are used in the construction of the shield, 1) borated graphite, 2) thermal insulation, and 3) lithium hydride. An eight-inch thickness of borated graphite faces the reactor, followed by 2 inches of thermal insulation and 19.6 inches of lithium hydride. The graphite is used in the shield because of its high temperature capability. It aids in reducing the heat generation and therefore the temperature in the lithium hydride. The purpose of the thermal insulation is to reduce the heat flux from the graphite to the lithium hydride. Lithium-7 instead of lithium-6 is used in the lithium hydride portion of the shield in order to reduce its operating temperature. This was shown in the shield analysis for the one megawatt powerplant where extremely high temperatures were generated with the use of lithium-6 due to an (n, α) reaction. This does not occur in lithium-7.

d. Primary EM Pump and Piping

An electromagnetic pump circulates the lithium coolant in the primary subsystem. A typical design for the pump is shown in Figure 10 of Report PWA-2224. The design parameters for the pump were selected on a minimum overall system weight basis. The pump cells and the interconnecting busbars are constructed of Cb-1Zr and are insulated from each other by Al_2O_3. A cobalt-iron alloy with a high Curie point (1790°F) was selected for the pump magnet in order to prevent the loss of permeability at the high operating temperature. The magnet windings consist of copper wire wrapped with Crystal M, an inorganic paper type insulation. A more detailed description of the design features of this pump is also given in Report PWA-2224.

The primary piping consists of four pipes which complete the coolant flow path for the primary system. Two of the pipes are connected to the two reactor outlet nozzles and allow the coolant to flow from the reactor to the heat exchangers' inlet manifold. The coolant then flows through the heat exchangers and is collected in the outlet manifold. From there the coolant flows through the two remaining primary pipes which branch off at the reactor to provide for four coolant inlets to the reactor. The inside diameter of the pipes was determined on a minimum weight basis by the systems analysis and the pipe wall thickness was sized to provide adequate meteoroid protection.

e. Cesium Reservoir Heat Rejection System

This system consists of a single-segment space radiator and an EM pump. The pump circulates a low temperature lithium coolant through the upper head of the reactor vessel (in which are contained the cesium reservoirs) and through the radiator. This fluid cools the reservoirs to their prescribed temperature and conducts the heat to the radiator where the heat is rejected to space. The design of this pump is similar to that of the primary pump but much smaller in size due to the reduced pumping power requirements. A tube-fin type radiator similar to

that used in the main heat rejection system is employed here and is optimized in the same way. However, the tube wall thickness of the radiator as well as the pipe wall thickness are sized to provide meteoroid protection.

The radiator consists of two panels through which flow the same coolant in series. The panels are located forward of and in the same plane as the main radiator and are constructed of Cb-1Zr.

2. Secondary Subsystem

The secondary subsystem is comprised of the sixteen coolant loops of the main heat rejection system. Each loop contains an EM pump, a heat exchanger and a radiator segment. Segmentation was used to achieve minimum weight and to provide redundancy. The coolant used in this system is lithium. All components in contact with the coolant are constructed of Cb-1Zr to give the radiators a high temperature capability which greatly reduces radiator area and eliminates the necessity of folding.

a. Radiators

The radiator segments are rectangular in shape and are composed of inlet and exit manifolds with interconnecting finned tubes. The arrangement of the segments in a plane is as determined by the plan area of the Saturn payload envelope. Design parameters such as tube and fin dimensions were determined on a minimum weight basis in the system analysis. Wall thicknesses were determined from meteoroid criteria. For even flow distribution, the inside diameters of manifolds were sized to give a pressure drop 10 per cent of that for the tubes. Emissivity of radiator surfaces was assumed to be 0.9. This value was based upon results of extensive testing[1] which indicate that this value may be attainable in the future.

Support of individual radiator segments is accomplished by emplacement of the segments in the radiator support structure. Two such structures contain all of the radiator segments, one structure on each side of the powerplant axis. The segments are hung from their upper manifolds which are oriented perpendicular to the powerplant axis and are allowed to grow against

[1] Pratt & Whitney Aircraft, Determination of the Emissivity of Materials, Report PWA-2206

leaf-type springs contained in the lower manifold supports. Lateral growth is accommodated by springs located in the outboard tube supports. The two support structures are connected at their ends to the fore-and-aft support rings. The structures are hung from the forward ring and are attached to the aft ring through a cruciform structure. At the four points of the cross are located expansion joints to accommodate any difference in thermal growth between the radiator structure and the launch structure during the system preheat cycle. Lateral support of the radiators is accomplished at launch by the four-quadrant launch structure which sandwiches the planar radiator between the paired quadrants.

b. Heat Exchangers

The secondary system contains sixteen lithium-to-lithium, counterflow, tube-and-shell heat exchangers, one for each of the heat rejection loops. The heat exchangers are of a straight tube design with the tubes welded to tubesheets and the sheets welded to the outer shell. Design parameters such as tube inside diameter, length and log mean temperature difference, were determined in the system analysis. A typical design for a heat exchanger is shown in Figure 9 of Report PWA-2224. The straight tube design was based upon experience at Pratt & Whitney Aircraft indicating that this design is capable of withstanding the stresses imposed at operating conditions. Spacers are provided between the tubes to prevent sagging which could cause blockage of flow. The inlet and exit plenums for the shell side are toroidal in shape and are welded to the tubesheets and the outer shell. These plenums have thin walls to allow for differences in thermal expansion between the tube bundle and the shell. The inlet and exit plenums for the tube side are hemispherical in shape and located at both ends of the heat exchanger. All exterior wall thicknesses were determined from meteoroid criteria.

The heat exchangers are grouped in the powerplant in a cylindrical cluster and are located behind the nuclear shield. This location is an optimum which was determined by trading off the pipe weights and the required pressure drops.

c. Secondary EM Pump and Piping

The electromagnetic pump employed in the secondary system

contains sixteen separate pumping channels, one for each of the heat rejection loops. Design parameters for this pump were also determined on a minimum weight basis in the system analysis. The design features and the materials utilized for this pump are similar to those presented in Figure 11 of Report PWA-2224. Two of the more obvious features of the pump are, 1) the electrical connection of the pumping cells in series, and 2) the provision for cooling the channel walls with a separate coolant loop. The cells were electrically connected in series to increase the pump voltage requirements, since the calculated voltage for each cell was very small. A higher voltage for the pump reduces busbar losses and the weight of power-conditioning equipment. The ribbon-shaped coolant loop is interwound between the pump cells and provides cooling for the cell walls in the event of a loss of coolant due to a radiator puncture. Loss of fluid in a cell leaves only the cell walls to conduct the high pumping current so that the possibility of melting the walls exists.

The pump is mounted on the inflight support structure at the center of the main radiator. Long lengths of secondary piping which connect the radiator segments with the pump are designed with expansion bends to absorb thermal motion and relieve the pump of any excessive stresses. The piping inside diameter was optimized and the wall thickness was determined from meteoroid data.

3. Auxiliary Subsystem

The auxiliary system consists of DC-to-DC power-conditioning equipment and its required heat rejection system. Power-conditioning equipment is required in the powerplant to process the output power of the reactor to match the characteristics required by the ion engines. The reference thermionic reactor produces electrical power at 218 volts DC which must be increased to 5000 volts for utilization by the ion engines.

a. Power-Conditioning Equipment

Components for the conditioning equipment are shown in Figure 9 which was taken from a Westinghouse systems study[1]. The

[1] Westinghouse Electric Corporation, Aerospace Electrical Division, Space Electric Power Systems Study, Volume 5, NAS3-1234.

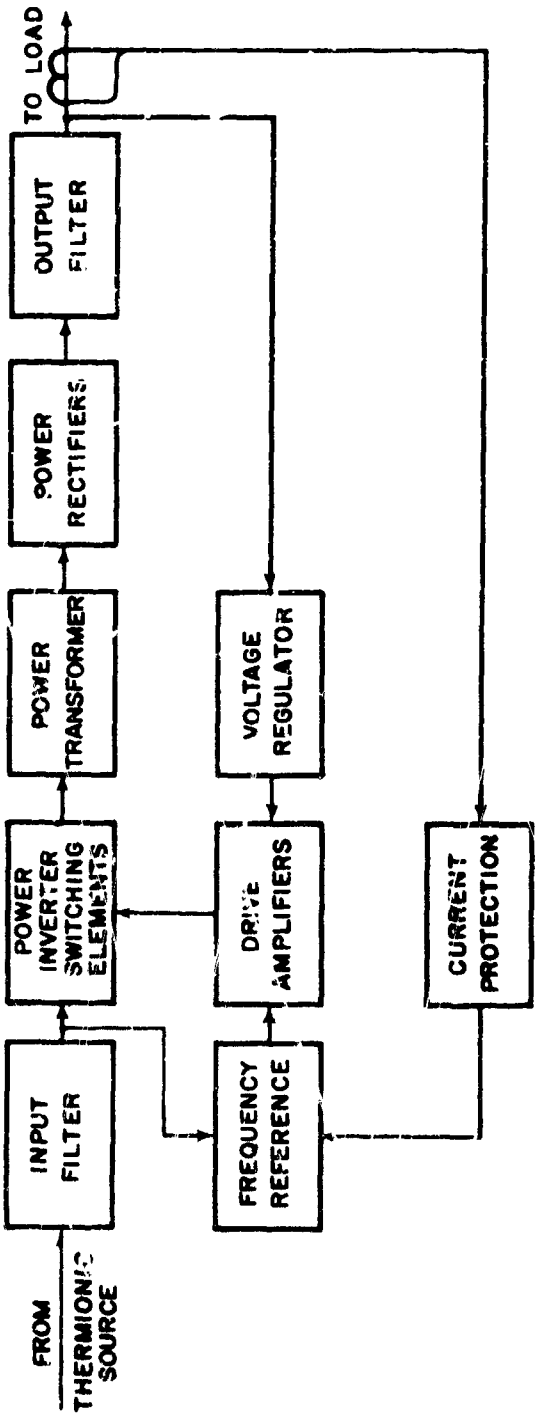

Figure 9 DC-to-DC Converter Block Diagram

Westinghouse report contains a parametric study for space power-conditioning equipment capable of processing power in the range of from 0.5 to 5 megawatts at various input and output voltages. Two types of equipment were considered in the study, high temperature and low temperature. The high temperature equipment employed gas-tube inverter components while the low temperature employed either silicon power transistors or silicon-controlled rectifiers as inverters. All systems considered, used the system components shown in the block diagram in Figure 9.

For the present study, it was assumed that the conditioning equipment weight was 5 lbs/KW(e) and that the equipment utilized high temperature components capable of operating at about 500°F. It was also assumed that the equipment efficiency was 93 per cent. The data presented in the Westinghouse study was received after the selection of a system design so that the powerplant design presented here is not based on this data. However, Appendix 5 presents the results of the Westinghouse study, and Appendix2 presents some of the important system parameters which would result with the inclusion of the new data in the powerplant design.

b. Auxiliary Heat Rejection System

Each loop of the auxiliary heat rejection system employs a motor-driven centrifugal pump to supply the pumping requirements. Each segment consists of an inlet and an outlet manifold with interconnecting finned tubes. Inside diameters of the radiator tubes were optimized, and wall thicknesses were calculated from meteoroid criteria. Fin width and thickness were calculated to give required surface radiating area for minimum weight.

The selection of monoisopropylbiphenyl as the coolant was based on the Westinghouse study presented in Appendix 5 of Report PWA-2240, and the aluminum radiator was chosen because of its light weight.

The auxiliary four radiator segments are supported in a manner similar to the main radiator segments and are the last four segments contained in the radiator support structure. The power-conditioning equipment is located within and supported by the aft support ring.

c. Busbars

The designs of the busbars employed throughout the powerplant reflect a trade-off between minimum busbar weight and the increment of weight that would be added to the system weight because of I^2R losses in the busbars.

Power is drawn from the reactor through two cylindrical Cb-1Zr busbars which pierce the lower head of the vessel. Each of these busbars is connected to two flat copper busbars which conduct the power to the power-conditioning equipment. The flat copper busbars are oriented parallel to the main radiator, and the side of the busbar facing the radiator is thermally insulated. With this arrangement the busbars will operate at a temperature of approximately 1000°F. Other busbars employed throughout the powerplant to deliver power to various loads are also of copper.

The current generated in the reactor is conducted first to the power-conditioning packages, then to the loads and finally back to the reactor. A study of the possible methods of wiring the power-conditioning modules is given in Section IV. G. It is desirable to wire the powerplant in such a way as to reduce power perturbations in the reactor and power-conditioning modules due to system component failures.

Busbars employed within the reactor are constructed of Cb-1Zr because of the high-temperature environment. The Cb-1Zr busbars are insulated with BeO and clad with Cb-1Zr to protect them from the lithium environment. Copper busbars are used outside of the reactor because of the low electrical resistivity and high operating temperature capability of this material.

D. Weight Analysis

1. Powerplant Weight

Since the weight of a system to be launched into space is of prime importance, the design of the thermionic powerplant was based on a minimum-weight philosophy. However, the practical design of the system components necessitated the choice of off-optimum parameters. Also, based on material-property and space-environment data, conservative engineering assumptions were made to ensure the reliability of the system. These assumptions in

all cases entailed system-weight penalties. A weight analysis was performed to determine the weights of all of the system components. Table 2 lists these weights and includes the weight of the powerplant support structure, the fairing, and the onboard auxiliary-power unit required for startup. The estimated inflight powerplant weight is 76,100 lbs or 23.4 lbs/KW(e). The total powerplant weight on the launch pad is 123,400 lbs or 37.9 lbs/KW(e).

Comparing these weights with those of the one-megawatt powerplant shows that the inflight specific weight for the present powerplant is lower and the launch weight higher. The former result occurred primarily because the specific weights are lower for the shield and the main and auxiliary radiators. The shield specific weight is lower because a gamma shield was not required for this powerplant as it was in the one-megawatt system (see Appendix 3 for the analysis of the shield). The main radiator specific weight is less because of a decrease in the meteoroid barrier thickness predicted by a new correlation. A much higher heat rejection temperature caused the reduction in the specific weight for the auxiliary radiator. The launch specific weight for this powerplant is significantly greater because of the large increase in the length of the powerplant which requires a disproportionate increase in launch structure weight. It can be anticipated that as the size and weight of a space powerplant increase, the specific weight of required launch structure will increase.

The specific weight of this powerplant is dependent upon the operating cathode temperature selected. The selection of this temperature can be based on either of two limiting criteria as is discussed in Section IV.H. Due to a lack of experimental data and for consistency with the previous one-megawatt study, a maximum cathode temperature of 3200°F was selected. If the thermal criterion of maximum open-circuit temperature had been chosen, an increase of 20 per cent in reactor power and a decrease of 8 per cent in specific weight could have been obtained.

As was discussed in Section IV.C., the weight of the power-conditioning equipment was based on preliminary assumptions. Later data published by Westinghouse showed that high temperature conditioning equipment can be expected to be significantly heavier than the weight assumed in this study. A discussion of the powerplant weight as affected by this new data is given in Appendix 2.

TABLE 2

System Component Weights

reactor (core, pressure vessel, reflector, control drums and actuators)	19,200 lbs
shield	7,200
primary piping and coolant	2,350
primary EM pump	500
heat exchangers (16)	750
secondary EM pump	300
high temperature heat rejection system (main radiator, secondary piping and coolant)	11,900
cesium reservoir coolant pump	150
cesium reservoir heat rejection system (radiator, piping and coolant)	300
auxiliary heat rejection system (radiator, pump, piping and coolant)	1,100
power-conditioning equipment	16,300
busbars	6,750
inflight support structure	8,800
Total Inflight Weight	76,100 lbs
onboard APU	200
launch structure	33,000
aerodynamic fairing	14,100
Total Launch Weight	123,400 lbs

2. Vehicle Weight

The total weight of the space vehicle, consisting of the powerplant, the propulsion system and the payload, is limited to 226,000 pounds. This weight is the maximum that the Saturn 5 is capable of lofting into a 300-nautical mile earth orbit. Since it is desirable to maximize the payload, a mission study was performed (Appendix 2) to determine the effect of the launch and inflight powerplant weights on payload weight. The study estimated the cesium propellant weight required by the ion engines, and the payload that the vehicle will be capable of delivering to Jupiter as a function of both the inflight and launch weights. It was found that to maximize the payload, it was more important to reduce the inflight rather than the launch weight. That is, a greater payload could be delivered for the lighter inflight powerplants even though their launch weights might be heavier. This result is important since it affects the selection of a powerplant configuration (see Appendix 2 for a comparison of planar and cylindrical radiators).

The propellant and payload weights are dependent on the thrustor efficiency assumed. Since a more efficient thrustor requires less propellant to complete the same mission, the reduction in the propellant weight for a more efficient thrustor can be added to increase the payload weight. Presented below are the payload and propellant weights for two thrustor efficiencies. The payloads shown are gross amounts that include the weights of the equipment required for guidance and navigation.

	85% Efficiency	95% Efficiency
powerplant launch weight	123,400 lbs	123,400 lbs
propellant weight	89,500	85,000
payload weight	13,100	17,600
total vehicle weight	226,000 lbs	226,000 lbs

E. Powerplant Performance

Studies have been performed to determine the performance of the system selected for design. The purpose of the studies was to determine in detail the characteristics of the individual components and the interaction of the components in the overall system.

1. Converter Performance

The performance of a thermionic converter is ultimately governed by the geometry, the materials and the operating conditions chosen. Once these parameters have been established the thermal and electrical characteristics and, therefore, the performance of the converter are specified. Both characteristics must be considered in the evaluation of performance because of their intimate relationship in the thermionic process. The discussion that follows will be mainly concerned with performance as affected by operating conditions. Discussions pertaining to the effects of geometry on performance as evidenced by their effects on system weight are given in Section V. C. of Report PWA-2319 (it should be noted that the system weights of PWA-2319 are less than those presented in this report because they do not include weight estimates of layout designs). Section IV.C. above presents the engineering considerations concerning geometry and materials that were taken into account in arriving at a final converter design.

An operating parameter that affects converter performance and system weight seriously is the cathode temperature. A plot of relative system weight versus cathode temperature, shown in Figure 10, indicates the variation in system weight for systems optimized at each of the given cathode temperatures. This curve was prepared assuming that there was no limit on fuel evaporation. With the maximum cathode design temperature selected, the variation in power output of a converter during powerplant operation can be discussed.

It is assumed for this discussion that the thermal power input to a particular converter contained in the reactor is held constant while the load resistance is varied. This causes the electric power output and the cathode temperature to vary. Since only a single converter is considered, the characteristics of the converter are different from those of a fuel element or the reactor, as will be shown below. Figure 11 shows the sensitivity of the power output to changes in cathode temperature. As can be seen, a 50 per cent decrease in power results when the temperature is decreased 200°F or increased 500°F from the temperature corresponding to maximum power. The cathode

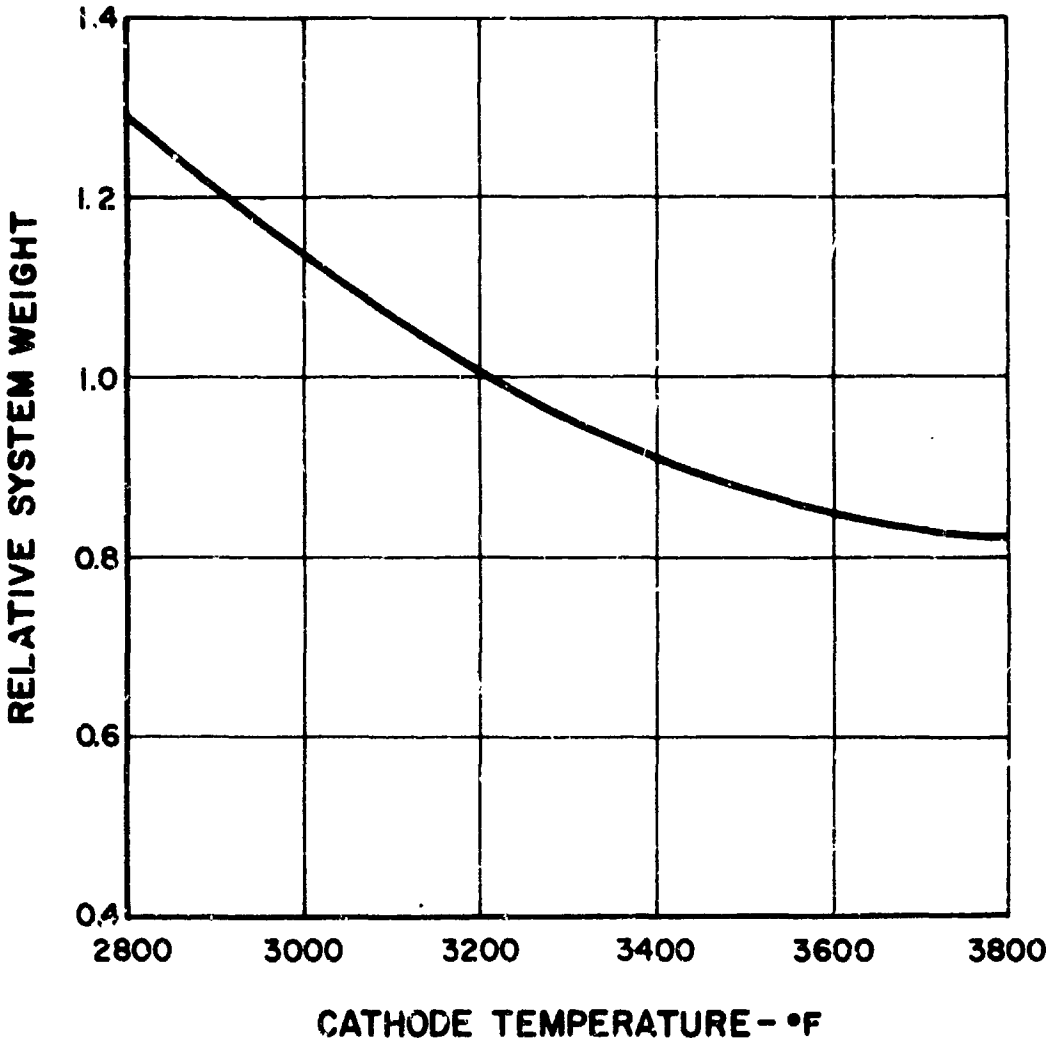

Figure 10 Relative System Weight vs Cathode Temperature

temperature at which the maximum power output occurs for a particular converter is dependent upon the thermal power input. For this converter, the maximum power output occurs at a temperature which is only slightly higher than the limit imposed on the cathode temperature.

Other converters in the reactor will have much different thermal inputs and therefore the temperatures at which they produce their maximum power will be far from the 3200°F limit. These con-

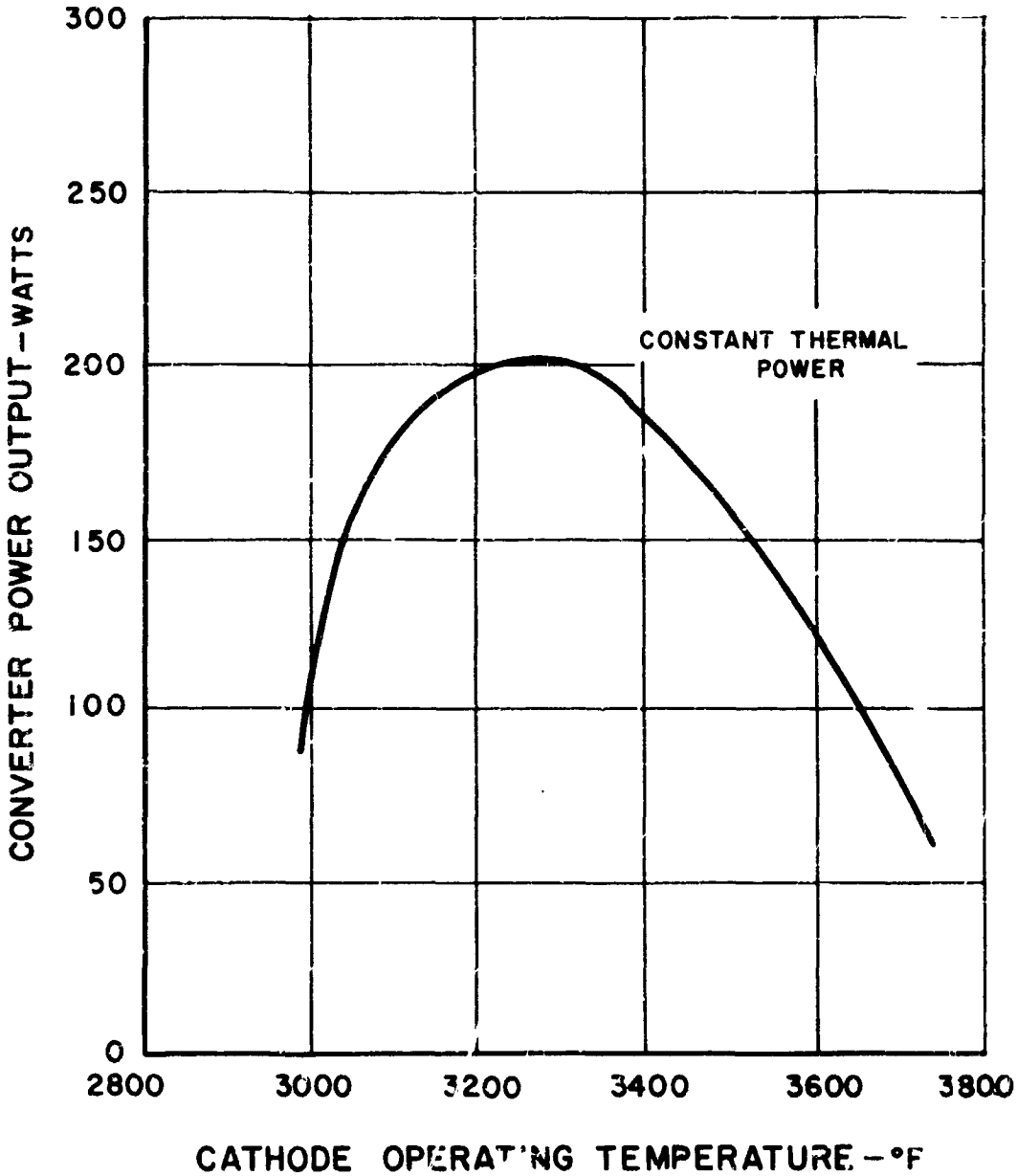

Figure 11 Converter Power vs Cathode Temperature

verters will operate at an off-optimum condition since they will not be operating at the point where they can produce their maximum power output. This is important since it gives rise to a weight penalty which is incurred due to the nonuniform power generation

in the reactor. A discussion of this problem is given in the following section which is concerned with fuel element performance.

To aid in understanding the performance of an operating converter and the relationships of the variables involved, consider the simplified model of a converter presented below.

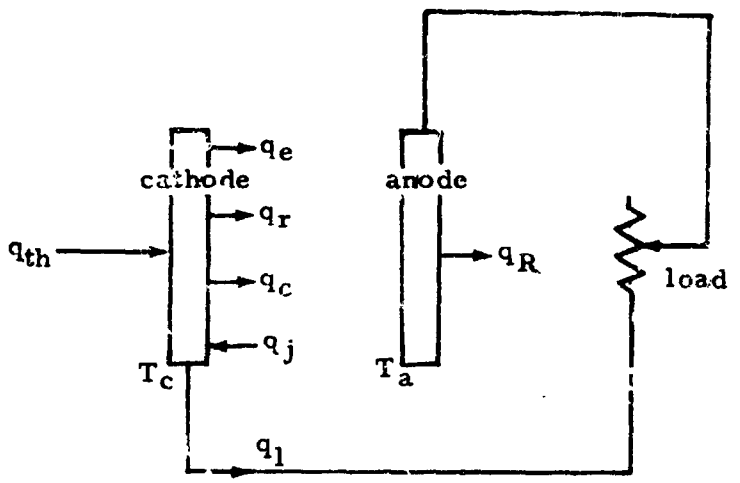

q_{th} = thermal power input
q_e = electron cooling
q_r = radiation loss
q_c = thermal conduction through cesium plasma
q_l = thermal loss through the lead
q_j = Joule heating in cathode
q_R = thermal power rejected

An energy balance taken on the cathode yields the equation

$$q_{th} = q_e + q_r + q_c + q_l - q_j \qquad (1)$$

From the equation it can be seen that the energy loss from the cathode is both thermal and electrical. Each term on the right side of the equation can be written explicitly in terms of the cathode temperature. Assuming a given thermal power input, an anode temperature and an electric current, the temperature of the cathode and the value of each term can be determined. A change in the value of the load resistance changes the current through the converter, which

in turn changes the value of each term on the right side of the equation. Since the thermal power input has been kept constant, the values of the thermal and electrical losses must adjust themselves by an adjustment of the cathode temperature. Figure 12 shows the variation in these terms as a function of the current flowing through the converter and the converter voltage. It is assumed that the converter is initially at an open-circuit condition (infinite load resistance) which produces the highest cathode temperature and the highest converter voltage, since all energy losses from the cathode are thermal. At this condition no current flows and the major loss is by thermal radiation to the anode, with only minor losses by lead and plasma thermal conduction. When the load resistance is reduced, a current

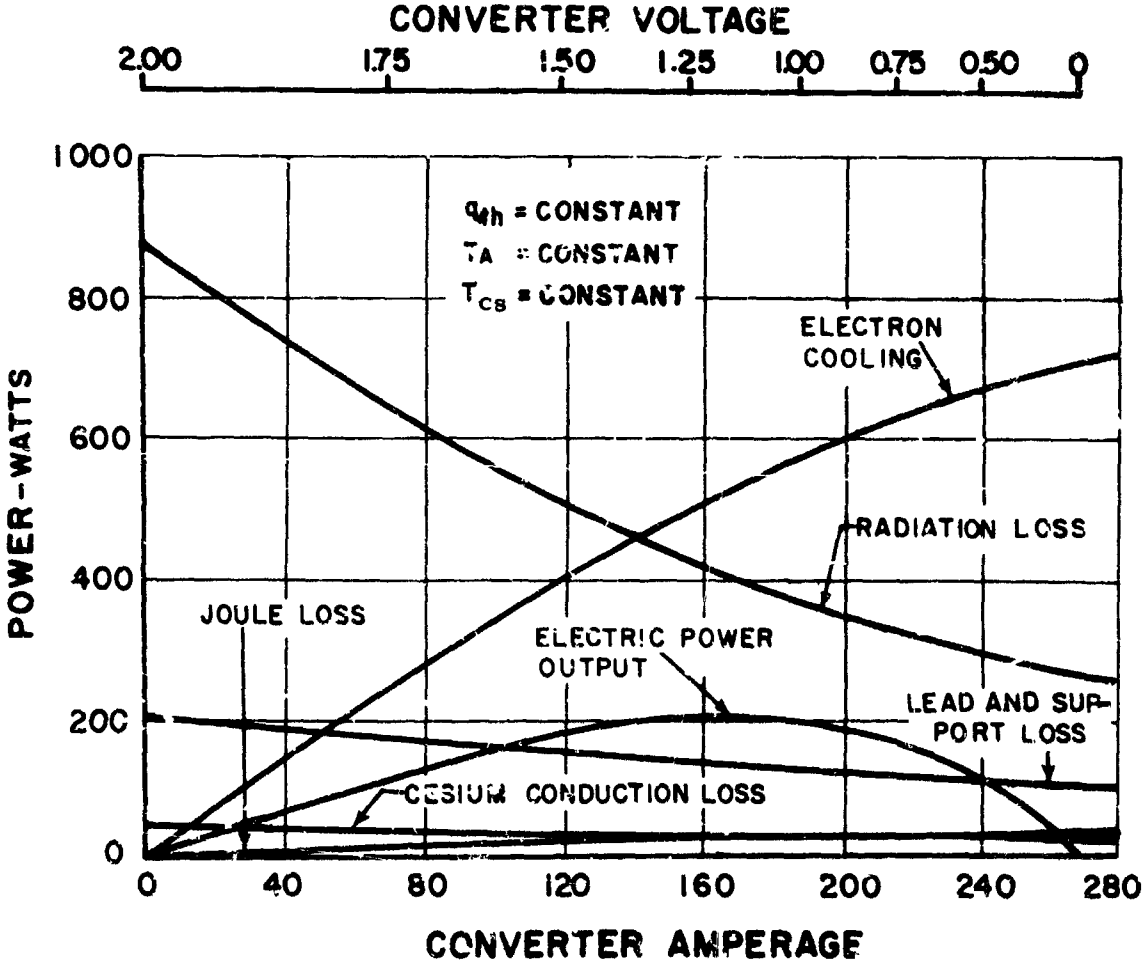

Figure 12 Converter Performance

flow is initiated and electrical energy (electron cooling) now flows from the cathode. Since the thermal energy input is held constant, a reduction in the cathode temperature must occur to reduce the thermal losses. Continuing the reduction in load resistance increases the electron cooling from the cathode and decreases the cathode temperature, the converter voltage and the thermal losses from the cathode. The electric power output of the converter also increases. This occurs because the power output of the converter is the product of the current and the voltage, and since the voltage decreases as the current increases, the product of the two can be expected to pass through a maximum.

The determination of the electrical characteristics can be demonstrated by again considering Equation (1). Neglecting the terms q_c, q_l and a_j which are usually small, and rewriting the equation in approximate form, the following expression results

$$q_{th} = i (\phi_c + 2kT_c) + \sigma A \epsilon T_c^4 \qquad (2)$$

Since the work function ϕ_c is a function of temperature, the equation can be written

$$q_{th} = i \left[f(T_c) + 2kT_c \right] + \sigma A \epsilon T_c^4 \qquad (3)$$

Assuming the function $f(T_c)$ is known, the equation can be solved for T_c. If the relation between T_c and converter voltage is also known from experimentation, the relationship between the current and voltage is known. A plot of this last relationship gives the I-V characteristics for a converter. Figure 13 is a plot of these characteristics for the particular converter discussed previously. Also shown in the figure is the variation in cathode temperature with current. Equations 2 and 3 and Figure 13 show the intimate relationship between the thermal and electrical characteristics of a converter which results in a distinct current-voltage plot for each converter with a different thermal power input.

The cathode temperature referred to previously is the maximum temperature occurring on the cathode. Due to the lead and support connections on either side of the cathode which supply paths for heat loss, a temperature distribution results as shown in Figure 14. The temperature distribution is determined by dividing the fuel and the

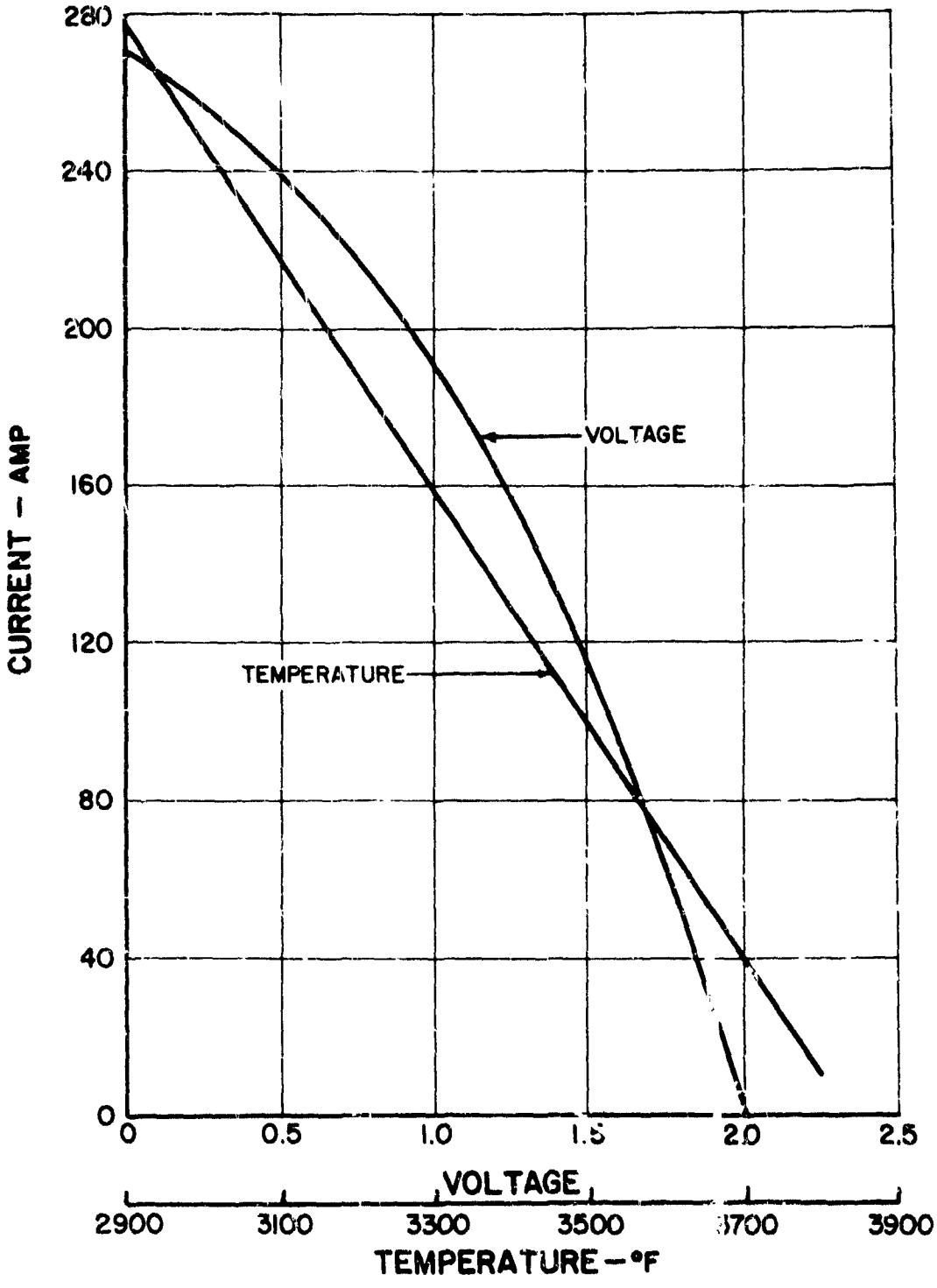

Figure 13 Current-Voltage Characteristics

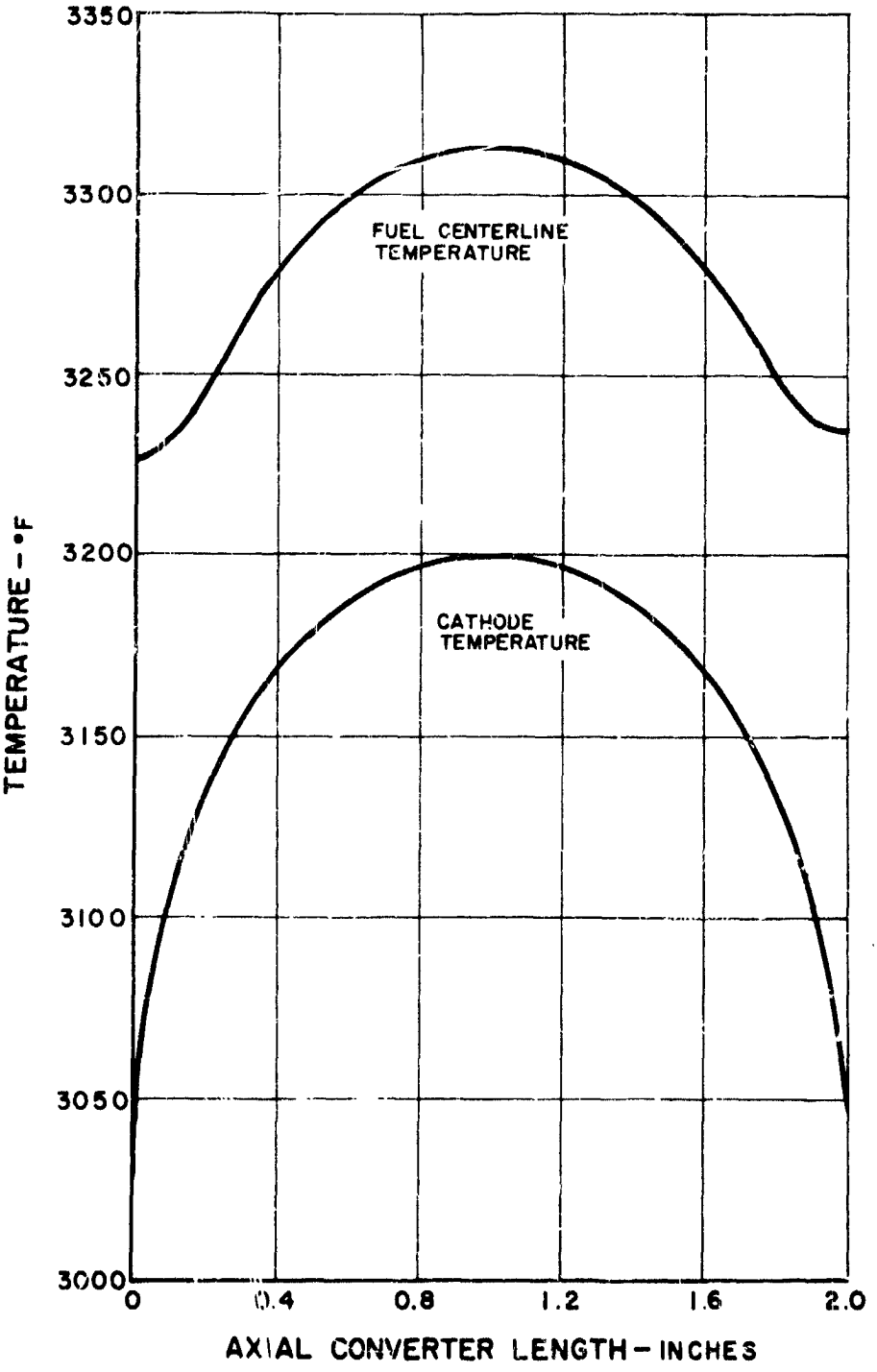

Figure 14 Converter Temperature Distribution

cathode into ten axial sections and by performing a heat balance on each section. The heat source for the fuel is the nuclear energy which is assumed to be generated uniformly through the volume of the fuel. Heat losses for a fuel section are the radial heat conduction to the cathode and the axial heat conduction through the fuel. The ends of the fuel region are essentially insulated by the radiation shields.

Heat inputs to the cathode section consist of the heat conducted radially from the fuel (no thermal contact resistance assumed between the fuel and the cathode) and the electrical resistance heating of the cathode. Heat losses from the cathode consist of the axial heat conduction to adjacent cathode sections, thermal radiation exchange with the anode, electron cooling, and heat conduction through the cesium in the interelectrode gap. End sections also have heat losses through the cathode support and the electrical lead. The electric lead thermal loss calculation included the effect of electrical resistance heating in this structure.

The power output of a converter is also affected by the operating anode temperature. A particular optimum anode temperature which results in a maximum power output exists for any converter. This temperature is not selected for the anode operating temperature because it does not result in a minimum system weight. To produce a minimum weight system the anode temperature is optimized by a tradeoff between reactor weight and radiator weight. This compromise results in an optimum system anode temperature which is higher than the optimum thermionic value.

The effect of the circumferential temperature variation on the anode due to uneven cooling of the close-packed elements was previously investigated for the elements of a one-megawatt system, and was described in Report PWA-2224. That study indicated that the effect of the temperature distribution is negligible. Since the converter and element designs for this powerplant are similar to those for the previous study, it can be concluded that the effect here will also be negligible.

Four modes of converter operation were considered in this study, 1) constant voltage, 2) constant thermal power, 3) constant cathode temperature, and 4) maximum efficiency. The design of the converters for the reactor was based on the constant volt-

age mode of operation with maximum cathode temperature limit of 3200°F. A discussion of the relative merits of each mode and the reasons for the selection of the constant voltage mode are given in the section covering reactor performance.

2. Fuel Element Performance

The thermionic fuel element consists of sixteen converters connected in series. This connection of converters with varying thermal inputs due to the nonuniform thermal power distribution in the reactor, gives rise to a number of problems which do not exist for individually operating converters. A circuitry analysis was conducted for the designed fuel element to investigate these problems. A description of the analysis is given in Report PWA-2224. The analysis considered the thermal and electrical characteristics of each of the converters and determined the variations in the converter operating parameters as a function of their axial location in the reactor.

Figure 15 shows the axial thermal power distribution occurring in the core. The thermal power input for each converter was averaged according to this distribution, which results in differing thermal inputs to each converter as shown in Figure 16. The increase in anode

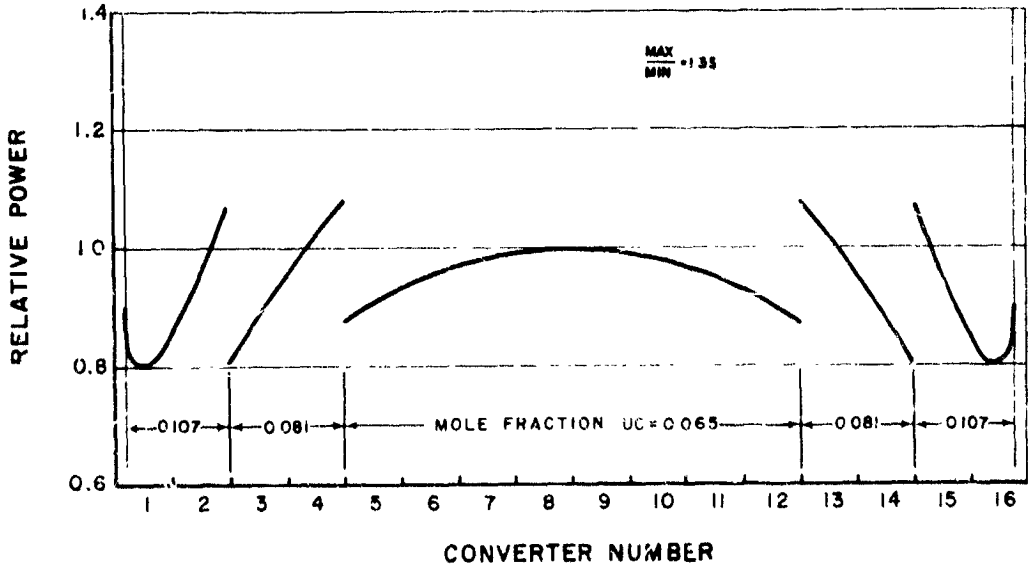

Figure 15 Axial Power Distribution

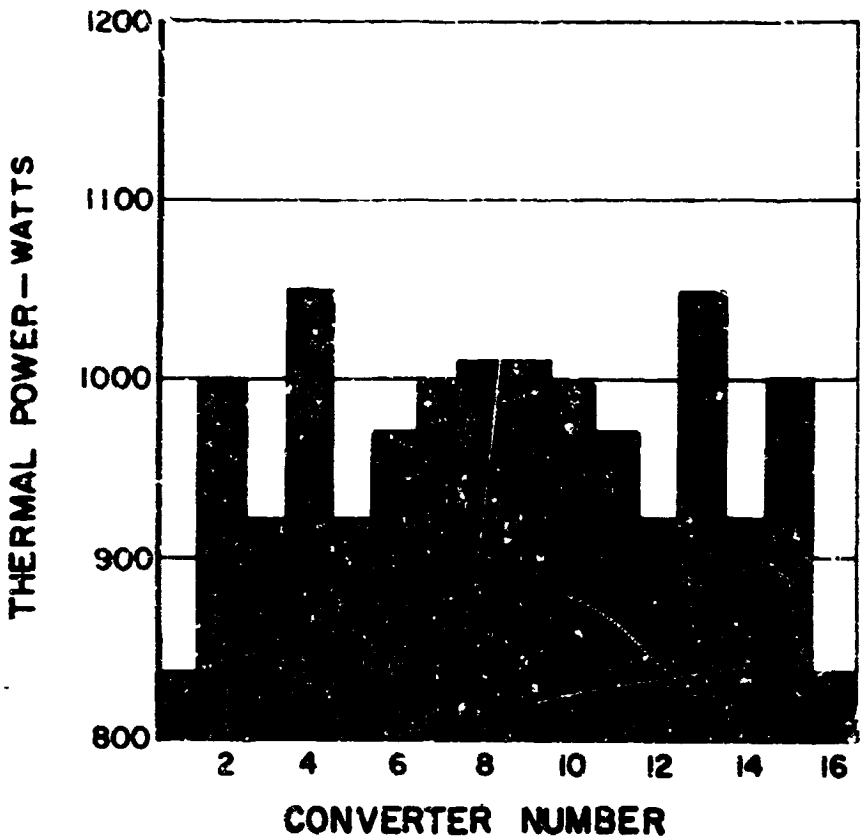

Figure 16 Thermal Power Input

temperature due to the coolant temperature rise in the reactor is shown in Figure 17. Since the thermal input to each converter is different, the thermal and electrical characteristics are different. Figure 18 shows the difference in the cathode operating temperature for each converter at the reference operating condition. This condition was set by limiting the cathode temperature of the hottest converter to 3200°F. (Of course, the current through each converter is the same). As can be seen, only a few of the converters attain this condition due to the different thermal inputs to each converter. For the same reason, the electrical power output from each converter is also different as shown in Figure 19. Moreover, as will be shown below, the power delivered from each converter is not the maximum power output that the converter is capable of, since the maximum occurs at different currents for each of the converters. To attain the maximum power output from the fuel element requires obtaining the maximum power output from each con-

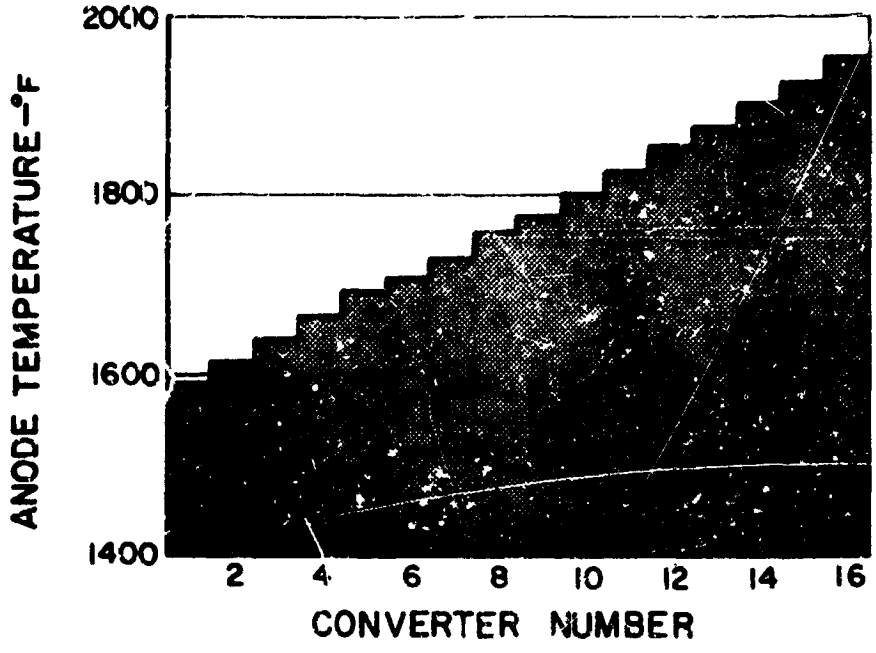

Figure 17 Anode Temperature

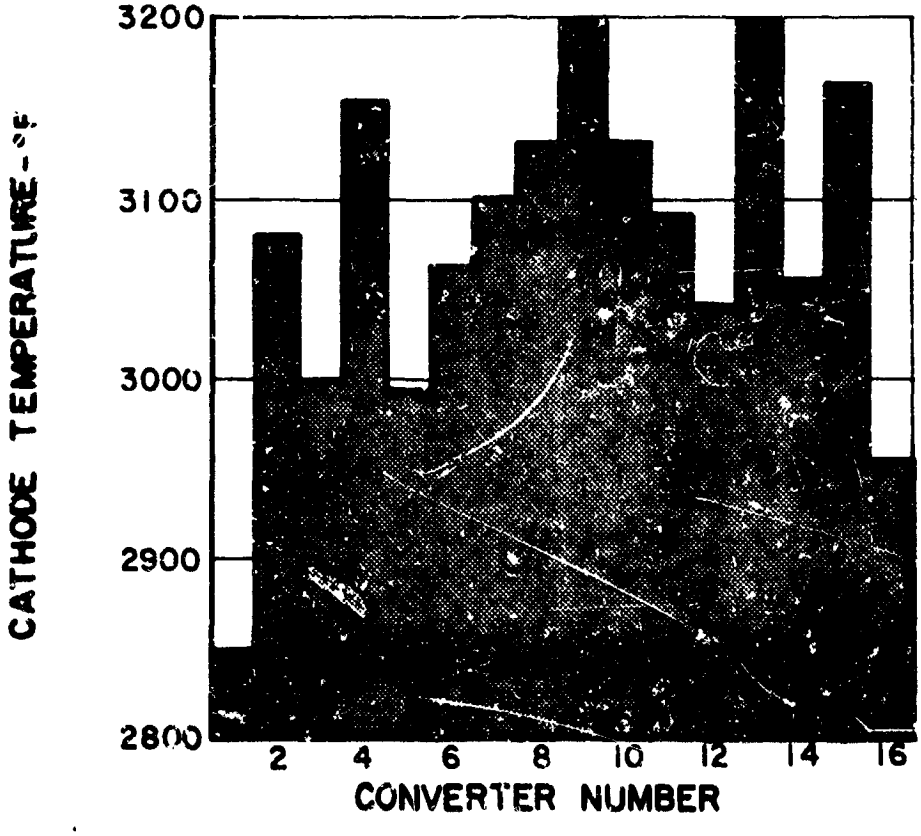

Figure 18 Cathode Temperature

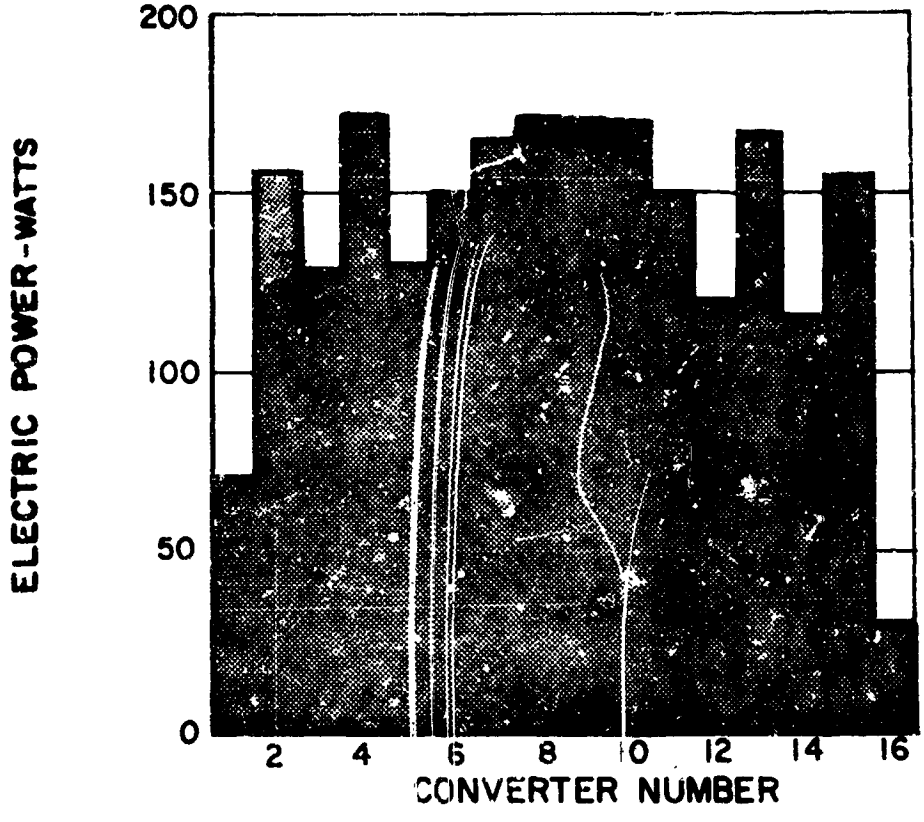

Figure 19 Electric Power

verter at the same series current. Essentially this means that the electrical characteristics of the converters must be matched by adjusting the thermal power inputs. A study has been made to investigate this problem and is presented in Appendix 6.

Figure 20 shows the current-voltage characteristics for three converters in the fuel element. The characteristic of each converter was determined by the method given in Section IV. E. 1. above. Shown in Figure 21 is a plot of power output versus current for the same three converters. As can be seen, the maximum power output from each converter occurs at a different current so that at the reference current converters two and three are operating at less than their maximum power output. This situation occurs for a number of the converters in the fuel element. Obviously it would be desirable in order to reduce system weight for each converter to produce peak power. Appendix 5 also gives the results of the studies concerned with the methods possible for accomplishing this.

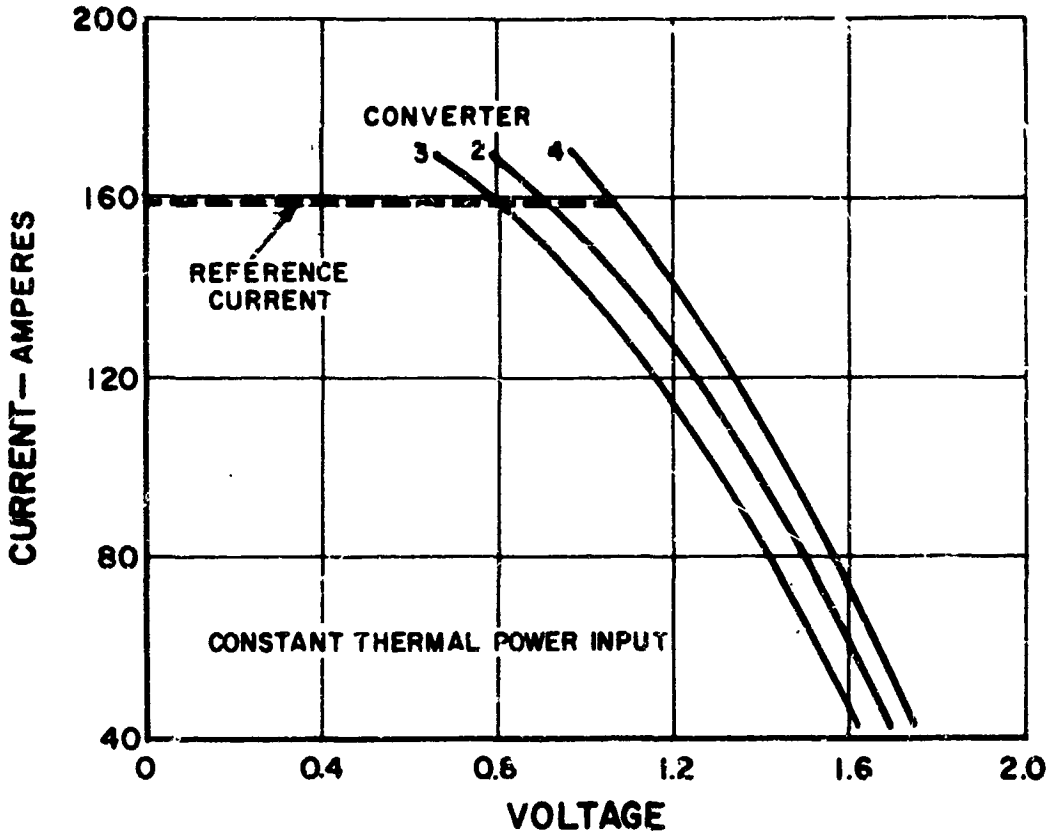

Figure 20 Current-Voltage Characteristics for First Three Converters

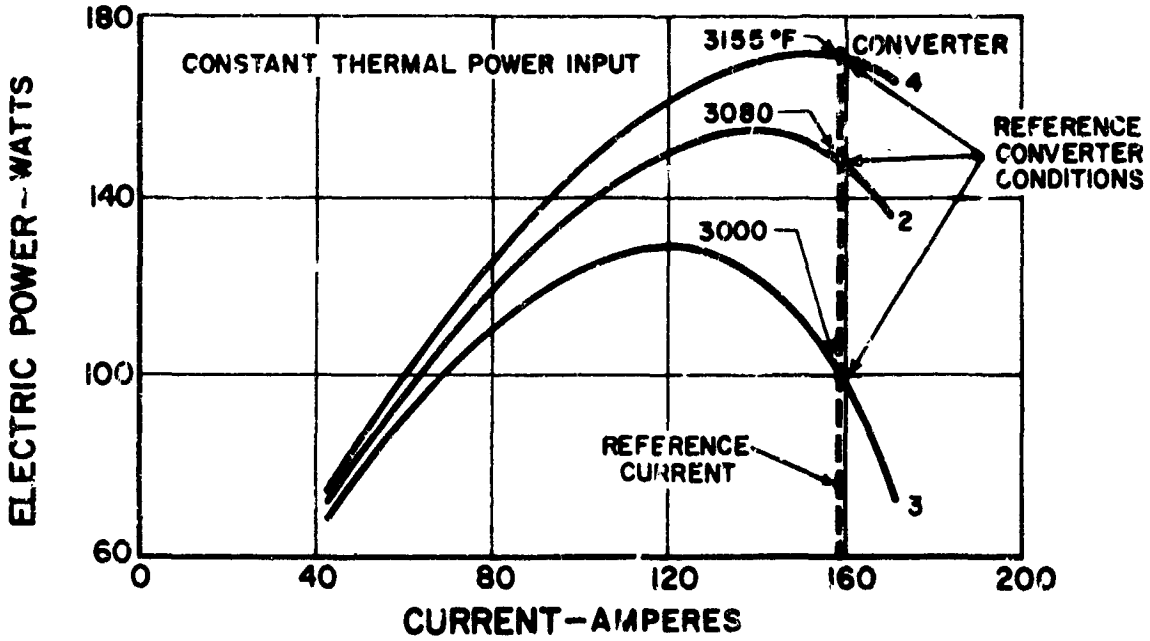

Figure 21 Electric Power vs Current

The variations in performance of the converters discussed above are a result of the nonuniform thermal power distribution in the reactor. In order to account for this in calculating the number of converters required to deliver the rated power of the reactor, an effective cathode temperature was employed. This temperature was determined so as to represent the thermal and electrical characteristics of an average converter. To show the penalties incurred due to the nonuniform power distribution in the reactor, as opposed to a hypothetical uniform distribution, calculations were performed for the previous one megawatt powerplant study and the results are presented in Report PWA-2224. Those results showed that an 18 per cent degradation in power was incurred for the one megawatt reactor due to nonuniform power distribution. Also, those results showed the reduction in effective current density and efficiency and the increase in optimum cathode temperature.

To operate each diode at its optimum cesium pressure would involve severe design problems. For this reason all of the fuel elements in each assembly were designed with a common cesium reservoir. A study was performed for the previous one megawatt reactor to determine the sensitivity of the reactor power output to cesium reservoir temperature. The result of that study showed that the reactor power output was fairly insensitive to variations in cesium temperature.

3. Reactor Performance

The severity of the effects of reactor thermal power distribution was reduced by dividing the reactor core into regions and adjusting the fuel composition to compensate for neutron leakage. The resulting radial and axial thermal power distributions are shown in Figures 22 and 15 respectively. The reactor fuel composition and material volume fractions for each region are shown in Tables 3 and 4, respectively. As can be seen from Table 3, the fuel compositions required vary over a broad range of UC concentrations, from 14 to 56 mole per cent of UC. This indicates that many different fuel compositions must be investigated to allow a flattened power distribution. For this reactor study, fuel evaporation rates for all regions were less than about 2 mils/year. However, for smaller higher temperature reactors where higher concentrations of UC will be required, fuel evaporation may present a significant problem.

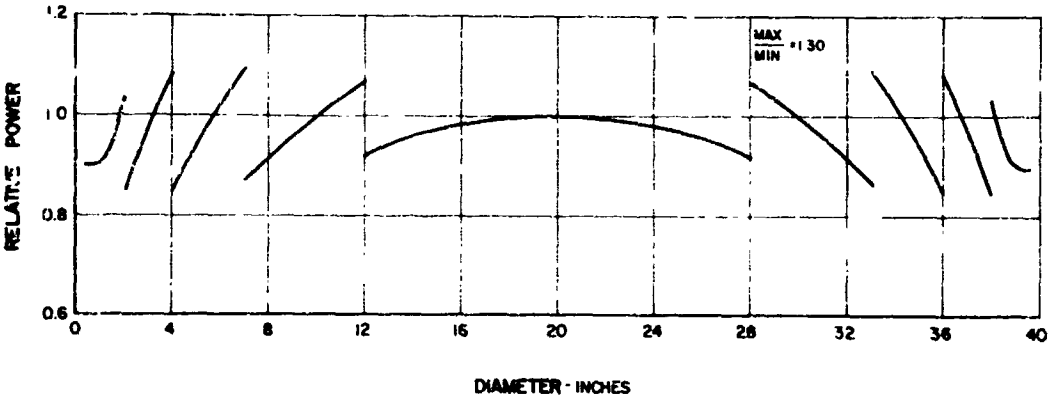

Figure 22 Radial Power Distribution

TABLE 3

Reactor Fuel Composition

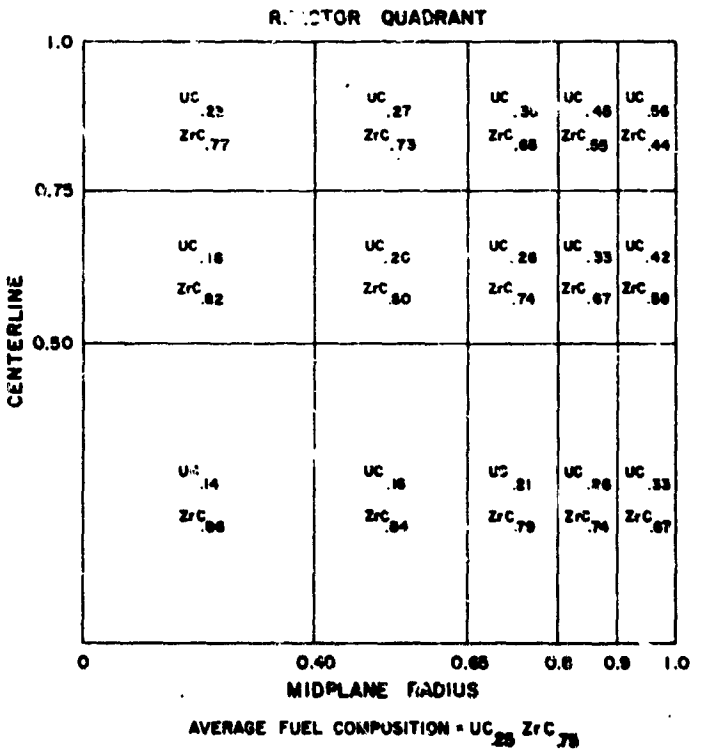

TABLE 4

Reactor Region Volume Fractions

Region	UC(93%)	ZrC	Cb	W	Ta	BeO	Li^7
1	.065	.343	.229	.081	.014	.041	.093
2	.075	.333					
3	.095	.313					
4	.121	.287					
5	.148	.260					
6	.081	.327					
7	.094	.314					
8	.119	.289					
9	.151	.257					
10	.185	.223					
11	.107	.301					
12	.124	.284					
13	.157	.251					
14	.200	.208					
15	.244	.164					

The criticality calculations for the reactor were determined utilizing multigroup two-dimensional diffusion theory. The fuel loading required to achieve and maintain criticality for the mission is 1251 kilograms of 93.5 per cent enriched uranium monocarbide. The reactor is not criticality limited, but limited rather by the number of converters necessary to meet the electric power requirements. As a result, ample room exists for the fuel in the converters and the fuel is diluted with ZrC.

As was mentioned previously, four modes of converter or reactor operation were selected for consideration. Figure 23 shows a plot of the reactor electric power output as a function of the load resistance for three of the operating modes. This plot was determined for the one megawatt study and is included here for illustrative purposes.

The first mode, constant voltage operation, shown by the lines of constant voltage in Figure 23, requires a variation in thermal power input as the load resistance and the electric power output vary. This mode of operation causes the cathode temperature to decrease as the electric power output decreases from the design point of 100 per cent electric power.

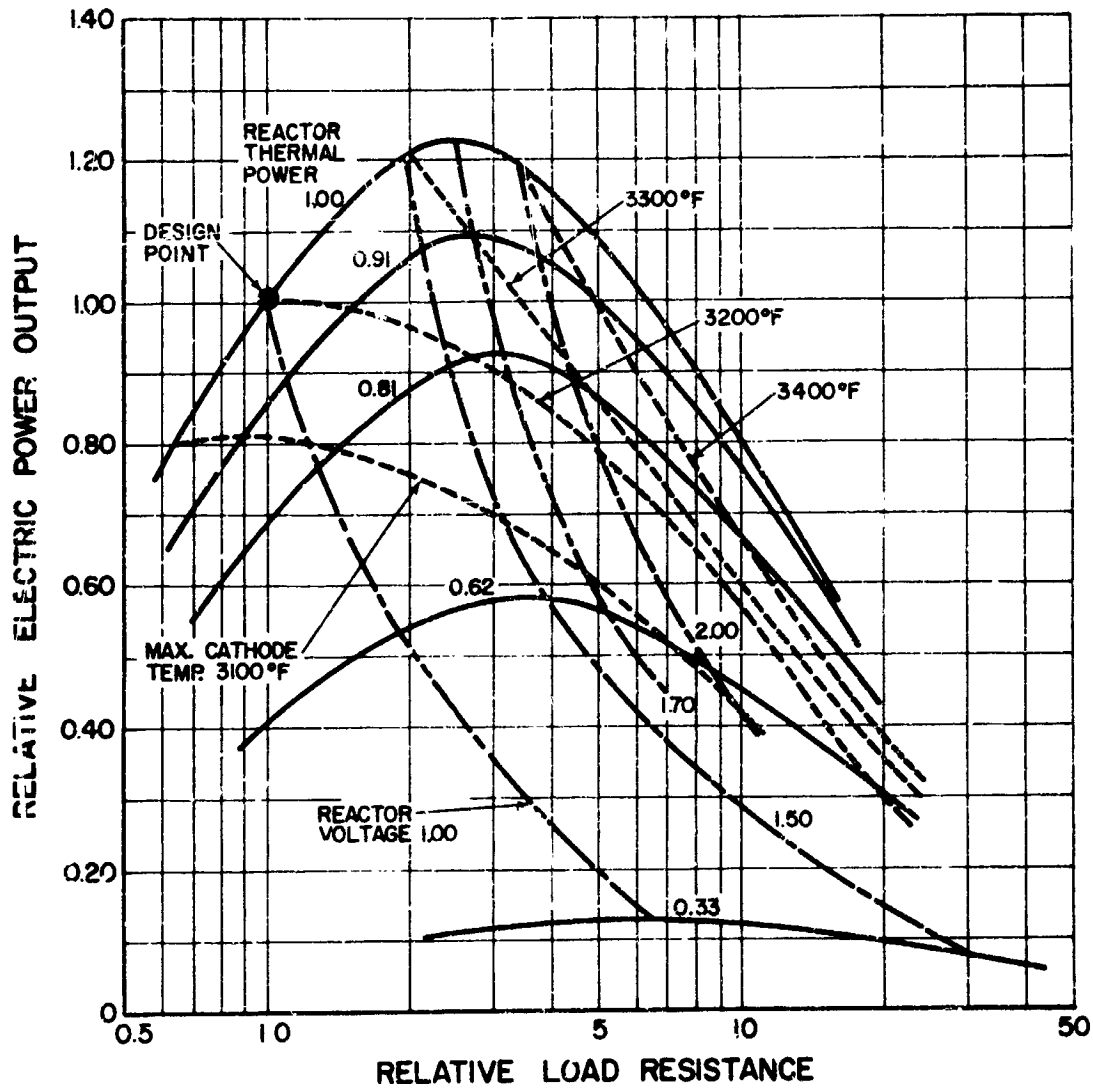

Figure 23 Reactor Performance

The second mode, constant cathode temperature operation, also requires a variation in the thermal power input as the load demand varies. This mode causes the reactor voltage to increase as electric power output and thermal power input decrease. The voltage output can also be made to decrease with decreased electric power demand by increasing the thermal power input. However, the latter method of operation is inefficient since increased fuel burnup is incurred at reduced electric power levels.

The third mode of operation, constant thermal power, requires variations in the cathode temperature and the output voltage. As can be seen, an increase in electric power output can be attained from the design point by an increase in cathode temperature and voltage. The reason for this will be given below. A reduction in electric power from the design point is attained by decreasing both cathode temperature and voltage.

The last mode, maximum efficiency operation, is not shown in the figure but it can be visualized by a line connecting the points of maximum electric power output on each of the constant thermal power curves. Figure 24, a plot of the current-voltage characteristics for the 3.25 MW(e) reactor, shows this operating line. The line connects the points of maximum efficiency which coincide with the points of maximum power output on each of the constant thermal power curves, so that the maximum electric power output is extracted for the given thermal power input.

The mode of operation selected in this study is the constant voltage mode, based on the desire to supply constant-voltage power to the power-conditioning equipment. A maximum cathode temperature limit of 3200°F was selected as the limiting criterion so that at 100 per cent electric power output the temperature of the hottest converter in the fuel elements does not exceed 3200°F. The converters as well as the entire system were optimized at 100 per cent power output based on this mode of operation. The converter operating parameters determined with this criterion dictated a given set of thermal and electrical characteristics for the converters.

The selection of a limiting criterion, that is, the selection of a parameter and a particular value for that parameter which must not be exceeded, and the selection of an operating line are uncertain at this time, due to a lack of experimental data. Therefore, in the control analysis for the powerplant, two operating lines, constant voltage and maximum efficiency were studied with their corresponding limiting criterion, maximum operating cathode temperature and maximum open-circuit temperature, respectively.

Since it was a purpose of this study to produce a minimum weight system, consideration of a limiting criterion was undertaken. For this purpose, consider a plot of the current-voltage characteristics

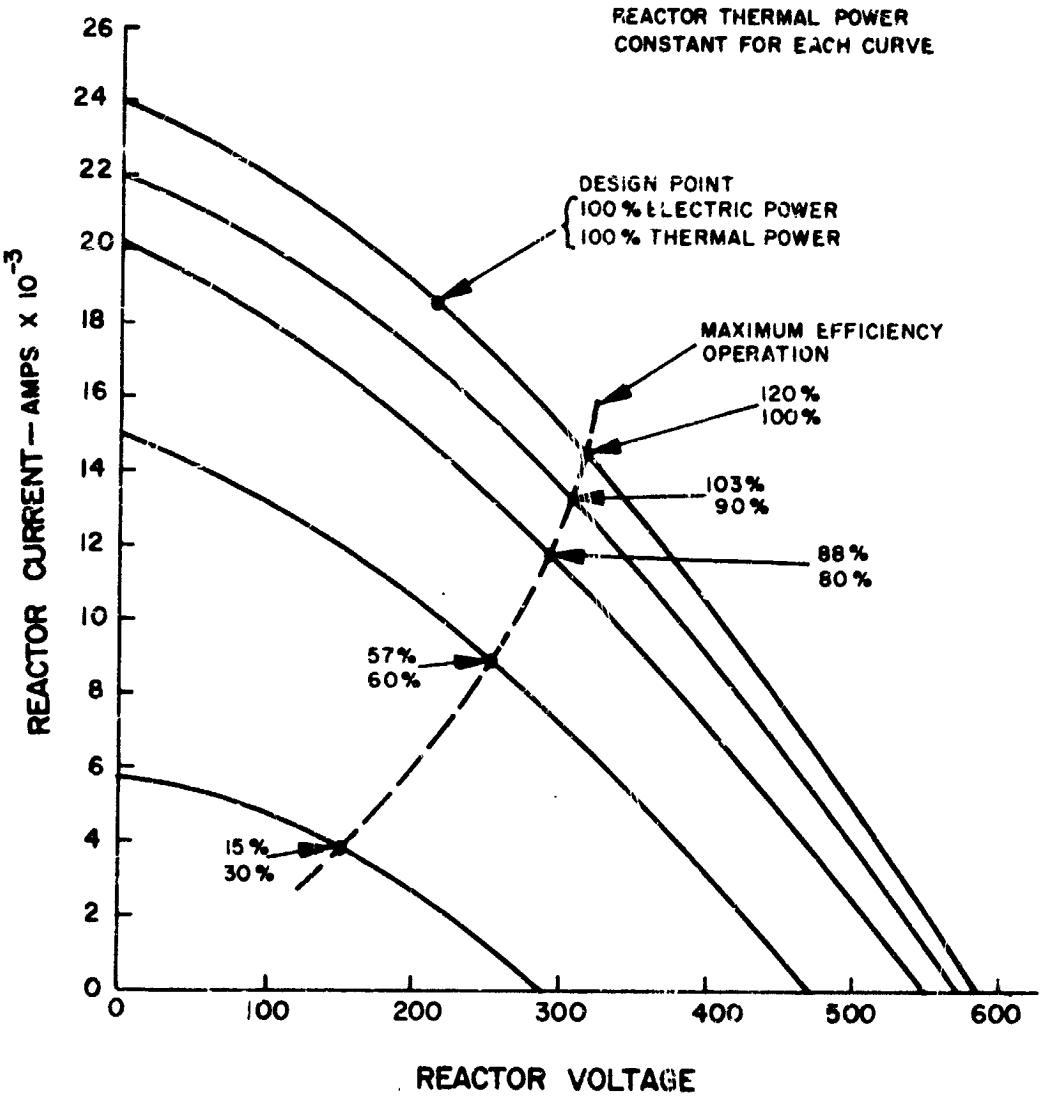

Figure 24 Reactor Electrical Characteristics

of the reactor for constant cathode temperature operation which would produce a plot similar to that shown for constant thermal power in Figure 24. The optimized design point at 100 per cent electric power occurs at the point of maximum power output on the 3200°F temperature line. This point does not correspond to the point of maximum reactor efficiency at the same thermal input

Figure 23 shows that the point of maximum power output and efficiency, based on the thermal power input determined above, does not coincide with the point of maximum power based on constant cathode temperature operation. As the figure shows, a significant increase in electric power could be attained by shifting the design point. With the consideration of the possible increase in power output and the additional consideration of the probability of open-circuit failures in the converters, it appears desirable to shift the limiting criterion to the maximum open-circuit temperature. That is, when optimizing the system, a maximum open-circuit temperature should be selected rather than the maximum operating cathode temperature, since the latter results in a reactor with lower efficiency. However, the two criteria available have two completely different set of requirements, and at present it is not known which requirements are the more stringent. Additional analytical and experimental work is required before the selection of this criterion can be made with confidence.

4. System Performance

a. Main Heat Rejection System

The probability that the system will not be disabled by a meteoroid penetration was assumed to be 0.9000 for this study. This total system probability is the product of the survival probability of each of the following subsystems, 1) primary loop, 2) main radiator and piping, 3) auxiliary power-conditioning radiator and piping, and 4) cesium reservoir coolant radiator. It was assumed that if one of these subsystems is unable to function, then the system as a whole cannot function.

The main radiator system is divided into 16 segments. If one segment fails, the remaining segments continue to function, and it was assumed that any 4 out of the 16 segments would fail during the mission.

There are 16 heat exchangers, each with reactor coolant flowing on the tube side and radiator coolant on the shell side. The heat exchangers are a necessity for redundant heat rejection systems. Film coefficients on the tube and shell side were computed from the Kaufman-Lubarsky correlation for liquid metals with a 1.3 factor on the temperature drop for uncertainty due to

data scatter. Tube and shell pressure losses considered friction and plenum losses.

The heat exchanger tube diameter and tube spacing were held at the minimum values determined from design studies since these parameters had little effect on system weight. The heat exchanger diameter was optimized. The trade-off in weight between the heat exchanger and radiator was accomplished by varying the log mean temperature drop of the heat exchanger.

The radiator panels, which consisted of coolant tubes with straight fins and meteoroid barrier around the tubes, rejected heat from both sides. Coolant pipes carry coolant between the heat exchangers and the radiator panels, and manifolds distribute and collect coolant to tubes in a panel. The heat rejected from the radiator system was computed by the equation below. Components considered to radiate heat are pipes, manifolds, panel tubes (with barrier) and fins. Heat loss from the primary piping is also taken into account.

$$Q = \sigma \left(\sum_i \epsilon_i S_i F_i \eta_i \right) T_m^4$$

where
- Q = total heat rejected
- σ = Stefan-Boltzmann constant
- ϵ_i = component emissivity
- S_i = total component surface
- F_i = component geometric factor
- η_i = component radiating efficiency
- T_m = mean radiator coolant temperature

Radiator tube and fin view factors were computed, assuming that the tube surface is at the mean coolant temperature and that all incident radiation is absorbed (a valid assumption for high emissivities). Manifold and piping view factors were estimated by dividing twice their projected area by their total surface area. The efficiency factor is the ratio of actual heat transfer to the heat that would be transferred if the component surface were at the mean coolant temperature. The radiator tubes, manifolds and pipes were assumed to be at the coolant temperature and therefore had efficiencies of unity.

The fin temperature distribution was determined by an analytical solution given by the equation below. Incident radiation from the radiator tubes was approximated by the use of the calculated view factors but radiation from the sun or planets was neglected.

$$k_f t_f \frac{d^2 T_f}{dZ^2} = 2 \sigma \epsilon_f T_f^4 - q''(Z)$$

where k_f = fin conductivity
t_f = fin thickness
T_f = fin temperature
ϵ_f = fin emissivity
$q''(Z)$ = incident absorbed radiation

The radiator tube pressure drop is the sum of friction and entrance and exit losses. The manifolds were sized to give a total pressure drop (momentum plus friction) of 0.1 times the tube pressure drop. Thus the manifolds will produce negligible flow maldistribution to tubes in a radiator panel. Pipe pressure drop is the sum of pipe friction losses and losses in pipe fittings.

The radiator fin geometry was optimized for minimum weight. The tube diameter was selected at the optimum value while tube lengths were determined from the powerplant design. Radiator panel aspect ratios and segment pipe lengths were estimated from design data. In analyzing the reference design, an average radiator panel was studied rather than considering each panel

The meteoroid barrier thickness was computed as shown below. A segment reliability of 0.8394 was used which, in conjunction with other loops, gave a total system reliability of 0.9000. The barrier equation contains factors for spalling and thin plate behavior. Vulnerable area was taken to be the total outside surface of fluid-containing ducts.

$$t_b = 0.01118 \frac{1}{\rho 1/2\ C^{2/3}} \left[\frac{(A\ \theta)}{-\ln P} \right]^{0.2485}$$

where t_b = barrier thickness, inches
A = vulnerable area, ft^2
θ = mission time, hours
P = probability of no punctures during time θ
ρ = density of barrier, gms/cc
C = velocity of sound in barrier, km/sec

b. Auxiliary Radiator

The components of the power-conditioning equipment must be cooled to maintain their temperature less than 500°F. The rejection of this heat to space requires a large radiator because of the relatively low temperature. However, this radiator is light in weight because all-aluminum construction was used.

For the purpose of calculating meteoroid barrier thickness, the radiator was considered to be a nonredundant system. It was

assumed that the powerplant would cease to function if a segment were punctured. Actually the conditioning equipment is divided into 4 modules, each with its own radiator, and failure of a segment would reduce the power-handling capability of the conditioning equipment by only one-quarter.

The hydraulic and heat transfer analyses for the auxiliary radiator are essentially identical to that of the main radiator. The performance was determined for deep space.

The heat removed by the auxiliary radiator was 7 per cent of the power input to the conditioning equipment. The radiator inlet coolant temperature was fixed at 500°F and the fin dimensions and coolant flow rate were optimized for minimum system weight. The radiator tube diameter was held at the optimum value.

c. Cesium Reservoir Coolant Radiator

Heat is transferred through the thermal insulator plate between the reactor coolant inlet plenum and the cesium coolant. This heat is rejected by an auxiliary radiator to maintain the reservoir at the required temperature. The heat transfer and hydraulic calculations are similar to those of the other radiators. The mean radiator coolant temperature was set equal to the optimum cesium temperature for best system performance.

d. Electromagnetic Pumps

Support studies conducted for the one megawatt powerplant included a study of multichannel electromagnetic pumps for the reactor coolant and for the main radiator circuit (see Appendix J of Report PWA-2224). The results of the study established pump weight as a function of pump efficiency and coolant flow rate. This data was used to determine pump efficiencies for the best system performance. The final pump design is not the optimum design indicated by the powerplant performance study. Because of the low pump voltages the pumps were connected in series to increase the voltage of the pump power supplied by the power-conditioning equipment. This necessitates a redesign of the pumps since the circuitry requires the matching of currents of different pumps connected in series. The final design therefore, was a compromise between the optimum pump design and a desire to build up high voltage by series connection.

e. System Analysis Methods

The methods used to analyze the reference system are an extension of those used to conduct the parametric studies described in Report PWA-2319. Certain detailed considerations were added to permit greater depth in the analysis and a better understand-

ing of powerplant characteristics. The most significant addition includes the effects of nonuniform reactor power distribution. A discussion of these effects is given in Section IV. E. 3. above. The methods used for analysis are given in Report PWA-2224 under the heading of circuitry analysis.

F. System Startup

A preliminary study of powerplant temperature and environment control during powerplant startup was performed. The purpose of this study was to outline a launch and startup procedure within current tentative temperature, loading and safety considerations, and to estimate the weight of required system startup equipment.

Powerplant startup as considered in this study comprises three phases. The first phase includes the final assembly of the powerplant, preparatory to launch. The second phase is the period between final system assembly and booster firing. The third phase is the time between booster firing and reactor power operation.

The general procedure for startup is to preheat and fill all lithium-containing components on the launch pad, allow them to cool slowly during the time between launch and orbit confirmation, and lastly to start the reactor for power operation. Preheating and filling the lithium components on the ground increases the reliability and practicality of this operation. Allowing a system cooldown reduces the weight of on-board auxiliary power sources by eliminating the need for thermal energy input to the lithium after launch. Startup of the reactor in space is required by safety criteria which preclude reactor startup until a proper orbit is confirmed. Component temperatures must be maintained during this time, since the liquid metal loops are filled on the launch pad. Therefore, the liquid metal must be kept hot and circulating to prevent it from freezing in local cold spots. While the powerplant is on the ground external power can be supplied to maintain the proper thermal conditions. However, after the vehicle is launched all power sources for the vehicle must be carried aloft. Obviously, it is desired to obtain a system which requires the minimum amount of weight. Based on this study and on the previous study for a one-megawatt powerplant, a temperature control system using a low-emittance coating applied over the high-emittance coating on the high-temperature main radiator and on the fairing was chosen. This method of controlling the powerplant temperature consists of heating the powerplant to some prescribed temperature on the ground and allowing it to cool after launch. The rate of cooling and hence the temperature achieved at any given time after launch are controlled by the emissivity of the radiator and the fairing surfaces.

It should be noted that a high evaporation rate for the low emissivity coating applied to the main radiator is required to allow this coating to evaporate when the radiator temperature begins to increase, after the initiation of reactor power operation.

An additional problem which complicates the system startup procedure is the high rate of oxidation of columbium - 1 zirconium in air. To prevent the oxidation of this alloy requires the containment of powerplant components in an inert atmosphere while the powerplant is on the launch pad, and during the time between launch and attainment of orbital altitude. The containment of components is accomplished with the use of component enclosures which can be jettisoned in orbit.

A summary of prelaunch, launch and orbital startup procedures is given in the following outline.

1) Pre-Startup

   a) Assemble powerplant to booster vehicle
   b) Evacuate air from inside component enclosures
   c) Fill enclosures with helium
   d) Circulate helium through remainder of fairing
   e) Fill low temperature auxiliary radiator with oil and circulate
   f) Fill and circulate helium in main piping and heat to 700°F
   g) Evacuate helium from main piping
   h) Fill main piping with lithium at 700°F
   i) Circulate lithium and supply heat to maintain at 700°F

2) Umbilical Cord Components

   a) Electric power for pumps and controls
   b) Instrumentation and control leads
   c) Electric power for heating lithium
   d) Helium piping for fairing coolant

3) Startup

   a) Launch
   b) Switch to on-board power for lithium pumps
   c) Bleed helium from fairing
   d) Bleed helium from component enclosures
   e) Achieve criticality, after establishing orbit
   f) Jettison fairing and enclosures
   g) Go to full thermal power with no load
   h) Calibrate neutron counting with reactor thermal power. This establishes maximum thermal power with neutron counting

i) Connect reactor to conditioning equipment and load
j) Bring cesium temperature up to operating temperature (650°F) from about 460°F

The status of each of the powerplant components is given in the table below during the startup sequence.

Stage	Component	Status
pre-launch (after lithium fill)	reactor	external power on, heated to 700°F, EM pump idling
	main radiator	external power on, heated to 700°F, EM pump idling
	auxiliary radiator	external power on, pump operating at 200°F
	cesium radiator	external power on, heated to 700°F, EM pump idling
	power-conditioning equipment	at auxiliary radiator temperature
	fairing package	helium flowing through at 150°F
launch and orbit	reactor	internal power on for idling EM pump, temperature decaying
	main radiator	internal power on for idling EM pump, temperature decaying
	auxiliary radiator	pump not operating, temperature slowly decaying
	cesium radiator	internal power on for idling EM pump, temperature decaying
	power-conditioning equipment	temperature slowly decreasing
	fairing package	internal vacuum after first 6 minutes
reactor startup	reactor	go critical, temperature increases
	main radiator	temperature increases, coating evaporates off
	auxiliary radiator	pump operating
	cesium radiator	adjust temperature for optimum cesium pressure
	power conditioning equipment	heats to operating temperature
	fairing package	jettison fairing and enclosures

The relative location of components inside the fairing at launch condition is shown in Figure 25. Also shown in the figure are the individual component enclosures. This method of maintaining an inert gas over the

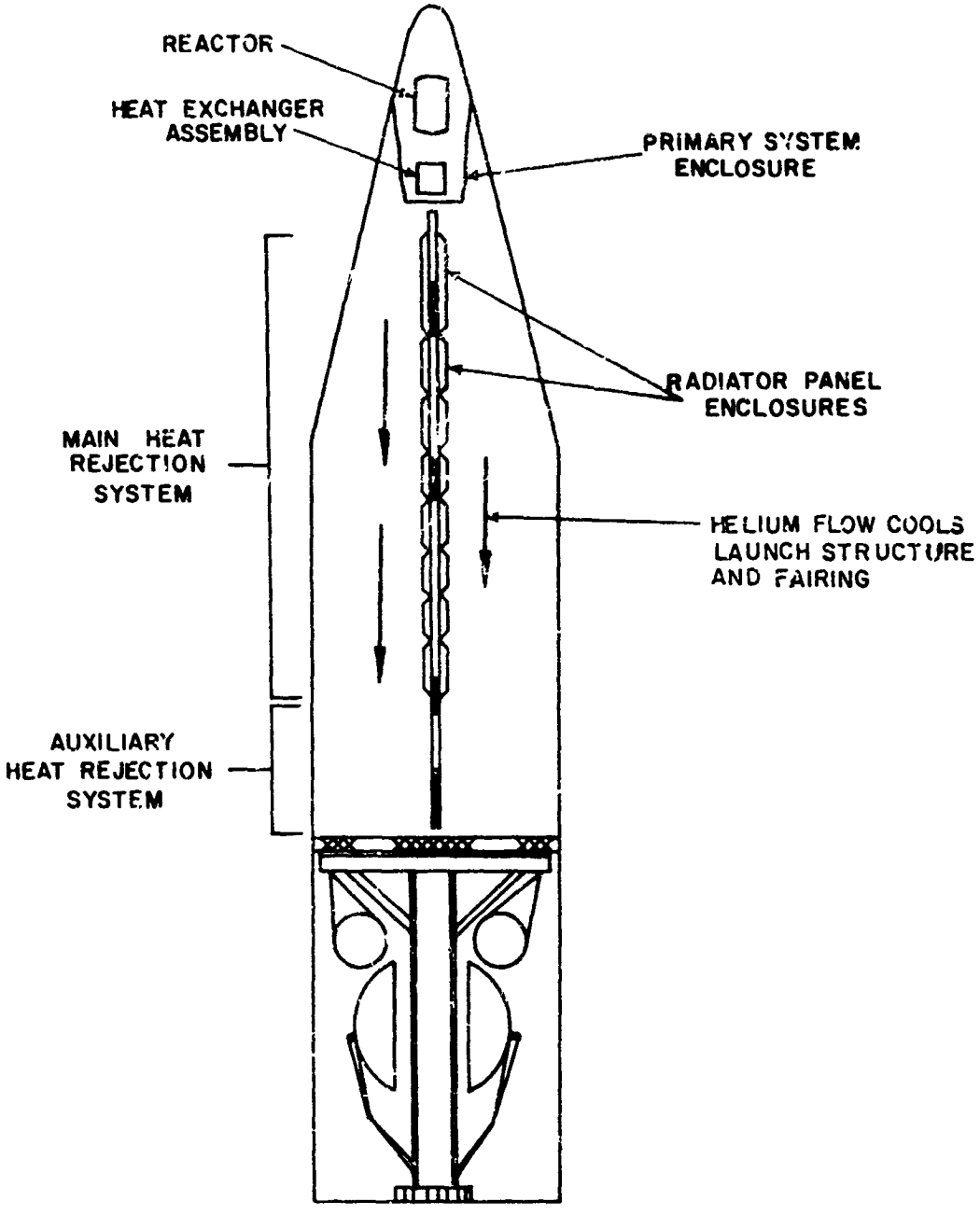

Figure 25 Powerplant Arrangement at Prelaunch Condition

components was selected instead of using the entire fairing, because of the extremely large size of this system. A single fairing enclosure would present difficult fabrication and sealing problems. In addition, the use of individual enclosures allows a flow of helium in the fairing which cools the fairing, the support structure and the aluminum auxiliary radiator system. Maintaining these components as cool as possible is important in order to insure their structural adequacy during launch. Temperatures less than 200°F can be maintained in these components by insulating the component enclosures and by causing a cooling gas to flow through the fairing which has an average temperature of 150°F and a temperature increase of about 50°F.

The monoisopropylbiphenyl coolant in the low temperature auxiliary radiator should remain in the vicinity of 200°F during the pre-launch period without any special cooling or heating other than the fairing cooling gas. The low temperature aluminum radiator is not enclosed but employs radiation baffles so that the radiator does not see the fairing opposite the main radiator. To prevent hot spots in the power-conditioning equipment package, the MIPB coolant is circulated during the pre-launch period. The MIPB pump for this purpose requires about 0.6 KW of external power.

After completion of the liquid metal fill, the lithium must be continuously circulated so that local freezing does not occur. If the primary and secondary electromagnetic pumps can be operated satisfactorily at 10 to 15 per cent of their rated power, then electrical pumping power requirements for the primary and secondary loops will be about 5 KW. An additional pre-launch power requirement will be to supply heat at the rate of 215 KW to compensate for losses from the primary and secondary loops to the fairing and its cooling gas.

During the pre-launch period, component temperatures are as follows:

secondary loop - 700°F
primary loop - 700°F
fairing - 200°F
power-conditioning equipment - 200°F
low temperature radiator - 200°F

At the time of launch, all external heating and cooling power is removed from the powerplant package and it undergoes a thermal transient until full power reactor operation is achieved. The flow of cooling gas through

the inside of the fairing also stops at launch and the gas is allowed to bleed from the fairing so that space conditions exist within the fairing at orbital altitude. The time consumed from launch to orbital altitude is approximately 6 minutes. The helium within the protective enclosures can be bled off slowly when launch is initiated, as long as the blanket of inert gas remains to protect the Cb-1Zr until the vehicle is beyond the atmosphere. The main on-board power requirements during the orbital period and prior to startup are for the primary and secondary lithium circulating pumps. These pumps operating at reduced flow rates will require approximately 5 KW of auxiliary power for about ten hours. The three most probable auxiliary power unit systems are fuel cell, chemical dynamic, and primary batteries. From the estimates of weight and volume presented below, the fuel cell at 230 pounds appears to be the best choice.

Comparison of Auxiliary Power Units for 5 KW, 10 Hours, 7-10 Volts

Components	Primary Batteries Ag/Cd Weight (lbs)	Ag/Cd Volume (ft^3)	Ag/Zn Weight (lbs)	Ag/Zn Volume (ft^3)	Fuel Cell Open Cycle Weight (lbs)	Fuel Cell Open Cycle Volume (ft^3)	Chemical Dynamic H_2 and O_2 Weight (lbs)	Chemical Dynamic H_2 and O_2 Volume (ft^3)
Power unit	1660	8.8	665	4.25	175	3.5	81	7.5
Reactants and tankage	-	-	-	-	55	2.5	150	10.0
Power-conditioning	10	-	10	-	-	-	40	-
Estimated Total	1670	8.8	675	4.25	230	6	271	17.5

Temperature control methods for this study were limited to the use of radiator coatings of 0.1 and 0.2 emissivity in addition to the normal radiator coating emissivity of 0.9. The low-emissivity coatings will evaporate off the main radiator as its temperature increases during startup, leaving the normal 0.9 emissivity surface. Other coatings as well as combinations of coatings and super-insulations were investigated in the previous one-megawatt powerplant startup study. Figure 26 shows the cooldown rate assuming a 0.1 emissivity coating on the main radiator as well as on both the inside and outside surfaces of the fairing. As the figure indicates, the lithium temperature has dropped to about 460°F after 10 hours, or about 100°F above the freezing point. For a system employing a NaK radiator, a much longer cooldown time would be allowed, (about 50 hours) due to the low melting point of NaK.

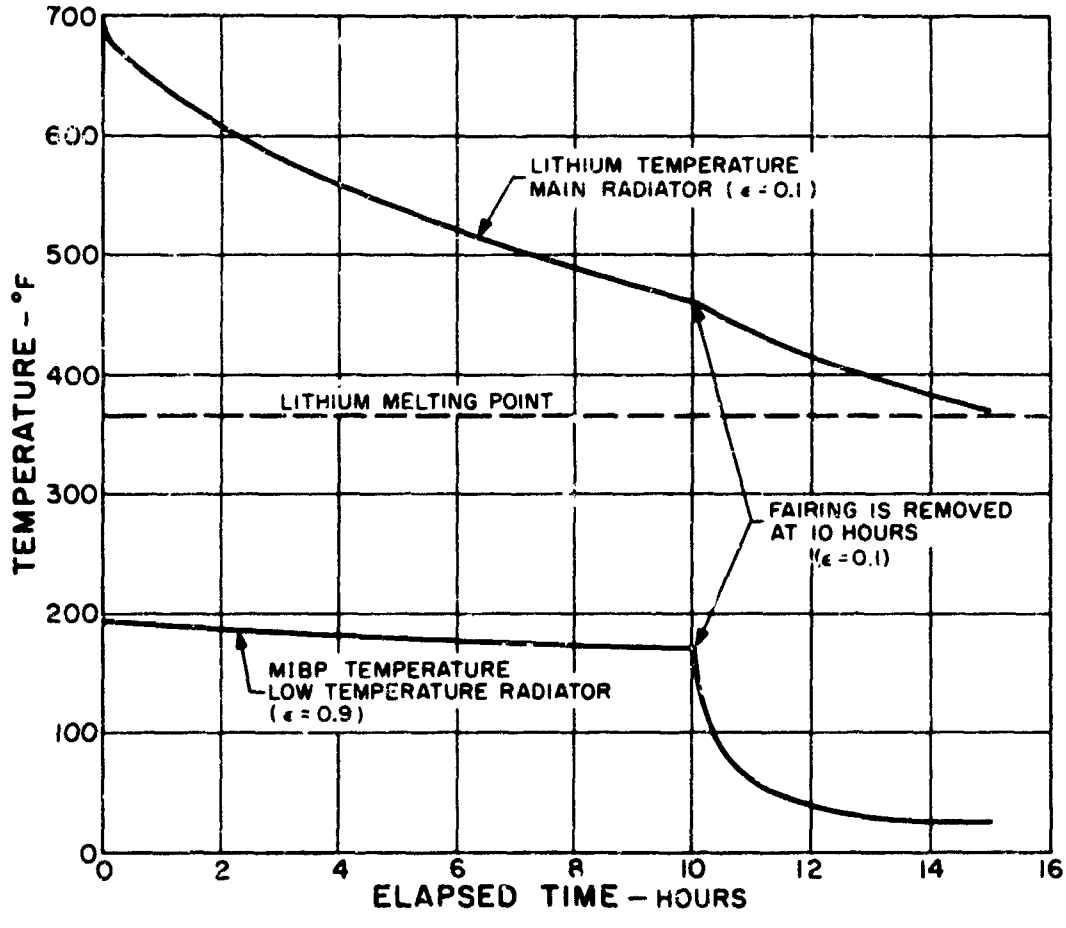

Figure 26 Prestartup Radiator Temperatures. Main Radiator $\epsilon = 0.1$

Also indicated in the figure is the cooldown rate for the low-temperature auxiliary radiator which has an emissivity of 0.9. A low-emissivity coating is not used for the latter because it does not reach high enough temperatures to evaporate the coating. The MIPB coolant temperature drops very slowly to about 170°F after 10 hours and then cools rapidly when the fairing is removed in preparation for startup. Similar calculations were performed for the main radiator using a coating emissivity of 0.2 throughout. These results, presented in Figure 27, indicate that the lithium has reached its freezing point of 367°F after 10 hours. It should be noted that the effect of the component enclosures acting as a heat resistance is not included in these calculations and will present another radiation barrier to further reduce the cooldown rates shown in both figures.

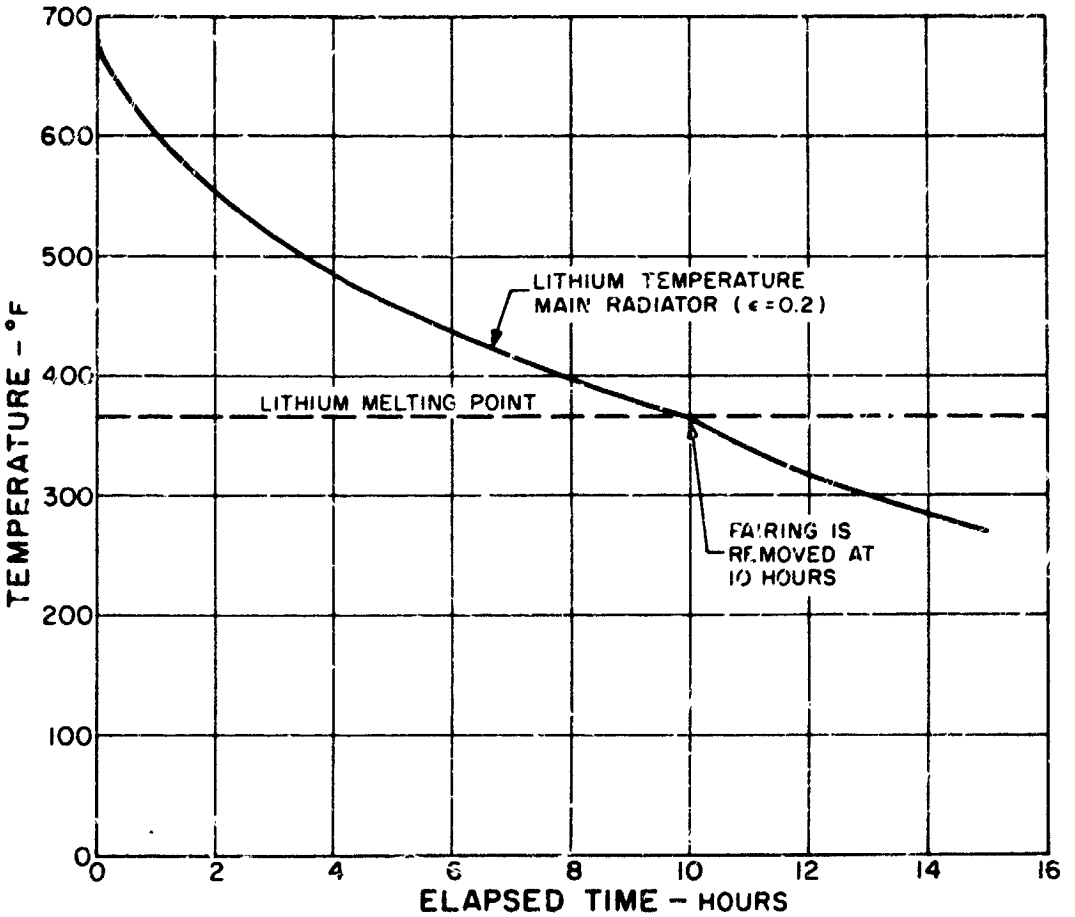

Figure 27 Prestartup Radiator Temperatures. Main Radiator $\epsilon = 0.2$

Radiator cooling rates are greater for the 3.25-megawatt system study than for the one-megawatt system study, due primarily to the lower mass per unit area of the former compared to the latter. This has occurred because of the new meteoroid barrier thickness calculation which has reduced the barrier and also because of the lower minimum radiator tube diameter used in the 3.25-megawatt study.

After a satisfactory vehicle orbit has been confirmed, the reflector segments of the reactor are brought into position and the control drums rotated to achieve criticality. The fairing structure and component enclosures are then jettisoned by explosive connectors as shown in Figure 28. The next step is to go to full thermal power under no-load conditions

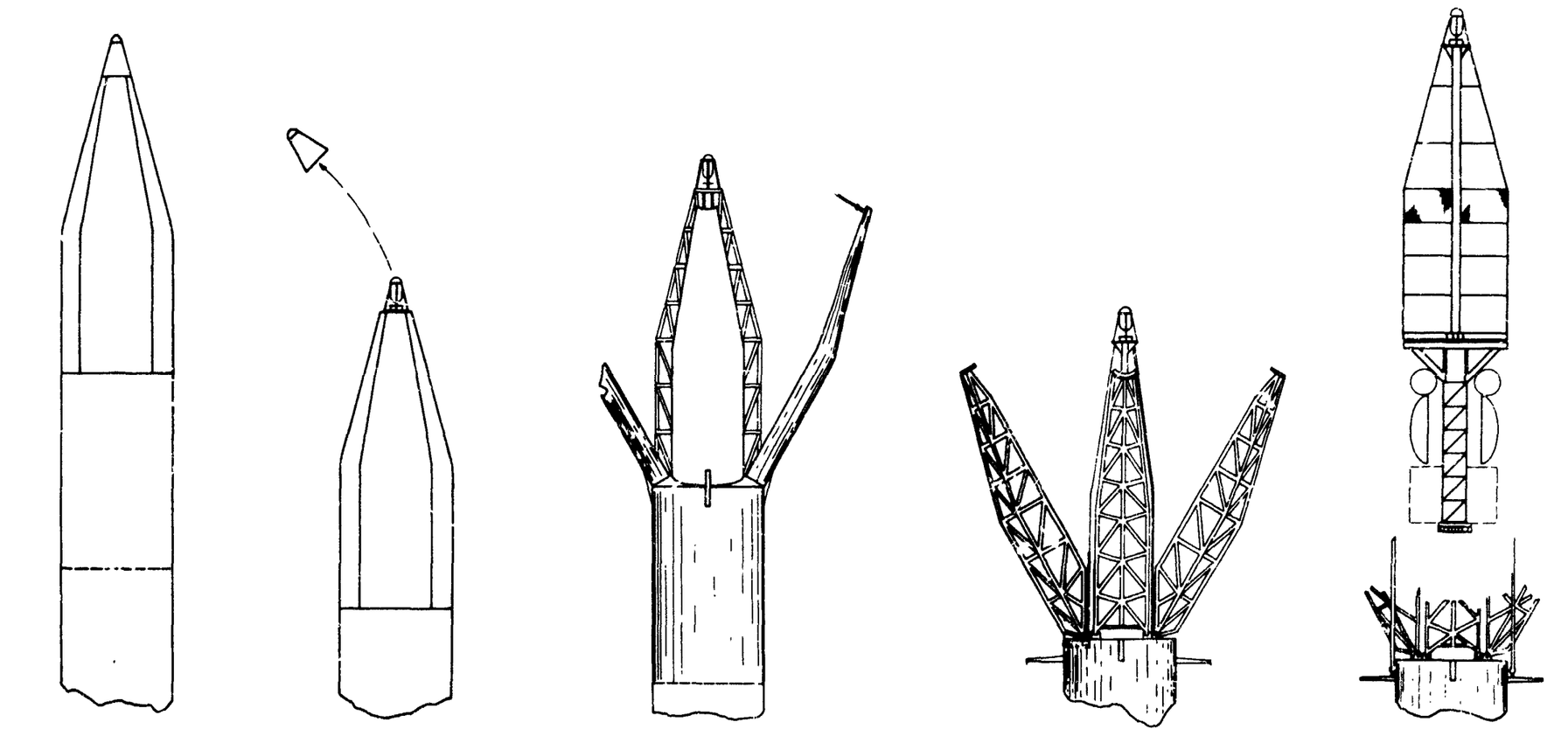

Launch Configuration | Jettison Nosecone | Jettison Fairing | Jettison Launch Structure | Inflight Configuration

Figure 38 Jettisoning of Launch Structure and Fairing

and calibrate the neutron counting with the maximum thermal power. The circuit connecting the reactor with the power-conditioning equipment and the load is closed and cesium temperature adjusted to an optimum value.

Problem Areas

To reduce internal power requirements, it was assumed that the DC EM pumps can be idled at 10 to 15 per cent of their design power without cessation of fluid flow. Approximately 90 to 95 per cent of the onboard power is consumed by these pumps so that development of EM pumps with good reduced power performance is desirable.

Another problem area in the present startup procedure is the point at which the reactor is taken to full thermal power for control calibration. At this point the liquid metal pumps are operating on auxiliary power at reduced flow rates since power is not yet available from the reactor. A detailed startup study would be required to determine component temperatures as reactor power is increased.

As shown in the cooldown curves of Figures 26 and 27, component temperatures can be maintained at satisfactory levels with an emissivity of 0.2 on the fairing and main radiator surfaces. However, if a pre-startup period of longer than 10 hours is required, some additional means of temperature control is necessary.

Detailed temperature studies for the system as well as for the individual components are necessary. A detailed study of transient sink temperature and radiator orientation for the particular orbit will be required. The assumption of a 0°F constant temperature sink for this study is only approximate since equivalent sink temperatures vary over several hundred degrees with radiator orientation to sun and earth, and with position in the orbit. Sink temperatures are also greatly different for the two radiating faces of the panel. Temperature control of the entire launch package or of each component individually is possible by controlling the orientation of the surface and its radiation characteristics. Surface orientation such as always parallel or perpendicular to the sun-earth vector would require attitude control. Surface radiation characteristics which affect heat loss and heat input are primarily solar absorptance (α_s) and thermal emittance (ϵ_t). Since the main purpose of temperature

control on a system such as this is to maintain liquid metal temperatures well above the freezing point, the most desirable ratio of these two properties would be a high ratio of α_s to ϵ_t. Other factors tending to maintain radiator temperature are the longer time of sun exposure than of dark side exposure for a typical 300-mile earth orbit and the high specific mass and heat capacities of the radiators.

Calculations of maximum and minimum coolant equilibrium temperatures with fairing removed were made for the main radiator for assumed values of α_s / ϵ_t and for a constant radiator attitude perpendicular to the earth-sun vector. α_s / ϵ_t values of 1, 3, and 5 were assumed, resulting in maximum lithium temperatures of 160°F, 345°F, and 456°F and minimum lithium temperaturesof 140°F, 280°F and 354°F respectively. These results show that very high values of α_s / ϵ_t will be required for this method of temperature control since the lithium cools down as far as 345°F with an α_s / ϵ_t as high as 5. The minimum desirable lithium temperature would probably be about 100 degrees above the freezing point or about 470°F. Since the power-conditioning equipment radiator has a 500°F operating temperature it cannot use special coatings which evaporate off at higher temperatures. This is the reason for the 0.9 emissivity on this radiator during the pre-startup period, and also necessitates a relatively low α_s / ϵ_t. Using a typical α_s / ϵ_t of 0.3 and $\epsilon_t = .9$ for this radiator, maximum and minimum equilibrium temperatures were calculated as 40°F and -42°F respectively.

The MIPB coolant has a melting point of -65°F and is not being circulated during the pre-startup period. The minimum allowable temperature for this coolant therefore is that at which the pump can satisfactorily circulate the MIPB at startup. Limiting high values of MIPB viscosity will probably occur between -20 and -40°F.

It should be mentioned that if the above method of powerplant temperature control were used before startup, the radiator would have to be rotated 90 degrees (radiator parallel to earth-sun vector) after startup. This is required to limit the auxiliary radiator temperature to its operating value when the powerplant is brought to full power.

Transient heat transfer radiator calculations for this study were performed with a computer program which utilized a one-dimensional finite difference machine solution. Using symmetry about the vertical centerline of the main radiator and omitting the titanium enclosure shown in Figure 25, the analysis takes into account heat transfer by the following modes for the main radiator:

1) Conduction through the lithium and its containing Cb-1Zr tubes

2) Convection in the gas (helium) between main radiator and fairing for the first 6 minutes after launch was approximated by using a film coefficient of K/L. This approximation for natural convection appears to be validated by McAdams' discussion of vertical enclosed air spaces[1]

3) Radiation from main radiator to fairing

4) Conduction through the fairing which was approximated as a 0.25 inch thickness of titanium

5) Radiation from the outside of the fairing was assumed to be to 70°F sink temperature for the first 6 minutes and to 0°F for the remainder of the calculations

The above calculations were duplicated in determining the MIPB curve presented in Figure 26. Material dimensions used in these calculations are for a preliminary 3.25-megawatt system. Dimensions may differ slightly from final design table values. Where the thickness of a material is not constant, as for a radiator panel, an effective overall uniform thickness is calculated. The total volume of lithium contained in the secondary system is assumed to be present at the radiating area since the lithium is being circulated. A list of material properties used in these calculations is presented in the table below.

Material Properties for Transient Heat Transfer Calculations

Material	Specific Heat Btu/lb °F	Thermal Conductivity Btu/Hr Ft °F	Density lb/ft^3
lithium	1.0	22	30.7
Cb-1Zr	0.07	29.3	534
aluminum	0.22	106	169
monoisopropylbiphenyl	0.44	0.07	59.5
titanium	0.126	8.6	283
helium	1.25	0.234	0.008

[1] McAdams, W. H., Heat Transmission, 3rd edition, 1954, pp 181, 182

G. Powerplant Control

System control studies for the 3.25-megawatt powerplant have been conducted to establish its operating characteristics during the mission and to define the requirements of the major system components and methods of powerplant control. The study assumed system performance characteristics based on two possible limiting thermal criteria, 1) a maximum operating cathode temperature, and 2) a maximum open-circuit cathode temperature. With the first limiting criterion it was assumed that a constant reactor output voltage would be maintained as the load demand varied, while with the second it was assumed that the optimum reactor output voltage, which varies with load demand, would be used. Discussions presented in Sections IV. E. and IV. H. gave the relative merits of the two types of operation.

The system control study was conducted in three basic steps. First, maximum operating limits were established for the major system components where estimates could be made. Second, failure rate estimates were made for the main powerplant radiator, based on the meteoroid barrier criterion used for the system study. When no estimate could be made of a failure rate for other components, a failure was assumed to occur. The third step in the control study was to impose the component operating limitations and failure rate on the power-time profile for the mission, and to analyze the performance of the system using a minimum amount of instrumentation to assure the highest reliability.

The following control mode was used in the studies, 1) control of reactor thermal power level through nuclear instrumentation, 2) a reactor coolant exit temperature control that would limit the maximum temperature to 2000°F, 3) voltage regulation and load-impedance matching on the input of the power-conditioning equipment, and 4) constant cesium temperature. The plant control scheme requires control drum motion to change thermal levels in the reactor caused by changes in the electrical power demand and by radiator segment failures.

Control of the reactor thermal power is required to maintain temperature limits within the fuel element. The temperature of primary concern is the cathode operating temperature which is a complicated function of both the thermal and electrical output and will vary as the load demand and as physical properties (such as electrode emissivity) vary during the mission. Since it is physically impossible to measure the cathode temperature directly and since it is impossible to calculate this temperature (due to physical property changes), all that can be done is to establish a maximum temperature limit at the open-circuit condition. Before this can be done, the total thermal power produced by the reactor must be measured, and nuclear instrumentation is required for this purpose. Nuclear measurements are preferred since the only other method of determining thermal power is by measurement of both the reactor's electrical output and the heat pickup by the coolant. The latter measurements will require computation to determine the reactor thermal power because the reactor electric power and the coolant inlet and outlet temperatures can be expected to change during the mission.

Calibration of the nuclear instrumentation can be done during reactor startup in space, under a no-load condition. The thermal power calibration can be performed by measuring reactor coolant temperatures and flow rate since no electrical power is delivered. Although computation is required during the calibration, the performance of the powerplant during the mission can be checked without it.

Measurement of the reactor outlet temperature is required to prevent this temperature from exceeding 2000°F. Increases in the coolant temperature will occur as radiator segments fail so that the thermal power must also be limited by this temperature.

1. Nuclear Control

Control Requirements

In order to maintain the reactor in a steady state, the effective

multiplication constant must remain at unity, that is, the reactor must be critical. Several factors exist, however, which tend to disturb the criticality by either increasing or decreasing the multiplication constant. The major sources of change that were considered are fuel depletion and temperature effects. The former source is due to the depletion of the fissionable material or burnup as the reactor operates. Thus, to continue operation for the lifetime of the reactor it becomes necessary to increase the fuel in excess of the initial critical loading.

The criticality calculations were determined utilizing multigroup diffusion theory. The fuel loading necessary to achieve criticality for the reference design at room temperature and beginning of life was calculated to be 1210 kilograms of 93.5 per cent enriched uranium monocarbide. In addition to the initial loading, 31 kilograms of fuel is required for the reactor to function for 20,000 hours at full thermal power. The correlation of reactivity and fuel is given by the material coefficient of reactivity. The average coefficient, $\Delta K/K / \Delta m/m$, for the reference reactor is 0.58.

The temperature coefficient of reactivity was determined for the change in physical properties with temperature by adjusting the material density and reactor dimensions. This produced a negative temperature coefficient of 2.68×10^{-4} per cent $\Delta K/K/°F$. The neutron flux energy distribution at the center and outer edge of the core is shown in Figure 29. The distribution results in a mean fission energy of 0.338 Mev. Because of the high fission energy the contribution to the temperature coefficient due to the change in

the slowing down range and the thermal group cross-sections is negligible.

Another source of variation of reactivity with temperature is the Doppler effect due to uranium resonance cross-sections. At the resonance energies the cross-section is extremely high, producing a reduction in the neutron flux such that, for a given energy integral of cross-section, the number of events is less than the number that would occur if the resonances were smoothed out. Due to the increased kinetic energy of the uranium nuclei with increasing temperature, the width of a resonance is increased but the height is decreased, keeping the integrated cross-section invariant. Thus, an increase in temperature results in a larger number of reactions. For small, highly-enriched reactors, the temperature coefficient due to the Doppler effect is positive. A somewhat conservative estimate of the coefficient for the reference design is about $+.85 \times 10^{-4}$ per cent $\Delta K/K/°F$. The total isothermal temperature coefficient is therefore negative with a value of 1.83×10^{-4} per cent $\Delta K/K/°F$. Because of the negative temperature coefficient an additional 6.7 kilograms of fuel is required in order to overcome the decrease in reactivity as the reactor proceeds to operating temperature during startup.

As a result of the lifetime and temperature demands, 37.7 kilograms of fuel must be added to the initial fuel loading of 1210 kilograms, which results in a 1.79 per cent excess reactivity at room temperature. A shutdown requirement of 2 per cent will therefore require a 3.79 per cent reactivity worth in the reactor control system.

Control Drum Analysis

The excess reactivity will be controlled by regulating the neutron

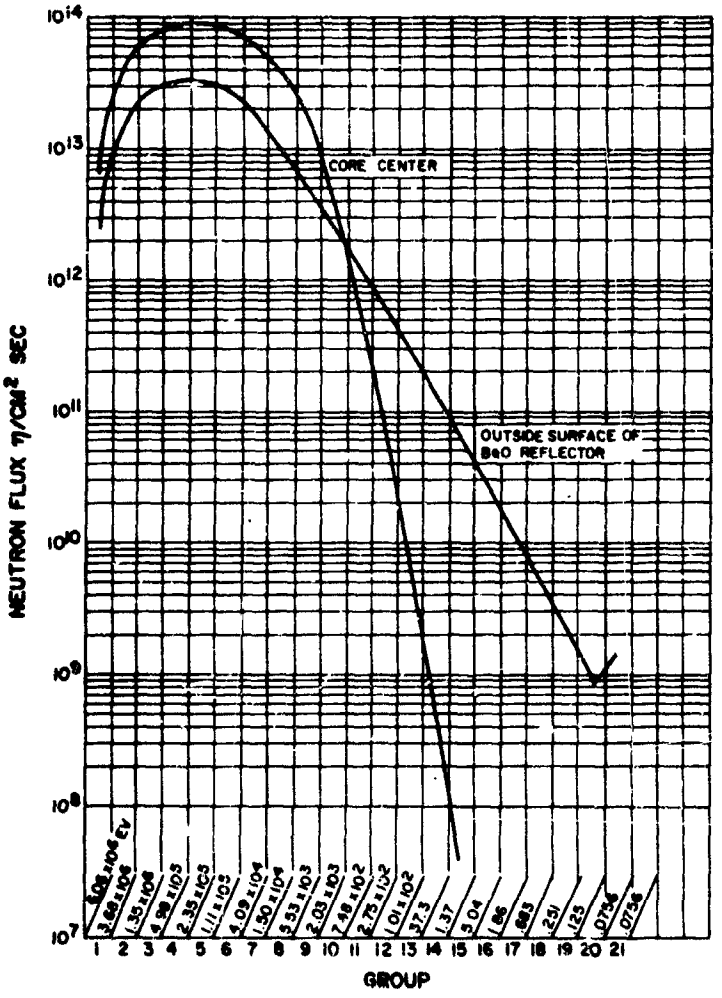

Figure 29 Neutron Flux Spectrum

leakage out of the core. This is achieved by eight rotatable drums symmetrically placed about the core and containing a segment of the reflector. To decrease reactivity, the drums are rotated out of the reflector. Initial studies were conducted to determine the thickness of radial reflector that would permit the incorporation of control drums of the required reactivity worth. It was found that

a two-inch reflector would be adequate for control. Two-dimensional r - θ multigroup diffusion theory was used to determine the change in reactivity with drum position. The control worth as a function of drum position is shown in Figure 30. The drum position at beginning of life and operating temperature is 45 degrees.

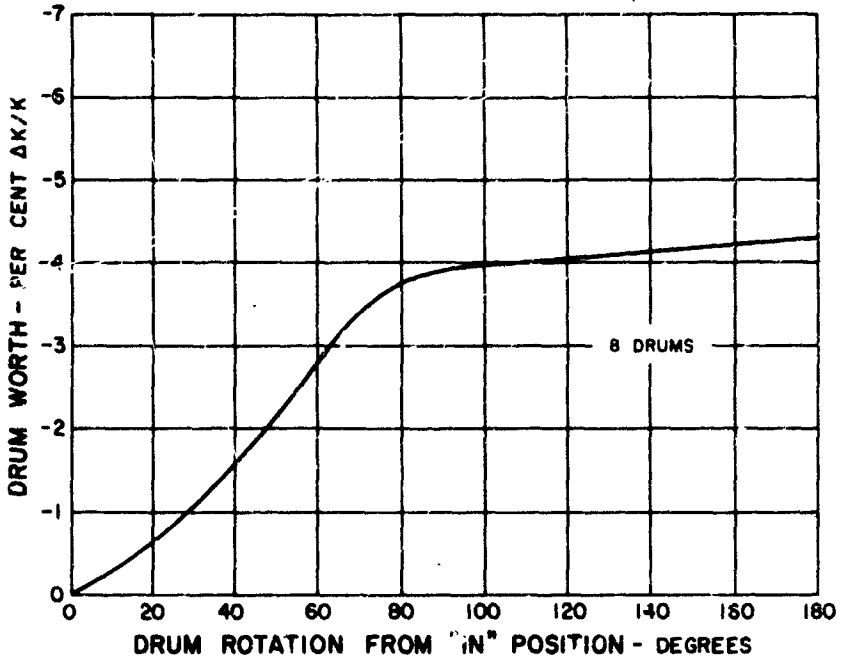

Figure 30 Control Drum Worth vs Drum Rotation

2. System Control

There are a number of possible events that may occur during operation of a thermionic power system. The occurrence of these events is postulated and the control of the system is checked to insure that it is adequate to prevent disabling of the system. The events to which the system is assumed to be subjected are, 1) changes in electric power demand, 2) anticipated radiator failure by meteoroid puncture, and 3) open-circuiting of some thermionic converters by lead failure or loss of cesium. The analysis of an assumed mission is discussed below and pertinent results are given.

Electric Power Demand

The assumed power requirements for a Jupiter mission are given in the table below.

Jupiter Mission Electric Power Requirements

Mission Phase	Interval, hrs	% Electrical Power
geocentric orbit	0 - 2,400	100
heliocentric orbit	2,400 - 6,700	100
coast	6,700 - 11,000	10
Jupiter capture observations and communications	11,000 - 15,300	100
	15,300 - 24,000	100

During the coast phase the electric power demand is appreciably less than 100 per cent. It is desired to reduce thermal power level in the reactor during this phase for the following reasons, 1) reduce fuel burnup to limit reactor reactivity changes during life, 2) lower operating temperatures of components when possible to increase reliability, and 3) to lower the magnitude of swings in reactor output voltage which would otherwise complicate design of the power-conditioning equipment.

Segment Failure

The meteoroid protection was distributed on the powerplant components to meet the following requirements, 1) a 90 per cent probability that the reactor coolant piping, the auxiliary radiator, and 12 or more of the 16 main radiator segments will be intact at the end of the mission, and 2) that the system weight with meteoroid barrier will be a minimum. At various times in the mission the number of operating main radiator segments will fall between the limits indicated on Figure 31 with 90 per cent probability. For the mission discussed here the number of segments was taken to be the least number of segments, the most adverse situation for a 90 per cent reliability.

The major consequence of a radiator segment failure is the loss of radiating area with a subsequent rise in temperature throughout the

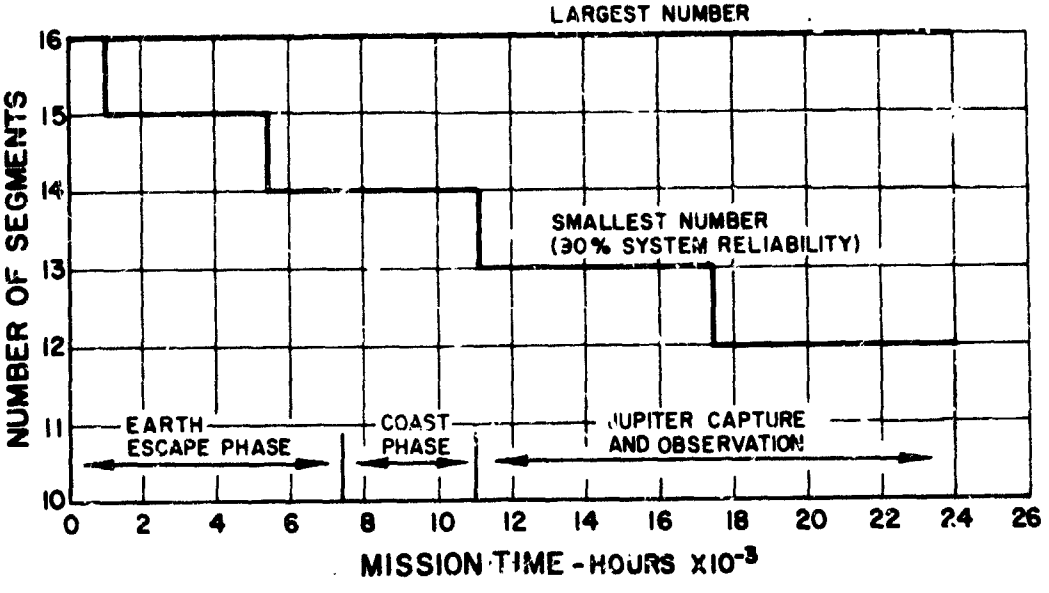

Figure 31 Number of Main Radiator Segments in Operation during Mission

system and particularly in the main heat rejection system if the thermal power level is not changed. If the system is operating at peak capacity and a failure occurs, then the thermal power must be cut back to avoid exceeding the thermal limits on the system. In Figure 32 is shown the maximum power capability of the system with different numbers of segments in operation. Whether operating with limits on cathode operating temperature or cathode open-circuit temperature, the limit on the maximum coolant temperature will severely reduce the power capability of the system when operating with fewer than 15 segments. This situation could be changed by increasing the area of the radiator panels and thus increasing the power capability of the system with fewer segments in operation (see Section IV.H. for an evaluation of a system capable of delivering full power with only 12 segments in operation at the end of the mission).

Another consequence of radiator failure is a reduction in reactor and radiator coolant flow rate. A meteoroid puncture will empty a channel of the main radiator pump of liquid metal. The result is an increase in the resistance of the pump circuit which reduces current and thus reduces flow in operating pump channels. This effect is shown in Figure 33.

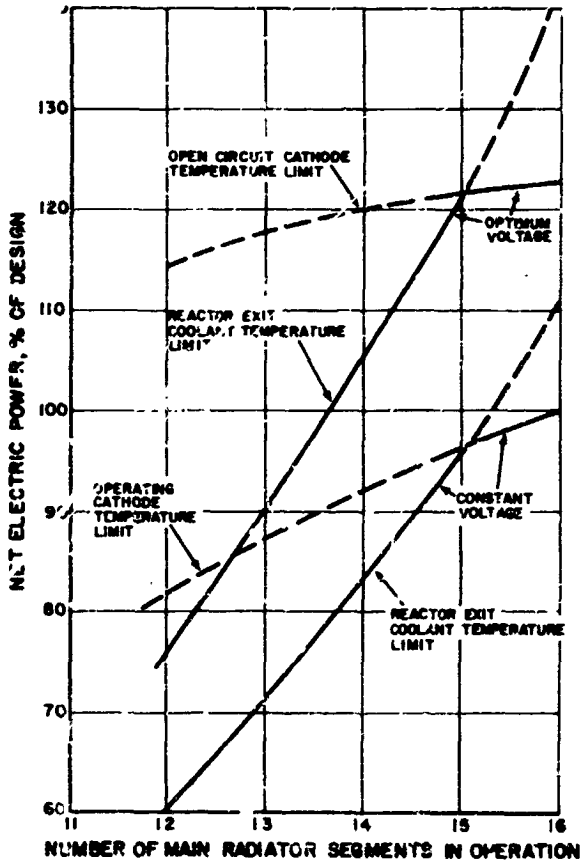

Figure 32 Maximum Power Capability of Nuclear Thermionic System at Constant Voltage

In Figure 34 is shown the thermal power level, the effective full thermal power hours and the variation in reactor exit temperature during the mission. With operation at constant voltage, the limit on reactor exit coolant temperature is reached after the first radiator panel failure. If the operating cathode temperature were not the limit, the system could be operated at a more efficient voltage which would reduce the coolant temperature and allow operation at higher thermal power and with much higher electrical power output.

Maximum Operating Cathode Temperature

The cathode operating temperature during the mission is shown in Figure 35. The solid curve refers to the operation of the system

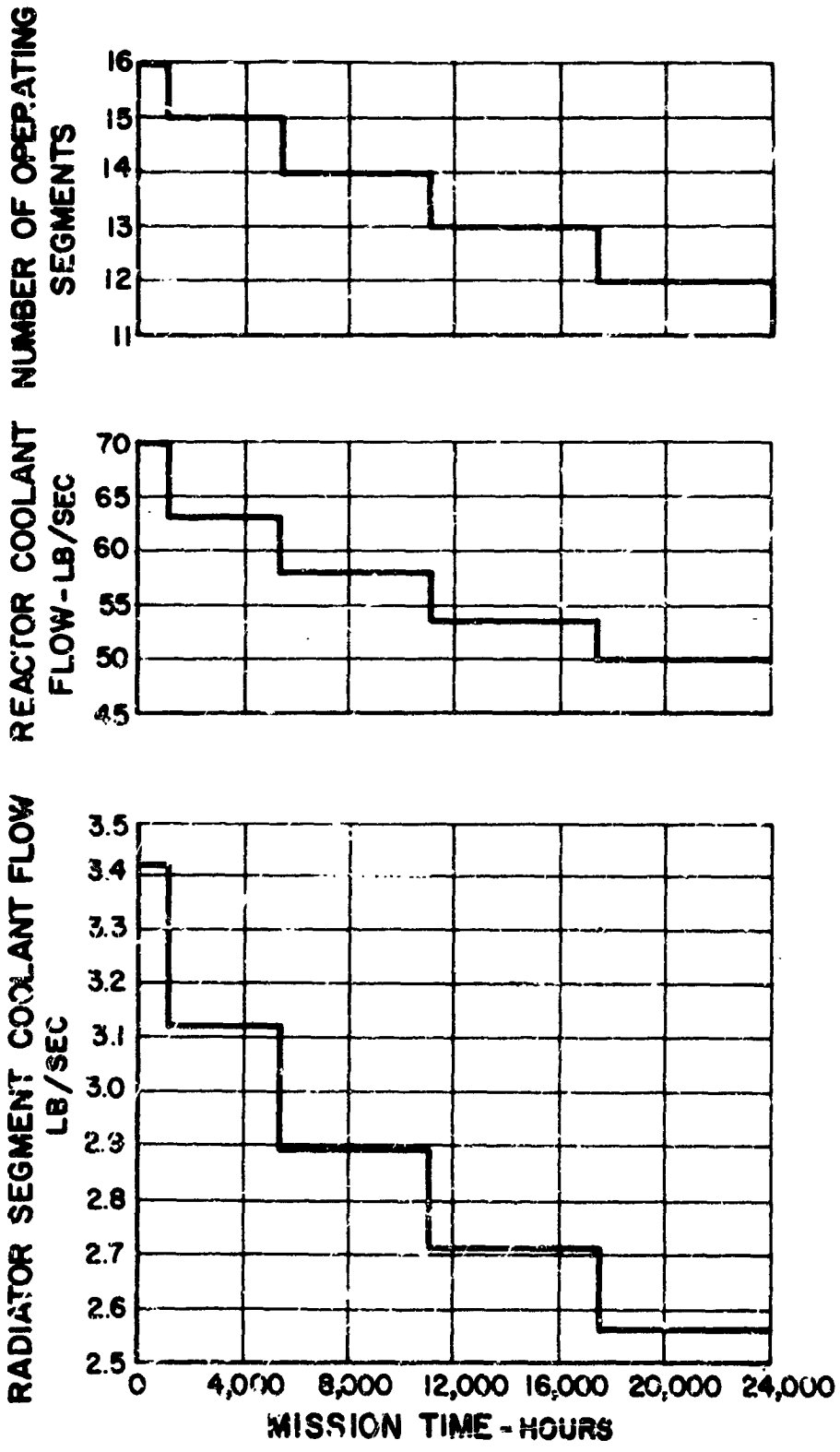

Figure 33 Powerplant Performance during Mission. System Operating Characteristics

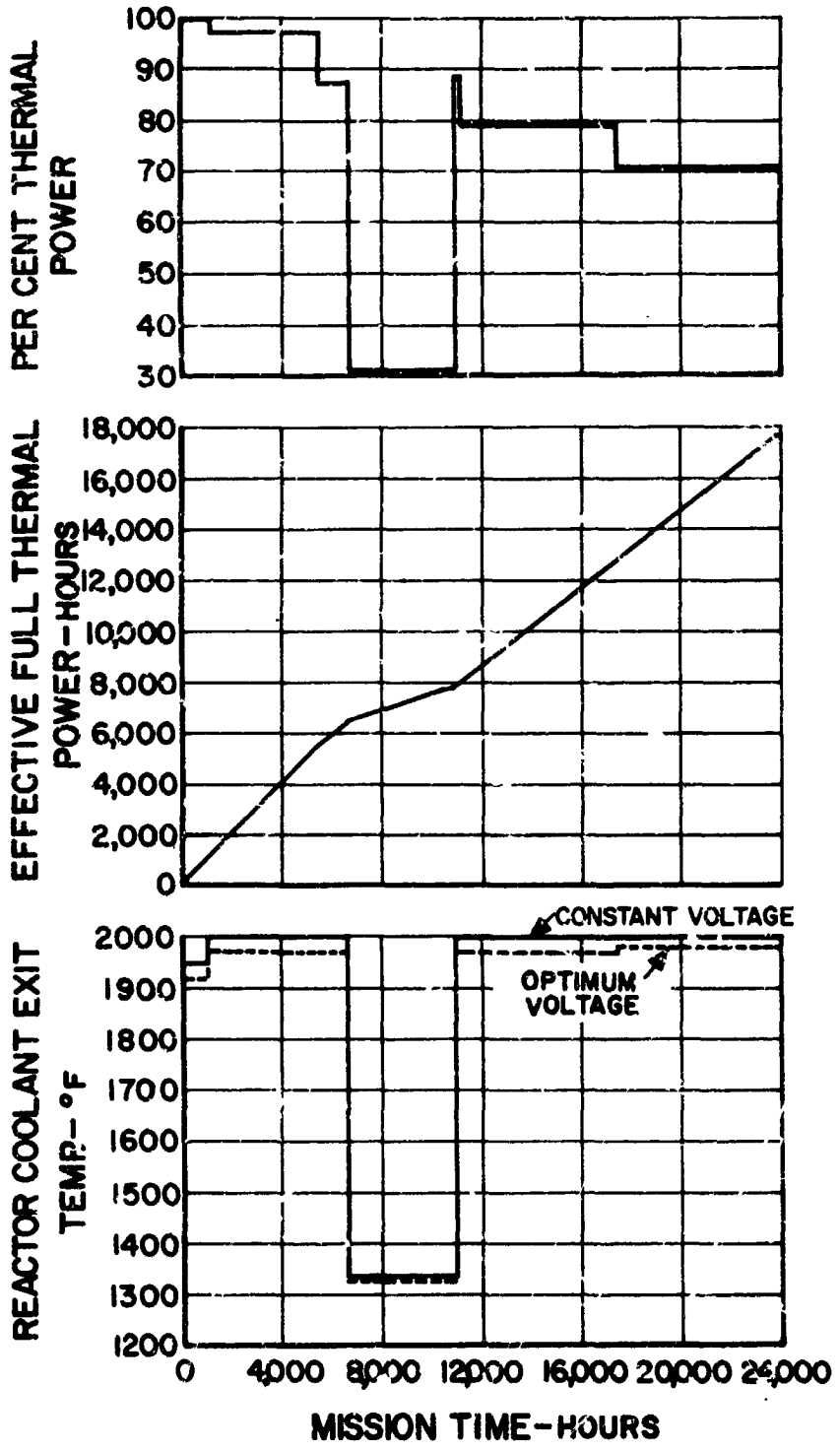

Figure 34 Powerplant Performance during Mission. System Thermal Characteristics

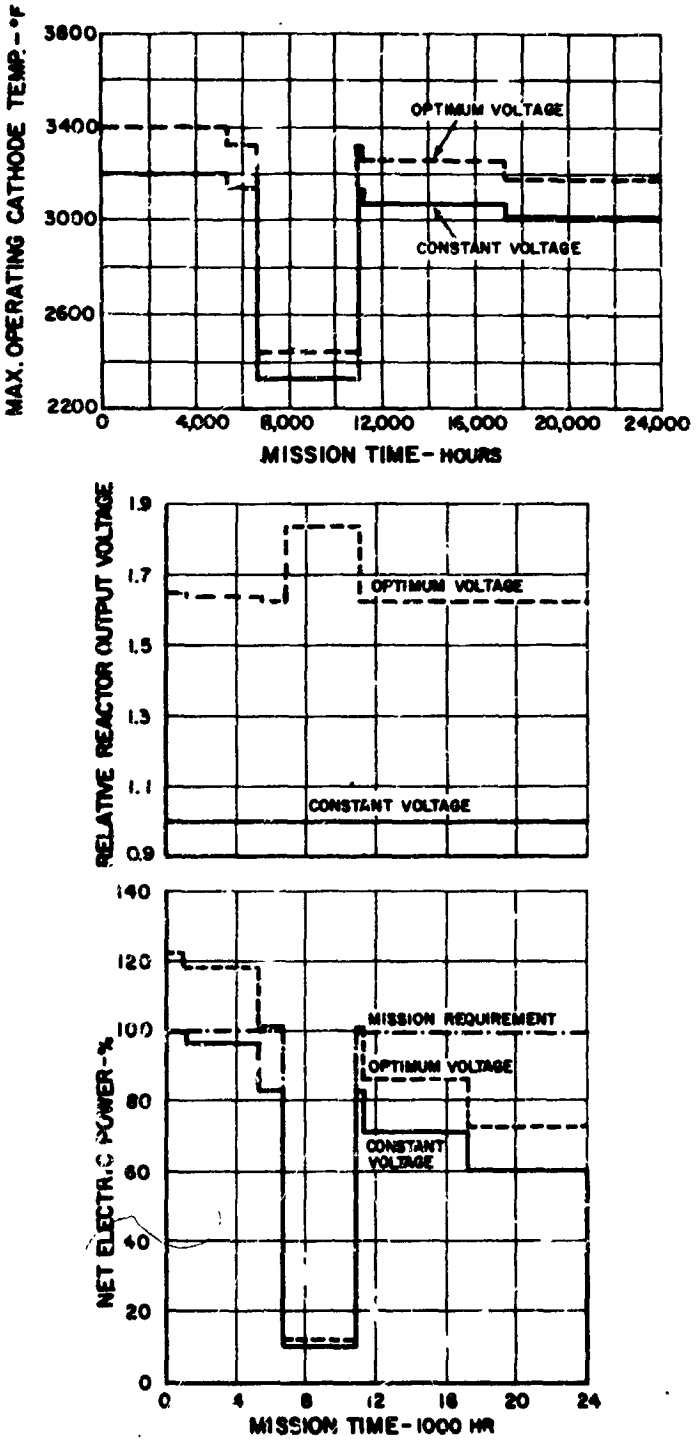

Figure 35 Powerplant Performance during Mission. Reactor Electrical Characteristics

with voltage optimized at the beginning of the mission for maximum power with a limiting operating cathode temperature of 3200°F. Also the voltage is held constant later in the mission when the reactor exit coolant temperature is limiting for about the first 5000 hours of operation. The reactor voltage and power output for this case are shown by the solid curves labeled 'constant voltage'. The power output capability is seen to drop below the assumed mission requirements after the first radiator failure.

Open-Circuit Cathode Temperature

The maximum open-circuit cathode temperature is the highest cathode temperature that can occur with a constant thermal power level. Figure 36 shows that the open-circuit cathode temperature is appreciably higher than the operating cathode temperature. This is a consequence of the loss of electron cooling in a failed reactor fuel assembly.

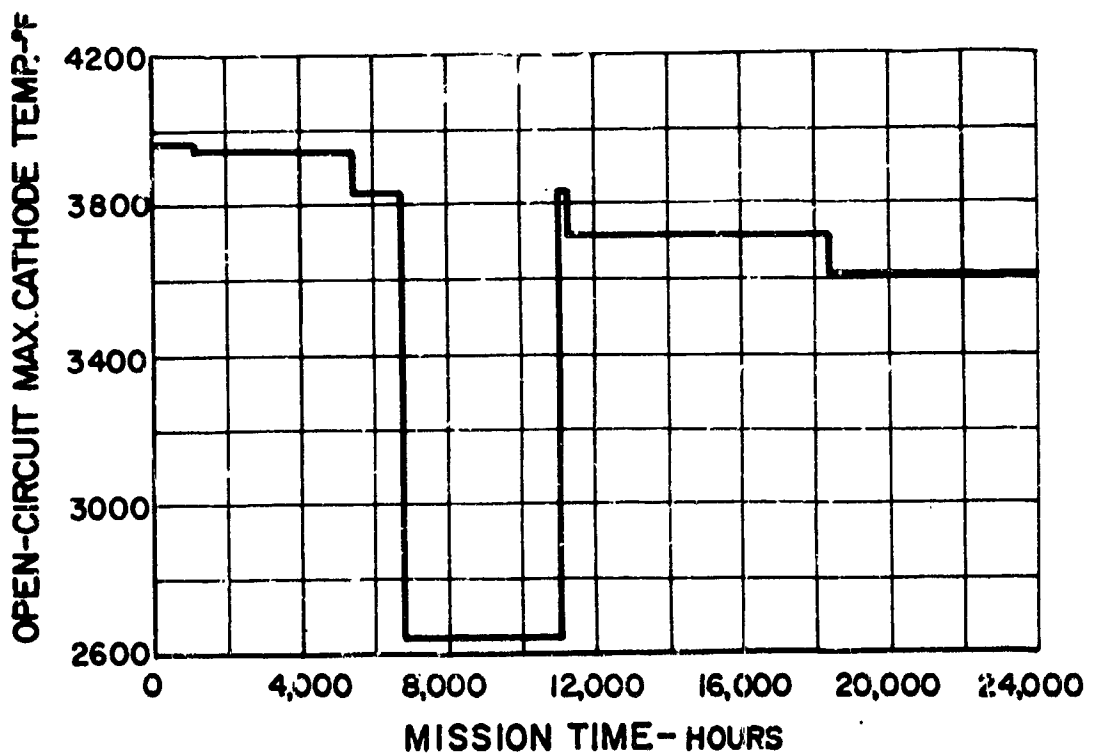

Figure 36 Powerplant Performance during Mission. Reactor Electrical Characteristics

Possible causes of open-circuiting of a converter are loss of electric load on the reactor, failure of a converter lead in the reactor, loss of cesium vapor, or contamination of the cesium vapor by fission gases. For the case of loss of electric power demand on the reactor, corrective action could be taken to lower the reactor thermal power and prevent or reduce the temperature excursion. The other conditions which lead to open circuits in single fuel assemblies cannot be readily detected and corrective action would not be possible. Reactor failure could occur due to the open-circuited fuel assembly in the event that fuel evaporated to space with a loss in reactor criticality or the fuel element cladding ruptured.

The open-circuit cathode temperature is relatively insensitive to anode temperature and therefore insensitive to the reactor voltage and number of main radiator segments at a given thermal power level.

The major effect of the change in thermal criterion will be in the reactor power output and reactor voltage output, which are discussed in the next section.

Reactor Power and Voltage

With cathode operating temperature limiting, the maximum power output is obtained at low reactor voltage and high reactor current. The resulting power output and voltage are shown as the solid lines on Figure 35 which are labeled 'constant voltage'.

If the operating cathode temperature limit is not used, the voltage can be optimized to obtain a higher power output. The reactor voltage and power are higher for this situation, as shown by the dashed lines labeled 'optimum voltage' in Figure 35. As mentioned previously, this change in operating voltage has no appreciable effect on the open-circuit temperature. However, the lower current output results in higher cathode temperature due to a partial loss of electron cooling as seen in Figure 35. The increased power output is in part due to the increase in cathode temperature.

In Figure 34 it is shown that the optimum voltage operation gives lower coolant temperature due to the lower heat rejection from more efficient thermionic performance. This means that higher thermal power could be used late in the mission when the reactor coolant temperature is limiting.

3. Failure Studies

Several failure studies concerned with reactor component and power-conditioning equipment failures were conducted for the one-megawatt powerplant and are described in Report PWA-2224. These studies were not repeated for this powerplant since the results of the previous study are applicable. Instead a summary of those results will be given.

a. Reactor Component Failure

Converter Short Circuit

A converter short circuit can occur by the cathode and anode coming into contact. If only a few of the converters in an assembly are shorted the power output from the reactor is decreased slightly by the power corresponding to the number of converters shorted. However, if a large number fail in an assembly, the electrical circuit in the reactor will be significantly disturbed which can result in a large decrease in power output from the reactor. Additional studies are required to evaluate the reactor power loss as a function of the number of converters shorted in an assembly.

An investigation of the temperature distribution occurring on the cathode showed that a temperature decrease can be expected for the cathode of the shorted diode with this type of failure.

An open-circuit failure occurring in a converter is a more serious problem and since it affects an entire fuel assembly it will be discussed in a later section.

Fuel Element Failure

A short circuit from anode to ground could result in the failure

of a number of fuel elements comprising an assembly. The location of the short determines the number of elements shorted out of the circuit. As the previous study showed, the loss of up to 50 per cent of the elements (9) in a single assembly would not seriously degrade the power output of the reactor. However, if as many as 75 per cent of the elements (13) are shorted, an appreciable power degradation of the reactor may result. The degradation could occur because the voltage output of the remaining assemblies may have to be shifted from the optimum value to keep the operating fuel elements in the partially-failed assembly operating in the power producing range. Otherwise, these elements would shift to the power-consuming range with the possibility of creating an over-temperature condition in the elements. This, of course, could lead to a fuel element failure and the loss of fuel from the reactor.

The failure mode described above can be serious, because only a single short circuit from anode to ground can result in a significant reduction in reactor voltage and power output. Although additional study is required to evaluate this problem in greater detail, the severity of the possible results again points out the importance of the anode trilayer.

Fuel Assembly Failure

The failure of a complete assembly can occur as a result of an open-circuit condition. Loss or contamination of cesium in the interelectrode spaces or the mechanical failure of an electrical lead can produce the open circuit. The reduction in the electric power output of the reactor is equal to the power output of the open-circuited assembly. This is due to the nature of the failure which does not affect the electrical output of the normally-operating assemblies.

A more important consequence of this type of failure is the occurrence of a very high cathode temperature which is attained when electron cooling from the cathode ceases. This open-circuit temperature depends upon the thermal power input and can be high enough to create serious temperature problems within the elements. A discussion of this problem is given in Section IV.H. of this report.

Power-Conditioning Module Failure

The powerplant design uses the power-conditioning equipment divided into four modules, each of which supplies power for the ion

engines and any other on-board power requirements. A description of the components included in this equipment is given in a Westinghouse systems study[1]. The results of the failure analysis conducted for the previous 1 MW powerplant study are presented in Table 5. That study was concerned with the effects of a single module failure upon the remaining portions of the power-conditioning equipment and the reactor. Various methods of connecting the load to the power-conditioning modules were investigated as shown in Figure 37, to determine an electrical system that would minimize failure effects. Table 5 shows the effects of a single module failure (which can result from radiator segment, coolant pump or electrical equipment failure) upon the reactor and the power-conditioning equipment, for the various types of load and equipment connections. The study assumed that cathode open-circuit temperature was the limiting thermal criterion. The obvious advantage for some wiring schemes is that no corrective action is required when a module fails. As can be seen, the effects vary for the different types of connection, so that the selection of a particular wiring scheme will, in the event of a failure, determine the power output of the powerplant. At the present time it is not possible to make this selection, because of the lack of data concerning both the reactor and the power-conditioning equipment. A study has been performed by the Westinghouse Corporation[1] concerning a single-channel (module) power-conditioning system. This study points out the reliability deficiencies inherent in single-channel systems and the need for additional studies for multichannel systems. Obviously, much work remains to be performed before permissible operating conditions for a thermionic reactor can be ascertained.

H. Design Criteria

1. Thermionic Reactor

a. Limiting Criteria

A significant question existing for the thermionic reactor is the selection of a thermal criterion to limit the operation of the

[1] Westinghouse Electric Corporation, Aerospace Electrical Division, Space Electric Power Systems Study, Vol. 5

TABLE 5

Effects of Power-Conditioning Module Failure

Mode of Operation of Power-Conditioning Equipment	Relative Reactor Power Output	Relative Reactor Output voltage	Relative voltage across Load	Relative reactor output current	Relative power in operating conditioning equipment	Relative Current in operating conditioning equipment	Reactor coolant outlet temp. °F	Max. operating cathode temp. °F	Corrective action required
No failure	1.00	1.00	1.00	1.00	1.00	1.00	1850	3350	--
Parallel connection	1.00	1.00	1.00	1.00	1.33	1.33	1850	3350	reduce load
Separate loads, no output voltage regulation	.97	1.14	1.14**	.85	1.29	1.13	1860	3440	reduce load
Separate loads, output voltage regulation	.75	1.44	1.00**	.52	1.00	.70	1890	3670	none*
Series connected no volt reg.	.90	1.26	0.95	.71	1.20	.95	1870	3540	none*
Series connected, volt reg.	.56	1.54	0.75	.37	.75	.49	1910	4100	none*

* No corrective action required if cathode open circuit temperature is limiting thermal criterion. Reactor thermal power must be lowered if operating temperature is limiting criterion. However conditioning equipment must be designed to operate at increased voltage or otherwise reactor thermal power must be reduced

** Across each load section

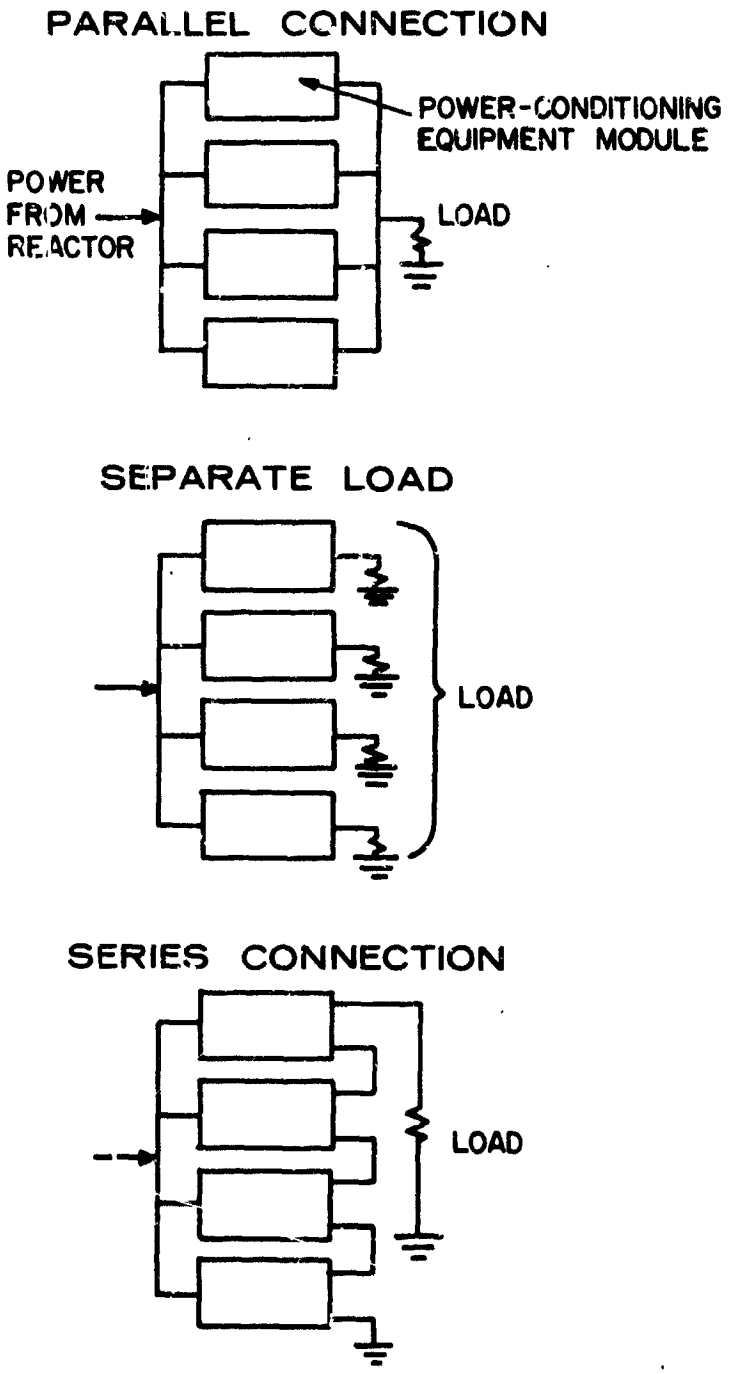

Figure 37 Load Circuit Diagrams

converters. This question exists because insufficient experimental data for converters is available at this time. Two criteria appear desirable and either might be selected as limiting, 1) maximum operating cathode temperature, and 2) maximum open-circuit temperature.

The cathode operating temperature naturally arises as a limiting criterion since it is the temperature to which the converters are subjected during the mission. The converter components and the fuel must be capable of withstanding the conditions of reactor operation at this temperature.

The maximum open-circuit temperature arises as a limiting criterion because of the possibility of an open-circuit failure in the system and the possibility of increasing the power output from the reactor. Open-circuit failures can occur either by an open circuit outside of the reactor or by a failure within the reactor resulting in a stoppage of electrical current. With either type of failure, the cathode temperature increases due to the cessation of electron cooling from the cathode.

The possibility for increasing the power output of the reactor with the second criterion occurs because it permits the operation of the converters at maximum efficiency. Referring to Figure 23, if operation is limited by the maximum operating cathode temperature the point of operation is selected at the maximum in the constant temperature curve. The thermal power input varies along this curve and although this point results in the maximum power output, it does not correspond to maximum efficiency. Instead, if converter operation is based on maximum open-circuit temperature which is determined by the thermal power input and described by the lines of constant thermal power in the same figure, the point of maximum power corresponds to that of maximum efficiency. This results in an increase in electrical power output from the reactor, an increase in the cathode operating temperature and the converter voltage.

Figure 38 shows the increase in relative electric power output as the relative reactor voltage varies. The relative voltage of unity is the optimum voltage corresponding to constant cathode temperature operation. Corresponding to this point is a thermal power input which if held constant as the voltage is allowed to increase results in an increase in electric power output. A

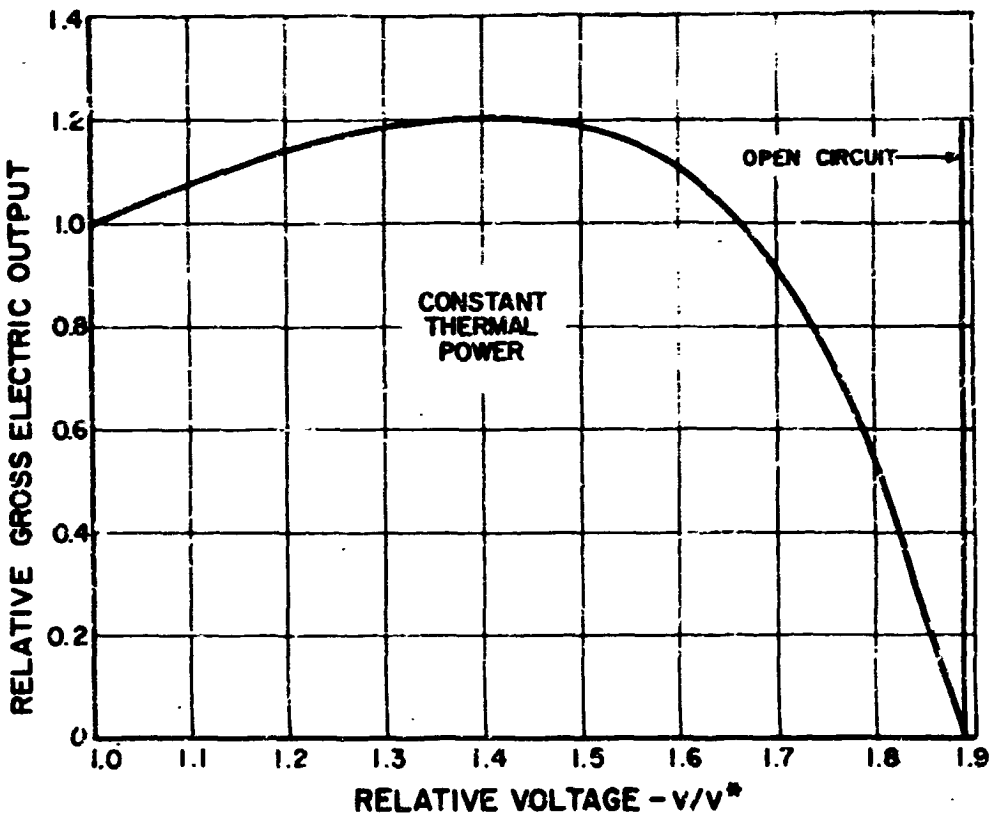

Figure 38 Relative Gross Electric Output vs Relative Voltage

maximum occurs at a relative voltage of about 1.4 with a corresponding increase of 20 per cent in electric power. This is the increase that can be attained by proceeding from the maximum cathode temperature criterion to that of maximum open-circuit temperature. Figure 39 shows that an 8 per cent saving in system specific weight also results for the latter criterion. The figure also shows that an increase in weight results as the voltage is increased for constant cathode temperature operation.

b. Converter Power Density

Figure 40 shows the effect of converter power density on relative system weight. The relative power density of unity corresponds to 10 watts/cm^2 which is the predicted value from the thermionic performance prediction system presented in Report PWA-2240 for a converter at optimum conditions and a cesium gap of 0.020 inch. This value was varied at a fixed cathode temperature (3200°F), the reactor perform-

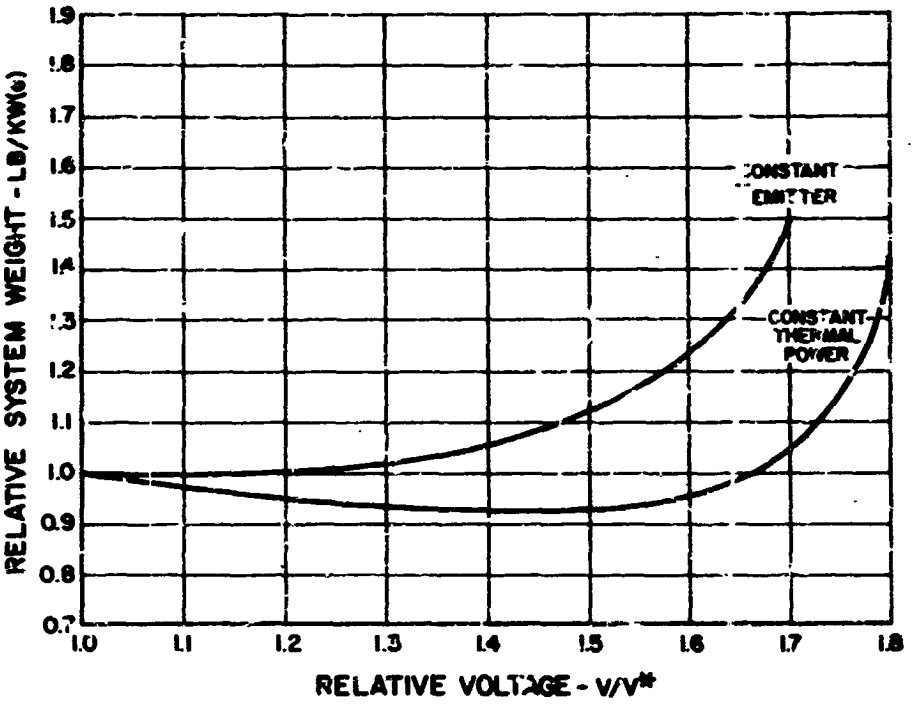

Figure 39 Relative System Weight vs Relative Voltage

ance was recalculated including the effects of nonuniform power distribution, and the powerplant weight was determined. The curve shows, as could be expected, that the greater the converter power density, the lower the system weight. However, a closer inspection of the curve shows that if the power density could be doubled from the reference value, only a 12 per cent saving in system weight can be realized. Conversely, if only one-half the power density can be attained, then the system weight increases by 25 per cent. This slow variation in system weight is due to relatively small increase in reactor efficiency (from 12.1 to 15.1 per cent) with doubling of the power density and the large amount of powerplant weight little affected by changing efficiency, such as the power-conditioning system, structure, pumps and piping.

c. Optimum Anode Temperature

The optimum anode temperature based on thermionic performance is that anode temperature which corresponds to the maximum power output from a converter. This temperature is different

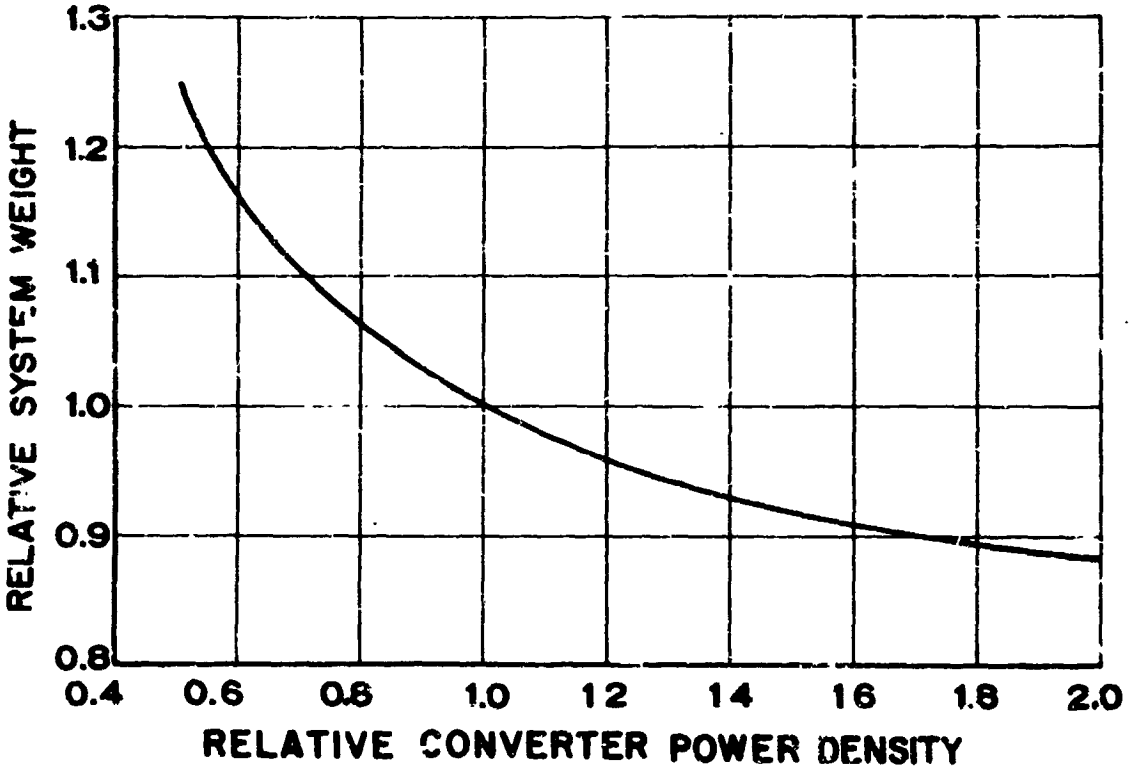

Figure 40 System Weight vs Converter Power Density

from the actual anode temperature used in the system which was calculated to produce minimum system weight. In the design of the powerplant, the optimum thermionic anode temperature was calculated from an experimental prediction system presented in Report PWA-2240. However, since there is still insufficient experimental performance data, a calculation was performed to determine the effect of varying optimum thermionic anode temperature. The results of the calculation are shown in Figure 40a where system weight is plotted as a function of actual anode temperature at constant optimum thermionic anode temperature, T*. The figure shows that increases in system weight can be expected if the predicted T* is low by a few hundred degrees. For example, T* for this powerplant was calculated to be about 1500°F which results in a system weight of 23.4 lbs/KW(e). If T* were actually 1300°F, a system weight increase of about 2 lbs/KW(e) would

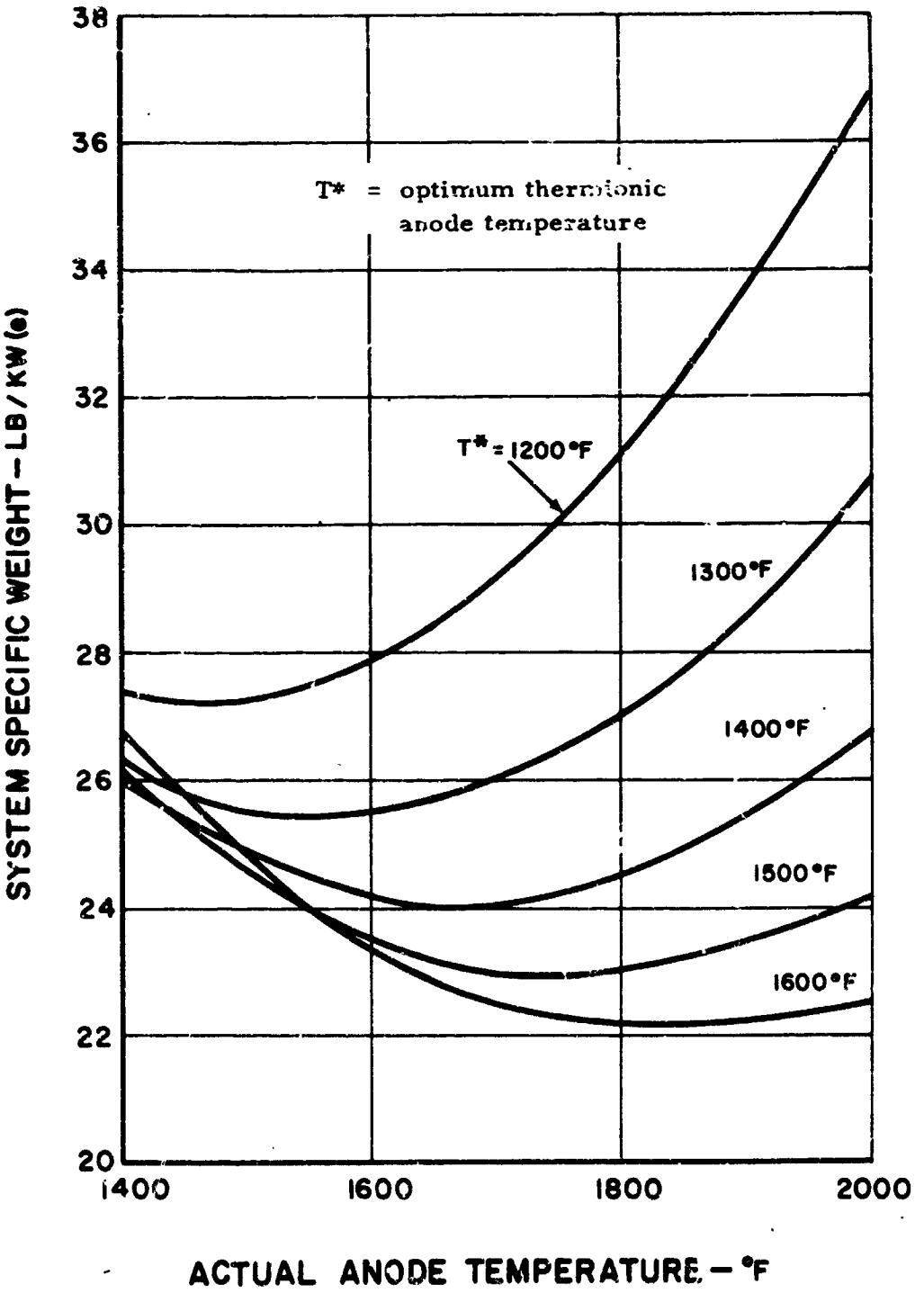

Figure 40a System Specific Weight vs Actual Anode Temperature

be incurred. Also, as the figure shown, the actual anode temperature calculated for the system would decrease, which would cause a decreased radiator temperature. If the resulting radiator temperature were low enough, a beryllium radiator might be optimum. This result is important since it points out that the optimum thermionic anode temperature affects the selection of the radiator material.

As was mentioned above, T* is not the anode temperature selected for the system, since it does not result in a minimum weight system. Each of the curves in Figure 40a was generated for a constant T*, and as can be seen the anode temperature which gives a minimum weight is higher than the T* for that curve. The reason for this is a weight trade-off between the reactor, which wants the anode temperature to be equal to the thermionic optimum, and the radiator, which wants as high an anode temperature as possible, to increase the radiator heat rejection temperature and therefore decrease the radiator size and weight. For example if an anode temperature lower than T* is selected, the reactor is heavy due to poor thermionic efficiency, and the radiator is heavy due to both the poor thermionic efficiency and the low heat rejection temperature. At an anode temperature equal to T*, the reactor weight is a minimum due to maximum thermionic efficiency, but the radiator is still fairly heavy. At temperatures higher than T*, the reactor weight begins to increase due to decreased efficiency, the radiator wants to be bigger and heavier for the same reason, but because the heat rejection temperature is higher the radiator weight is lowered to such an extent that it overcomes the increase in reactor weight. This trend continues as the anode temperature increases until the decreased conversion efficiency causes such large increases in reactor weight that they overcome the decrease in radiator weight and the overall effect is an increase in system weight. Therefore, the minimum weight system occurs at an anode temperature where the total of the reactor and the radiator weight is a minimum and not at the optimum thermionic anode temperature, where only the reactor weight is a minimum.

d. Anode Trilayer

The resistivity of the BeO used in the anode trilayer is an important parameter because of the power loss that can occur by leakage of current to ground. This is shown in Figure 41 where it can be seen that a large portion of the power generated can be lost due to an insufficient resistivity. For this design a resistivity

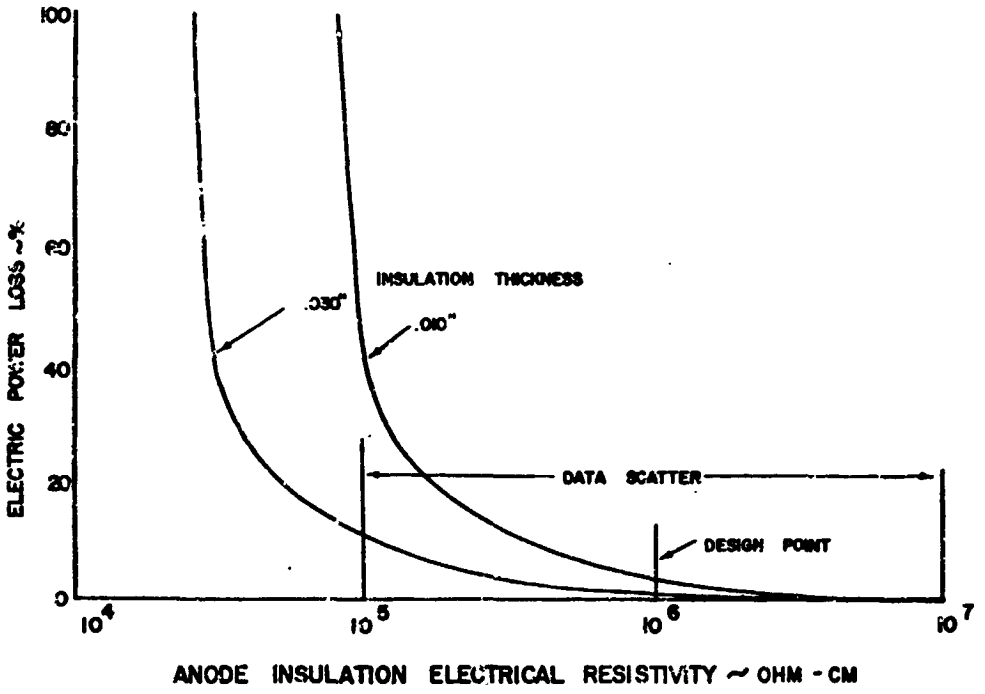

Figure 41 Electric Power Loss vs Anode Insulation Electrical Resistivity

of 10^6 ohm-cm and a thickness of 0.010 inch were chosen. The curve shows for these values only a 4 per cent loss is incurred. However, a review of experimental data available reveals investigators have reported values varying from 10^5 to 10^7 ohm-cm (at 2000°F) depending on material properties such as density, purity and method of fabrication. As the curve for 0.010 inch thickness shows, a resistivity of 10^5 results in about a 40 per cent loss in electric power and resistivities less than this are completely intolerable. Increasing the thickness of the insulation to 0.030 inch gives only a small improvement in this situation.

The problem of insulation resistance is compounded by the high-temperature nuclear environment within which the insulation must operate. Insufficient in-pile experimental data is available upon which can be assigned a reliable value of the resistivity. More-

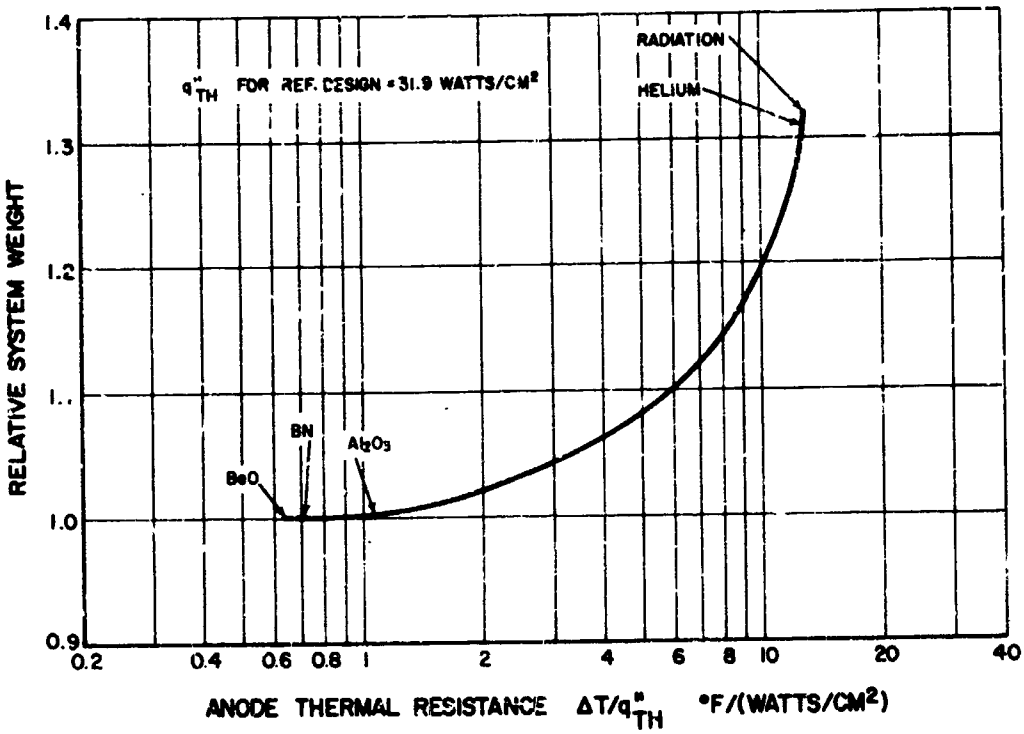

Figure 42 Anode Thermal Resistance vs Relative System Weight

over, some work performed indicates many problems can be anticipated with the use of ceramic insulators in reactors. Such problems as cracking and helium generation in BeO have been observed.

An additional requirement for the trilayer is that it must present a low resistance to heat flow. This requires fabrication into an integral body without the presence of voids. Pratt & Whitney Aircraft[1] is currently developing a trilayer using BeO as the insulation. Figure 42, a plot of relative system weight versus trilayer thermal resistance, shows the weight penalty incurred due to a high resistance trilayer. The three points indicated by ceramics were calculated by assuming an integral trilayer (no thermal contact resistance between layers), and indicate that either of the electrical insulation materials may

[1] Pratt & Whitney Aircraft, Liquid Metal-Heated Space Radiator-Mounted Thermionic Generator, APL TDR 64-121

be used. The point designated 'radiation' assumed a complete void in the trilayer across which heat transfer occurs by radiation only. The 'helium' point was calculated assuming that the void was filled with helium. Obviously, it does not appear that the presence of helium will be of any benefit. Preliminary experimental data from Pratt & Whitney Aircraft and Radio Corporation of America[1] concerning temperature drops across a trilayer indicate that system weight increases ranging up to 30 per cent can be expected. Also, large increases in radiator area will result due to the decrease in reactor coolant temperature.

Although the anode emissivity has only a small effect on system weight, it does have a significant effect on the maximum open-circuit cathode temperature. An increase in anode emissivity causes a decrease in the open-circuit temperature. This is important since in the event of an open-circuit failure it is desirable to have the lowest open-circuit temperature possible so as to minimize evaporation, gas release and swelling of the nuclear fuel. Figure 43 shows the effect of increased anode emissivity on system weight and open-circuit temperature, with the operating cathode temperature held fixed. The open-circuit temperature decreases with increased anode emissivity due to the increase in radiation heat loss from the cathode. However, since the heat loss from the cathode is increased, the efficiency of the converter decreases which causes an increase in system weight. Also, increased fuel burnup is incurred since an increase in thermal power input is required to maintain the cathode temperature constant. It is interesting to note that although an increase in emissivity causes an increase in the thermal power input, the overall effect is a decrease in open-circuit temperature.

Figure 44 shows the effect of the increase in anode emissivity on system weight and cathode operating temperature with a fixed open-circuit temperature. As anode emissivity increases, the heat loss from the cathode increases so that an increase in thermal power input is required to maintain the open-circuit temperature constant. The overall effect is an increase in the operating cathode temperature which increases the converter power density, even though the converter efficiency is decreased. As

[1] Radio Corporation of America, The Development of an Auxiliary Electrode Thermionic Converter, ASD-TDR-63-442

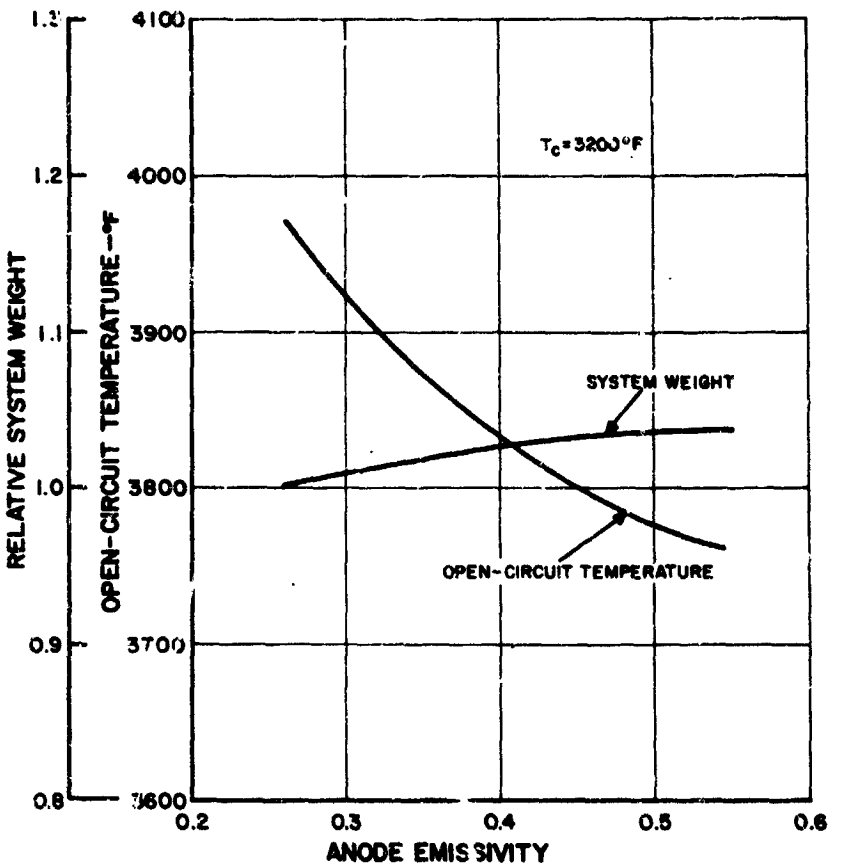

Figure 43 Anode Emissivity at Fixed Cathode Temperature

a result, a slight decrease in system weight occurs, but at the cost of a high cathode operating temperature.

The importance of Figures 43 and 44 is that the problem of a high open-circuit temperature can be somewhat alleviated by an increase in anode emissivity. However, a penalty must be paid by either an increase in system weight or cathode operating temperature.

e. Reflector Control

As a part of the study of high power thermionic powerplants, a study was performed to determine the limits on the size of

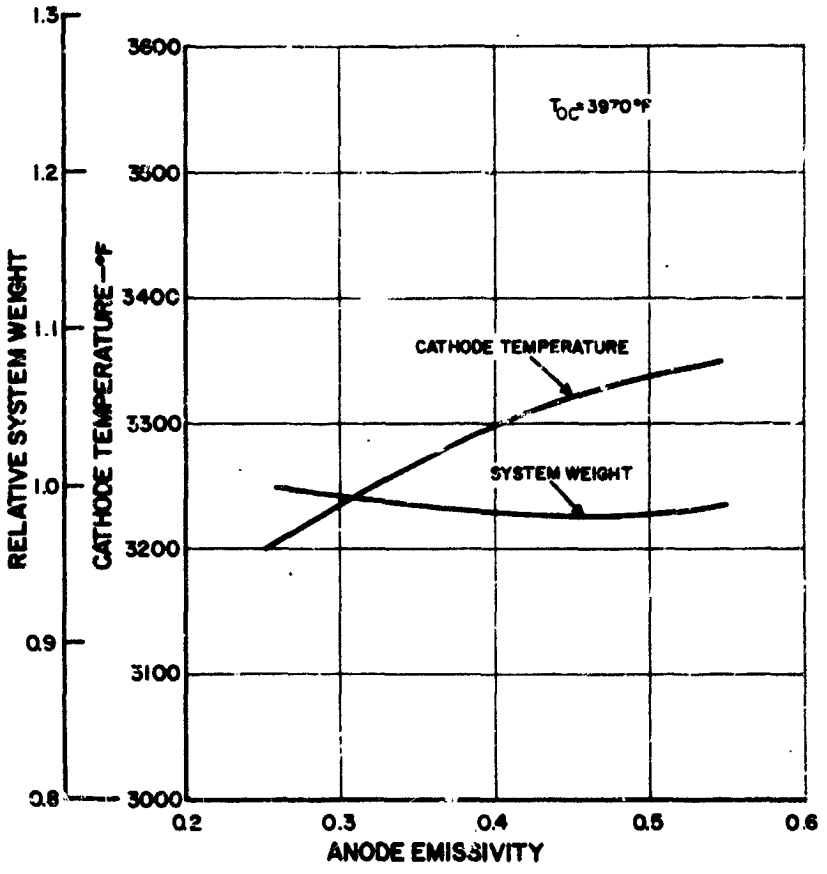

Figure 44 Anode Emissivity at Fixed Open-Circuit Temperature

thermionic reactors capable of reflector control. Obviously, due to the emitting area requirement for a thermionic reactor, the size of the reactor will determine the maximum electrical power output at a given temperature. As the core dimensions increase, the neutron leakage decreases and consequently the ability to control excess reactivity by a movable reflector concept diminishes. It is of course possible to employ control rods for large reactors; however, this concept perturbs the reactor power distribution and results in p r thermionic performance.

The reactivity worth of an infinite reflector was determined for several core diameters and for a length-to-diameter ratio of one. A 1/4-inch columbium pressure vessel was situated between the core and the reflector. The worth was obtained using a one-

dimensional multigroup neutron-transport program. The total worth is presented as the difference in the effective multiplication constants obtained by proceeding from a bare core to one with an infinite radial reflector. In the study an 8-inch reflector was assumed to be infinite. The radial reflector worth is shown as a function of core diameter in Figure 45 for a 2-inch axial reflector.

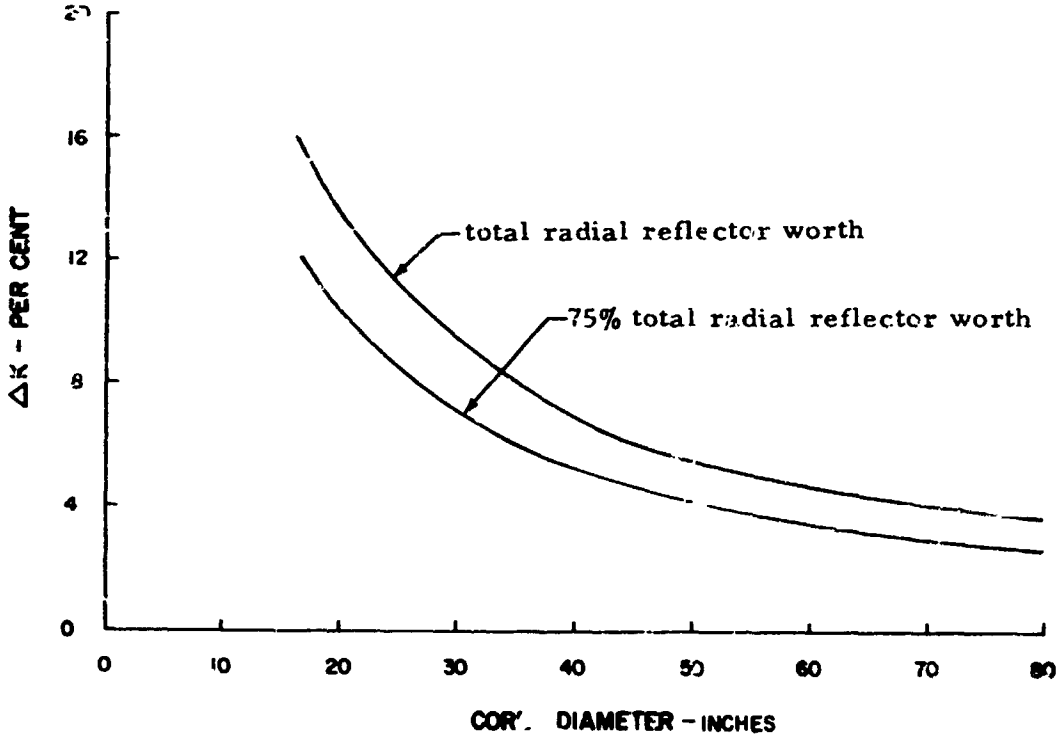

Figure 45 Reactivity Worth of an Infinite Radial Reflector vs Core Diameter

The power output was determined for various reactor diameters and cathode temperatures using the thermionic system program. A columbium radiator was employed in the analysis. Core diameter is shown as a function of cathode temperature and power output in Figure 46.

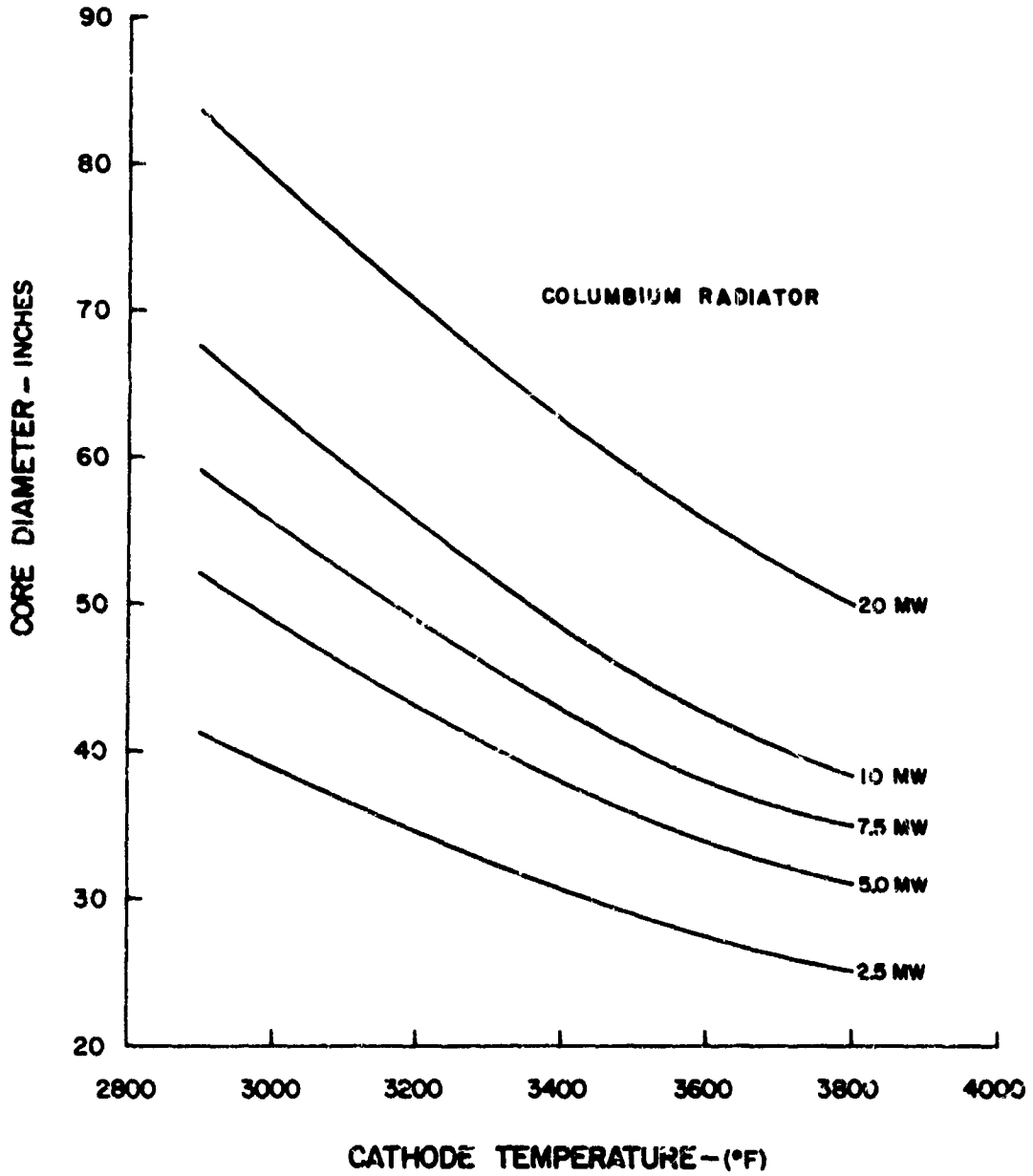

Figure 46 Core Diameter vs Cathode Temperature

Using a 4 per cent ΔK control requirement, Figure 45 indicates a maximum core diameter of 70 inches. Applying this value to Figure 46 re-

sults in a 20 megawatt power output for a 3200°F cathode temperature. A more realistic approach, however, is to assume that only 75 per cent of the infinite radial reflector worth can be achieved. This reduces the maximum core diameter to 53 inches and the resulting maximum power is 9 megawatts at the 3200°F cathode temperature.

2. Meteoroid Criteria

The selection of a meteoroid criterion for vehicles destined for deep space probes is uncertain due to lack of data. Therefore, since this uncertainty exists a study was made to determine the effect different criteria would produce on system weight. Figure 47 shows a plot of relative system weight versus relative barrier thickness. The thickness was allowed to vary from 0.5 to 1.5 times the thickness predicted by the criterion selected for this study. The plot indicates

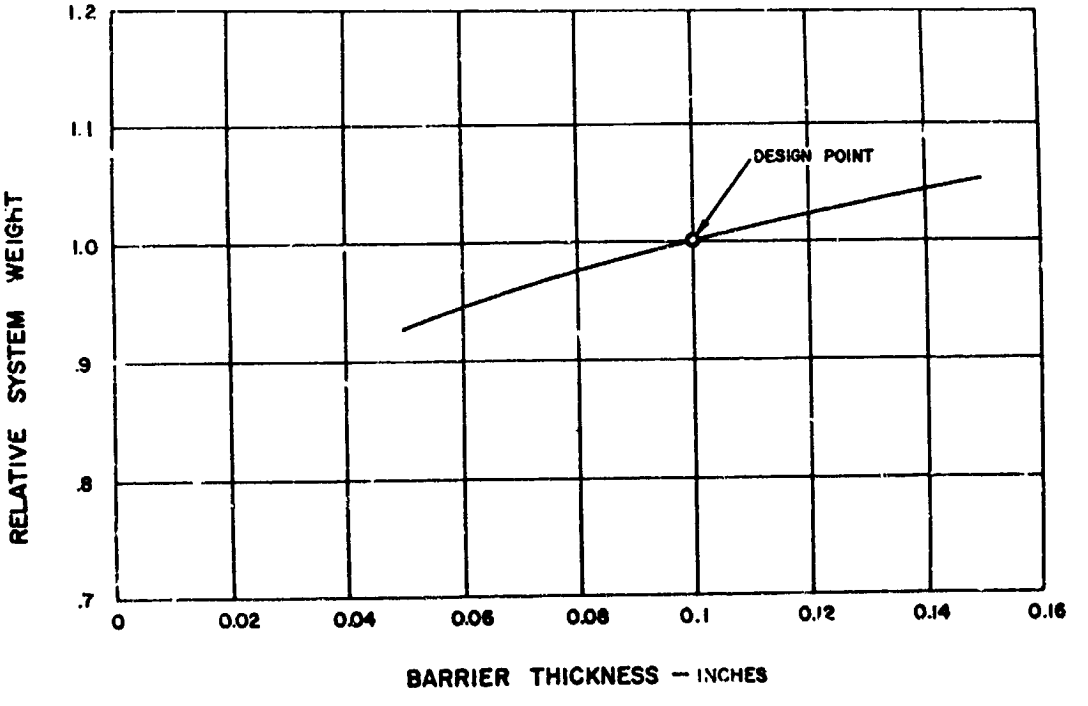

Figure 47 Relative System Weight vs Relative Meteoroid Barrier Thickness

that this variation produces system weight variations of less than 10 per cent over the entire range. Therefore, it can be concluded that for high power thermionic systems, the meteoroid criterion selected will not have a drastic effect on system weight within the thickness range used here.

3. Powerplant Reliability

For this study meteoroid protection was provided for a 90 per cent probability that three-fourths or more of the radiator segments would be in operation at the end of the mission. From Section IV.G. above, it was seen that the powerplant is not capable of completing the assumed mission. This occurred because as radiator segments failed, the reactor coolant outlet temperature increased until it reached the 2000°F temperature limit early in the mission.

To allow the powerplant to fulfill the mission, an increase in the main radiator area is required. A calculation was performed to determine the system parameters for a powerplant designed to produce the rated power at the end of the mission. The radiator area of each of the sixteen segments was increased to permit completion of the mission when only twelve segments are in operation. The total area of the 12 segments is sufficient to reject the heat corresponding to 3.25 megawatts. Table 6 presents a list of some of the system parameters, and shows that a 2.6 lbs/KW in-flight specific weight increase results from this design criterion. However, the specific weight of 26 lbs/KW(e) quoted in the table is based on the end-of-mission power, and since the powerplant has a higher power capability at the initiation of the mission the system specific weight on this basis is 23.6 lbs/KW(e). Table 6 presents a comparison of the full power system parameters at the beginning and end of the mission. A 21 per cent increase in power at mission initiation results from the increase in radiating area which lowers the mean radiator and reactor coolant temperatures. The decrease in the latter temperature improves thermionic efficiency, which allows the higher power output at the beginning of the mission.

TABLE 6

System Parameters*

inflight system specific weight, lbs/KW(e)	26
emitter temperature, °F	3,200
system lifetime, hrs	24,000

	Beginning of Mission	End of Mission
net electric power, MW(e)	3.94	3.25
radiator area, ft^2	1,867	1,400
radiator segments	16	12
mean radiator temperature, °F	1,595	1,669
mean anode temperature, °F	1,670	1,780
thermionic efficiency, %	12.4	12.1
reactor thermal power, MW	38.4	33.4

*System designed for full power at end of life

IV. AREAS OF MAJOR TECHNICAL UNCERTAINTY

Many areas of uncertainty exist in the design of nuclear thermionic space power systems which require considerable experimental effort. The reactor especially presents many formidable problems and some work is currently in progress to solve them. However, most of the basic problems that were presented in the previous one-megawatt powerplant study are still unsolved. Report PWA-2224 presents the important problems and a summary of these will be given here.

A. Fuel Element

1. Thermionic Prediction System

The thermionic prediction system used in the powerplant analysis (given in Report PWA-2240) agrees quite well with test data in the region of maximum power. However, some doubt exists for short-circuit and open-circuit conditions, and for the transition from the extinguished to the arc-mode. This data must be known to be able to predict converter performance and open-circuit temperature.

2. Thermionic Efficiency

The emissivities of the converter electrodes are important because of their effect on performance. The effects of cesium plasma and plating of materials on the electrodes during operation are not yet known. These effects may be deleterious to performance since thermionic efficiency may degrade during converter operation.

3. Thermal Criterion

The selection of a cathode temperature and the operating condition corresponding to that temperature is a major uncertainty affecting the whole system design. Data are required to select the critical condition needed to establish reasonable design limits.

4. Fission Gas Products

The disposition of fission products for a thermionic fuel element is still questionable. Vented and contained gas designs are possible

but both present significant problems. The vented gas designs present the problem of condensation of products in vents and passageways which could result in a stoppage of flow and a buildup of pressure within the converters. The gases could be allowed to permeate the interelectrode spaces where they would be vented by flushing with cesium vapor. However, the effect of plating of condensables on the electrodes and the effects of contaminating the cesium vapor are as yet unknown. Contained gas designs incur system weight penalties due to the containment volume required in the reactor. Also, the contained gases present the problem of cathode distortion and possibly cathode failure due to pressure buildup.

5. Arcing Problems

The relatively high electrical conductivity of the cesium plasma and the voltages existing in the fuel element raise the possibility of arcing in the elements. This can occur between converters and between the cesium reservoir and the converters. Either case will produce a degradation in power, the latter being the more serious since it could produce a complete short circuit of an assembly.

6. Materials and Fabrication

Although efforts are currently in progress in these areas, much additional work is required to determine, 1) the radiation stability of the fuel element materials, especially the fuel and ceramic insulators, 2) the compatibility of the materials, and 3) the fabrication of the element components.

7. Structural Requirements

The structural requirements for the thermionic fuel element are severe due to the extreme operating conditions existing within the element and the use of complex ceramic and metal structures. In particular, the cathode lead, the cathode support, the graded seal and the ceramic trilayer pose difficult structural problems. These components are highly stressed due to large thermal gradients, differences in coefficients of expansion and launch loads. In addition, thermal cycling and thermal shocks must be sustained during power-plant transients, especially those caused by system component failures. Extensive analytical, design and experimental work are required to insure the structural integrity of the element.

B. Reactor

A number of problems arise concerning the fabrication and operational feasibility of the reactor. These include the operation of external control drums having bearing surfaces that must operate in a space environment without welding. The control of the reactor by control drums without severe scalloping should be experimentally verified to insure a flattened power distribution. The support of the fuel assemblies and the containment of two coolants present problems that must be solved. Endurance of the reflector at high temperature in the vacuum environment is questioned at high radiation dose.

C Shield

The major technical uncertainty in the shield design is the containment of LiH. At elevated temperatures such as 800°F, LiH dissociates to form gaseous hydrogen and liquid lithium, and therefore an overpressure of hydrogen is required. Hydrogen gas diffuses through most materials, such as stainless steel, so that hydrogen will be lost during operation for extended periods at high temperatures. The ability of the shield to stop neutrons will be decreased. Also, liquid lithium will be liberated with the attendent corrosion problem. Further analytical and experimental efforts should be made to resolve the shielding problems.

D. Radiator

The design of space radiators is still somewhat uncertain due to lack of meteoroid occurrence and penetration data. Current radiator designs are based on theories and correlations of little data which have not yet been substantiated.

High-emissivity coatings require development to insure a high emissivity at high temperatures in a space environment for long periods of time. Low-emissivity coatings appear attractive for startup to eliminate the weight of auxiliary heating units or the use of cumbersome insulating blankets. Such properties as emissivity, evaporation and compatibility need to be evaluated to determine the worth of the coatings.

E. Power-Conditioning Equipment

Future missions into deep space will require large blocks of electric power for propulsion, communications, and other systems. Power-conditioning equipment will undoubtedly be required to tailor the primary power output to the system requirements. The design criteria for space power-conditioning equipment are minimum weight, maximum efficiency, and high operating temperatures, in addition to high reliability. Unfortunately, space power-conditioning equipment using state-of-the-art components is rather heavy, and operates at relatively low temperatures. The low operating temperature offsets the high efficiency of the equipment, since the power lost must be dissipated at a low temperature with a subsequent high auxiliary radiator weight. Requirements to condition power for the electromagnetic pumps have not been examined and may result in difficult problems.

F. Electromagnetic Pumps

Direct current electromagnetic pumps in use today are both heavy and inefficient. To develop electromagnetic pumps suitable for use in space, extensive analytical and experimental work must be conducted. Such problems as magnetic fringing, magnetic saturation and current losses must be solved to produce lightweight pumps. Materials investigations should be conducted to find high-temperature materials possessing high Curie points and low electrical resistivities for magnetic and electrical conductors. Also, compatibility investigations should be conducted to determine the types of high-temperature insulation that can be employed in pump design.

G. Powerplant Operation

Control schemes must be analyzed as to powerplant stability, accuracy and reliability of control, and whether maximum powerplant performance can be achieved without exceeding thermal limits in normal operating transients. The powerplant should respond to changes in electric power demand and expected radiator failures.

Powerplant reliability analyses now consider only component failures from meteoroid punctures. More complete reliability analyses which consider other failure modes are desired, but data on component reliability are lacking.

The control of the powerplant is possible only if instrumentation can be developed to operate in a nuclear space environment for long periods of time. Experimental verification is required for instrumentation such as neutron counters.

V. RECOMMENDED FUTURE PROGRAMS

Report PWA-2224 presented a thorough listing of experimental programs required to solve the many materials problems present in a one megawatt nuclear thermionic space power system. Since the powerplant study presented in this report is encumbered with the same problems, the recommended future programs remain the same and will not be repeated here.

Since the issuance of Report PWA-2224, additional experimental work has been performed. Appendix 8 of this report presents a compilation of the significant results obtained from these efforts.

APPENDIX 1

Powerplant Structural Analysis

APPENDIX I

Powerplant Structural Analysis

Structural analyses were performed for the critical structure areas in the powerplant. The analyses considered the problems involved in supporting the reactor vessel, the core, the radiators and the entire powerplant. Since data is not yet available for Saturn 5 loading, data for the Saturn 1 was used. A compilation of this data given in Report PWA-2224, shows that a maximum load of 15G axial and 7G side can be anticipated during transportation and that a 12G axial and a 5G side load can be expected during launch.

Support of the reactor is accomplished as shown in Figure 1-1. A cylindrical skirt extending from the upper head of the vessel supports the reactor in tension during axial loading. Eight cross-links attach to the lower head of the vessel at the lower control drum mounts and support the vessel during side loading. The support structure within which the vessel is hung consists of three rings with four interconnecting struts as shown in Figure 1-2. The upper ring attaches to the reactor skirt, and the lower ring attaches to the forward support ring.

Figure 1-3 shows the attachment of the reactor to the reactor support, the thermal gradient along the reactor during space operation, and the accompanying stresses for transportation and launch. Also shown are thermal stresses encountered during space operation. The stresses for launch and transportation are below the yield strength. During space operation, local yielding due to thermal stresses, occurs at the attachment of the core support to the reactor vessel. Although the vessel yields, space maneuver loads are negligible and the plastic strain is less than the design allowable for a 100-cycle life.

Figure 1-4 shows a summary of reactor support structure stresses for transportation and launch loads. Titanium AMS 5613 was selected as the material since it resulted in smaller ring and strut sizes and is easier to fabricate than AMS 4910 titanium. The strength-weight ratio for both materials at the launch temperature is the same, indicating negligible weight difference.

In Figure 1-5 is shown the reactor core support, its attachment to the outer shell of the reactor, and the pertinent stresses due to vertical loads. Lateral loads are distributed along the length of the reactor shell and do not present a significant problem at this location.

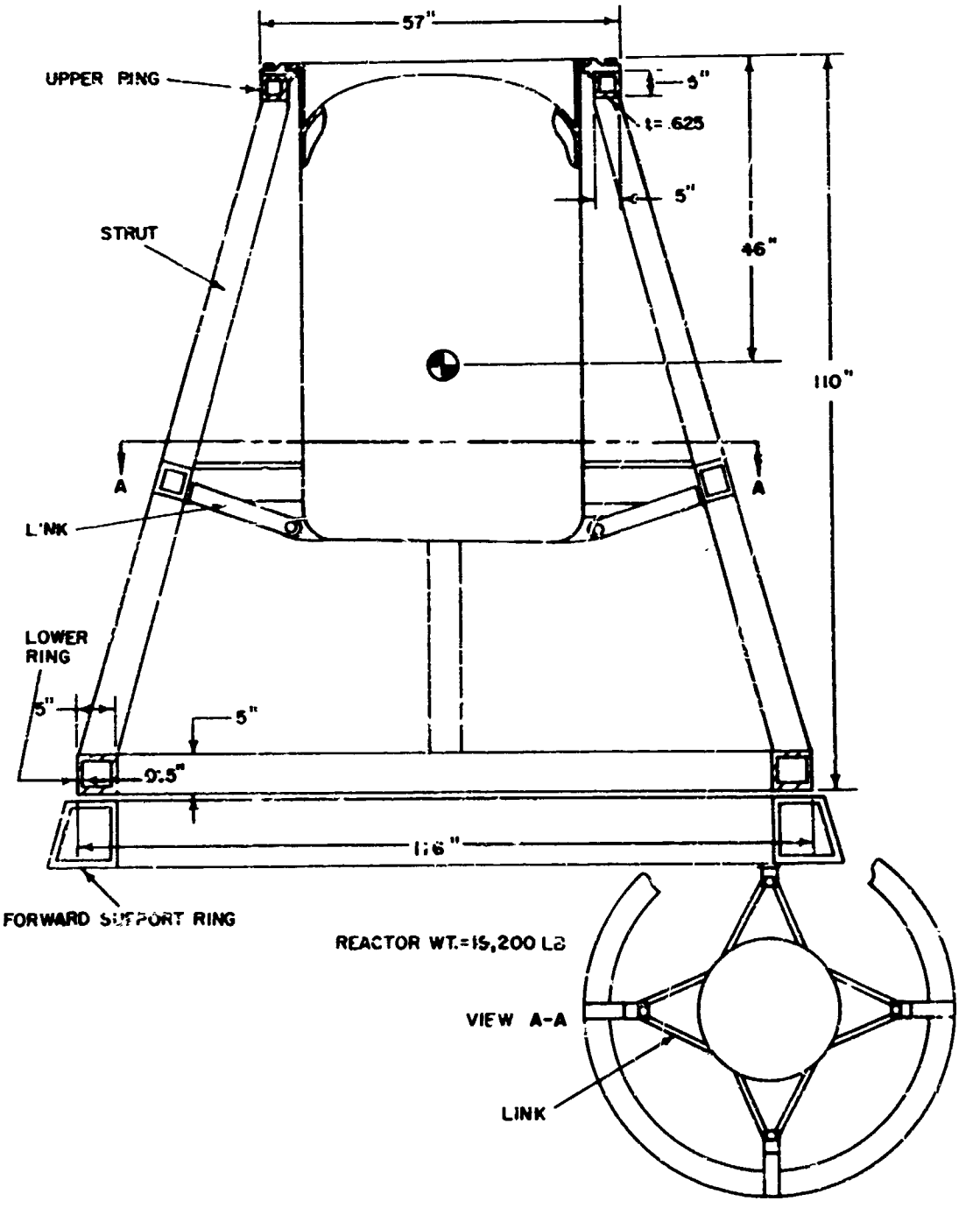

Figure 1-1 Reactor and Support

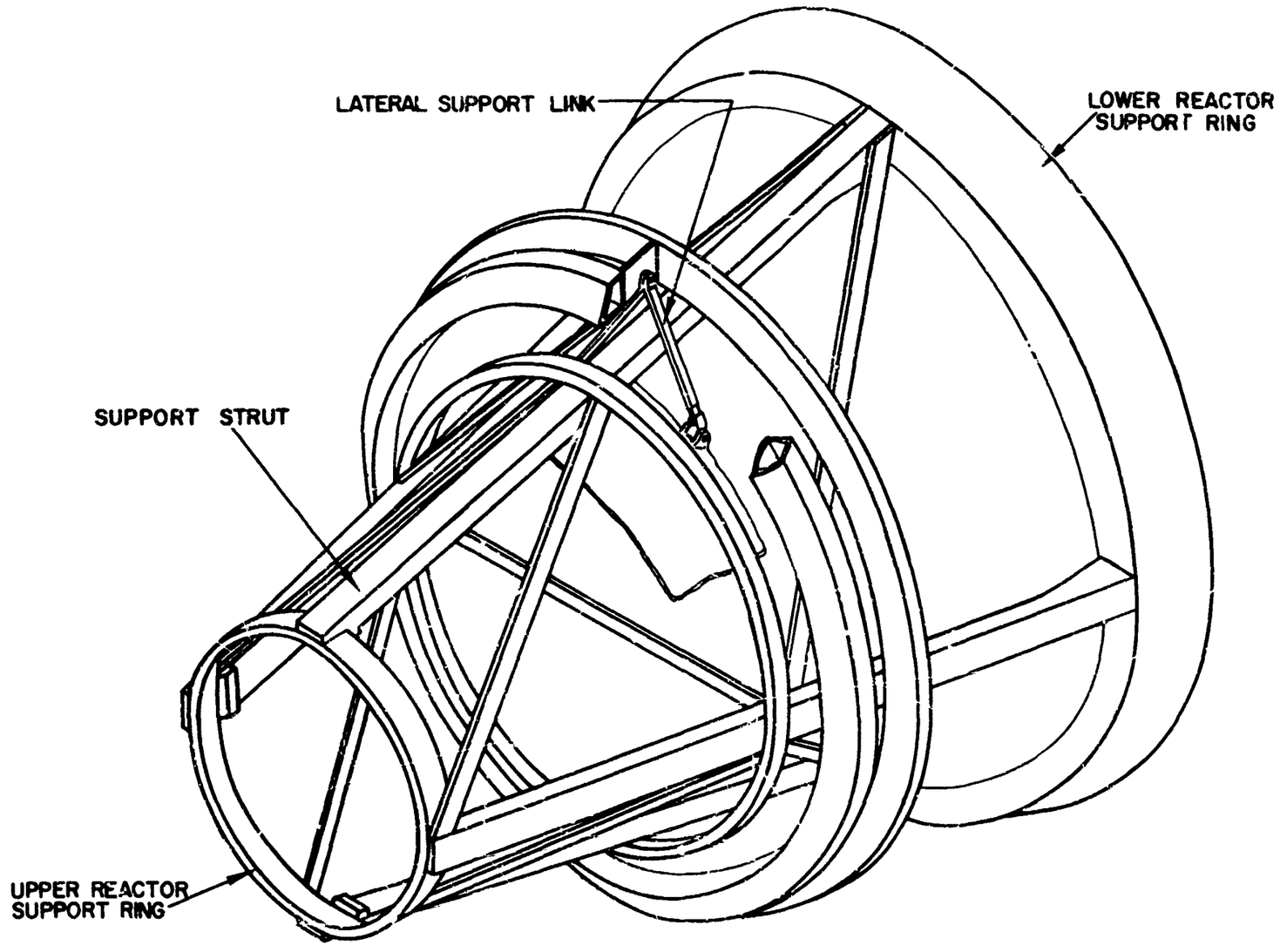

Figure 1-2 Reactor Support Structure

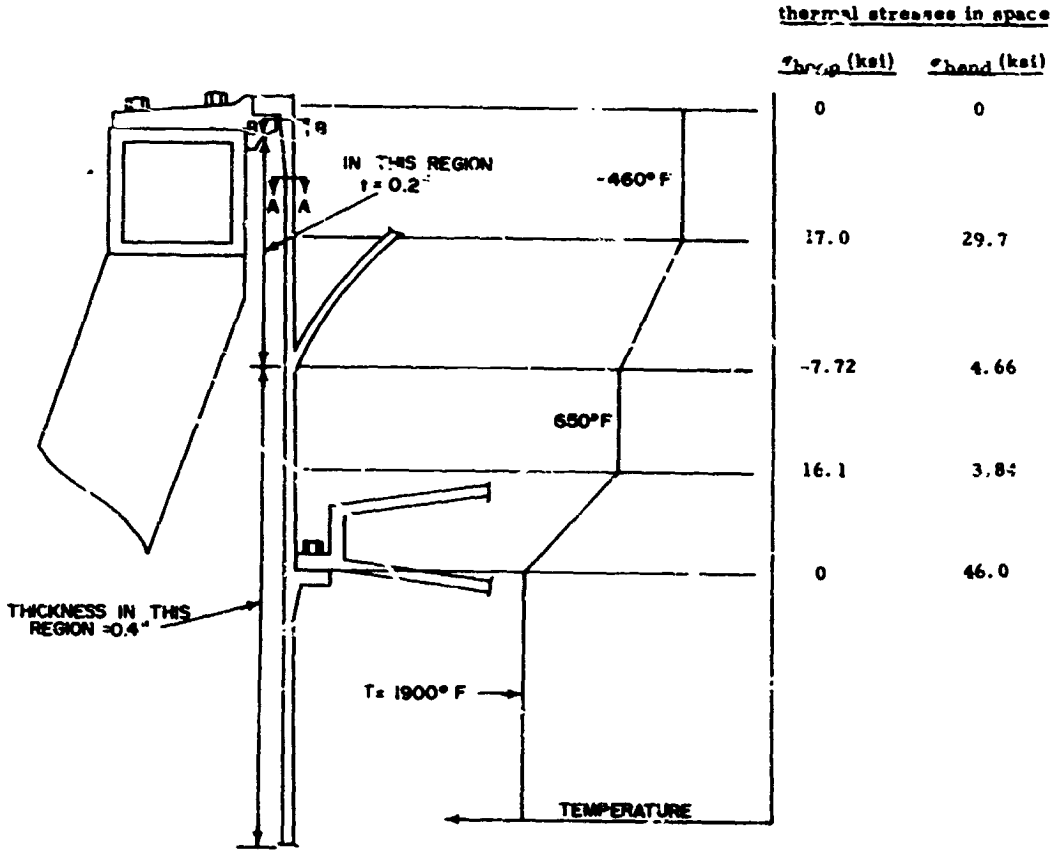

section	t, inch	T	transportation (higher of 15G vert. or 7G side) $\sigma_{max}\left(\frac{Mc}{I}+\frac{P}{A}\right)$, psi	T(max)°F,	launch (higher of 12G vert. or 5G side) $\sigma_{max}\left(\frac{Mc}{I}+\frac{P}{A}\right)$, psi
A-A	0.2	ambient temp.	14,200	700	11,400
B-B	0.34	ambient temp.	34,800	700	27,800
yield strength			36,000		30,500

Figure 1-3 Reactor Attachment Stress Summary and Temperature Profile of Reactor in Space

		TRANSPORTATION		LAUNCH T = 700°F (Max)	
		15 G Axial	7 G Side	12 G Axial	5 G Side
Upper Ring 5" x 5" x 5/8" (min)	M_{in}	113,000 in-lb	196,000 in-lb	90,500 in-lb	140,000 in-lb
	M_{out}	198,000 in-lb	1,080,000 in-lb	159,000 in-lb	770,000 in-lb
	T_{max}	29,800 in-lb	1,750,000 in-lb	23,800 in-lb	1,250,000 in-lb
	σ_{max}	26,200 psi	108,000 psi	21,000 psi	76,800 psi
	τ_{max}	1,500 psi	74,000 psi	1,200 psi	52,800 psi
	$\sigma_{y.s.}$	110,000 psi	110,000 psi	90,000 psi	90,000 psi
Lower Ring 5" x 5" x 1/2" (min)	M_{in}	105,000 in-lb	406,000 in-lb	84,000 in-lb	290,000 in-lb
	M_{out}	-	-	-	-
	T_{max}	-	-	-	-
	σ_{max}	8,900 psi	34,200 psi	7,100 psi	24,500 psi
	τ_{max}	-	-	-	-
	$\sigma_{y.s.}$	110,000 psi	110,000 psi	90,000 psi	90,000 psi
Strut 5" x 5" x 1 3/16"	M_{max}	-	2,000,000 in-lb	-	1,430,000 in-lb
	P_{max}	47,400 lb	62,000 lb	37,900 lb.	44,300 lb
	σ_{max}	3,000 psi	110,000 psi	2,500 psi	78,500 psi
	$\sigma_{y.s.}$	110,000 psi	110,000 psi	90,000 psi	90,000 psi
Link A = 1 in^2	P_{max}	-	25,600 lb	-	18,200 lb
	σ_{max}	-	25,600 psi	-	18,200 psi
	$\sigma_{y.s.}$	-	110,000 psi	-	90,000 psi

Material - AMS 5613 RC 30-38

M_{in} = Ring, in-Plane Moment
M_{out} = Ring, Out-of-Plane Moment
T_{max} = Ring, Maximum Twisting Moment

Figure 1-4 Reactor Support Stress Summary

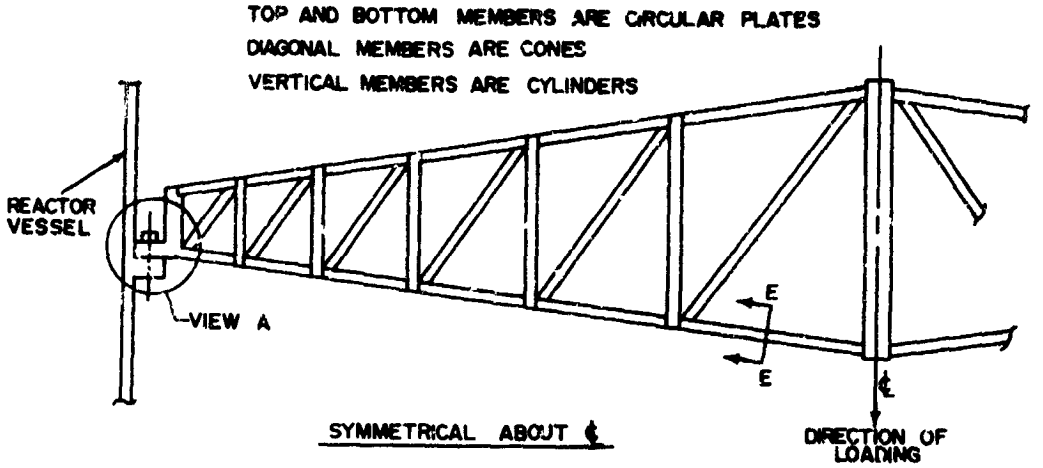

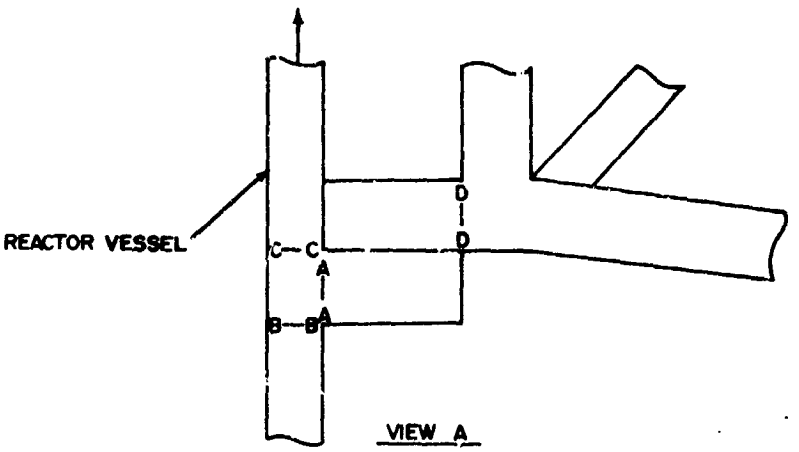

		transportation (15G)		launch (12G)	
section	t, inch	T	$\sigma_{max}(\frac{Mc}{I}+\frac{P}{A})$, psi	T(max), °F	$\sigma_{max}(\frac{Mc}{I}+\frac{P}{A})$, psi
A-A	0.5	ambient temp.	17,500	700	14,000
B-B	0.4	"	19,300	700	15,500
C-C	0.4	"	23,000	700	18,400
D-D	0.5	"	18,000	700	14,400
E-E	0.3	"	33,800	700	27,000
yield strength			36,000	700	30,500

Figure 1-5 Reactor Core Support

All of the radiators in the powerplant are coplanar and are supported within the radiator support structure, one-half of which is shown in Figure 1-6. The radiators are secured within this structure and are allowed to grow thermally against leaf springs located within the lower manifold supports. Attachment for this structure occurs at the main forward and aft support rings. The structures are hung in tension from the upper ring and can grow thermally relative to the launch structure by four expansion joints located on the aft support ring. During launch the radiator structure is free to grow axially and radially but is guided laterally by the launch structure.

Figure 1-7 shows the main and auxiliary radiator tube stresses. Provided the launch structure is essentially rigid, the vibratory input will be attenuated to less than 1 G in the first mode. However, resonance could occur if the higher modes are excited. Damping or methods to ensure that the higher modes will not be excited can be incorporated in the design.

The powerplant support structure is divided into two sections, the launch structure and the inflight structure. The launch structure which supports the powerplant above the launch vehicle is hinged to the vehicle at the aft support ring (Figure 1-8). This structure is rotated outboard at the time of vehicle separation. The inflight structure supports the vehicle in space.

The launch structure is divided into four quadrants, each quadrant forming a trussed column approximately 95 feet long. When installed, the four quadrants are mechanically tied together by shear webs (Figure 1-8, Section S-S) to comprise a single structure unit of high rigidity. This single unit becomes the launch weight support system for all liquid metal components, including the main radiators. Individual truss members are sized on the basis of buckling and load carrying requirements. Where necessary, wall thicknesses are increased in weld zones to provide adequate weld areas.

The primary liquid metal system is mounted on top of the launch structure (Figure 1-8). The secondary liquid metal system is hung inside the launch structure, i.e., the radiators and all secondary system plumbing are supported by permanent structure which is attached to the forward and aft support rings. This arrangement places the inflight structure in tension during launch, an arrangement that precludes the nec-

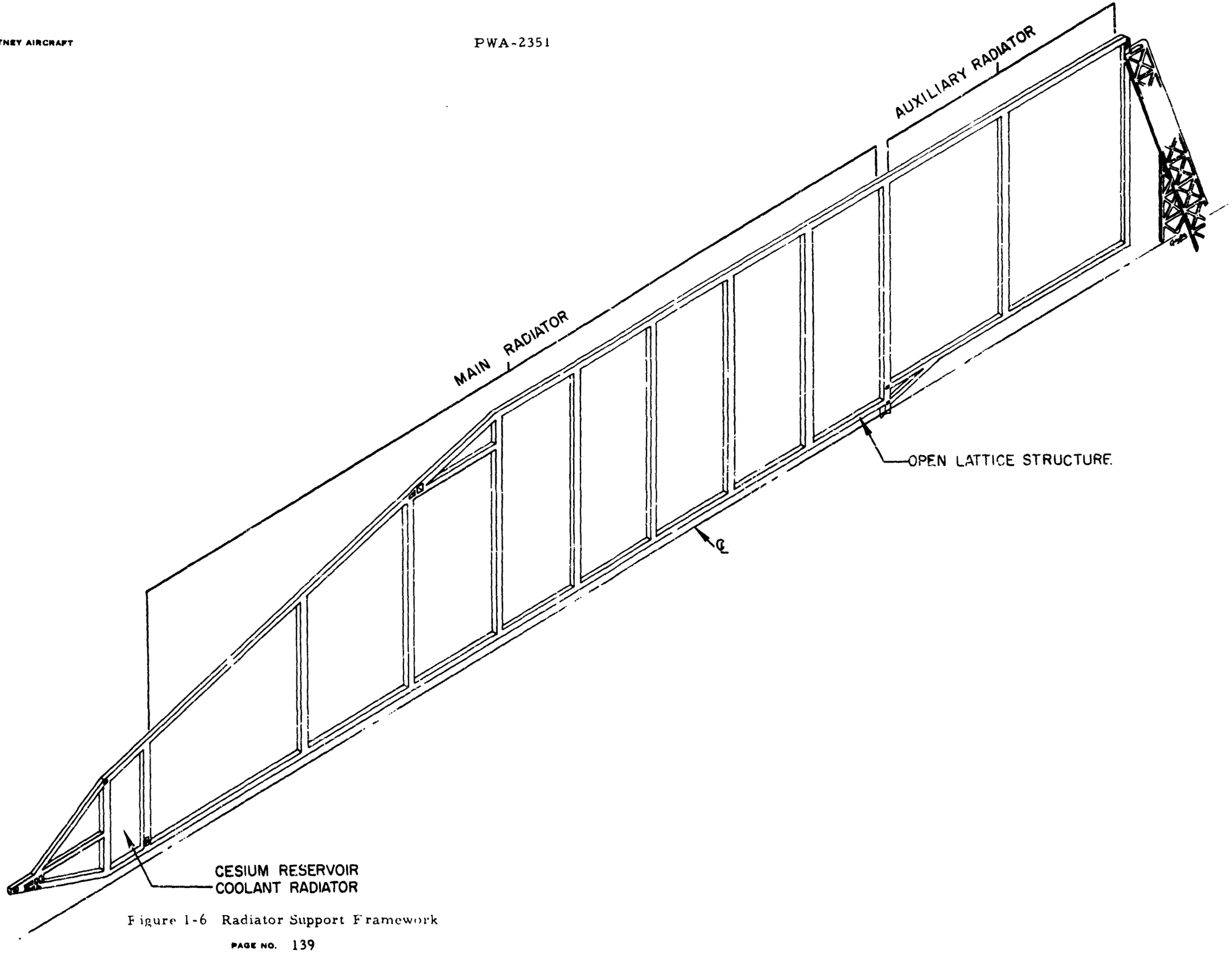

Figure 1-6 Radiator Support Framework

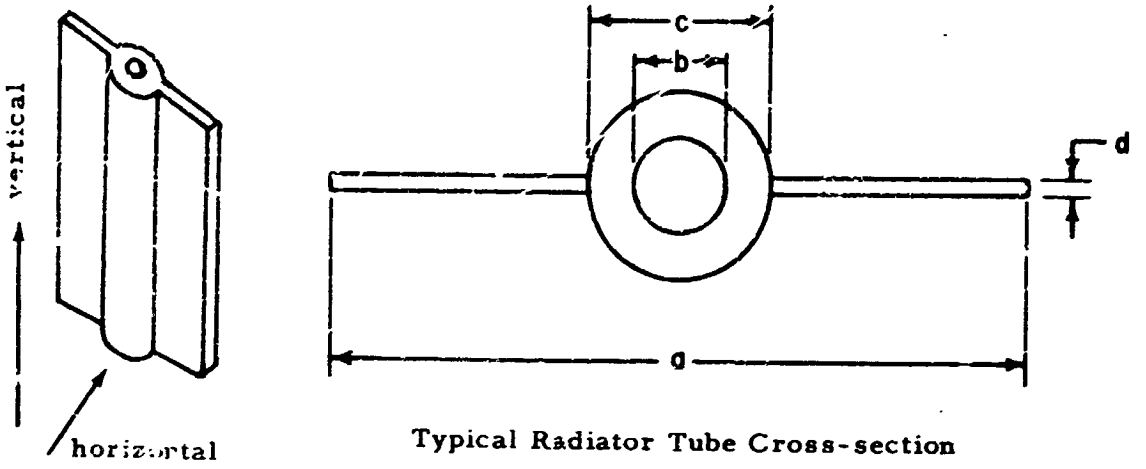

Typical Radiator Tube Cross-section

	secondary loop cooling system	auxiliary cooling system
material	Cb - 1Zr	6061 aluminum
inlet temp	1919°F	500°F
length	77 in.	99 in.
a	1.256 in.	7.53 in.
b	.142 in.	.126 in.
c	.376 in.	.712 in.
d	.028 in.	.028 in.
12G vert. σ	370 psi	180 psi
5G horiz. σ	27,500 psi	10,100 psi
launch temp.	700°F (max)	500°F(max)
yield strength at launch temp.	30,000 psi	14,000 psi
natural frequency	3.2 cps	4.7 cps

Stresses in space due to assumed propulsive load of 0.01G are well below the 0.5% creep stress in 20,000 hours

Figure 1-7 Radiator Tube Stresses

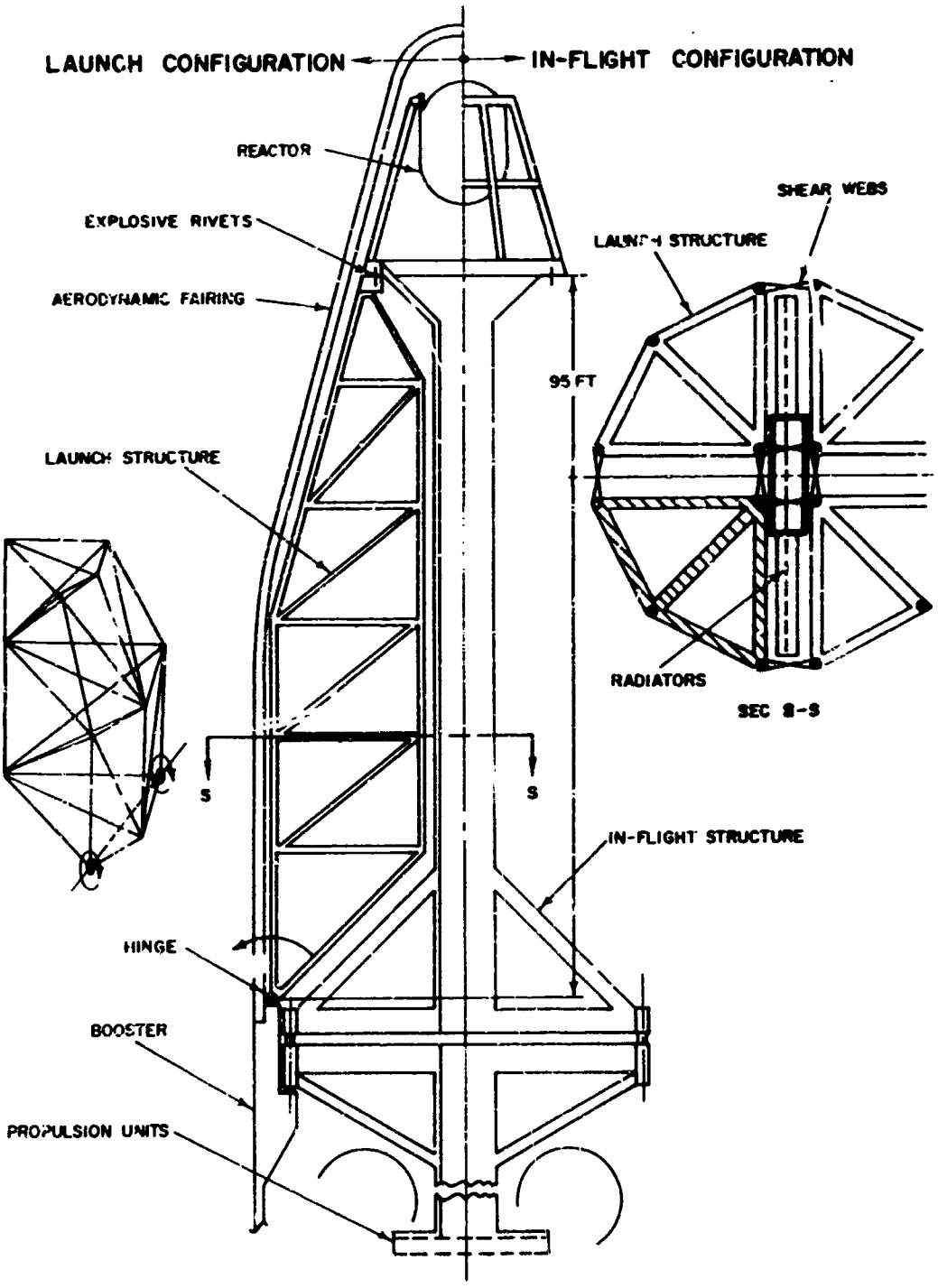

Figure 1-8 Structural Schematic

essity of designing for buckling. This arrangement also provides the intermediate permanent structure with good transverse support and full freedom for axial thermal expansion.

Prior to launch, all liquid metal-containing components (reactor, piping, pumps, and radiators) will be preheated to 700°F by means of inert gas. A gas-tight insulated enclosure will be provided around all of these components as shown by Figure 25. This blanket will be stripped away from the radiator surfaces by the removal of the launch structure. From the startup studies, it is anticipated that the launch structure will attain a temperature of approximately 300°F prior to launch.

Figures 1-9 and 1-10 show the primary structure and a summary of the critical members in the structure. The size of these members at the base of the structure is 13.75 inches in outside diameter to reduce the stress below the yield strength and to get a minimum buckling margin of 30 per cent.

total weight = 67,000 lbs

launch loads
a) 12G vertical
b) ± 5G horizontal

critical member summary

material AMS 4910 titanium
T_{max} = 300°F

max. load 5C horiz. = 445,000 lbs
max. load 12G vert. = 92,000 lbs
σ_{max} = 72,000 psi
yield strength at 300°F = 80,000 psi
buckling load = 575,000 lbs

section properties
outside diameter = 13.75 in.
inside diameter = 13.60 in.

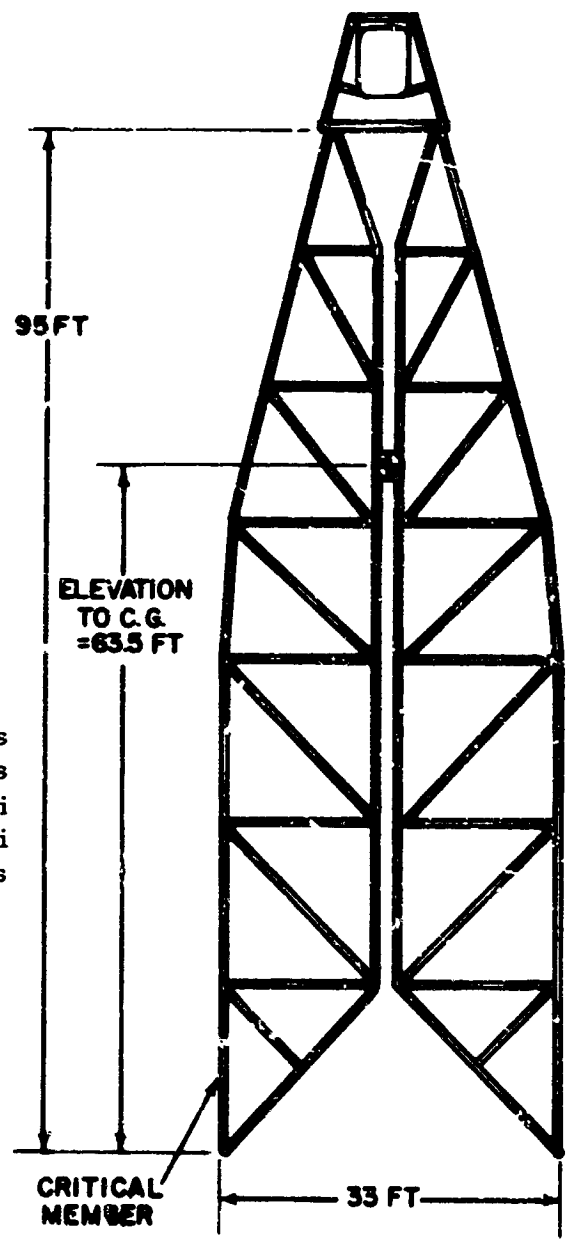

Typical Cross-Section

Figure 1-9 Launch Structure

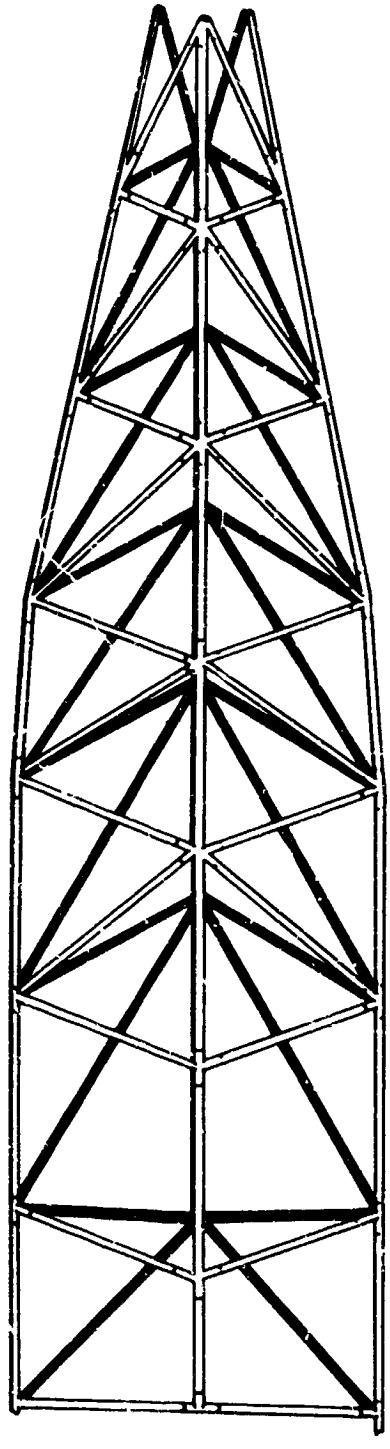

Figure 1-10 One Quadrant of Launch Support Structure

APPENDIX 2

Powerplant Configuration and Vehicle Payload Studies

APPENDIX 2

A. Comparison of Powerplant Configurations

This appendix presents the results of a preliminary study performed to compare the weights of 3.25-megawatt powerplants with two radiator configurations, 1) planar, and 2) cylindrical. The purpose of the study was to aid in the selection of a minimum weight arrangement for the reference powerplant design. This is desirable, both to minimize launch vehicle requirements and to maximize payload capability. The initial comparison was made as shown in Figure 2-1 using the parameters for the power-conditioning equipment that were available at the start of the design effort. Upon receipt of new conditioning equipment data from Westinghouse, a revision of the weight estimates presented in Figure 2-2 was made. Support studies were performed for cylindrical shields and radiators, and the results of these studies are presented in Appendix 3 and 4, respectively.

In addition to the two alternative configurations, two types of power-conditioning equipment were considered, 1) low-temperature solid state equipment, and 2) high-temperature gas tube equipment. The operating temperatures and the efficiencies for this equipment are important because they have a drastic effect on auxiliary radiator area, overall weight and powerplant configuration.

1. Initial Comparison

The alternatives given above result in four possible powerplant configurations which are shown in Figure 2-1. The estimated system specific weights which were based on the initial power-conditioning equipment data are also given in the figure. Comparing the planar configurations with the cylindrical (1, 2 vs 3, 4) it can be seen that the former have a lower weight. This is due primarily to the shield weights which are listed below.

	Shield Weight - lb	
	Low-Temperature Power-Cond. Equip.	High-Temperature Power-Cond. Equip.
planar	6,900 lbs	7,200 lbs
cylindrical	17,000	18,400

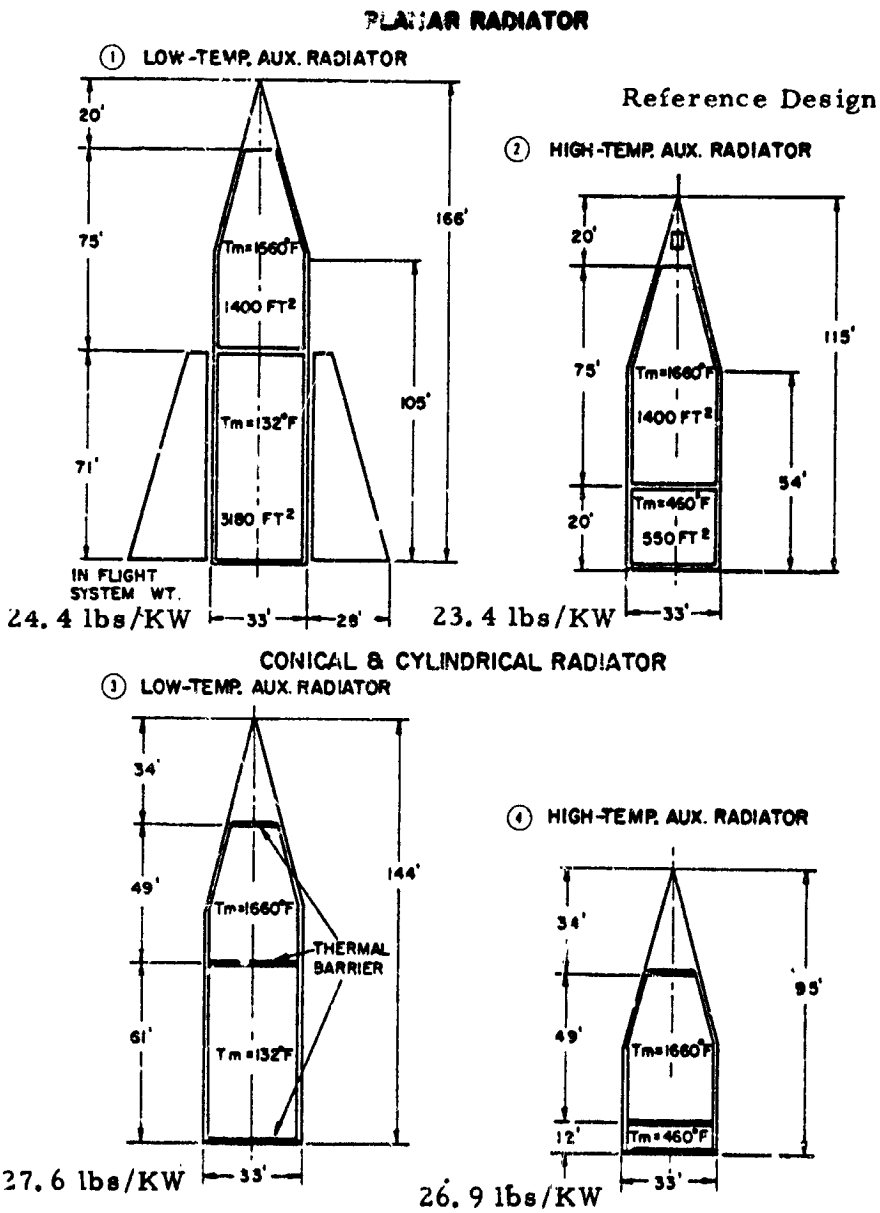

Figure 2-1 Radiators for 3.25-MW Thermionic Powerplant

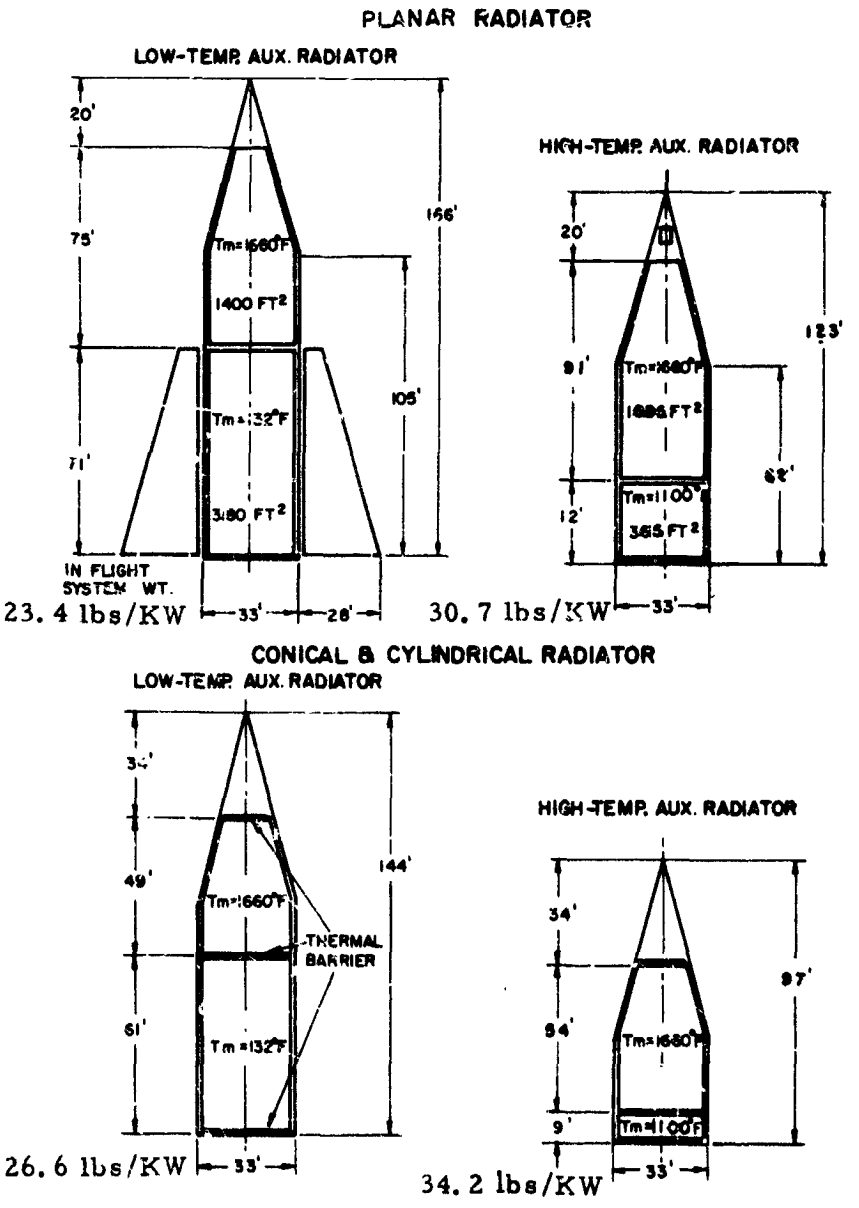

Figure 2-2 Revised Estimates Based on New Power-Conditioning Information

The cylindrical powerplant shields are larger and therefore heavier, since they must provide a solid angle of shadow defined by the conical portion of the powerplant. This requires the geometry of the shield for the cylindrical powerplant to be a truncated cone while only a slab-shaped shield is required for the planar powerplant. Also, since the cylindrical powerplants are shorter, the reactor is closer to the dose point which requires the axial thickness of these shields to be greater than the thickness for the planar configurations. A comparison of the weights of the radiators for both configurations shows that there is no significant difference between them (see Appendix 4 for cylindrical radiator weights).

Comparing the powerplants employing low-temperature power-conditioning equipment with those using the high-temperature equipment (1,3 vs 2,4) shows that the low-temperature powerplants are moderately heavier, but significantly larger. Since the payload enclosure of the launch vehicle is of fixed diameter, the low-temperature powerplants are much longer, requiring increased launch structure weights. In addition, the low-temperature planar configuration requires the deployment of a part of the auxiliary radiator which places an additional reliability restriction on this powerplant.

Based on the above comparisons, the planar configuration utilizing high-temperature power-conditioning equipment was selected for the reference design. This configuration results in the lowest inflight weight which, as shown in the analysis of payload capability, permits the greatest payload delivery at the end of the mission. The lightest powerplant in space requires the least amount of fuel for propulsion so that additional payload can be carried aboard. In addition, the planar configuration was selected over the cylindrical because the launch structure can be jettisoned more easily. Although the weights given in the figure do not include launch structure weights, it can be assumed that the in-flight weights of cylindrical powerplants will also be greater because of the inherent difficulty in jettisoning all of the launch structure. This can be anticipated, since some of the launch structure for the cylindrical powerplants will probably be contained within the radiators.

2. Revised Comparison

The study described above and the selection of the configuration for the reference design powerplant was made prior to the publication of Reference 1 which concerns space power-conditioning equipment. This report presented conditioning equipment weights and required heat rejection systems that were different from the data used for the reference design. For example, a specific weight of 5 lbs/KW(e) was assumed for both the high and low-temperature equipment whereas the report showed this estimate to be slightly pessimistic, by 1 lb/KW(e), for the low-temperature equipment but very optimistic, by 5 lbs/KW(e), for the high-temperature equipment. Also, an efficiency of 93 per cent was assumed for the high-temperature equipment where the report published efficiencies of less than 80 per cent. However, the error in this assumption was mitigated by the selection of a conservative operating temperature of 500°F, whereas the report indicated operating temperatures of 1100°F. The estimated heat rejection temperature and efficiency for the low-temperature equipment were correct. Therefore, the radiator area used in the original study for both the high and low-temperature equipment is within reason. The weight assumed for the high-temperature equipment, however, is not.

A re-evaluation of the specific weights and the system parameters was made based on the new data given in the referenced report. For the systems employing the high-temperature equipment, the auxiliary radiator employed NaK as a coolant and stainless steel as the containment material. The revised weights and powerplant dimensions are shown in Figure 2-2, and some of the system parameters are given in the table . As was mentioned previously, the initial assumptions concerning efficiency and heat rejection temperature were somewhat compensating so that the changes in the sizes of the radiators did not significantly change the powerplant dimensions.

---

[1] Westinghouse Electric Corporation, Aerospace Electrical Division, Space Electric Power Systems Study, Volume 5

Revised System Parameters

	Low-Temp. Equipment	High-Temp. Equipment
Powerplant Specific Weight (Inflight, lbs/KW(e)	23.4	30.7
Overall System Efficiency, %	10.5	8.8
Auxiliary Radiator Area (Projected one-side), ft^2	3180	365
Auxiliary Radiator Weight, lbs.	3250	1800
Average Auxiliary Radiator Temperature, °F	132	962
Average Auxiliary Radiator Materials	MIPB-AL	Nak-S.S.
Power-Conditioning Equipment Efficiency, %	93	78
Power-Conditioning Equipment Specific Weight, lbs/KW(e)	4	10

Comparing the new weights of the powerplants shows that the planar configuration utilizing high-temperature equipment is no longer the lightest. Both the planar and the cylindrical configurations employing low-temperature equipment are lighter. However, the much greater lengths of these powerplants will require heavier launch structure. Also, it can be anticipated that the inflight weight of the cylindrical powerplant will be greater than that shown, due to the difficulty in jettisoning launch structure.

There are other considerations and trade-offs that must be taken into account before a complete evaluation can be made. Therefore, although it may appear at first that the new data causes a change in the selection of the powerplant, additional design and analytical studies must be conducted to determine with confidence the best possible configuration.

B. Vehicle Payload Analysis

Payloads have been estimated for a typical one-way Jupiter orbiter using a propulsive powerplant with 3.25 megawatts net electric output. The powerplant ground launch weight and interplanetary flight weight were considered parametrically to permit comparison of vehicle performance with various powerplant configurations. The powerplant flight weight was found to be usually the more important factor in determining the spacecraft payload. For example, it was also found that for the reference powerplant, if the inflight weight is increased by 1 pound, and the launch weight decreased by 1 lb, the payload capability reduces by 0.4 lb. Whereas, if the launch weight is increased by 1 pound and the inflight weight decreased by 1 lb, the payload capability increases by 0.4 lb. This result is important when comparing powerplant configurations and indicates that the lighter inflight powerplant can deliver a greater payload even if the launch weight is heavier.

The Mission

The specific mission considered was an 825-day transfer from a 300-nautical mile earth orbit to a satellite orbit around Jupiter at an altitude of 50,000 nautical miles. For the various powerplant configurations examined, the transfer time from earth orbit to a high altitude elliptic orbit around Jupiter (a situation in which the spacecraft is barely captured by Jupiter's gravitational field) varies from about 630 to 650 days, and the minimum propulsion time required to spiral down from this condition to a 50,000 nautical mile circular orbit varies from about 195 to 175 days. The minimum total flight time is 825 days in all cases. The spiral time can be lengthened if desired (with a resulting increase in total mission time) by either reducing thrust or by using intermittent instead of continuous thrust. Observation time at various altitudes can be adjusted in this manner, as desired.

Performance Results

It was assumed that the launch vehicle could boost 226,000 pounds into a 300-nautical mile earth orbit.

With low-thrust electric propulsion systems, high acceleration loads will be encountered only during the initial launch from the ground int-

earth orbit. Consequently there will be a large portion of powerplant support structure which is required only during this high acceleration phase. Some powerplant designs may permit jettisoning of this structure once the spacecraft has reached its earth orbit. Jettisoning this structure is advantageous since it is merely dead weight so far as the remainder of the mission is concerned.

Figure 2-3 shows the spacecraft propellant requirement for this typical

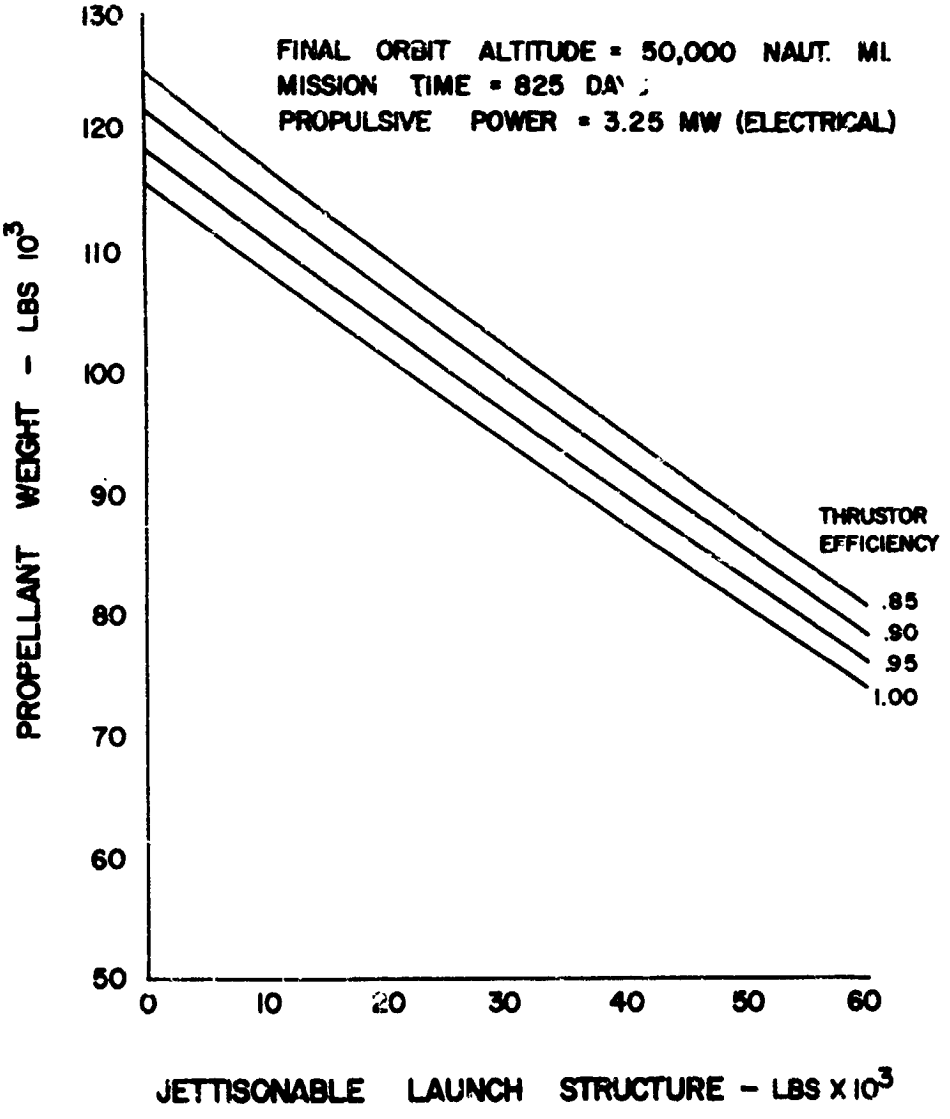

Figure 2-3 Propellant Requirement for Jupiter Satellite Mission

mission as a function of the dead weight that can be jettisoned, assuming that a total of 226,000 pounds is originally placed in earth orbit. Results are shown for various thrustor efficiencies.

Figures 2-4 and 2-5 show the resulting gross payload as a function of the powerplant flight weight (weight after jettisoning launch structure) and powerplant launch weight (weight before jettisoning launch structure).

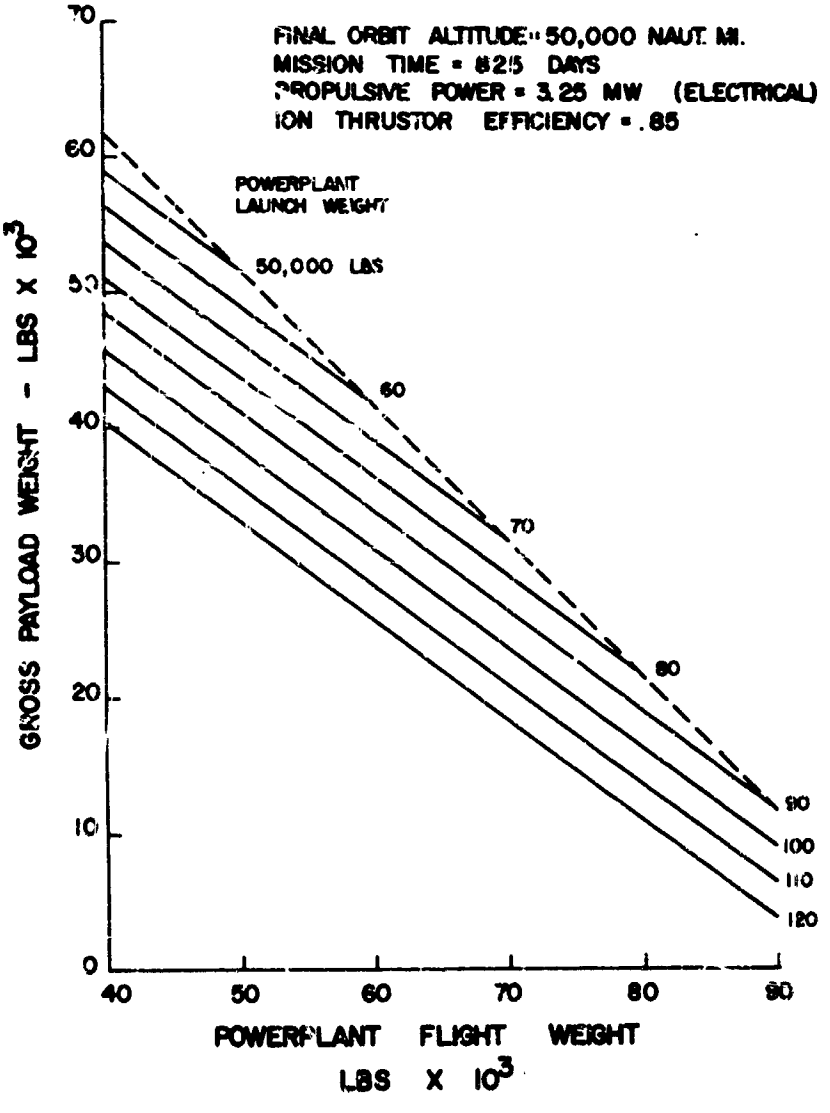

Figure 2-4 Jupiter Satellite Payload. Ion Thrustor Efficiency = .85

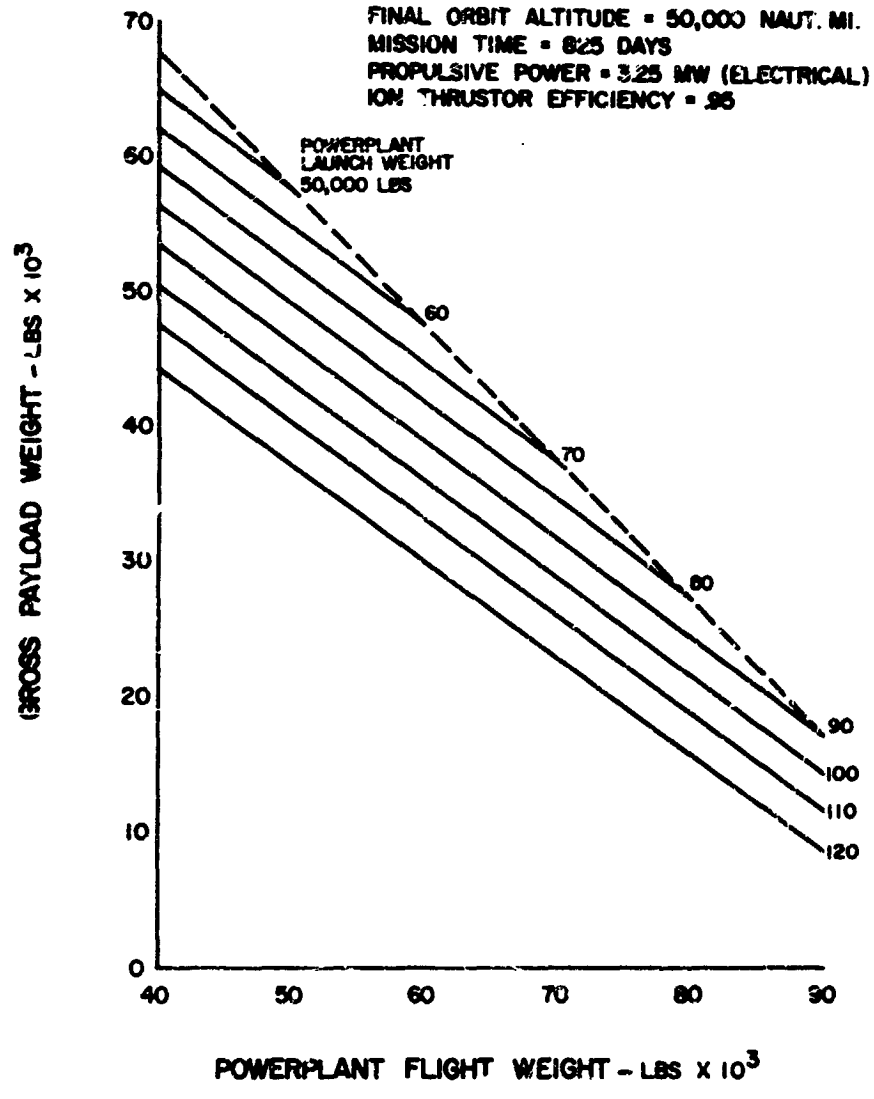

Figure 2-5 Jupiter Satellite Payload. Ion Thrustor Efficiency = .95

Thrustor efficiencies of .85 and .95 were used for Figures 2-4 and 2-5, respectively. To obtain net useful payload one must subtract, from the gross payload shown in the figures, an allowance for the weight of hardware such as thrustors, guidance and navigation equipment.

It can be seen from Figures 2-4 and 2-5 that the powerplant flight weight

generally influences the payload capability more significantly than does the powerplant launch weight. For an example, assume that the thrustor efficiency is .85. Then Figure 2-4 shows that a gross payload of 31,500 pounds can be obtained if the inflight powerplant weighs 70,000 pounds and no launch structure is jettisoned. The same payload can be obtained, however, if the powerplant weighs 90,000 pounds at takeoff provided that sufficient launch structure can be jettisoned in earth orbit to reduce the powerplant flight weight to 63,000 pounds. Similarly a powerplant with a 120,000-pound launch weight and a 52,000-pound flight weight would permit the same payload.

APPENDIX 3

Shielding Studies

APPENDIX 3

Shielding Studies

A nuclear shield is employed in the powerplant to provide shielding for the power-conditioning equipment. The semiconductor components of this equipment were used for setting the maximum allowable radiation dose. The total integrated dose over a 20,000-hour period was set at 10^{13} nvt (fast) for neutrons and at 10^{7} rads for gammas.

The shielding analysis was performed for the reference powerplant shield and for a cylindrical powerplant shield. Figures 3-1 and 3-2 show the models used for the nuclear analysis and the optimized dimensions. Studies for both shields were performed to aid in the selection of a configuration for the reference powerplant (see Appendix 2). Figure 3-3 shows the location of the shield and the distance between the reactor and the dose point (thepower-conditioning equipment) for both powerplants.

In the analysis, the shield is separated into a direct shield and a scatter shield. The direct shield is cylindrical and is equal in diameter to the outside diameter of the reflector which surrounds the reactor. The scatter shield fills the space between the direct shield and the powerplant envelope and attenuates neutron radiation striking the radiators which scatters into the power-conditioning equipment. The thicknesses of both shields were optimized on a minimum weight basis by varying the fraction of allowable dose through each portion of the shield.

Direct Shield

The direct shielding thicknesses required to achieve the allowable dose were calculated by use of a one-dimensional multigroup neutron diffusion code with a gamma and neutron shielding subprogram. The reference design reactor dimensions and composition were used in the code mockup.

Three materials were considered for use in the shield, 1) borated graphite for the high temperature portion of the shield, 2) tungsten for gamma shielding, and 3) lithium hydride for neutron shielding. It

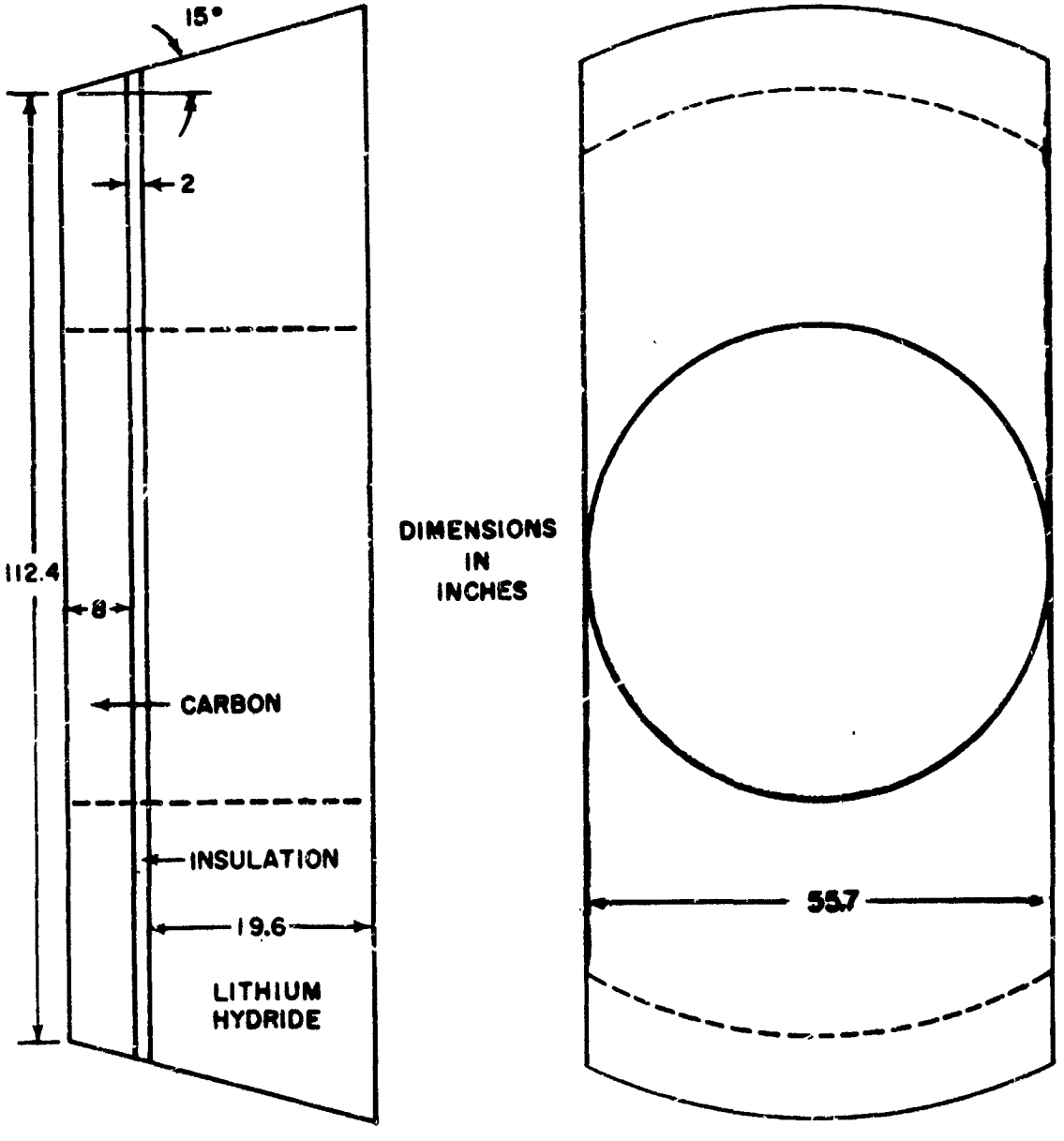

Figure 3-1 Reference Powerplant Shield
Specific Weight 2.22 lbs/KW(e)

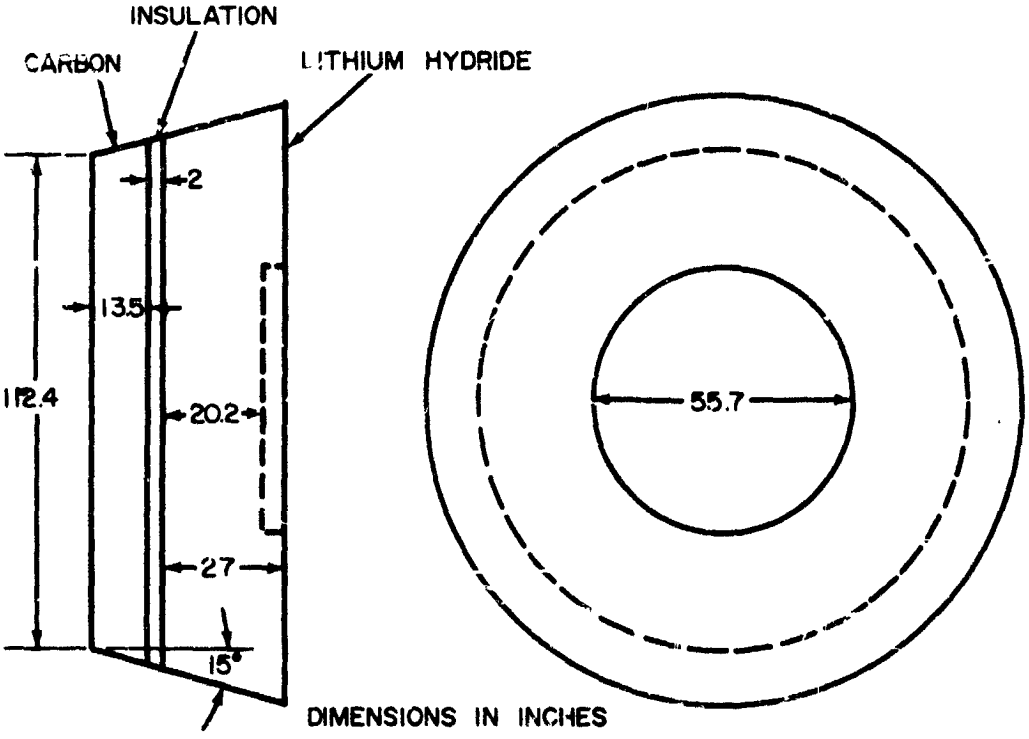

Figure 3-2 Cylindrical Powerplant Shield
Specific Weight 5.65 ibs/KW(e)

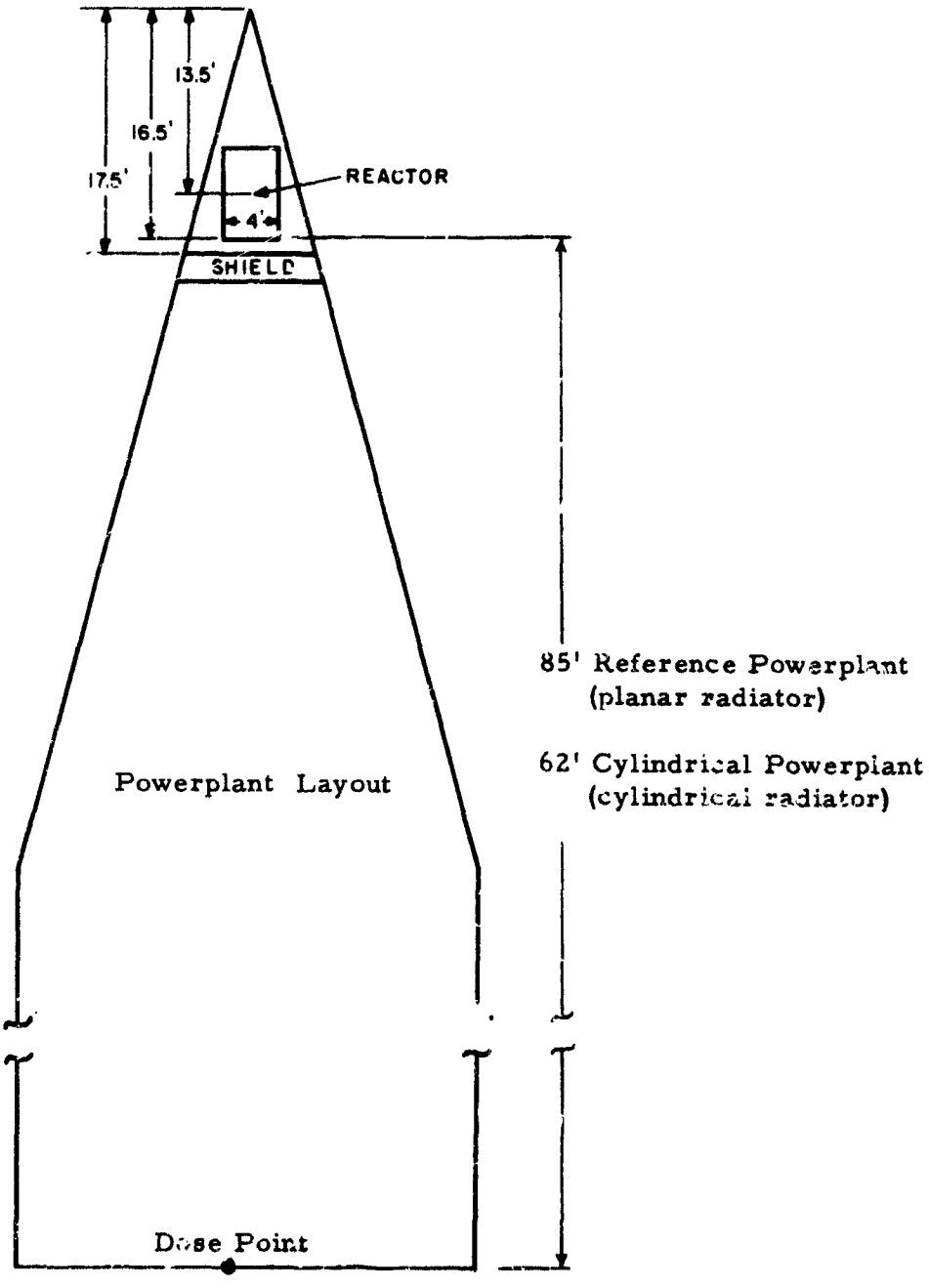

Figure 3-3 Vehicle Layout

was decided to use borated graphite in the shield to reduce the heat generation in the lithium hydride due to neutron heating. The addition of this material eliminated the need for gamma shielding so that the final shield designs contained only borated graphite and lithium hydride.

In the discussion of shield heating it will be shown that 8 inches of borated graphite is needed to thermally protect the reference powerplant shield and 13.5 inches is needed to protect the cylindrical radiator shield. From the shielding analysis, it was found that approximately 2 inches of borated graphite would replace 1 inch of lithium hydride. Thus, when the graphite shielding was added, the lithium hydride thickness was reduced accordingly.

The results of the analysis of the direct shield for the reference powerplant are given in Figures 3-4 and 3-5. Figure 3-4 shows the neutron dose rate at the dose point as a function of the neutron shield thickness. Figure 3-5 shows the gamma dose as a function of gamma shield thickness and neutron shield thickness. This figure is included for illustrative purposes only, since it was later found that the addition of borated graphite eliminated the need for gamma shielding. In determining the allowable dose rate, a conversion factor of 7,000 n/cm^2-sec equal to 1 rem/hr was used. For 20,000 hours this gives an allowable neutron dose rate of 19.8 rem/hr.

In the optimization of the shield, the allowable dose rate through the direct and scatter shields was varied. This caused the shield weights to vary as shown in Figures 3-7 and 3-9. The minimum weight shield for the reference planar powerplant results when the direct and scatter doses are equal. For the cylindrical powerplant, the optimum shield results when 30 per cent of the dose is allowed through the direct shield and 70 per cent through the scatter shield.

Scatter Shield

The scatter shield is sized so that the radiator does not have a direct unshielded view of the reactor from which to scatter radiation into the power-conditioning equipment. Thus, the scatter shield extends outward from the direct shield to cover the 60 degrees of the vehicle nose cone. The scatter shield for the reference powerplant has a thickness perpendicular to the radiator equal to the outside diameter of the reflector. For the cylindrical powerplant, the shield geometry is that of a truncated cone.

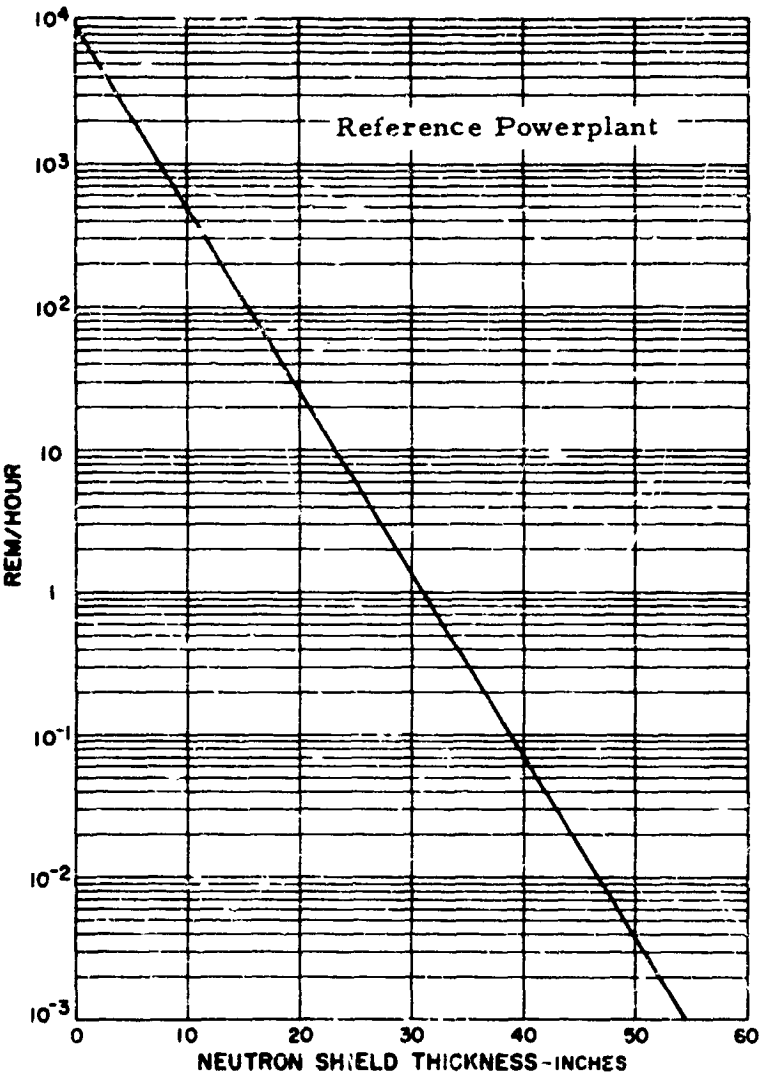

Figure 3-4 Neutron Dose Rate vs LiH Neutron Shield Thickness

The radiator can scatter both neutrons and gamma rays into the power-conditioning equipment. The dose from gamma scattering is not significant since the borated graphite reduced the gamma dose to well below the total allowable gamma dose.

To determine the neutron scattering off the radiators, the reactor was considered a point isotropic source. The neutron dose reaching the

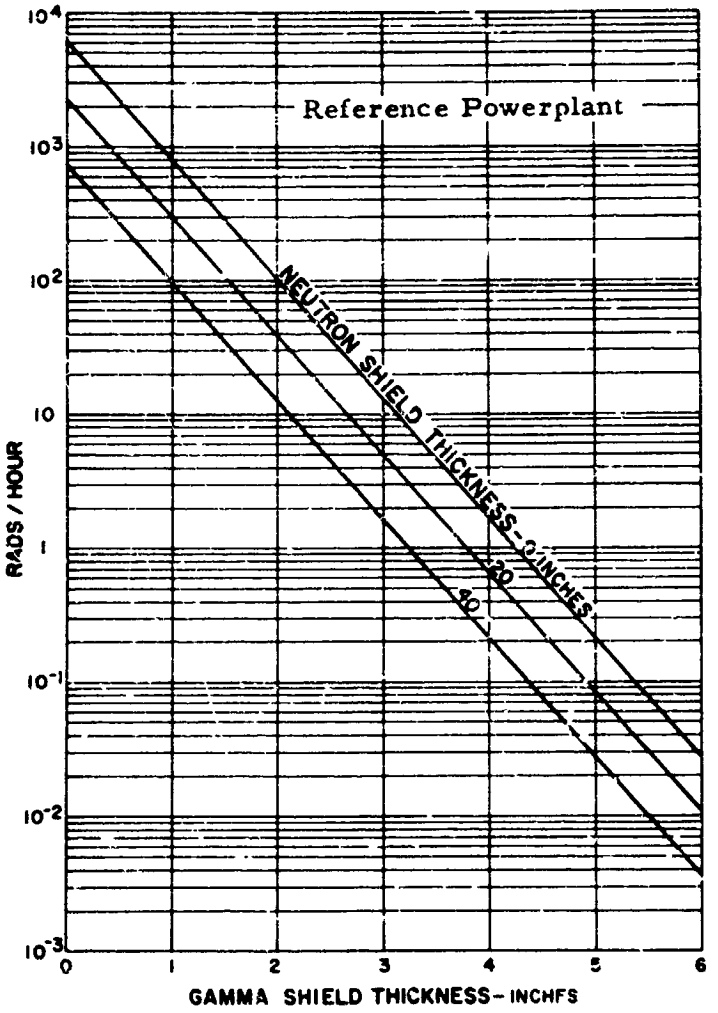

Figure 3-5 Gamma Dose Rate vs Tungsten Shield Thickness

power-conditioning equipment after originating in the reactor and being scattered off the planar radiator was determined by numerical integration. This integral considered single scattering, the solid angle between the reactor and radiator, and the solid angle between the radiator and power-conditioning equipment. Figure 3-6 shows a plot of the contribution to total dose from each section along the radiator length. The scatter shield thickness was determined by attenuating the scattered neutron dose until it equalled the allowable scatter dose. Figure 3-7 shows the scatter shield weight and total shield weight versus the allowable dose ratio for the planar radiator shield. These weights include the weight of the borated graphite thermal shield.

Reference Powerplant (planar radiator)

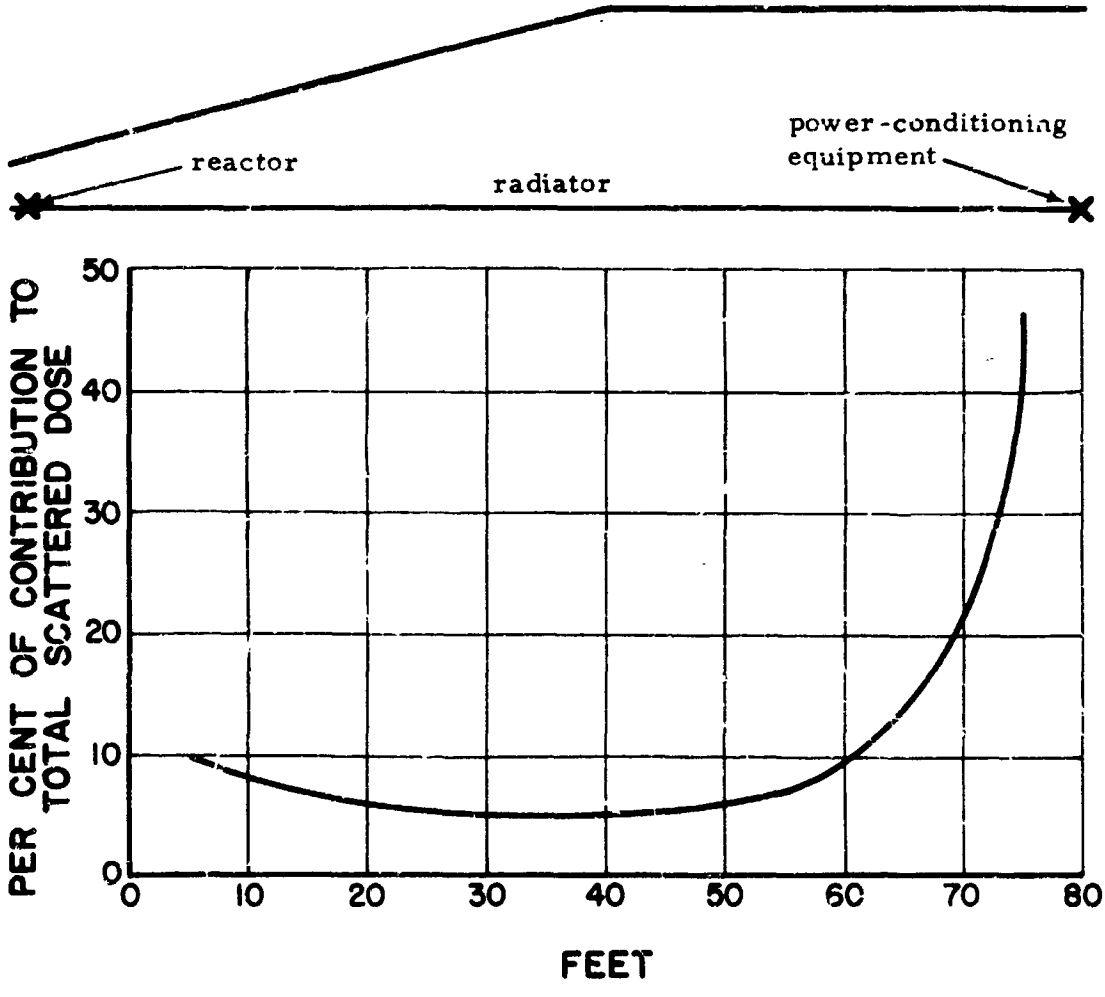

Figure 3-6 Scattered Dose. Planar Radiator

To determine the neutron scattering off the cylindrical radiator, an equation was devised using a cylindrical radiator model with the reactor as a point isotropic source. By considering single scattering, the solid angle between the reactor and radiator, and the solid angle between the radiator and power-conditioning equipment, the following integral was formulated.

$$d\phi_s = \frac{\Sigma_s \; t \; a \; S}{8\pi} \int_b^c \frac{dy}{(y^2 + a^2)\left[(y - y_1)^2 + a^2\right]}$$

where ϕ_s = scattered neutron flux, n/cm^2
Σ_s = macroscopic fast neutron Scattering cross-section
S = neutron source strength
t = radiator thickness
a = one half the raidator diameter
y_1 = source to dose point distance
y = variable axial distance between source and aft end of radiator
b = distance between source and forward end of radiator
c = distance between source and aft end of radiator

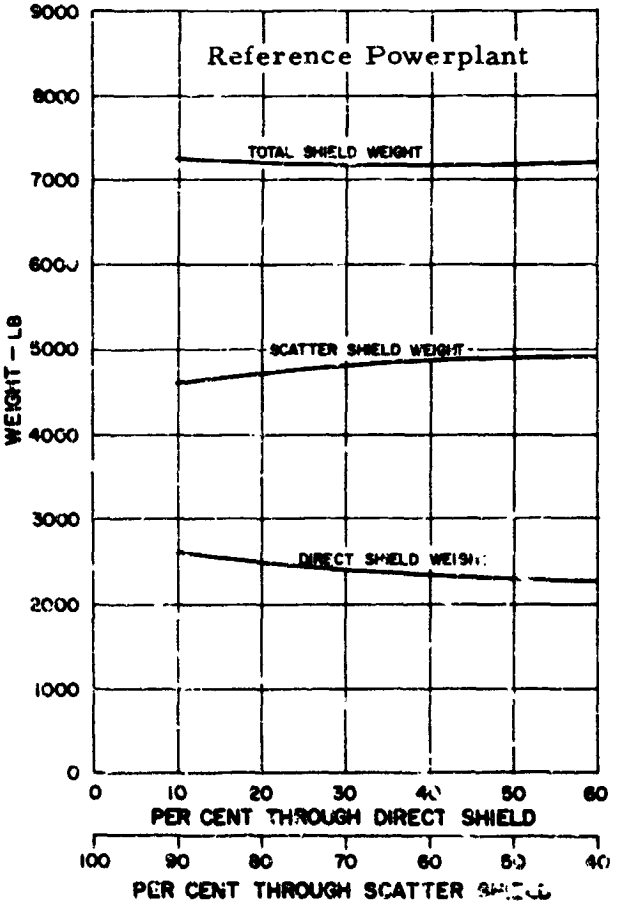

Figure 3-7 Shield Weight vs Allowable Dose Distribution.Flat Flate Radiator

After integration the equation reduces to the following form

$$\phi_s = \frac{\Sigma t\, a\, S}{4\pi(4a^2 + y_1^2)} \left[\frac{1}{a} \tan^{-1}\left(\frac{y}{a}\right) + \frac{1}{y_1} \ln \frac{y^2 + a^2}{(y-y_1)^2 + a^2} - \frac{1}{a} \tan^{-1}\left(\frac{y_1 - y}{a}\right) \right]_b^c$$

Since this equation is for a pure cylindrical model and the radiator actually has a small cone-shaped section tapering towards the reactor, a comparison was made to test the accuracy of the model. By numerically integrating the dose off the partially cone-shaped radiator, it was found the total scattered dose compared very closely with the total scattered dose from the analytical model. Figure 3-8 shows a plot of the contribution to total dose from each point along the radiator length for the anal-

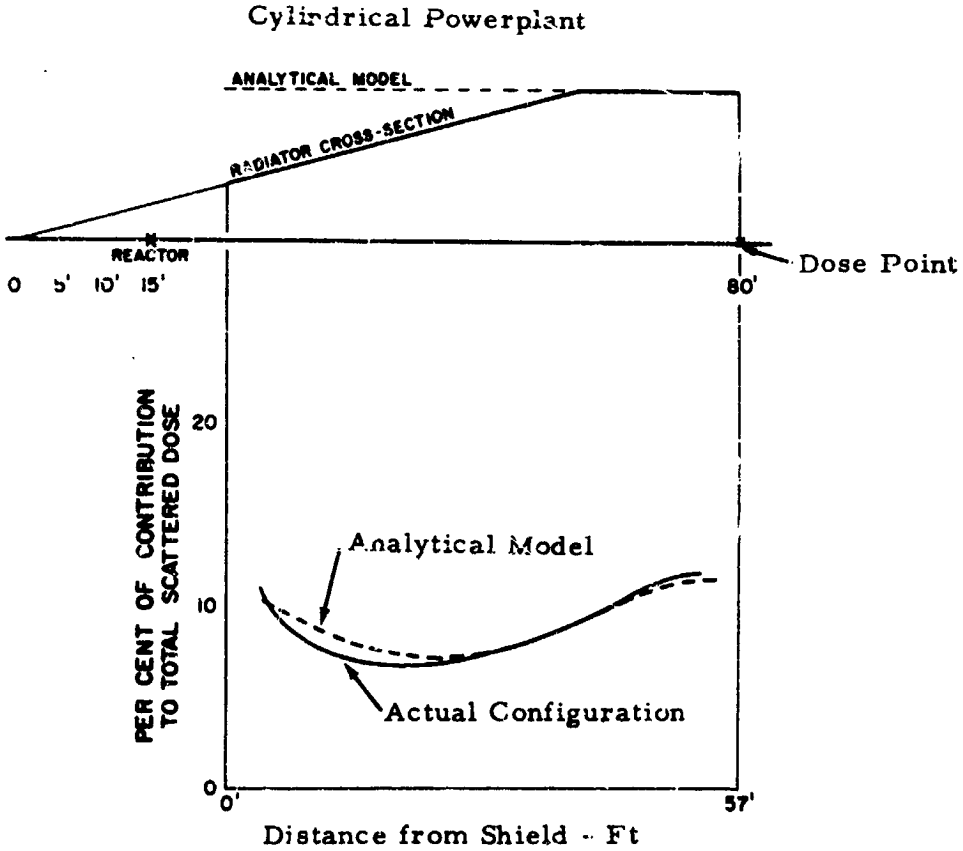

Figure 3-8 Scattered Dose. Cylindrical Radiator

ytical model and actual configuration. Again, the shield thickness was determined by attenuating the scattered neutron dose down to the allowable dose. Figure 3-9 shows the scatter shield weight and total shield weight versus the allowable dose ratio for the cylindrical radiator shield.

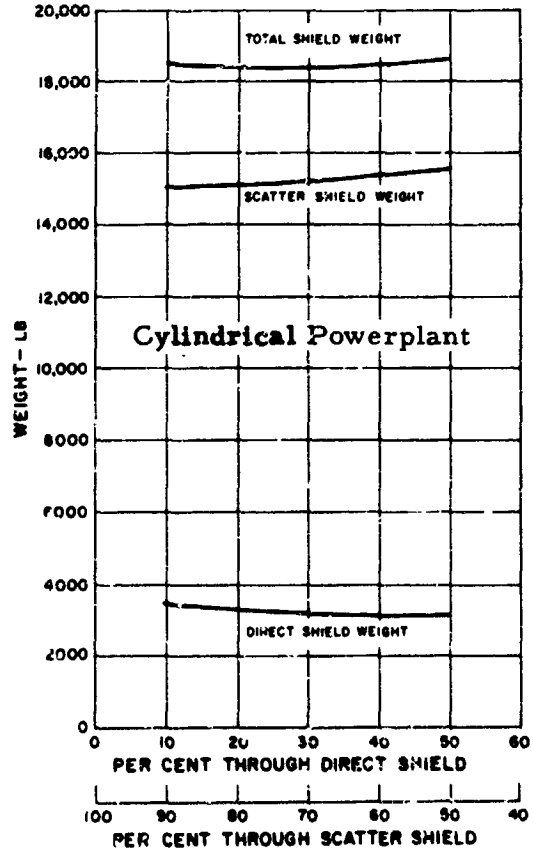

Figure 3-9 Shield Weight vs Allowable Dose Distribution. Cylindrical Radiator

Shield Heating

The heat generation due to neutron and gamma radiation from the reactor was determined by utilizing a one-dimensional multigroup neutron diffusion computer code with gamma and neutron heating options. Gamma and neutron heating was calculated both for an all-lithium hydride shield and a borated graphite-lithium hydride shield.

Li^7H was used for the neutron shield, due to the high alpha heating in Li^6. When a neutron is absorbed by a Li^6 atom, the atom disintegrates to form a helium atom and a tritium atom. This reaction is significant since the helium atom is stopped almost immediately and the heating is localized. The analysis considered both the reactor and plenum as consisting of homogeneous mixtures. The neutron heating in the reactor and in the planar radiator shield is shown in Figures 3-10 and 3-11. The gamma radiation heating is shown in Figures 3-12 and 3-13. In the homogeneous regions such as the core and plenum, the gamma heating was calculated in individual materials as indicated on the figure. The total heating in each of the shield components is shown in Figure 3-14.

To obtain the steady-state temperature distribution in the shield, a two-dimensional heat transfer analysis was employed. Heat removal from the shield was based on radiating to space from the shield surface. The heat generation in each of the shield components was approximated by an exponential equation in each component.

The sides of the shield facing the reactor and the radiator were insulated to prevent radiation heat transfer from these components to the shield. Therefore, in the analysis, adiabatic boundary conditions were imposed on these sides of the shield. For the reference powerplant, the shield has two dimensions perpendicular to the powerplant axis. One is equal to the outside diameter of the reflector and the other is sized to fit within the angle of the nose cone. The latter is the longest dimension and was considered as being infinite in the analysis. Therefore, it was assumed that there was no heat flow perpendicular to the surface shown in Figure 3-15.

In the first analysis, it was assumed that the shield contained Li^7H only. The high heating and low thermal conductivity produced a maximum temperature of 6826°F. Since this temperature is well over the maximum operating temperature of lithium hydride, borated graphite had to be added to reduce the heat generation in the lithium hydride. Several calculations were run at various thicknesses of borated graphite, to determine the thickness that would keep the lithium hydride temperature below its maximum operating value of about 800°F. The borated graphite is at a much higher temperature than the lithium hydride and heat flows into the lithium hydride causing increased temperatures.

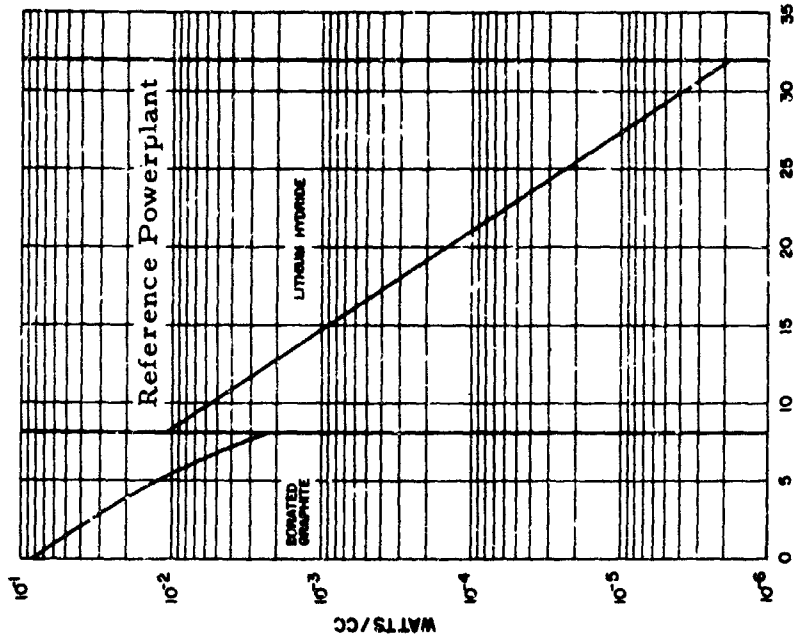

Figure 3-11 Neutron Heating vs Shield Thickness

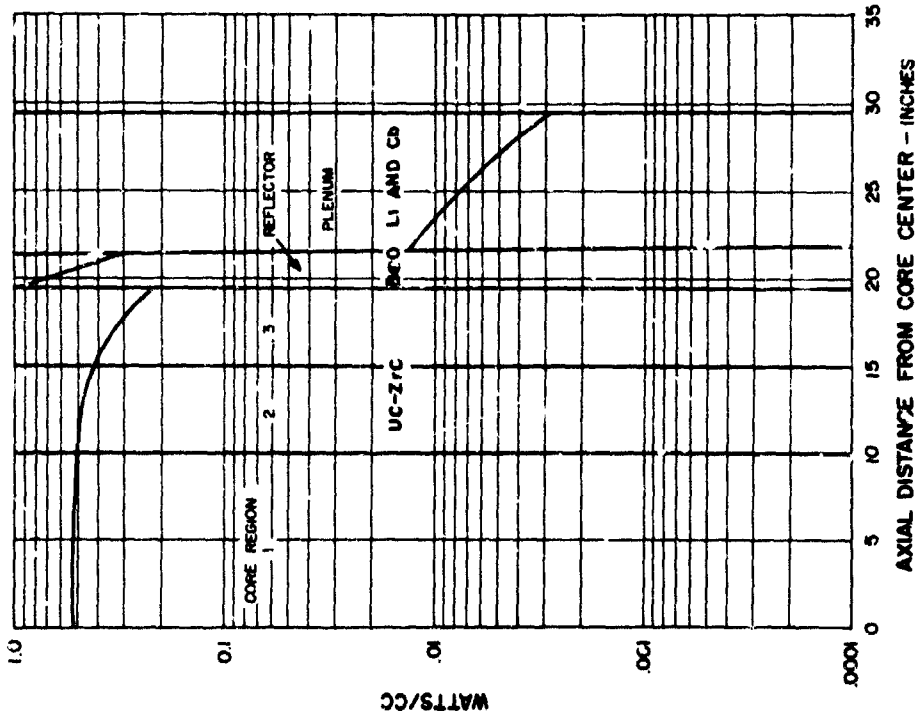

Figure 3-10 Neutron Heating vs Distance

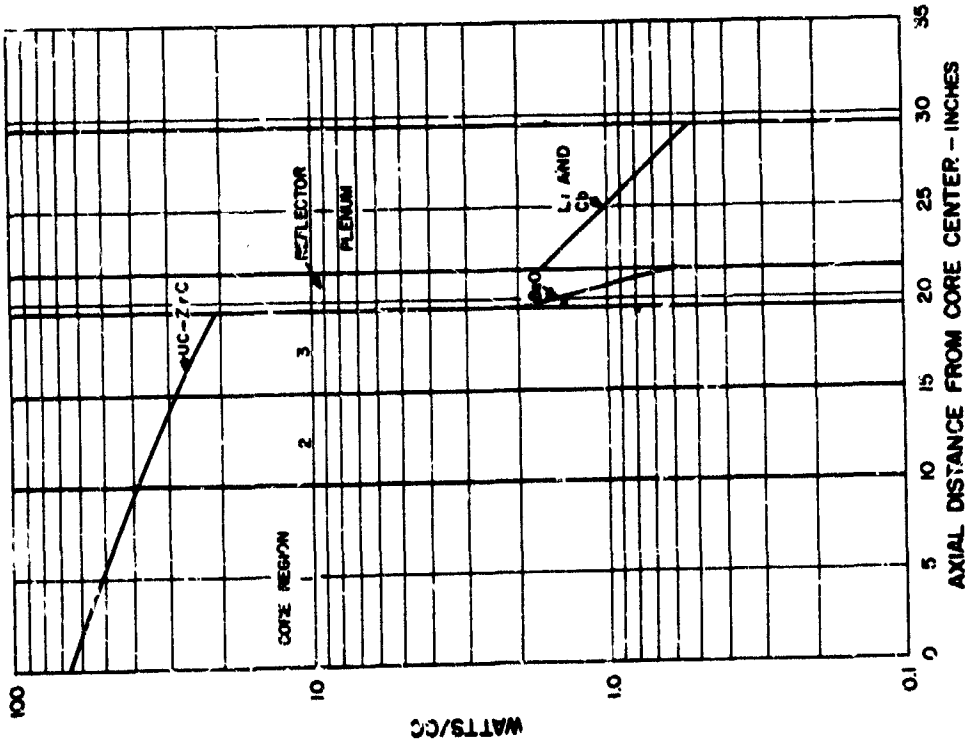

Figure 3-12 Gamma Heating vs Distance

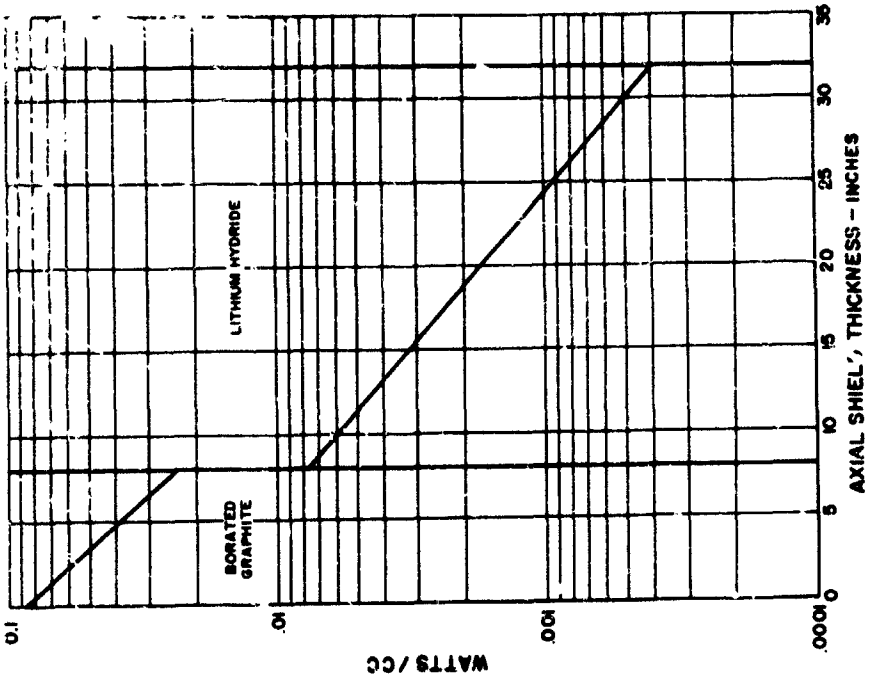

Figure 3-13 Gamma Heating vs Shield Thickness

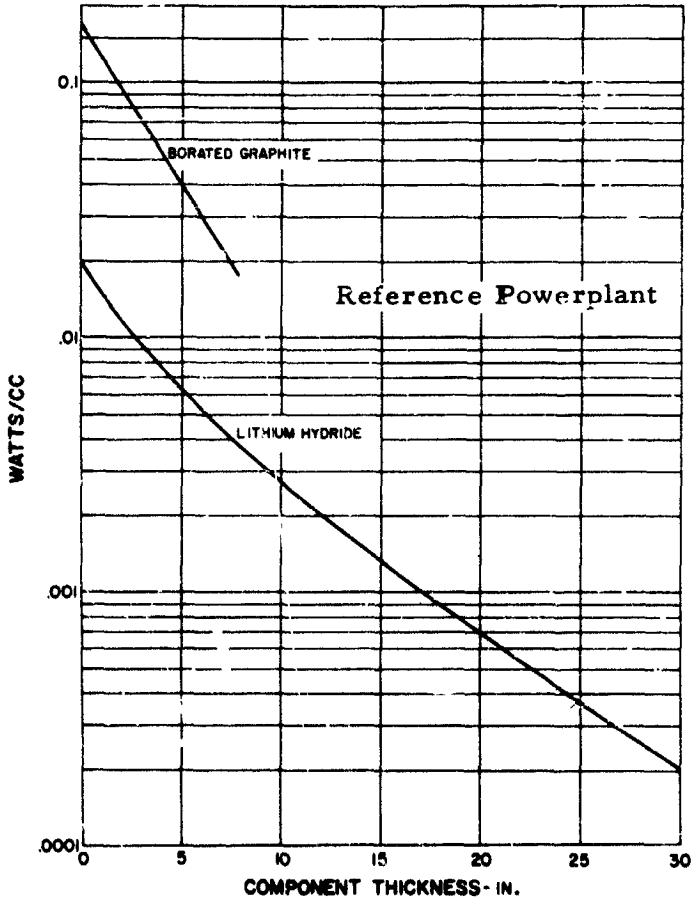

Figure 3-14 Total Shield Heating vs Shield Component Thickness

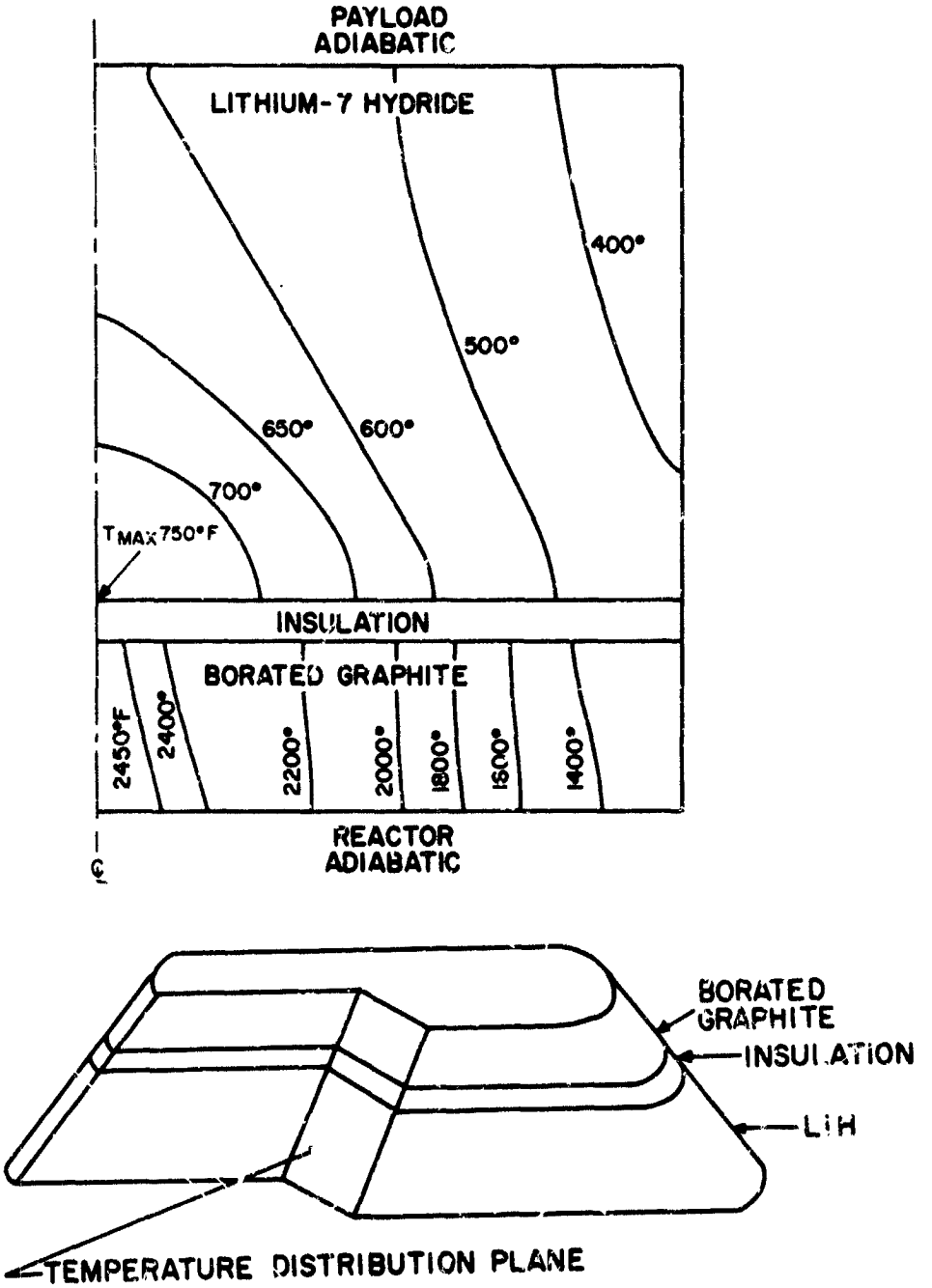

Figure 3-15 Shield Temperature Distribution

Therefore, it was necessary to insulate the lithium hydride from the borated graphite with a near-adiabatic layer of insulation. This insulation consists of layers of thin metal foil and results in an extremely low conductivity. Thus, it was determined that 8 inches of borated graphite was needed to keep the heating in the lithium hydride at an allowable level, and 2 inches of insulation was needed to prevent a large amount of heat flow from the borated graphite to the lithium hydride. The final shield temperatures are shown in Figure 3-15. Although a complete temperature grid was obtained, only representative temperatures are shown. The maximum lithium hydride temperature is 750°F, an allowable operating temperature. The total heat deposited in this shield is 59.6 kilowatts: 36.3 kilowatts in the borated graphite and 23.3 kilowatts in the lithium hydride.

The cylindrical radiator shield has the shape of a truncated cone, so it was mocked up in two-dimensional R-Z coordinates. With the two end conditions adiabatic, this allows for heat flow in the radial direction. Since the radial dimension is greater than the dimension of the narrow part of the planar radiator shield, heat has further to flow and consequently the maximum temperatures are greater in the cylindrical radiator shield. This increase in the maximum lithium hydride temperature dictated a greater thickness of borated graphite. To reduce the maximum lithium hydride temperature to that of the flat plate radiator shield, 13.5 inches of borated graphite were needed. The final shield temperatures for the cylindrical radiator shield are shown in Figure 3-16. The total heat deposited in this shield was 156.7 kilowatts: 137.2 kilowatts in the borated graphite and 19.5 kilowatts in the lithium hydride.

In the final design, perhaps more borated graphite might be needed in the shield due to the effect of variables not included in this study. For example, the lithium hydride was considered as being continuous when in actuality it may be discontinuous, thus reducing the effective thermal conductivity. Also, the temperatures may be higher due to the lack of a perfect thermal bond between the components and cladding.

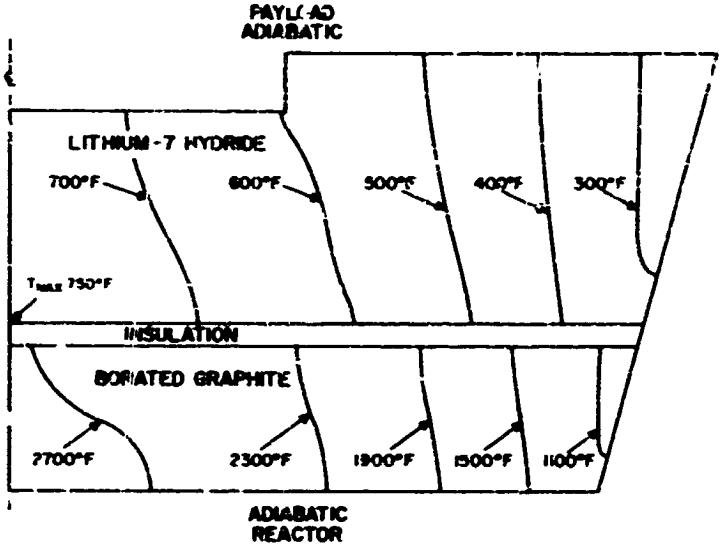

Figure 3-16 Cylindrical Powerplant Shield Temperature Distribution

APPENDIX 4

Cylindrical Radiator Study

APPENDIX 4

Cylindrical Radiator Study

The results of an analysis of cylindrical radiators performed to aid in the comparison of planar and cylindrical powerplants are presented. The study included the analysis of both the main and auxiliary radiators, and assumed heat rejection from the outside radiator surface only. The analysis was performed independently of a complete systems analysis so that the size and weight values determined may not be the exact optimums, but should be representative of the optimum values. Parameters such as pressure drop, radiator reliability, and heat rejection rate and temperature for the analysis were taken from the systems analysis for the planar powerplant.

Three fin-tube radiator designs, Figure 4-1, for the liquid lithium main radiator and two hidden-tube radiator designs, Figure 4-2, for the monoisopropylbiphenyl auxiliary radiator are presented.

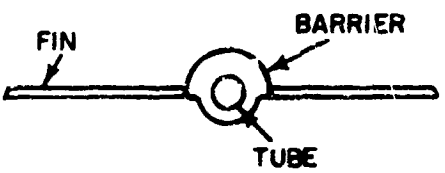

Figure 4-1 Fin-Tube Radiator Design

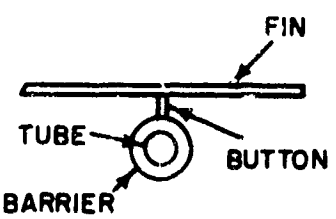

Figure 4-2 Hidden-Tube Radiator Design

Main Liquid Lithium Radiator

For the liquid lithium radiator the fin-tube radiator design demonstrated a weight advantage over the hidden-tube radiator design. The radiators

were designed to reject 9.13×10^7 Btu/hour from sixteen parallel circuits with a radiator pressure drop of 4.6 psi and to be compatible with the vehicle design shown in Figure 4-3.

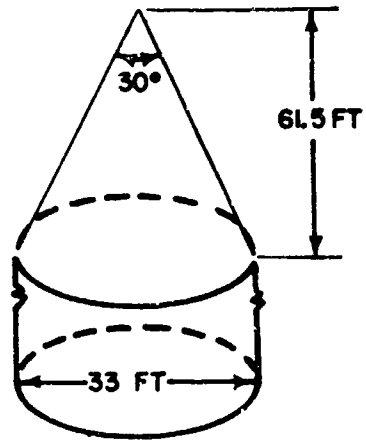

Figure 4-3 Vehicle Design

The following requirements were placed on the main radiator design:

1) Total heat rejection rate = 9.13×10^7 Btu/hour
2) Number of segments = 16
3) Inlet temperature = 2380°R
4) Outlet temperature = 1935°R
5) Flow rate per segment = 3.676 lbs/sec.
6) Radiator pressure drop = 4.6 psi
7) Coolant, liquid lithium
8) Tube and barrier-material, Cb-1Zr
9) Reliability per segment = 0.8696

The recommended design consists of four segments arranged as a cone, plus twelve segments arranged as a cylinder. This configuration is considered to provide the best balance between powerplant height and radiator weight. The results of a study of three designs for the liquid lithium main radiator are presented below.

Design	No. of Segments Cone	Cylinder	Total Radiator Weight, lbs	Area, sq. ft	Vehicle Height, ft
1	0	16	10,630	3846.4	99.65
2	4	12	10,498	3752.4	90.1
3	8	8	12,430	3627	80.57

Design 1 was rejected because the additional powerplant height would require an increase in support structure weight. Design 3 was rejected because of an excessive increase in radiator weight for the reduction in vehicle height gained.

The configuration chosen for the three designs was one in which the manifold and collector are parallel to the circumference of the vehicle and the tubes are parallel to the vertical axis of the vehicle. This offered the advantage of setting the number of tubes and hence the fin width by means of the pressure drop assigned.

A space radiator design computer program was used in the design of the radiator. The analysis which formed the basis of the program considered:

1) Different manifold and collector designs,
2) Location of fin to tube in determining their respective view factors to space,
3) Meteoroid protection and reliability,
4) Temperature drop in tube wall, root and fin,
5) Variation in heat transfer coefficients, and
6) Variation in fin effectiveness and fin thickness.

The program contains an optimization routine for computing a minimum-weight radiator by variation of any number of continuous independent variables.

In the analysis it was assumed that eighty per cent of the total radiator pressure drop was in the tubes and ten per cent in each of the headers. The radiator consisted of constant-thickness fins and a nontapered manifold and collector. The positioning of the manifold and collector was such that they were radiating to space. The meteoroid equation used in the analysis to calculate the thickness of the barrier material required for the manifold, collector and tubes was:

$$t_{in} = \frac{0.01118}{\rho^{1/2} C^{2/3}} \left[\frac{AT}{-\ln P} \right]^{0.2485}$$

where ρ = density of material, gm/cm^3
C = sound velocity in material, km/sec
A = vulnerable area, ft^2
T = mission time, hours
P = probability of no meteoroid penetration

The characteristics of the all-cylindrical radiator designed in this manner are tabulated below:

Total area = 4,272 sq ft
Total weight = 9,000 lbs
Inside diameter of tubes = 0.130 inch
Thickness of barrier = 0.104 inch
Number of tubes per segment = 219
Tube-to-tube distance = 0.90 inch
Thickness of fin = 0.0133 inch

The fin in this design was considered to be too thin to manufacture. To obtain a suitable fin thickness of 0.030 inch, an off-optimum radiator was chosen. The characteristics of this radiator are tabulated below and shown in Figure 4-4.

Total area = 3,346 sq ft
Total weight = 10,630 lbs
Inside diameter of tubes = 0.130 inch
Thickness of barrier = 0.[illegible]7 inch
Number of tubes per segment = 206
Tube-to-tube distance = 1.178 inch
Thickness of fin = 0.0319 inch

In an attempt to reduce the powerplant height, a design involving four segments on the cone and twelve on the cylinder was investigated. The basic planform of the segments on the cone was rectangular. These were arranged to cover a major portion of the surface of the cone. A trapezoidal planform would cover the entire surface of cone but a complex configuration is encountered in this design. Analysis requires the calculation of:

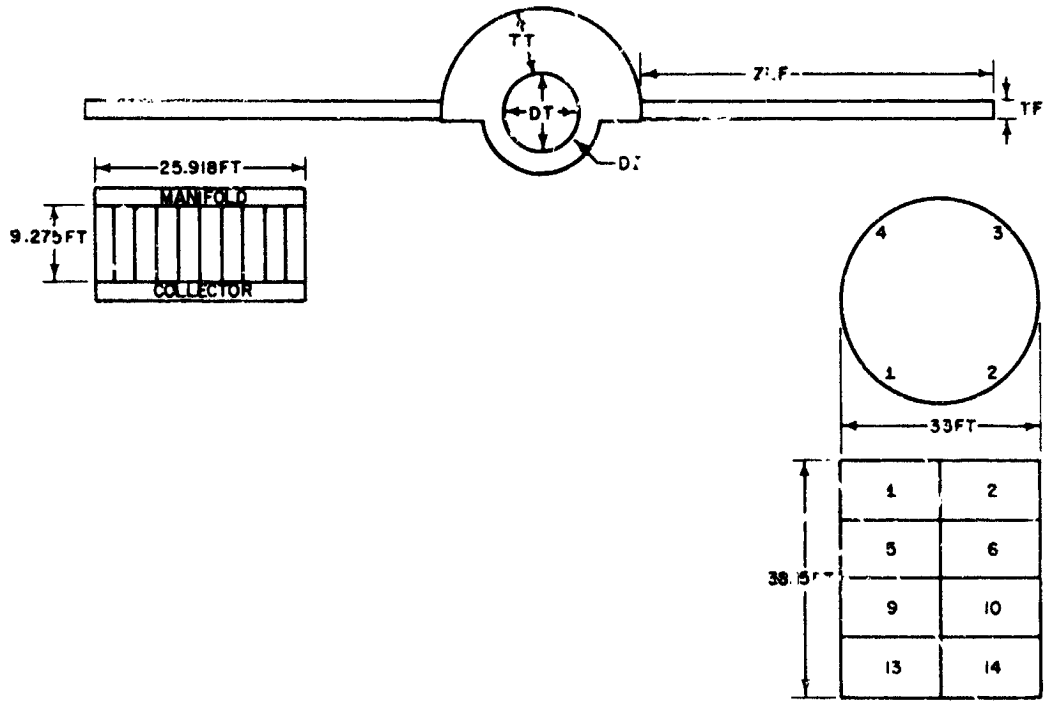

Radiator Data and Dimensions

plan area = 240.4 sq ft/segment
length of manifold and collector = 25.918 ft
length of tubes = 9.275 tt
number of tubes = 206
overall radiator effectiveness = 0.735
fin effectiveness = 0.72
radiator pressure drop = 4.6 psi
heat rejection per segment = 5.7×10^6 btu/hr
flow rate per segment = 3.67 lbs/sec
radiator weight = 10630 lb
diameter of tube (dt) = 0.130 inch
thickness of outer barrier (tt) = 0.1017
shielded barrier thickness (di) = 0.0373 inch
thickness of fin (tf) = 0.0319 inch
width of fin (zlf) = 0.589 inch
diameter of manifold = 1.5 inch
diameter of collector = 1.67 inch

Figure 4-4 Main Radiator. Fin-Tube Configuration. Radiator Data and Dimensions

1) Manifold and collector geometry due to change in length,
2) Fin thickness to maintain fin effectiveness with tapering fins,
3) Shielded barrier thickness due to varying fin thickness, and
4) The temperature drop in the root and fin.

The characteristics of the off-optimum radiator with a rectangular planform conforming to the stipulation of a minimum 0.030 inch fin thickness are tabulated below and shown in Figure 4-5.

Segments	Cone	Cylinder
Total area, sq ft	867	2,880
Total weight, lbs	2,525	7,973
Inside diameter of tubes, inch	0.130	0.130
Thickness of barrier, inch	0.1045	0.1017
Number of tubes per segment	219	206
Tube-to-tube distance, inch	0.812	1.178
Thickness of fin, inch	0.0266	0.0319

The last design investigated (Figure 4-6) consisted of eight rectangular planform segments placed on the cone and eight on the cylinder. This design was unsatisfactory since the weight of the additional four rectangular planform sections increased the weight of the entire radiator by approximately 2000 pounds. The characteristics of the design are tabulated below:

Segments	Cone	Cone	Cylinder
Total area, sq ft	836	867	1,923
Total weight, lbs	4,590	2,525	5,315
Inside diameter of tubes, inch	0.130	0.130	0.130
Thickness of barrier, inch	0.1223	0.1045	0.1017
Number of tubes per segment	250	219	206
Tube-to-tube distance, inch	0.517	0.812	1.178
Thickness of fin, inch	0.0260	0.0266	0.0319

Auxiliary Monoisopropylbiphenyl Radiator

The four-parallel-circuit design for the monoisopropylbiphenyl auxiliary radiator was determined as a function of pressure drop. The hidden-tube design exhibited a definite weight advantage over the fin-tube design for this particular radiator. The following requirements were placed on the design:

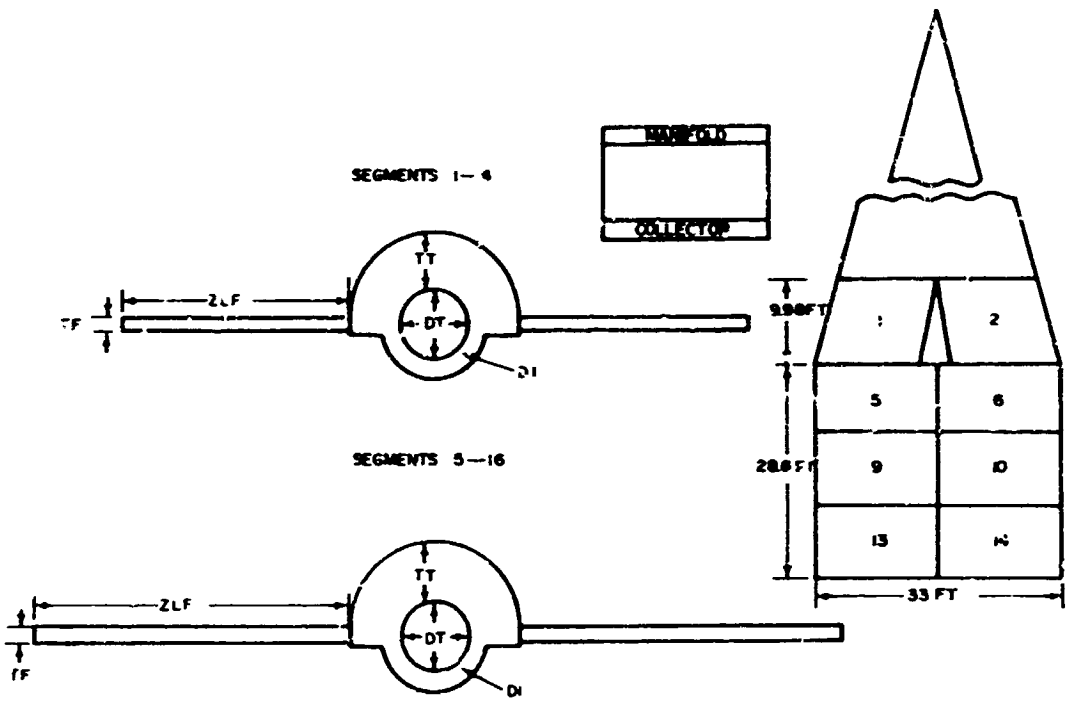

Data and Dimensions

	Segments 1-4	Segments 5-16
radiator and barrier material	Cb-1Zr	Cb-1Zr
plan area per segment	216.9 ft^2	240.4 ft^2
length of manifold and collector	21 ft	25.918 ft
length of tubes	10.33 ft	9.275 ft
number of tubes	219	296
overall radiator effectiveness	0.81	0.73
fin effectiveness	0.807	0.70
radiator pressure drop	4.6 psi	4.6 psi
heat rejection per segment	5.7×10^6 btu/hr	5.7×10^6 btu/hr
flow rate per segment	3.676 lbs/sec	3.676 lbs/sec
weight of segments	2525 lbs	7973 lbs
diameter of tube (dt)	0.13 inch	0.13 inch
thickness of outer barrier (tt)	0.1045 inch	0.1017 inch
shielded barrier thickness (di)	0.0355 inch	0.037 inch
thickness of fin (tf)	0.0266 inch	0.0319 inch
width of fin (zlf)	0.4086 inch	0.589 inch
diameter of manifold	1.42 inch	1.5 inch
diameter of collector	1.59 inch	1.67 inch

Figure 4-5. Main Radiator. Fin-Tube Configuration. Segments 1-4 and 5-16

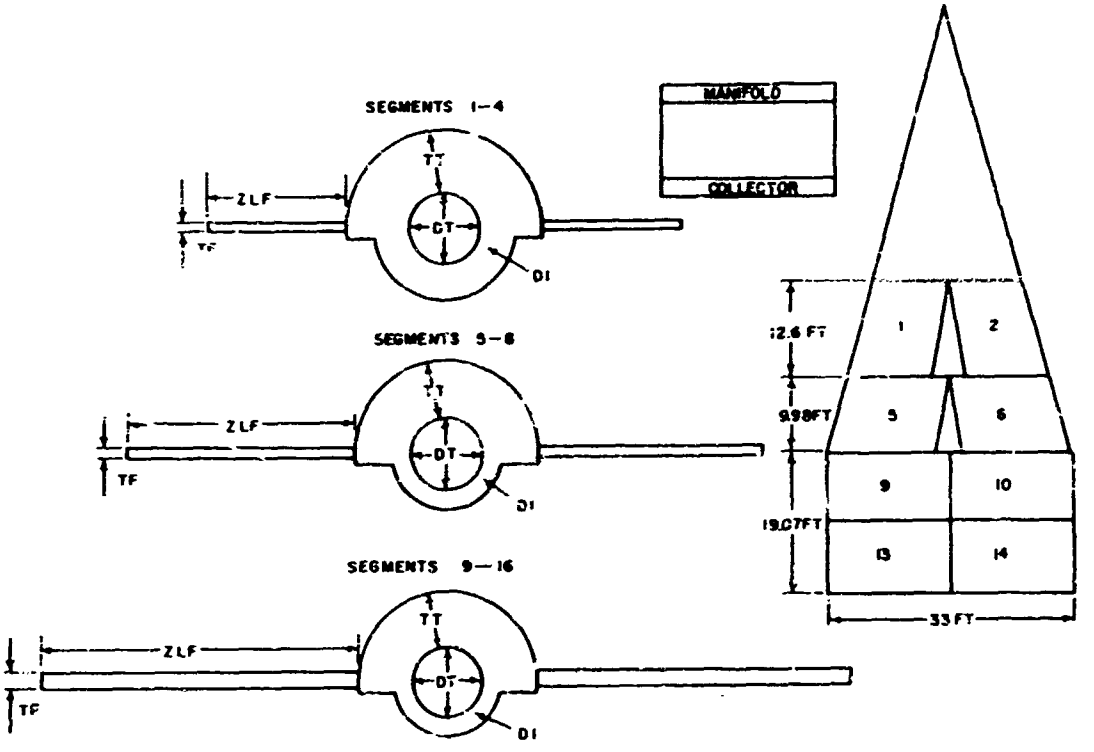

Data and Dimensions

	Segments 1-4	Segments 5-8	Segments 9-16
radiator and barrier material	Cb-1Zr	Cb-1Zr	Cb-1Zr
fin area per segment	209 ft^2	216.9 ft^2	240.3 ft^2
length of manifold and collector	16 ft	21 ft	25.918 ft
length of tubes	13.06 ft	10.33 ft	9.275 ft
number of tubes	250	219	206
overall radiator effectiveness	0.846	0.815	0.73
fin effectiveness	0.691	0.807	0.70
radiator pressure drop	4.6 psi	4.6 psi	4.6 psi
heat rejection per segment	5.7×10^6 btu/hr	5.7×10^6 btu/hr	5.7×10^6 btu/hr
flow rate per segment	3.676 lbs/sec	3.676 lbs/sec	3.676 lbs/sec
weight of segments	4590 lbs	2525 lbs	5315 lbs
diameter of tube (dt)	0.13 inch	0.13 inch	0.13 inch
thickness of outer barrier (tt)	0.1223 inch	0.1045 inch	0.1017 inch
shielded barrier thickness (di)	0.061 inch	0.0355 inch	0.0373 inch
thickness of fin (ft)	0.026 inch	0.0266 inch	0.0319 inch
width of fin (zlf)	0.2586 inch	0.4056 inch	0.589 inch
diameter of manifold	1.3 inch	1.42 inch	1.5 inch
diameter of collector	1.5 inch	1.59 inch	1.67 inch

Figure 4-6 Main Radiator, Fin-Tube Configuration, Segments 1-4, 5-8, and 9-16

1) Total heat rejection rate = 834,000 Btu/hour
2) Number of segments = 4
3) Inlet temperature = 960°R
4) Outlet temperature = 885°R
5) Flow rate per segment = 1.285 lbs/sec
6) Radiator pressure drop = 17.2 psi
7) Coolant, monoisopropylbiphenyl
8) Tube and barrier material, aluminum
9) Reliability per segment = .990765

The results of a study of the auxiliary radiator are presented below.

Cylindrical Segments	Pressure Drop, psi	Total Radiator Weight, lbs	Total Radiator Area, sq ft	Height, ft
4	7.5	768	969.2	9.38
4	10.0	642	1080.0	10.53
4	17.5	634	1224.0	11.90

The configuration chosen for the two designs was that of the hidden tube, Figure 4-2, with the headers parallel to the circumference of the vehicle and the tubes parallel to the vertical axis. The meteoroid equation used was the same as that for the main radiator. The four parallel segments were placed around the circumference of the powerplant as shown in Figure 4-7.

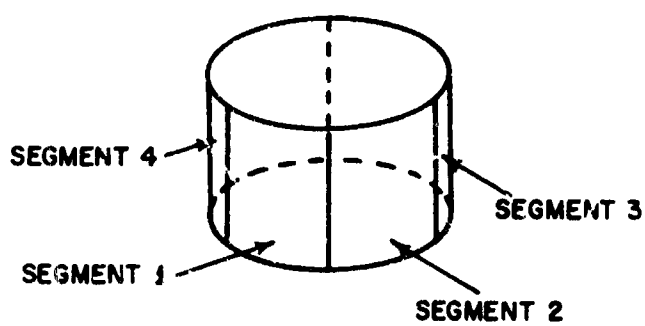

Figure 4-7 Location of Auxiliary Radiator Segments

The space radiator computer program was used in the design of these segments. A plot of radiator pressure drop versus radiator weight, Figure 4-8, revealed that the pressure drop specified was on a relatively shallow portion of the curve. The radiator pressure drop can be reduced from 17.5 to 10 psi with a negligible increase in weight. A further reduction to 7.5 psi may be obtained if the radiator weight is increased from 642 to 768 pounds. The radiators whose characteristics are listed below are off-optimum designs since it was desired to have a fin thickness close to 0.030 inch. The designs are shown in Figures 4-9 and 4-10.

Pressure drop, psi	7.5	10.0
Total area, sq ft	969	1080
Total weight, lbs	768	642
Inside diameter of tubes, inch	0.125	0.125
Thickness of barrier, inch	0.0786	0.0794
Number of tubes per segment	55	49
Tube-to-tube distance, inch	5.66	6.34
Thickness of fin, inch	0.036	0.026

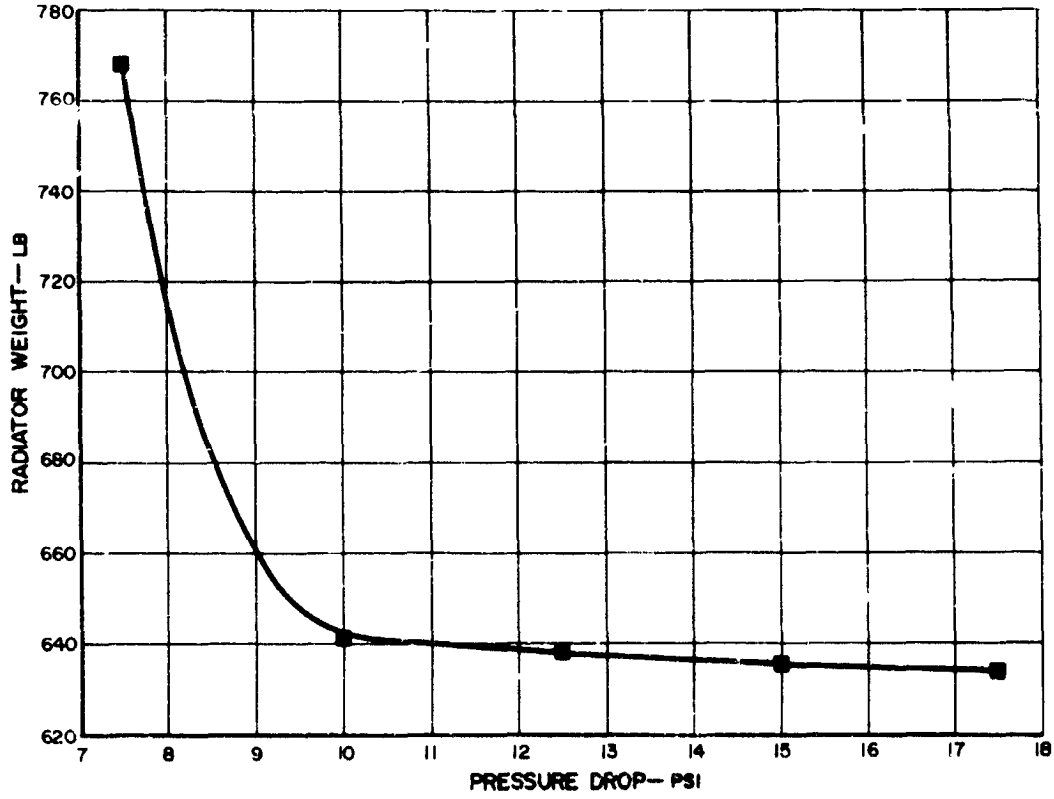

Figure 4-8 Auxiliary Radiator, Fin Type 3. Radiator Weight vs Pressure Drop

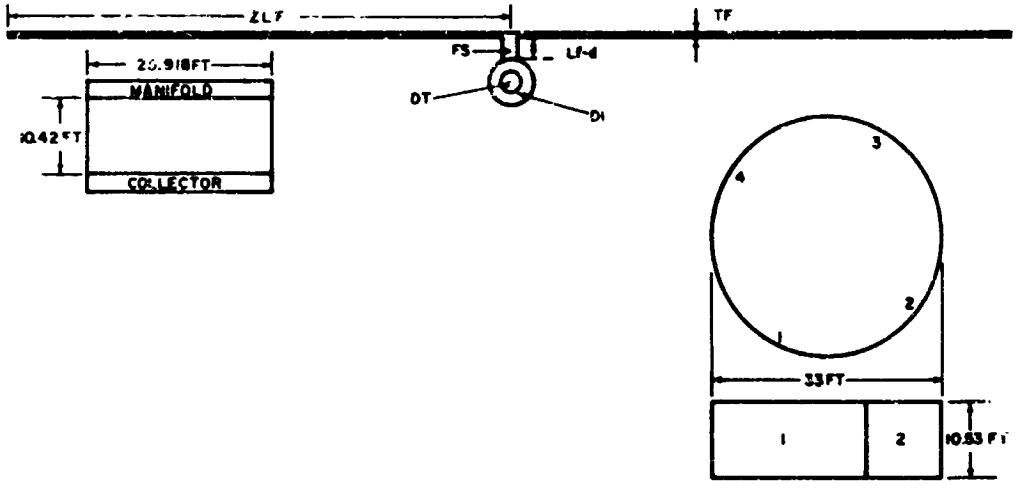

Radiator Data and Dimensions

plan area = 270 sq ft/segment
length of manifold and collector = 25.918 ft
length of tubes = 10.42 ft
number of tubes = 49
overall radiator effectiveness = 0.695
fin effectiveness = 0.763
radiator pressure drop = 10 psi
heat rejection per segment = 208,500 btu/hr
flow rate per segment = 1.285 lbs/sec
radiator weight = 642 lbs
diameter of tube (dt) = 0.125 inch
shielded barrier thickness (di) = 0.0794 inch
connecting strip length (lf-d) = 0.1 inch
connecting strip thickness (fs) = 0.0902 inch
thickness of fin (tf) = 0.026 inch
width of fin (zlf) = 3.17 inches
diameter of manifold = 0.632 inch
diameter of collector = 0.665 inch

Figure 4-9 Auxiliary Radiator. Hidden-Tube Configuration. Radiator Data and Dimensions

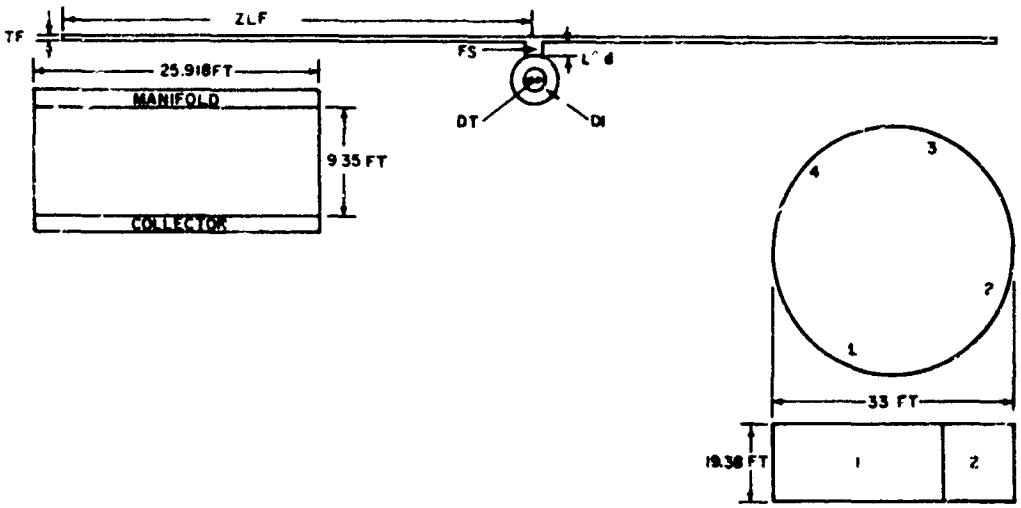

Radiator Data and Dimensions

plan area = 242.3 sq ft/segment
length of manifold and collector = 25.918 ft
length of tubes = 9.35 ft
number of tubes = 55
overall radiator effectiveness = 0.774
fin effectiveness = 0.843
radiator pressure drop = 7.5 psi
heat rejection per segment = 208,500 btu/hr
flow rate per segment = 1.285 lbs/sec
radiator weight = 768 lbs
diameter of tube (dt) = 0.125 inch
shielded barrier thickness (di) = 0.0786 inch
connecting strip length (lf-d) = 0.1 inch
connecting strip thickness (*fs*) = 0.126 inch
thickness of fin (tf) = 0.036 inch
width of fin (zlf) = 2.83 inches
diameter of manifold = 0.671 inch
diameter of collector = 0.708 inch

Figure 4-10 Auxiliary Radiator. Hidden-Tube Configuration. Radiator Data and Dimensions

APPENDIX 5

Power-Conditioning Equipment

APPENDIX 5

Power-Conditioning Equipment

This appendix presents the results of a new study performed by the Westinghouse Corporation[1] for DC-to-DC space power-conditioning equipment. The results of this study were not included in the reference powerplant presented in this report since the new results were received after the selection of the reference design. The data used for the reference design is given in Section IV. C. of this report, and was based partly on assumptions and partly on a previous Westinghouse study[2]. However, the effects of the new data on the design of the 3.25 MW(e) powerplant have been studied, and the results of this study are presented in Appendix 2.

The new Westinghouse study is of a more comprehensive nature than the previous one and was performed to investigate megawatt-rated DC-to-DC converter systems utilizing components which should be available within the next 5 years. All of the systems were considered to be operating with a nuclear thermionic power source to supply power in space for ion thrustor electric propulsion. Parametric data was generated for each of the components (See Figure 9) included in converter systems whose power output ranged from 0.5 to 5 megawatts with varying input and output voltages. Electrical characteristics of the nuclear thermionic power source were taken from Pratt & Whitney Aircraft's study of a 1MW system[2].

The results of the study are presented in Table 5-1 through 5-3 which give the weights, volumes and efficiencies of the systems using either silicon transistors or silicon-controlled rectifiers in the inverter switching circuits. The former component was included in the low input voltage (20 and 100 volts) systems and the latter was used for the higher input voltage (300 and 600 volts) systems. Both of these systems will be restricted to low temperature operation with maximum coolant temperatures of about 150°F. Also included in the tables under

---

[1] Westinghouse Electric Corporation, Aerospace Electrical Division, Space Electric Power Systems Study, Volume I, Contract No. NAS5-1234

[2] Pratt & Whitney Aircraft, Design Report, Advanced Nuclear-Electric Power Generator System Study, Thermionic Nuclear Space Powerplant, Report PWA-2224, Vol. I CRD

TABLE 5-1
Weight Summary

P_{out} & V_{out}	V_{in}	FUNCTIONAL BLOCK WEIGHT - (LBS)							Total Weight	Specific Weight (lbs/kw)
		Input Filter	Inverter	Pwr. Xfmr.	Pwr. Rect.	Output Filter	Drive Amp	Cont. Ckts.		
500 kw	20	-	2110	1570	37.6	200	195.2	31.4	4,144.2	8.26
	100	-	391	1215	37.6	200	48.0	28.6	1,920.2	3.84
	300	665	425	1095	37.6	254	45.6	30.8	2,553.0	5.1
5 kv	600	615	361	1095	37.6	254	45.6	30.8	2,439.0	4.87
1 mw	20	-	4220	3130	58.3	354	294	32.7	8,089	8.09
	50	1940	5770	-	166.4	-	-	-	*7,832.0	*7.83
	100	-	782	2430	58.3	354	63.5	28.6	3,716.4	3.71
5 kv	300	1278	610	2090	58.3	443	45.6	30.8	4,555.7	4.55
	600	1206	483	2090	58.3	443	45.6	30.8	4,356.7	4.35
2 mw	20	-	8450	6820	143.5	844	588	31.15	16,876.7	8.44
	100	-	1564	5230	143.5	844	116.8	31.0	7,929.3	3.96
20 kv	300	2550	1220	4620	143.5	1098	93.3	33.2	9,758	4.89
	600	2410	983	4620	143.5	1098	93.3	33.2	9,381	4.68
5 mw	20	-	21,250	15,900	281	2539	1469	51.7	41,490.0	8.29
	100	-	3920	12,300	281	2539	360	51.9	19,451.0	3.89
600 &	300	6470	3770	10,300	281	3490	367	61.7	24,739.0	4.94
5000 v	600	6200	3124	10,300	281	3490	367	61.7	23,823.0	4.77

Inverter Switching Frequency = 1000 cps
*These numbers are based on the three functional blocks indicated

TABLE 5-2
Volume Summary

P_{out} & V_{out}	V_{in}	FUNCTIONAL BLOCK VOLUME -CU. FT.							Total Volume
		Input Filter	Inverter	Pwr. Xfmr.	Pwr. Rect.	Output Filter	Drive Amplifier	Cont. Ckts.	
500 kw	20	-	92.7	7.28	1.07	1.29	3.0	0.67	115.01
	100	-	15.7	4.55	1.07	1.29	0.88	0.63	25.12
5 kv	300	11.03	11.2	3.70	1.07	1.56	0.16	0.67	29.39
	600	11.03	9.7	3.70	1.07	1.56	0.16	0.67	27.89
	20	-	185.2	14.6	1.93	2.2	4.62	0.67	209.22
1 mw	50	23.0	123.	-	4.9	-			*150.9
	100	-	31.4	7.36	1.93	2.2	1.40	0.63	44.9
5 kv	300	18.8	17.5	2.61	1.93	2.92	0.16	0.67	44.59
	600	17.7	12.3	2.61	1.93	2.92	0.16	0.67	38.29
2 mw	20	-	371	38.1	3.61	6.25	9.26	0.76	428.9
	100	-	62.8	21.4	3.61	6.25	2.65	0.76	97.47
20 kv	300	37.6	35.0	15.8	3.61	8.45	0.16	0.81	101.43
	600	35.4	24.6	15.8	3.61	8.45	0.16	0.81	88.83
5 mw	20	-	931	74.1	6.0	27.2	23.1	0.72	1062.1
	100	-	157.6	50.3	6.0	27.2	7.43	0.76	249.2
600 &	300	101.5	97.5	37.3	6.0	36.8	1.34	0.87	281.3
5000 v	600	97.1	86.6	37.3	6.0	36.8	1.34	0.87	278.07

Inverter Switching Frequency = 1000 cps
*This number is based on the three functional blocks indicated

TABLE 5-3
Efficiency Summary

P_{out} & V_{out}	V_{in}	FUNCTIONAL BLOCK LOSSES - KW								Total Efficiency
		Input Filter	Inverter	Pwr. Xfmr.	Pwr. Rect.	Output Filter	Drive Amp	Cont. Ckts.	Total Losses	
500 kw	20	–	36.6	38.4	1.431	1.140	1.65	0.546	79.76	86.5
	100	–	10.6	21.2	1.431	1.140	0.372	0.510	25.25	93.1
5 kv	300	1.192	8.5	11.5	1.431	1.341	0.072	0.517	23.55	95.6
	600	0.080	6.5	11.5	1.431	1.341	0.072	0.517	21.4	96.0
	20	–	73.2	78.0	2.813	1.552	3.3	0.577	159.4	86.5
1 mw	50	0.548	190.0	–	43.00	–	–	–	233.5	** 81.0
	100	–	21.2	42.?	2.813	1.552	0.744	0.510	69.5	93.6
5 kv	300	0.380	15.5	18.2	2.813	1.756	0.072	0.517	39.23	96.4
	600	0.148	12.0	18.2	2.813	1.756	0.072	0.517	35.5	96.7
2 mw	20	–	146.4	160.0	5.590	2.175	6.75	1.26	322.17	86.1
	100	–	42.4	91.2	5.590	2.175	1.488	1.26	144.11	93.4
20 kv	300	0.760	31.0	36.7	5.590	2.535	0.120	1.26	77.9	96.5
	600	0.298	24.0	36.7	5.590	2.535	0.120	1.26	70.4	96.6
5 mw	20	–	366	380.0	20.26	9.66	16.9	0.367*	793.7	86.5
	100	–	106	217.0	20.26	9.66	3.76	0.365*	357.0	93.1
600-	300	1.880	81.4	99.0	20.26	12.24	0.608	0.407*	215.7	95.8
5000v	600	0.730	66.1	99.0	20.26	12.24	0.608	0.407*	199.3	96.2

Inverter Switching Frequency = 1000 cps
*Output Voltage = 600 v
**This number is based on the three functional blocks indicated

1MW systems is the data for a system using high temperature vapor tube thyratrons in the inverter. This system was studied because its high temperature capability allows a drastic reduction in the required radiator area. The data listed in the tables for this system include the parameters for only those components indicated. An estimate of the data for the power transformer, output filters, drive amplifier and control circuits was made using the data for the 1 megawatt 20 and 100-volt input systems. Using these figures, the high temperature vapor tube system parameters would lie in the following ranges:

	Minimum	Maximum
voltage	20	100
weight, lbs	10,708.1	11,647.7
volume, ft^3	162.5	172.9
efficiency, %	76.0	78.1
total losses, KW	279.0	316.9

From all of the data given the gross conclusions that can be made concerning power-conditioning equipment for megawatt-rated nuclear thermionic space powerplants are that, 1) its weight will represent a significant fraction of the total powerplant weight, 2) its volume will be small so that it should not affect powerplant configuration, and 3) higher efficiencies and lower specific weights can be expected for the low temperature equipment than for the high temperature equipment. The latter conclusion indicates that the low temperature equipment would be the most desirable for space powerplants. However, the low operating temperature for this equipment will result in very large radiators which cause problems with powerplant configuration and system weight increases, due to the increased size of the radiator and the additional meteoroid barrier required. Also, the shield weight may be heavier for the low temperature equipment because, 1) this equipment is more sensitive to radiation than the high temperature equipment, and 2) deployment of the radiator outside the shadow of the shield may be necessary which will cause an increase in the size and weight of the shield.

APPENDIX 6

Variable Length Converter Study

APPENDIX 6

Variable Length Converter Study

1. Introduction

A major design objective of a thermionic reactor is the reduction of the effects of nonuniform thermal power distribution in order to attain minimum system weight. This requires matching the electrical characteristics of each of the converters in the circuit.

For the reference design reactor a variable fuel loading technique was employed to reduce the effects of nonuniform power distribution. This appendix presents the results of a study performed to determine the value of varying converter geometry, and discusses the interplay of converters operated in a series circuit.

Since thermionic converters are fundamentally high current, low voltage devices, it becomes necessary to connect them in series to obtain desirable voltages. Also, since neutron leakage from the reactor causes a nonuniform spacial power generation, the thermal power input to each converter varies. Therefore, the electrical characteristics which are intrinsically affected by the thermal characteristics are different for each converter. The important point is that the maximum power output from each of the converters in the reactor occurs at a different operating point, and since in a series circuit a constant current must be maintained, it becomes impossible to operate all of the converters at their peak power. In addition to this, a more severe problem exists if the electrical characteristics of a number of series-connected converters are so badly mismatched that some of the converters act as a load in the circuit and consume power.

The penalties incurred due to nonuniform reactor thermal power distribution can be reduced generally by two methods, 1) a variation of the fuel concentration in certain regions of the core, and 2) a variation of the converter geometry. In the former case, the fuel concentration is varied to flatten the thermal power distribution so that with the use of constant-geometry converters a more equal thermal power input to each

converter occurs. This results in matching of the converter electrical characteristics. In the latter case, the fuel concentration is held constant while the converter geometry, especially the electrode length, is varied to improve the matching.

2. Variable Geometry Criteria

A number of geometric parameters can be varied in a converter, but only variations in electrode length will be considered in the following discussion. In a later section of this appendix variations in lead geometry are also discussed.

Considering a fixed thermal power distribution the converter length can be so varied that either the thermal flux or the thermal power to each converter comprising a series circuit are equal. In order to demonstrate the criterion that will yield the maximum electric power output for a fixed thermal power input and a maximum operating temperature, a simple analytical model was constructed. This consisted of three thermionic converters electrically connected in series, subjected to a cosine thermal power distribution with a maximum-to-minimum power ratio of four. The converter dimensions were those for the reference design with the exception of the lengths, and the total thermal power for the three converters was maintained constant. The anode temperatures of the converters were equal.

Three investigations were conducted to determine the effects of varying converter lengths. In the first the converter lengths were set equal to the value of the reference design. In the second the lengths were adjusted so that the thermal flux in each converter was equal, and in the third the lengths were adjusted so that the thermal power in each converter was the same. The cosine power distribution and the converter lengths corresponding to the preceding requirements are shown in Figure 6-1. The values of converter length, thermal flux, and thermal power for the three criteria are listed in Table 6-1.

TABLE 6-1

Equal Converter Lengths

Converter No.	Converter Length - Inches	Thermal Power - Watts	Thermal Flux - Watts/cm^2
1	2.0	1388	52 8
2	2.0	1117	42.4
3	2.0	603	23.0

Equal Thermal Flux

Converter No.	Converter Length - Inches	Thermal Power - Watts	Thermal Flux - Watts/cm^2
1	2.89	1520	40.0
2	2.00	1051	40.0
3	1.04	545	40.0

Equal Thermal Powers

Converter No.	Converter Length - Inches	Thermal Power - Watts	Thermal Flux - Watts/cm^2
1	1.45	1035	54.2
2	1.66	1035	47.4
3	2.89	1035	27.2

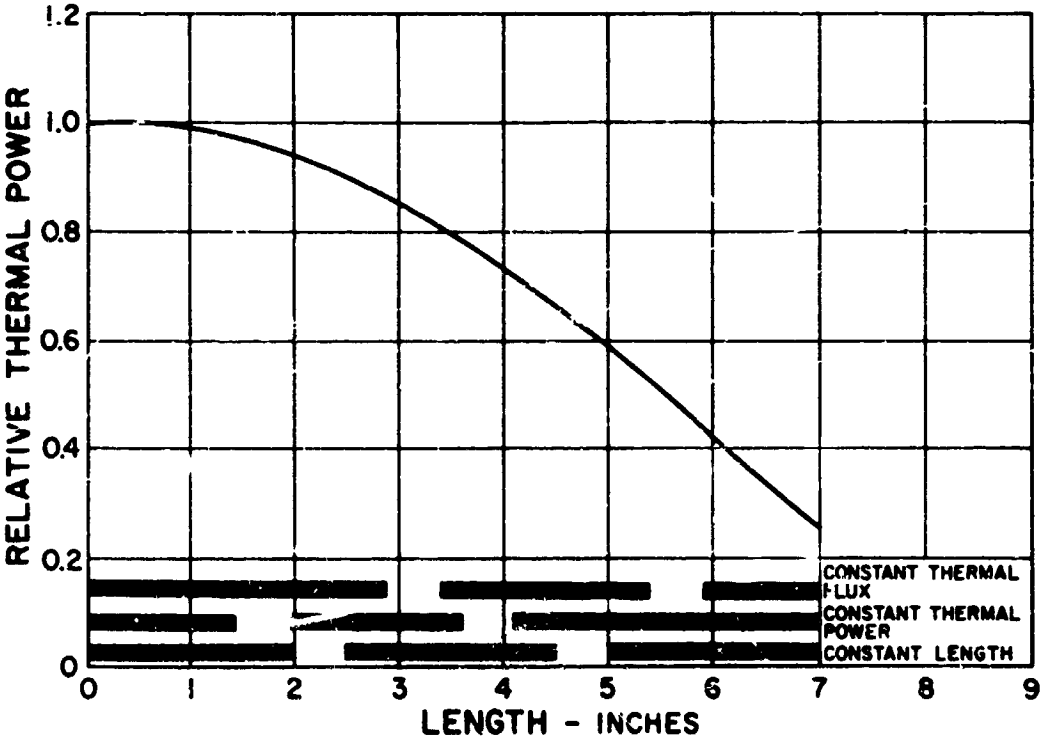

Figure 6-1 Thermal Power Distribution. Converter Length Criterion

Circuitry analyses were performed to determine the individual performance of each converter in the circuit and the combined performance of the three converters. The initial phase of the analysis involved the determination of the current-voltage characteristics for each converter. Because the analysis was concerned with constant thermal power rather than constant cathode temperature, the current-voltage characteristics were determined to balance thermal input with the cathode energy loss due to electron cooling, radiant heat transfer, lead thermal conduction, and cesium thermal conduction. This entailed iterating upon the cathode temperature to maintain the heat balance. The change in cathode temperature with respect to current was determined, thus enabling the cathode temperature to be obtained for each series circuit current. The corresponding converter voltages were determined utilizing the thermionic correlations presented in Report PWA-2240 for constant cathode temperature. With the current voltage characteristics thus determined, the electric power is presented as the products of the sum of the voltage output of each converter and the series circuit current.

The relative electric power output for each of three criteria is shown in Figure 6-2 as a function of relative cathode temperature. The values are normalized with respect to the optimum power and the corresponding cathode temperature occurring for the equal converter length criterion. Each of the converters in series operates at a different cathode temperature due to the difference in thermal power input. The temperatures in the figure correspond to the highest cathode temperature in the circuit. This requires the electron cooling to be different for each converter, which necessitates a variation in cathode temperature to maintain the thermal balance.

It is seen that the equal power criterion results in a 27 per cent increase in power, whereas the equal flux criterion results in a slight degradation in power. The optimum for both the equal flux and equal power criteria occur at lower cathode temperatures, that is, 4 and 8 per cent respectively. This result is important since maximum operating cathode temperature is frequently employed to determine operating criteria. The open-circuit conditions for equal length, equal flux and equal power results in an 8, 2.5, and 7 per cent increase in cathode temperature respectively. It should be noted that both the equal-flux and equal-power criteria result in lower open-circuit temperatures than the constant-length criterion.

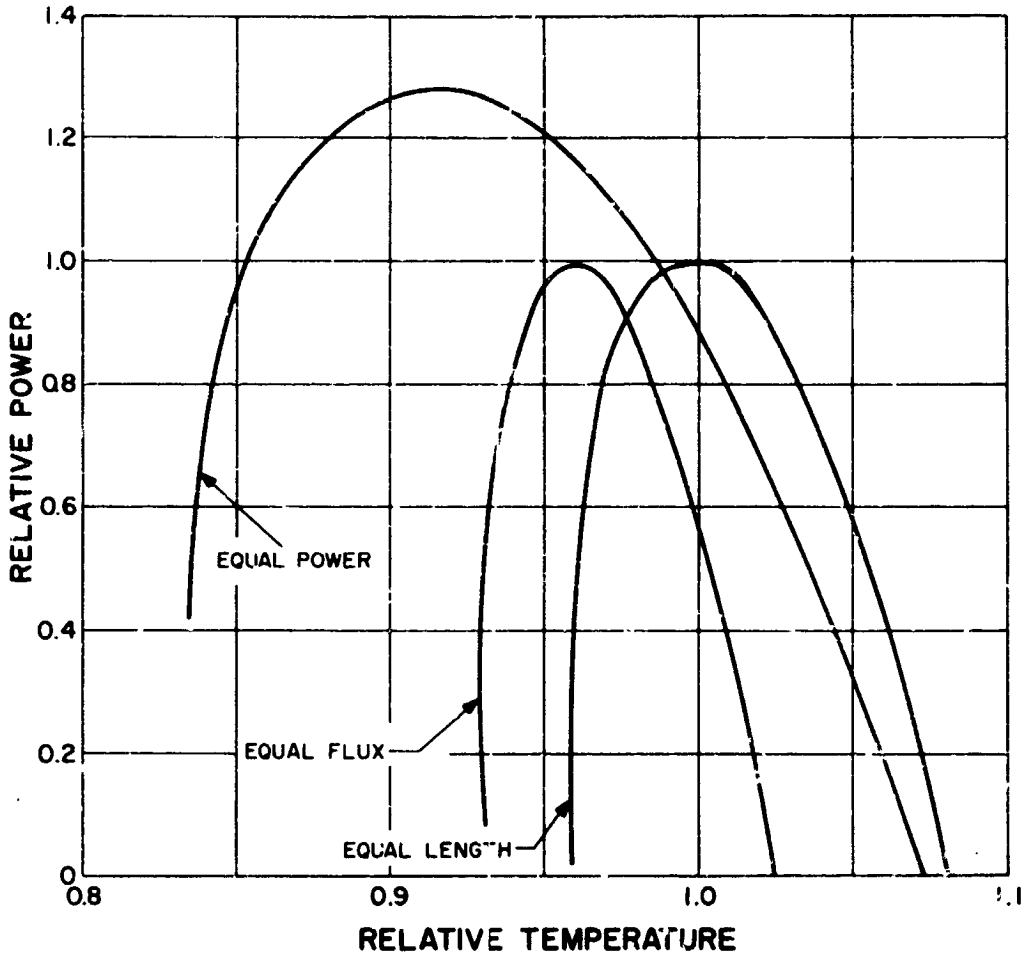

Figure 6-2 Circuit Performance. Cathode Length Criterion

The aforementioned relations can be accounted for by considering the converter current-voltage characteristics for each criterion. The converter characteristics for equal-thermal-power, equal-thermal-flux, and equal-length criteria are shown in Figures 6-3 to 6-5, respectively. The individual thermal flux and thermal powers are indicated along the lines of constant thermal power. Lines of constant cathode temperature are also shown. The striking aspect of the curves is the similarity of the characteristics for the equal-thermal-power criterion and the contrast in characteristics which exists for the other criteria. It is this mismatch of current-voltage characteristics which limits the series circuit current, thus resulting in a degradation in electric power.

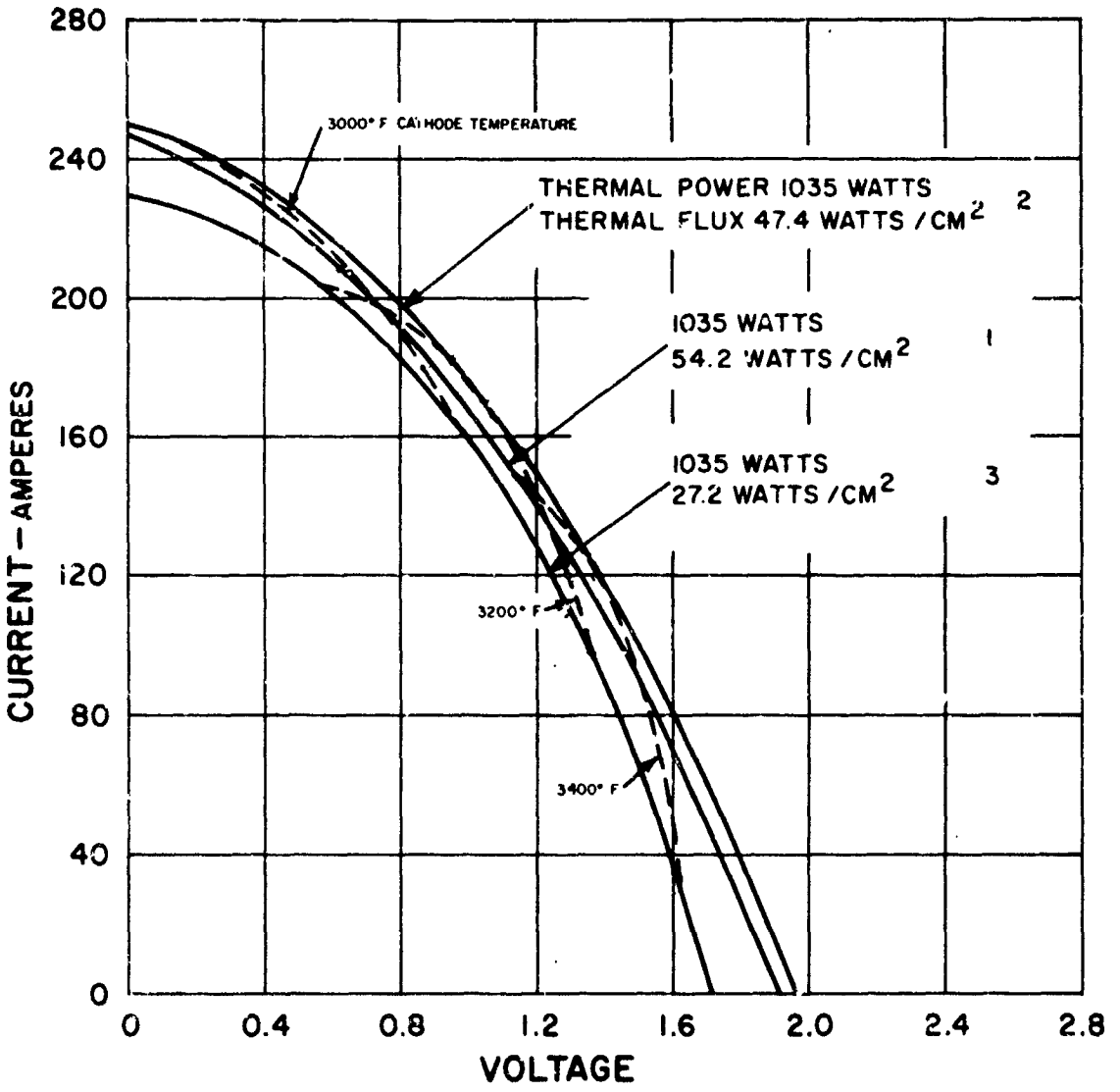

Figure 6-3 Current-Voltage Characteristics. Equal Thermal Power

The converter characteristics can be accounted for by considering Table 6-2 which lists the cathode open-circuit temperature and the change in cathode temperature with respect to current. The open-circuit temperature is the cathode temperature which exists when no current emanates from the converter. The major thermal energy losses are therefore radiant heat transfer and lead thermal conduction, the former

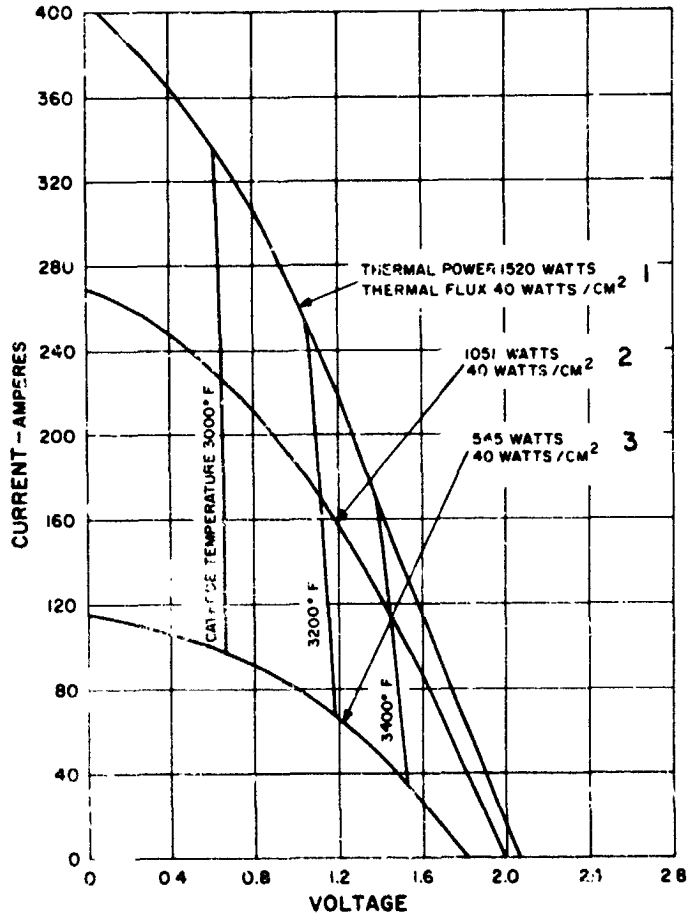

Figure 6-4 Current-Voltage Characteristics. Equal Thermal Flux

being the predominant mode. Table 6-2 indicates that the open-circuit temperatures for each criterion increase as the heat generation decreases, converter number one being at the maximum end of the cosine distribution and converter number three at the minimum. The change in cathode temperature with respect to current increases in a similar manner for the equal-length and equal-flux criteria. The change in cathode temperature with respect to current for the equal-power criterion, however, decreases as the heat generation decreases. Thus, as current begins to flow in the circuit utilizing the equal-power criterion,

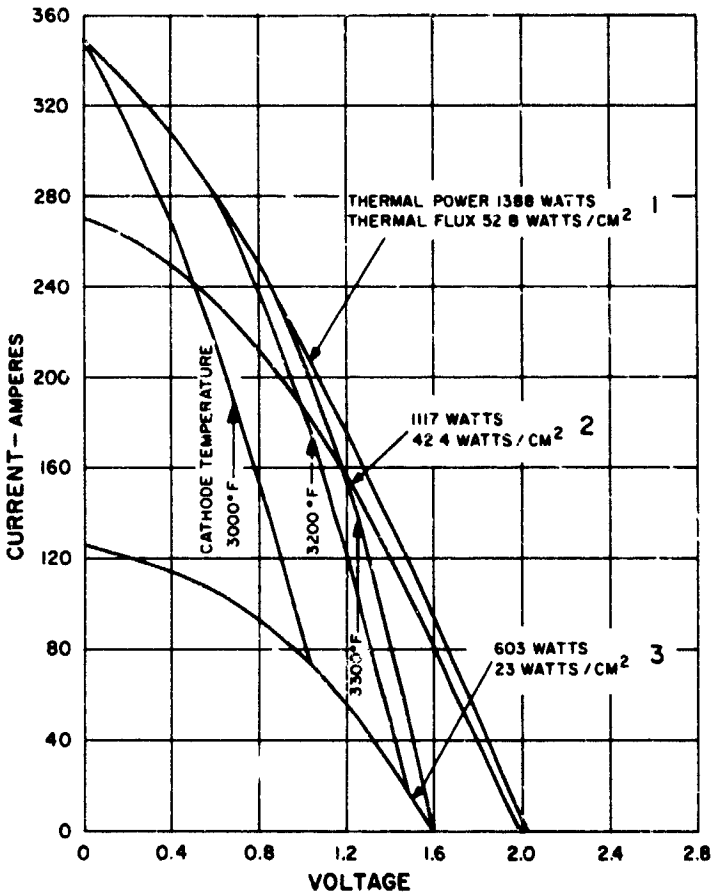

Figure 6-5 Current-Voltage Characteristics. Equal Cathode Length

the differences between the cathode temperatures in each converter decrease, and because the converter voltages are linear functions of cathode temperature, the current-voltage characteristics approach matched conditions. Conversely for the remaining criteria, the differences between cathode temperature in each converter increase, resulting in mismatch conditions and the associated power degradation.

TABLE 6-2

Equal Length

Converter No.	Open-Circuit Temperature - °F	ΔT/ ΔI °F/amps
1	4050	3.038
2	3840	3.409
3	3295	4.559

Equal Thermal Flux

Converter No.	Open-Circuit Temperature - °F	ΔT/ ΔI °F/amps
1	3840	2.527
2	3785	3.447
3	3630	6.550

Equal Thermal Power

Converter No.	Open-Circuit Temperature -°F	ΔT/ ΔI °F/amps
1	4020	4.015
2	3915	3.760
3	3500	3.102

Thus, adjusting the cathode length so that the thermal power input to each converter is equal results in an increase in electric power output and a decrease in both operating and open-circuit cathode temperature. For this reason it was decided to investigate the effects of varying cathode length in the reference design utilizing the constant-power criterion.

3. Reference Design

a) Variable Fuel Loading

The two methods indicated above, variable fuel loading or variable converter length, that can be used to reduce the power degradation due to nonuniform power distribution, each present problems.

Varying converter length necessitates the accurate determination of the spacial power distribution and the fabrication of each converter individually to achieve equal thermal power. Varying fuel distribution, on the other hand, requires dividing the reactor core into regions and varying the fuel concentration to compensate for neutron leakage. This essentially results in a different fuel for each region of the core.

A circuitry analysis was conducted to determine the performance of the reference fuel element subjected to the power distribution for the variable fuel loading. Varying the fuel loading reduces the severity of the thermal power distribution, but does not provide a completely uniform distribution. Consequently, a mismatch exists in the current-voltage characteristics, which can be reduced by varying the converter lengths and the lead-length-to-area ratios. The lead length-to-area ratios were varied in an attempt to match cathode temperature by altering the lead conduction losses.

Three studies were performed employing a variable fuel form reactor. The first involved equal converter length, the second, varying converter length to yield equal thermal power input, and the third, varying converter length and lead length-to-area ratio. The power distribution due to the variable fuel loading is shown in Figure 6-6 as a function of fuel element half length. Also indicated are the converter positions for the constant and varying length studies.

The electric power for the aforementioned studies is shown in Figure 6-7 as a function of maximum cathode temperature. The values are normalized with respect to the reference design, which was established for a maximum operating cathode temperature. The thermionic reactor, however, provides constant thermal power to the converters. Thus, two modes of operation are possible, constant cathode temperature and constant thermal power. For an invariant thermal input, the maximum electric power for the latter mode is greater than that for the constant temperature mode. This is illustrated by the curve for equal converter length. It is seen that 31 per cent greater power can be achieved by proceeding from the constant temperature to the constant power mode of operation. The increase in power output, however, is accompanied by a 5 per cent increase in cathode temperature. This is because the values corresponding to maximum power output and maximum efficiency do not coincide for the constant temperature mode.

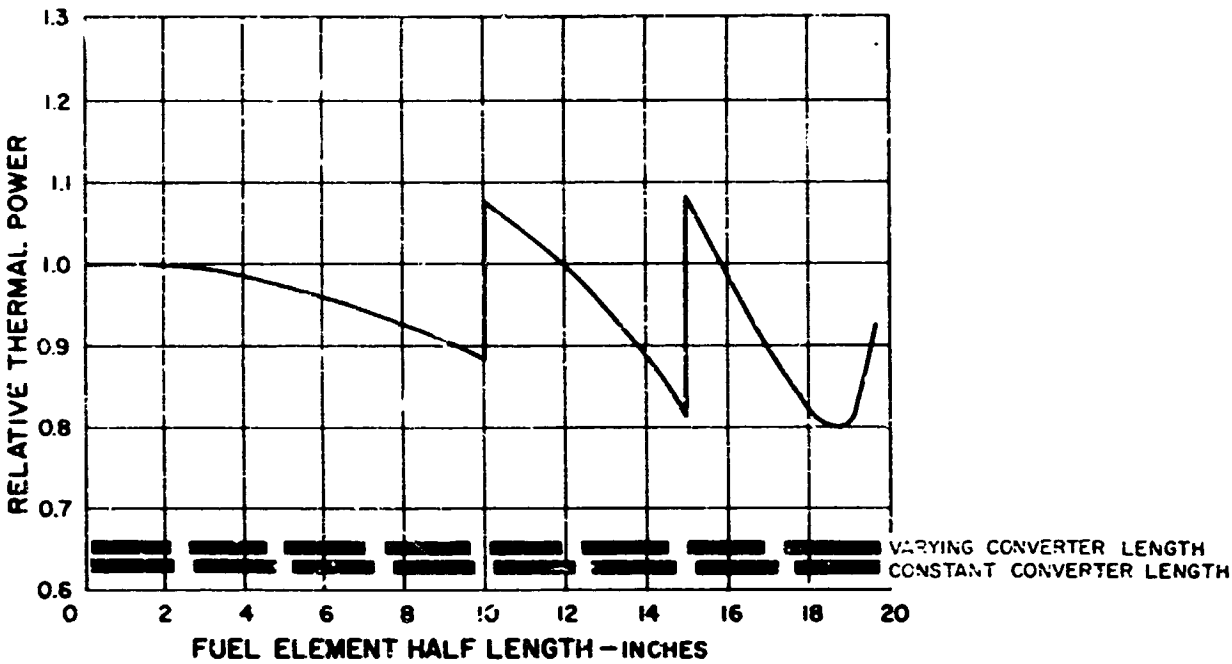

Figure 6-6 Thermal Power Distribution. Variable Fuel Loading

Varying the converter lengths so that the thermal power inputs are equal, results in a 27 per cent increase in electric power at the same cathode temperature. A further increase of 4 per cent is achieved by also also varying the lead length-to-area ratio. The ability of the lead length-to area ratio to match current-voltage characteristics is limited, but it does provide a method of fine adjustment.

The operating cathode temperatures are shown in Figure 6-8 as a function of converter position in the fuel element. The convergence towards matched conditions is evidenced by the convergence of the temperatures towards a uniform temperature condition.

b) Uniform Fuel Loading

A circuitry analysis was conducted to determine the performance of the reference fuel element subjected to the power distribution for a uniform fuel loading. As a means of comparing the variable fuel loading and constant length concept with the variable converter length uniform fuel loading concept the integrated thermal powers were set equal. The first part of the analysis entails determining the fuel ele-

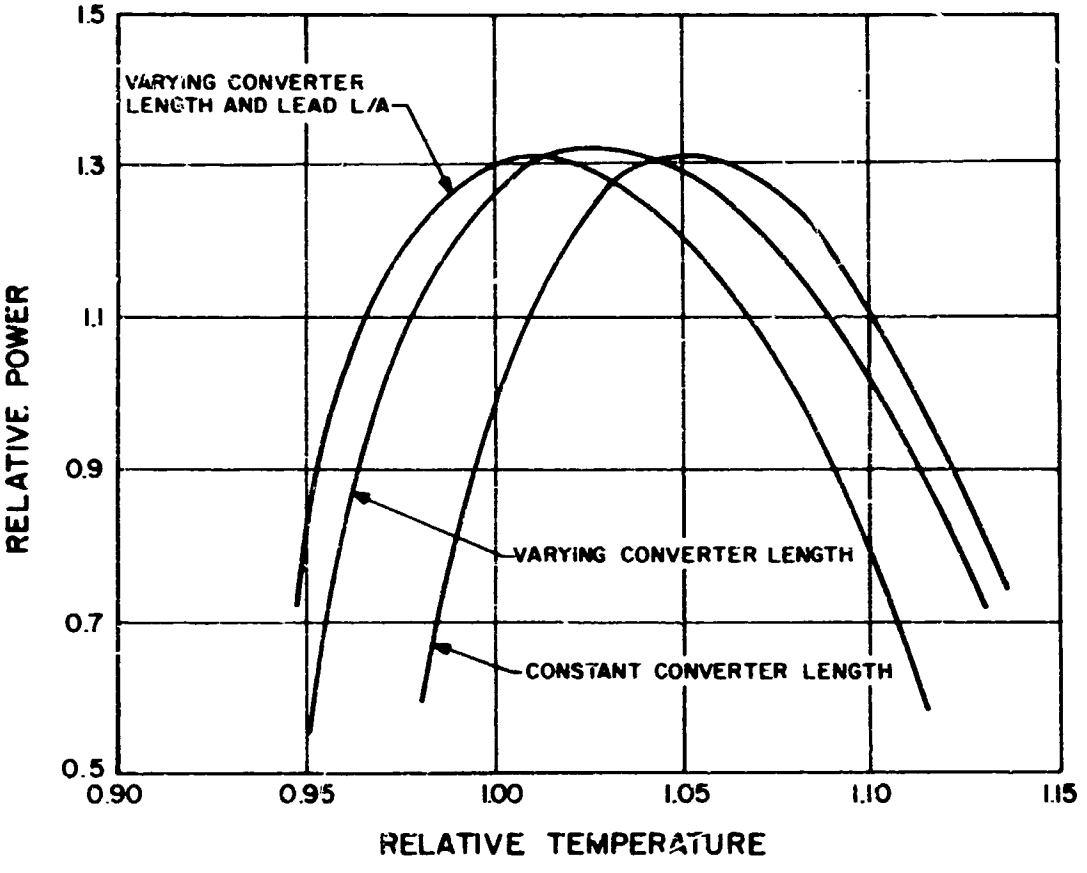

Figure 6-7 Fuel Element Performance. Variable Fuel Loading

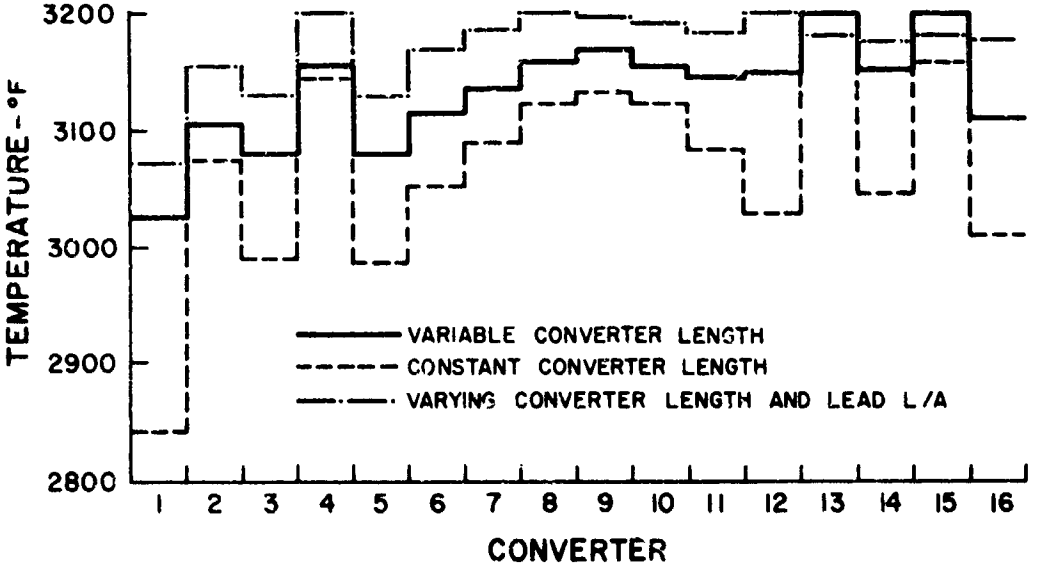

Figure 6-8 Cathode Operating Temperatures. Variable Fuel Loading

ment performance for equal converter length, the second, varying converter length to achieve equal thermal power, and the last, varying converter length and lead length-to-area ratio. The power distribution is shown in Figure 6-9 as a function of fuel element half length. Also indicated are the converter positions for the equal and varying length studies.

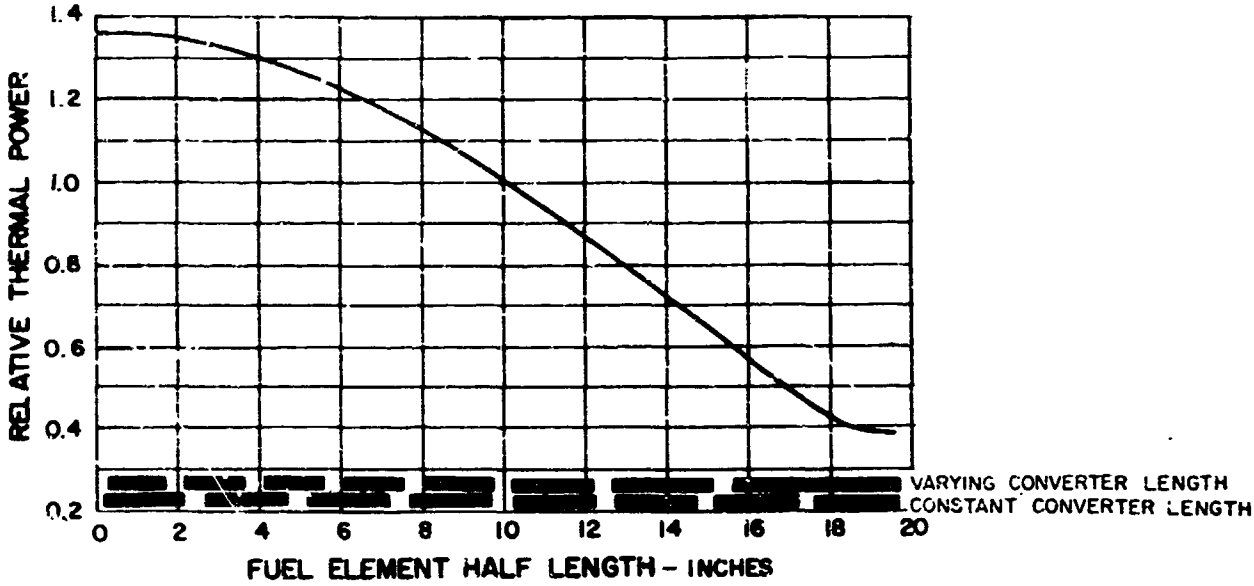

Figure 6-9 Thermal Power Distribution. Uniform Fuel Loading

The electric power is shown in Figure 6-10 as a function of maximum cathode temperature for each of the aforementioned studies. For the purpose of comparison the values are normalized with respect to the performance for the reference fuel element with variable fuel loading and equal cathode length. The mismatch between equal length converters with uniform loading is so severe that the maximum cathode temperature is always greater than the maximum operating cathode temperature for the reference design. Varying the converter length at a relative temperature of one results in a 17 per cent power degradation. The degradation is reduced to 7 per cent by varying the lead length-to-area ratio.

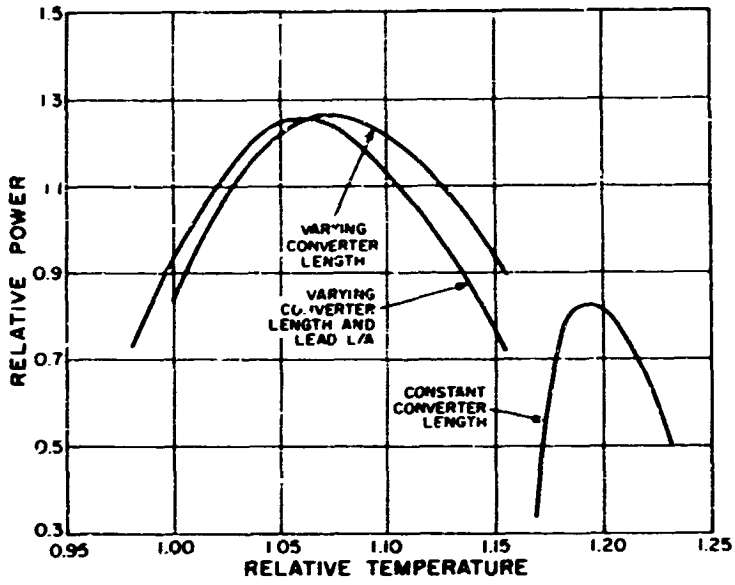

Figure 6-10 Fuel Element Performance. Uniform Fuel Loading

The operating cathode temperature is shown in Figure 6-11 as a function of converter position in the fuel element. The convergence towards matched conditions is evidenced by the convergence of temperatures towards a uniform value. Figure 6-12 shows a comparison of the various methods of improving reactor performance. Comparing the variable with the uniform fuel loading cases, it can be seen that all cases produce a reasonable power output at the reference temperature except for the case of uniform loading with uniform converter length. For this case, the optimum power output occurs at a much higher temperature and falls off so quickly with temperature that at 3200°F, practically no power output is obtained. Comparing the cases of variable fuel loading, it can be seen that improvements in power result from variations in converter length or converter length and lead geometry. However, the improvements in power are not great enough to overcome the problems associated with the fabrication and inventory of variable geometry converters. Comparing the cases for uniform loading it is obvious that constant geometry should not be employed, and that relatively small power degradations result with the variable geometry cases.

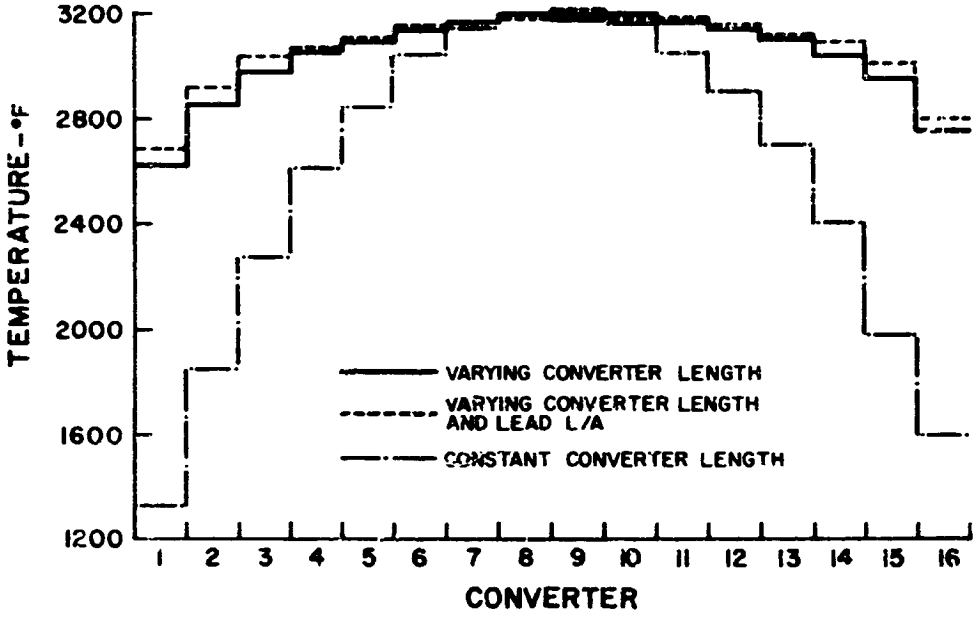

Figure 6-11 Cathode Operating Temperatures. Uniform Fuel Loading

c) Conclusions

The variable fuel loading concept with constant geometry and the variable converter length concept with uniform loading are comparable on the basis of performance. The former concept requires the reactor core to be divided into fifteen regions, each with a different fuel composition. This essentially results in fifteen different fuels which will have to be developed.

The variable length concept requires development of many different converter structures and complicates assembly. Combining both concepts results in a 26 per cent increase in electric power, but unfortunately involves combining the aforementioned problems.

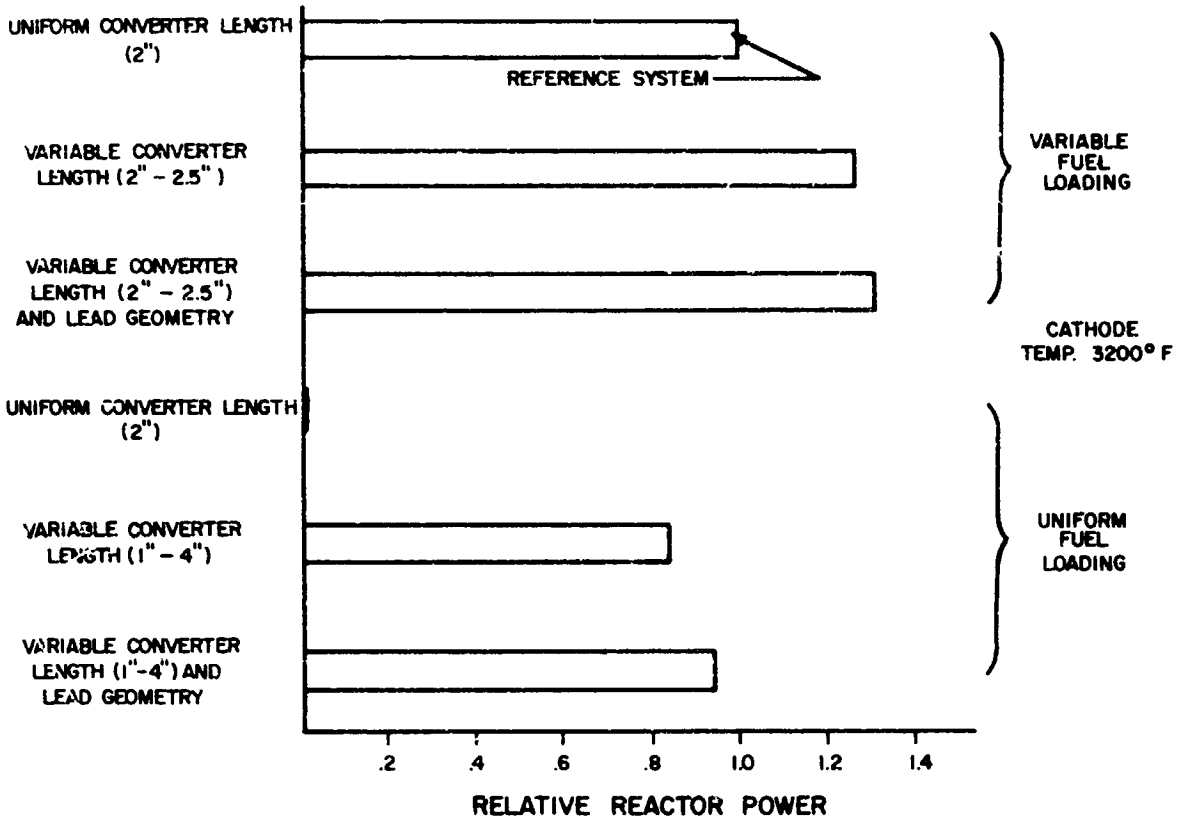

Figure 6-12. Reactor Performance

APPENDIX 7

Contained Fission Gas Fuel Element

APPENDIX 7

Contained Fission Gas Fuel Element

1. Introduction

Because of the long lifetimes associated with nuclear space power systems, the problem of gas pressure buildup due to fission products must be considered. This leads to the problem of either containing or venting the fission products. In the latter scheme, the products are vented to space through passages leading from the reactor core. Although this apparently presents a simple and direct solution, it may reduce the reliability of the system. This is due to the possibility of the fission products condensing at cold spots and eventually blocking the passages. Should this occur, the fission gas pressure buildup could rupture the cathode, producing fuel element failures. Because of the question concerning reliability, an analysis was conducted to determine the penalties in system specific weight that would be incurred by retaining the fission gas in the reactor core.

2. Fission Gas Buildup

A significant property of fission products is their radioactivity. The immediate decay products are also radioactive and, although the decay chains vary in length, each fragment is followed on the average by three stages of decay before a stable species is formed. Because there are about 60 different radioactive nuclides produced in fission and each is, on the average, the precursor of two others, there are approximately 180 radioactive species present among the fission products after a short time. In view of the complexity of the decay scheme it was assumed that for each fission product there exists one isotope which effectively represents the entire decay chain.

This isotope is the member of the chain which is present in the greatest quantity during the reactor lifetime. In this manner the number of isotopes was considerably reduced. The fission product burnup was neglected, since the mean fission energy for the reference design is high, resulting in low neutron absorption cross-sections. Because of the lack of data, thermal reactor yield values were in some cases substituted

for fast reactor yield values. The number of atoms per fission product was thus determined as a function of fission yield, reactor power and operation time.

3. Fission Gas Pressure

To determine the gas pressure due to fission products it was assumed that for any gas, there exists some critical temperature above which the pressure is given by the perfect gas law and below which the pressure is simply its vapor pressure. If, however, a number of atoms in a specified volume are at a temperature less than their critical temperature and the gas pressure as calculated from the perfect gas law is less than the gas pressure as calculated from the vapor pressure equation, it was assumed that there are not enough atoms present to constitute a liquid. The choice of the correct equation to determine the gas pressure was made according to the aforementioned conditions.

4. Fission Gas Volume

An analysis was conducted to determine the volume necessary to contain the fission gas at one end of the thermionic converter. This scheme shown in Figure 7-1 was used only as an analytical model and does not represent a suggested design. Further study would be required to de-

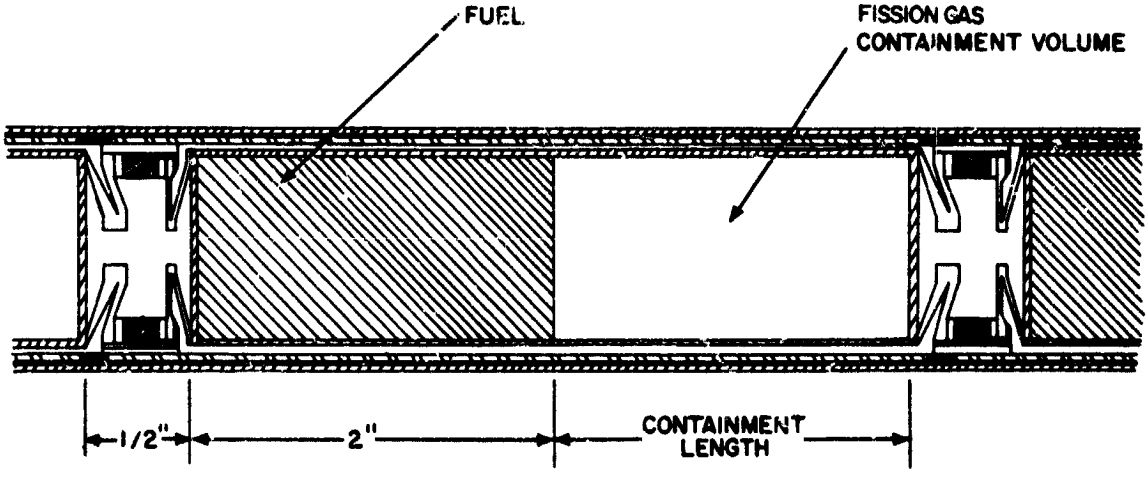

Figure 7-1 Converter with Contained Fission Gas

termine the most desirable configuration. The volume was determined using creep in a cylindrical pressure vessel under conditions of varying internal pressure as the governing criterion. The analysis assumes that for uniaxial tension specimens the logarithm of the minimum creep rate varies linearly with the logarithm of the circumferential stress. An expression was obtained for internal pressure as a function of material, temperature, time, strain, cylinder radius and thickness. The volume was varied by varying the containment length (the cathode outside diameter was held constant) which required a variation of cathode thickness until the fission gas pressure converged to the allowable internal pressure obtained by the preceding expression.

An initial analysis was conducted for 100 and 50 per cent fission gas release from the fuel. The volume was sized so that the cathode contained the fission gas at end of life. Three design criteria were employed for the reference converter. The first criterion was cathode rupture. The second was an allowable change in cathode radius, whereby the cathode was permitted to come in contact with the anode at end of life. The last criterion was an allowable cathode true strain of 1 per cent. Each was analysed for maximum operating and open-circuit cathode temperature. The distance between adjacent converters (the containment length) necessary to accomodate the fission gas volume for the preceding conditions is listed in Table 7-1. The striking feature of this table is the severe penalties in core volume and the ensuing increase in reactor weight that would occur should open-circuit temperatures govern the fission gas containment.

The ability of the anode to contain the fission gas, should the cathode rupture, was investigated for 100 and 50 per cent fission gas release. Because a failure of this nature would involve fission gas in the interelectrode space, the analysis was conducted for open-circuit conditions. The design criteria included anode rupture and allowable true strains of 1.0, 0.1 and 0.01 per cent. The results in Table 7-2 list the containment lengths necessary to contain the fission gas for the aforementioned conditions.

Figure 7-2 shows the allowable pressures at the end of the mission for cathodes with the specified thicknesses. Corresponding to each cathode thickness is a containment length for each of the assumed gas releases. Obviously, for a given cathode thickness the containment length increases as the gas release increases.

TABLE 7-1

Containment Lengths for
Fission Gases Contained Within Cathode

Fission Gas Release %	Cathode Temperature	Design Criterion	Containment Length inches
100	maximum operating temperature	cathode rupture	6.54
		electrode contact	7.27
		1 per cent strain	9.17
	open-circuit temperature	cathode rupture	22.1
		electrode contact	24.0
		1 per cent strain	31.7
50	maximum operating temperature	cathode rupture	3.27
		electrode contact	3.56
		1 per cent strain	4.63
	open-circuit temperature	cathode rupture	11.1
		electrode contact	12.5
		1 per cent strain	15.4

TABLE 7-2

Containment Lengths for
Fission Gases Contained Within Anode

Fission Release %	Design Criterion	Containment Length inches
100	anode rupture	.49
	1 per cent strain	.76
	0.10 per cent strain	1.18
	0.01 per cent strain	1.89
50	anode rupture	.24
	1 per cent strain	.38
	0.10 per cent strain	.59
	0.01 per cent strain	.94

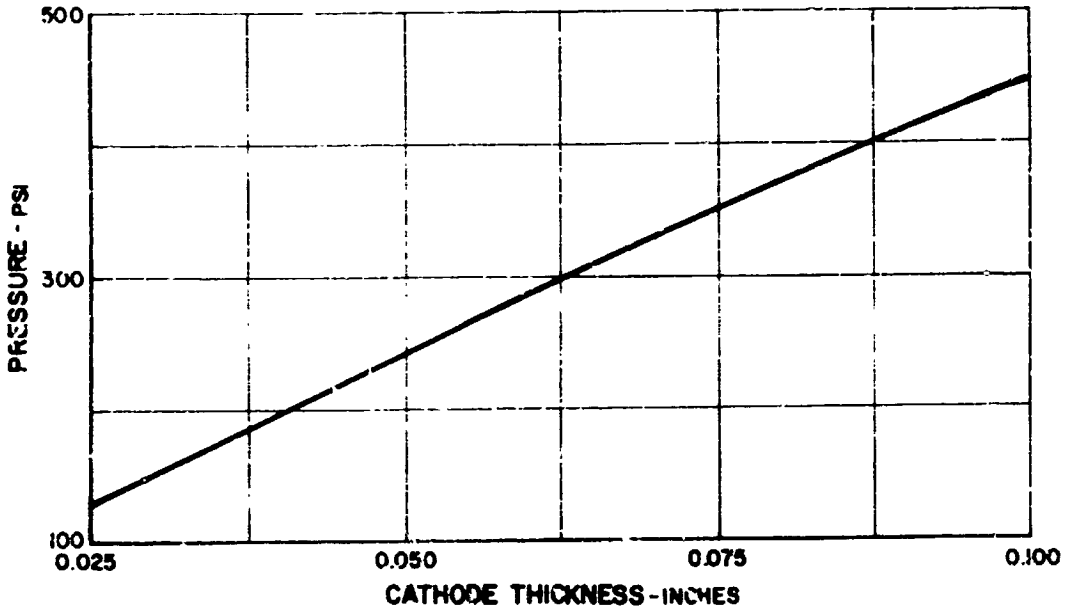

Figure 7-2 Fission Gas Pressure vs Cathode Thickness

A further analysis was conducted for the reference design employing maximum operating cathode temperature and an allowable change in cathode radius permitting contact with the anode at end of life. The cathode thickness and fission gas release were varied to determine the spacing necessary to contain the fission gas. The results are shown in Figure 7-3 where containment length is presented as a function of cathode thickness for constant values of fission gas release. The line labelled minimum weight connects the locus of points corresponding to the optimum values of containment length and cathode thickness for minimum system weight at each of the fission gas releases. The lines for 10 per cent increase in system weight are also shown. Values for the system weight were determined from the curves in Figure 7-4 which is a plot of relative system specific weight versus cathode thickness.

The containment length shown in Figure 7-3 is limited by the ability of the anode to contain the gases in the event of a cathode rupture. Therefore, the selection of a containment length and a cathode thickness should be based not only on the desire to attain minimum weight but also on the ability of the anode to contain the gases. This may require the selection of off-optimum parameters.

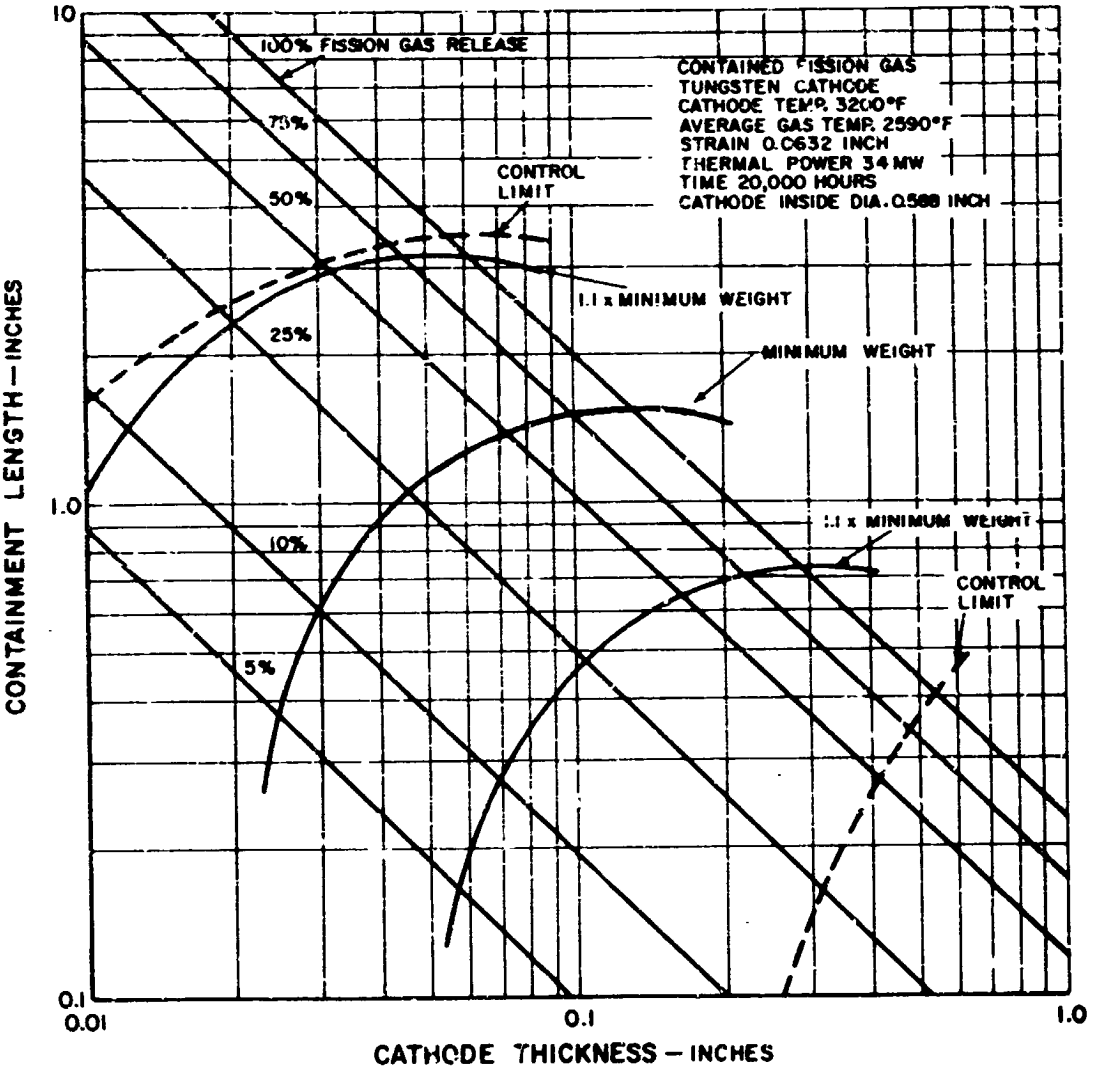

Figure 7-3 Containment Length vs Cathode Thickness

Also shown in Figure 7-3 are control limit lines which represent additional limitations on the containment length and cathode thickness. The control limits encompass the systems whose reactor diameters are small enough to be controlled by rotating reflectors. These lines were determined from Figure 43 which showed that the limiting diameter is about 50 inches. The values of reactor diameter for the contained gas systems are given in Figure 7-5.

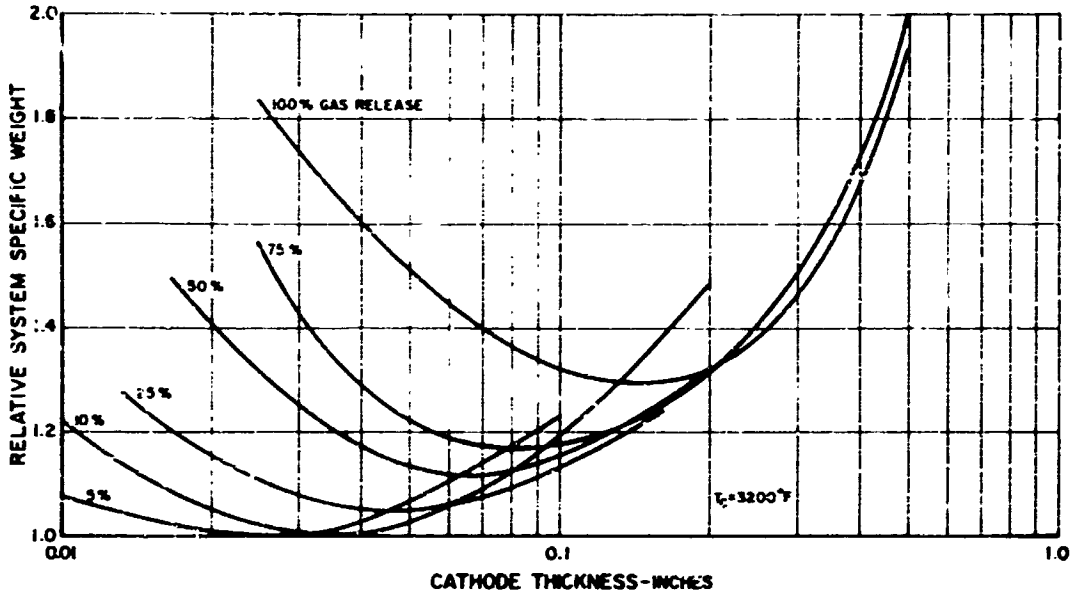

Figure 7-4 Relative Weight vs Cathode Thickness

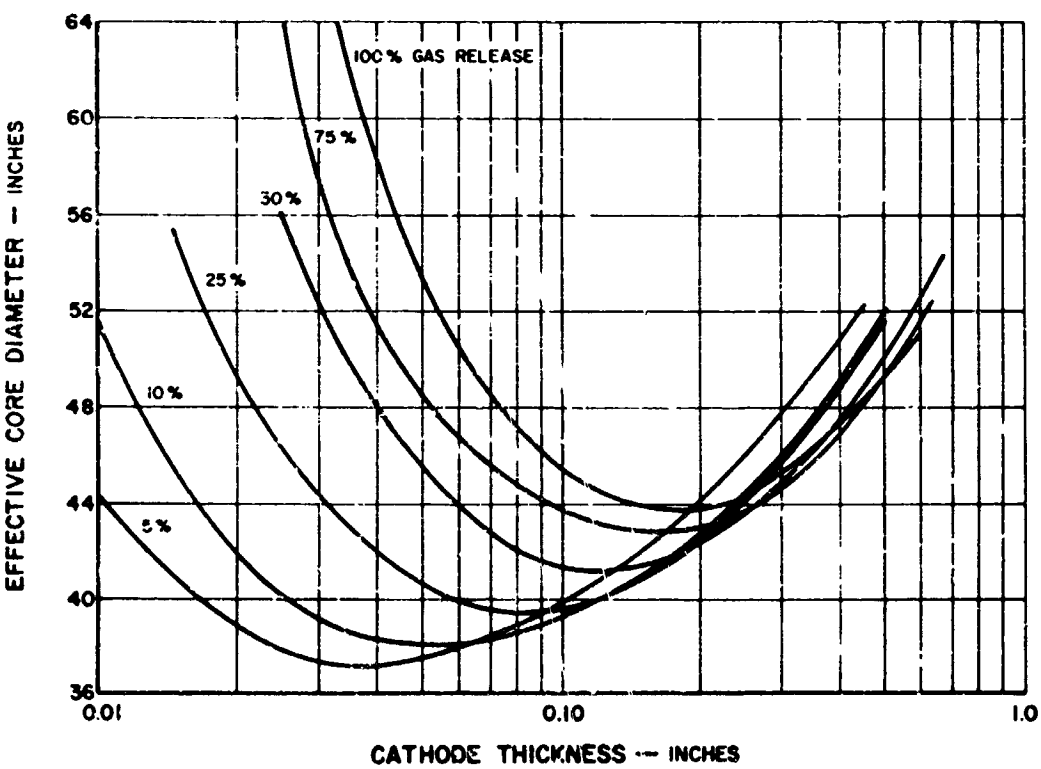

Figure 7-5 Core Diameter vs Cathode Thickness

DESIGN STUDY OF A HIGH POWER IN-PILE NUCLEAR THERMIONIC SPACE POWERPLANT

by
A. U. Buatti and J. W. Schmitt

ABSTRACT

A preliminary design study of a 3.25 MW(e) in-pile nuclear thermionic space powerplant required to complete an assumed 24,000-hour Jupiter-capture mission was performed. Engineering design criteria and preliminary system and component weights were established. The importance of component parameters and the requirements and limitations of components were identified. Also, alternate reactor concepts were investigated and estimates of their requirements and performance made. System parameters for the powerplant were taken from a parametric study of powerplants in the power range from 1 to 10 MW(e) (Report PWA-2319). The results of the parametric study shows specific weights of powerplants in this power range to be relatively constant. This design study incorporated the results of the parametric study and considerations of engineering practicality. The effects of nonuniform reactor power generation, powerplant structure and integration, power-conditioning equipment and mission requirements were also included. The results of the design study indicate that the in-flight powerplant specific weight is 23.4 lbs/KW and that the specific weight is relatively insensitive to increases in converter power density and converter configuration.